

https://dspace.org/

Pre-existing fluid-driven fracture: mathematical models and solution

Nchabeleng, Mathibele Willy

2021
https://hdl.handle.net/10539/32427

Downloaded from a DSpace repository. https://dspace.org/

DOCTORAL THESIS

Pre-existing fluid-driven fracture: Mathematical models and solution



WITS UNIVERSITY

MATHIBELE WILLY NCHABELENG

Supervisor:
Dr. Adewunmi G. FAREO

A thesis submitted to the Faculty of Science, University of the Witwatersrand, Johannesburg, South Africa, in fulfilment of the requirements for the degree of Doctor of Philosophy

February 24, 2021

DECLARATION

I, Mathibele Willy Nchabeleng, declare that the work in this thesis is my own unaided work except where due reference has been made. It is being submitted to the University of the Witwatersrand, Johannesburg, for the degree of Doctor of Philosophy. It has not been submitted before for any degree or examination at any other university.

Johannesburg, February 24, 2021

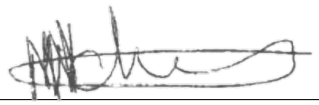

Mathibele Willy Nchabeleng

To my family

ABSTRACT

The problem of a two-dimensional, pre-existing, fluid-driven fracture propagating in a permeable rock is considered. The flow of fluid in the fracture is laminar and the fracture is driven by a viscous incompressible Newtonian fluid. Lubrication theory is applied to the fracturing fluid and the Cauchy principal value integral derived from linear elastic fracture mechanics is used to describe the elasticity equation relating the fluid pressure to the fracture half-width. The fluid leak-off at the fracture interface into the rock formation is modelled in two ways, namely, using a leak-off velocity term and by using Darcy's law. Appropriate initial and boundary conditions for the model are stated and discussed. Similarity solutions are derived for the fracture half-width, length, leak-off velocity and leak-off depth. Numerical results are obtained for a nonlinear diffusion equation with leak-off velocity term and for a nonlinear diffusion equation coupled with Darcy's model. The results are illustrated using computer generated graphs.

Mathematics, rightly viewed, possesses not only truth, but supreme beauty — a beauty cold and austere, like that of sculpture, without appeal to any part of our weaker nature, without the gorgeous trappings of painting or music, yet sublimely pure, and capable of a stern perfection such as only the greatest art can show. The true spirit of delight, the exaltation, the sense of being more than Man, which is the touchstone of the highest excellence, is to be found in mathematics as surely as poetry.

— Bertrand Russell

ACKNOWLEDGEMENTS

I wish to express my deep and sincere gratitude to my wonderful supervisor, Dr A.G. Fareo, for all his support and encouragement throughout my academic programme. His patience, wisdom and guidance has been invaluable and his confidence in me has been a major source of motivation which has driven me throughout my thesis. I am grateful to Dr M.J.S. Mphaka for sharing with me the necessary literature for me to develop my background in singular integral equations. I am also grateful to Prof D.P. Mason for his insightful comments.

I am thankful to my parents who have cared for me and given me unconditional love. To my siblings, Dr Molefe S. Nchabeleng, Dr Ntheno L. Nchabeleng and Matlale H. Nchabeleng, thank you all for being there for me. To my brother, Dr Mo, thank you for being the best "Big Brother" anyone can ask for. To my sister, Dr Lee, thank you for believing in me and always encouraging me to strive for the best and to push myself. To my sweet younger sister, Matlale aka "*Hunza*", thank you for always...always showing up when I needed you. You are next in line, get that red gown! *I love you all fam...*

My greatest appreciations and gratitude to my friends, Christopher Nchabeleng, Lungelo Mabuza, Simphiwe Mazibuko, Frank Nchabeleng, Ilish Seema, David Kgokolo, Manyano Nogoboka and my cousins, Matete Motubatse, Alfred Nchabeleng and Nape Makgolane. I will forever cherish the moments we shared together and thank you for the fun, game nights, traveling and hiking. I wish you all the best the world has to offer. I would also like to thank wholeheartedly, Mbalenhle Mandisa Nxumalo, for her support and encouragement. I have to offer my special thanks the one man who has, at all times, encouragement me to further my studies, Mr Thabo Chuene, may his soul continue to rest in peace. A big thank you to the leadership of Sego Sa Lesedi Foundation, Dineo Makoro, Jessica Phalafala and Matthews Sejeso.

Finally, I am very grateful to the National Research Foundation and University of the Witwatersrand for the financial support during my research. I would also like to acknowledge and thank the administrative

staff of the School of Computer Science and Applied Mathematics for their hospitality at all times and all the non-academic staff. A big thank you to everyone who has helped and encouraged me throughout all levels of my education. I cannot forget to thank the Almighty God, my creator.

As Mduduzi Dube would say "*Re mo spacing!*". Vele, re tsene! We are within. It is time to give the people what they want!

CONTENTS

I OVERVIEW OF THE STUDY 1

1 INTRODUCTION AND BACKGROUND 2
1.1 Introduction . . . 2
1.2 Background to hydraulic fracturing . . . 3
1.3 Literature review . . . 4
1.4 Theoretical background . . . 7
1.4.1 Mechanics of hydraulic fracturing . . . 7
1.4.2 Fracture geometry models . . . 9
1.4.3 Darcy's law . . . 11
1.5 Outline of research . . . 13

2 INTEGRAL EQUATIONS 15
2.1 Introduction . . . 15
2.2 Background to integral equations . . . 15
2.3 Classification of integral equations . . . 16
2.3.1 Fredholm integral equations . . . 17
2.3.2 Volterra integral equations . . . 20
2.3.3 Singular integral equations . . . 21
2.3.4 Volterra-Fredholm integral equations . . . 23
2.4 Structure of kernel . . . 24
2.5 Conclusion . . . 25

II MATHEMATICAL PRELIMINARIES AND MODELS 27

3 SOME NUMERICAL TECHNIQUES AND SOLUTIONS FOR CAUCHY-TYPE SINGULAR INTEGRAL EQUATIONS OF THE FIRST KIND 28
3.1 Introduction . . . 28
3.2 Cauchy principal value integrals . . . 28
3.3 An inversion technique using properties of Abel's equation 30
3.4 A survey of some numerical methods for singular integral equations . . . 33
3.4.1 Analytical solution . . . 33
3.4.2 Approximate analytical solution . . . 35
3.4.3 Finite difference method . . . 38
3.4.4 Spline method . . . 51
3.4.5 Comparison of the numerical methods . . . 60
3.5 Conclusion . . . 60

4 MATHEMATICAL MODELS AND GOVERNING EQUATIONS 61
4.1 Introduction . . . 61
4.2 Problem description . . . 61
4.3 Governing equations . . . 61
4.4 Boundary equations . . . 64
4.5 Solid mechanics equations . . . 66

4.5.1 Cauchy principal value integral 66
4.5.2 Fracture propagation criterion and the stress intensity factor 67
4.6 Nonlinear diffusion equation with leak-off velocity term 68
4.7 Conclusion 74

III MAIN RESULTS AND CONCLUSIONS 75

5 LEAK-OFF FLUID VELOCITY PROPORTIONAL TO FRACTURE HALF-WIDTH 76
5.1 Introduction 76
5.2 Leak-off fluid velocity proportional to fracture half-width 76
5.3 Tip asymptotics and the velocity ratio 79
5.4 Finite difference method 82
5.5 The Newton-Raphson method for a system of equations 85
5.6 Discussion on numerical method 88
5.7 Spline method 89
5.8 Discussion on numerical method 95
5.9 Numerical results and discussions 96
5.10 Conclusion 105

6 LEAK-OFF FLUID VELOCITY PROPORTIONAL TO GRADIENT OF FLUID-ROCK INTERFACE 106
6.1 Introduction 106
6.2 Leak-off fluid velocity proportional to gradient of fluid-rock interface 106
6.3 Tip asymptotics and the velocity ratio 108
6.4 Spline method 110
6.5 Numerical results and discussions 112
6.6 conclusion 120

7 TWO-DIMENSIONAL FLUID-DRIVEN FRACTURE WITH DARCY FLOW IN PERMEABLE ROCK FORMATION 122
7.1 Introduction 122
7.2 Fluid leak-off into the permeable medium 122
7.3 Two-dimensional fluid-driven fracture with Darcy flow model 123
7.4 Tip asymptotics and the velocity ratio 129
7.5 Spline method 129
7.6 Discussion on numerical method 132
7.7 Numerical results and discussions 133
7.8 Conclusion 142

8 CONCLUSION 144

IV APPENDIX 147

A APPENDIX A 148
A.1 Inversion of a Cauchy Integral Equation 148

B APPENDIX B 155
B.1 Solution of the dimensionless fracture half-width 155

C APPENDIX C 159
C.1 Differentiation under the integral sign 159

BIBLIOGRAPHY 162

LIST OF FIGURES

Figure 1 (a) Mode I (Opening) (b) Mode II (Sliding) and (c) Mode III (Tearing) deformations [6]. 8
Figure 2 The KGD model [15]. 9
Figure 3 The PKN fracture model [69]. 10
Figure 4 The Penny–Shaped model [28]. 11
Figure 5 Schematic of Darcy's experimental equipment [13]. 12
Figure 6 Structure of Fredholm and Volterra integral equations, adapted from [47]. 17
Figure 7 Central difference at midpoints on uniform grid [41]. 39
Figure 8 Graph of $h(x)$ plotted against x for (i) $n = 5$, (ii) $n = 50$ and (iii) $n = 100$ when $2 \leqslant i \leqslant n-1$, using the conventional finite difference approach. 43
Figure 9 Graph of $h(x)$ plotted against x for (i) $n = 5$, (ii) $n = 50$ and (iii) $n = 100$ when $1 \leqslant i \leqslant n-2$, using the conventional finite difference approach. 45
Figure 10 Graph of $h(x)$ plotted against x for (i) $n = 5$, (ii) $n = 50$ and (iii) $n = 100$, using the transformation method 48
Figure 11 Graph of $h(x)$ plotted against x for (i) $n = 5$, (ii) $n = 50$ and (iii) $n = 100$, using the integral approximation approach. 50
Figure 12 Linear spline interpolant $s(x)$. 52
Figure 13 Graph of $h(x)$ plotted against x for (i) $n = 5$, (ii) $n = 50$ and (iii) $n = 100$, using the spline method. 57
Figure 14 Graph of $h(x)$ plotted against x for (i) $n = 5$, (ii) $n = 50$ and (iii) $n = 100$. 58
Figure 15 Plots of the relative error for (i) $n = 5$, (ii) $n = 50$ and (iii) $n = 100$. 59
Figure 16 A pre-existing two-dimensional fluid-driven fracture propagating in a permeable rock where $h(t,x)$ represents the fracture half-width and $L(t)$ the fracture length. 62
Figure 17 Graph of $f(\xi)$ plotted against ξ for $\beta_1 = 0.01$, $Q_0 = 0.2$, $\gamma = 0.5$ when (i) $n = 50$, (ii) $n = 80$ and (iii) $n = 100$. 90

Figure 18 Comparison of the solution for the similarity function $f(\xi)$ obtained using the finite difference method and the spline method when $n = 100$. . 96
Figure 19 Graph of $h(t,x)$ plotted against x at times $t = 0, 10, 20, 50$ for $Q_0 = 0.2$, $\gamma = 0.5$ and for (i) $\beta_1 = 0$ and $c_2 = 0.022453$, (ii) $\beta_1 = 0.01$ and $c_2 = 0.019100$ and (iii) $\beta_1 = 0.04$ and $c_2 = 0.009068$. 98
Figure 20 Graphs of (i) the fracture half-width $h(t,x)$, (ii) leak-off fluid velocity $v_n(t,x)$ and (iii) the net pressure $p(t,x)$, plotted against x for $\beta_1 = 0$, 0.005, 0.01, 0.04 when $Q_0 = 0.2$ and $\gamma = 0.5$ at $t = 50$. 99
Figure 21 Graphs of (i) the fracture half-width $h(t,x)$, (ii) leak-off fluid velocity $v_n(t,x)$ and (iii) the net pressure $p(t,x)$, plotted against x for $Q_0 = 0.1$, 0.15, 0.2, 0.25 when $\gamma = 0.5$ and $\beta_1 = 0.01$ at $t = 50$. 100
Figure 22 Graphs of (i) the fracture half-width $h(t,x)$, (ii) leak-off fluid velocity $v_n(t,x)$ and (iii) the net pressure $p(t,x)$, plotted against x for $\gamma = 0$, 2, 4, 10 when $Q_0 = 0.2$ and $\beta_1 = 0.01$ at $t = 50$. . 101
Figure 23 Fracture length plotted for various values of (i) β_1, (ii) Q_0, (iii) γ. 102
Figure 24 Graphs illustrating (i) fracture volume plotted against t for $\beta_1 = 0, 0.005, 0.01, 0.04$ when $Q_0 = 0.2$ and $\gamma = 0.5$, (ii) velocity ratio $v_x^*(t,x)/L'(t)$ plotted against ξ for $\beta_1 = 0, 0.005, 0.01, 0.04$ when $Q_0 = 0.2$ and $\gamma = 0.5$, (iii) dimensionless pressure gradient plotted against ξ for $Q_0 = 0.2$, $\gamma = 0.5$ and $\beta_1 = 0.01$. 103
Figure 25 The constant c_2 plotted against (i) β_1, (ii) Q_0, (iii) γ. 104
Figure 26 Graph of $h(t,x)$ plotted against x at times $t = 0, 10, 20, 50$ for $Q_0 = 0.2$, $\gamma = 0.5$ and for (i) $\beta_2 = 0$ and $c_2 = 0.022433$, (ii) $\beta_2 = 0.01$ and $c_2 = 0.019125$ and (iii) $\beta_2 = 0.04$ and $c_2 = 0.009200$. 113
Figure 27 Graphs of (i) the fracture half-width $h(t,x)$, (ii) leak-off fluid velocity $v_n(t,x)$ and (iii) the fluid pressure $p(t,x)$, plotted against x for $\beta_2 = 0$, 0.005, 0.01, 0.04 when $Q_0 = 0.2$ and $\gamma = 0.5$ at $t = 50$. 114

Figure 28 Graphs of (i) the fracture half-width $h(t,x)$, (ii) leak-off fluid velocity $v_n(t,x)$ and (iii) the fluid pressure $p(t,x)$, plotted against x for $Q_0 = 0.1$, 0.15, 0.2, 0.23 when $\gamma = 0.5$ and $\beta_2 = 0.01$ at $t = 50$. 115
Figure 29 Graphs of (i) the fracture half-width $h(t,x)$, (ii) leak-off fluid velocity $v_n(t,x)$ and (iii) the fluid pressure $p(t,x)$, plotted against x for $\gamma = 0, 0.5, 1, 2$ when $Q_0 = 0.2$ and $\beta_2 = 0.01$ at $t = 50$. 116
Figure 30 Fracture length plotted for various values of (i) β_2, (ii) Q_0, (iii) γ. 117
Figure 31 Graphs illustrating (i) fracture volume plotted against t for $\beta_2 = 0$, 0.005, 0.01, 0.04 when $Q_0 = 0.2$ and $\gamma = 0.5$ (ii) velocity ratio $v_x^*(t,x)/L'(t))$ plotted against ξ for $\beta_2 = 0, 0.005, 0.01, 0.04$ when $Q_0 = 0.2$ and $\gamma = 0.5$, (iii) dimensionless pressure gradient for $Q_0 = 0.2$, $\gamma = 0.5$ and $\beta_2 = 0.01$. 118
Figure 32 The constant c_2 plotted against (i) β_2, (ii) Q_0, (iii) γ. 119
Figure 33 Graph of $h(t,x)$ plotted against x at times $t = 0, 20, 50, 200$ for $Q_0 = 0.25$, $\gamma = 0.01$ and for (i) $\alpha = 6$ and $c_2 = 0.003277$, (ii) $\alpha = 18$ and $c_2 = 0.0034975$ and (iii) $\alpha = 50$ and $c_2 = 0.003600$. . 134
Figure 34 Graphs of (i) the fracture half-width $h(t,x)$, (ii) leak-off depth $b(t,x)$ and (iii) the fluid pressure $p(t,x)$, plotted against x for $\alpha = 6, 18, 30, 50$ when $Q_0 = 0.25$ and $\gamma = 0.5$ at $t = 200$. 135
Figure 35 Graphs of (i) the fracture half-width $h(t,x)$, (ii) leak-off depth $b(t,x)$ and (iii) the fluid pressure $p(t,x)$, plotted against x for $Q_0 = 0.21$, 0.23, 0.25, 0.27 when $\gamma = 0.5$ and $\alpha = 8$ at $t = 200$. . 136
Figure 36 Graphs of (i) the fracture half-width $h(t,x)$, (ii) leak-off depth $b(t,x)$ and (iii) the fluid pressure $p(t,x)$, plotted against x for $\gamma = 0$, 0.005, 0.01, 0.03 when $Q_0 = 0.25$ and $\alpha = 8$ at $t = 200$. . . 137
Figure 37 Leak-off velocity $v_n(t,x)$ plotted for various values of (i) α, (ii) Q_0, (iii) γ, at $t = 200$. 138
Figure 38 Fracture length plotted for various values of (i) α, (ii) Q_0, (iii) γ. 139
Figure 39 Graphs illustrating (i) the fracture volume plotted against t for $\alpha = 6$, 18,30, 50 when $Q_0 = 0.25$, and $\gamma = 0.01$, (ii) the dimensionless pressure gradient plotted against ξ for $\alpha = 8$, $Q_0 = 0.25$, and $\gamma = 0.01$. 140

Figure 40 The constant c_2 plotted against (i) α, (ii) Q_0, (iii) γ. 141
Figure 41 The region of integration (shaded area). 151

LIST OF TABLES

Table 1 Stress intensity factors for different geometries. 8
Table 2 Comparison between traditional two-dimensional hydraulic fracture models 11
Table 3 Conditions for classifying integral equations. . . 16
Table 4 Frequently encountered integral equations, λ is a parameter 25
Table 5 Chebyshev polynomials of the Second kind ($n = 5$). 37

Part I

OVERVIEW OF THE STUDY

1 INTRODUCTION AND BACKGROUND

1.1 INTRODUCTION

Reservoir stimulation and artificial lifting are the two main activities for a production engineer in the oil and gas industry [16]. The main purpose of stimulation is to increase well productivity. One of the primary engineering techniques used to increase well productivity is hydraulic fracturing. Hydraulic fracturing has made it possible to access underground mineral resources where they were previously inaccessible and it has proved to be a very useful and standard technique for petroleum production, extraction of gas and the generation of geothermal energy [20]. This led many scientists and engineers, including mathematicians, to take an interest in this technique. Simple mathematical models of hydraulic fractures were introduced between the 1940s and 1950s [9, 11, 31, 35, 80]. These models included (i) the Khristianovic-Geertsmade Klerk (KGD) model [28, 44]; (ii) the Perkins-Kern-Nordgren (PKN) model [63, 66]; and (iii) the radial or penny–shaped model [79]. A notable number of hydraulic fracture problems in literature have been modelled with the use of the PKN formulation which gives a simple linear relationship between the net-fluid pressure and the fracture half-width [7, 21, 43]. The PKN concept is based upon the assumptions of plain strain condition in vertical planes [69, 87]. One of the shortcomings of this model is that the net pressure necessarily vanishes at the fracture tip and therefore the stress intensity factor K cannot be defined. The stress intensity factor can be described as a numerical value that measures the magnitude of the effect of the stress singularity at the tip of the fracture [24]. Essentially, the stress intensity factor provides a convenient mathematical framework for the study of fracture development and propagation.

In this thesis, we will extend the analysis of a pre-existing fluid-driven fracture from a case in which the PKN model is used to describe the elasticity equation to a more complex case in which the elasticity of the rock is modelled using the Cauchy principal value integral. This model will be formulated to describe the evolution of the fracture propagating in a permeable rock. The flow of fluid inside the porous rock matrix will be modelled in two ways, firstly, by using a leak-off velocity term and secondly, by using the Darcy's fluid flow model.

1.2 BACKGROUND TO HYDRAULIC FRACTURING

Hydraulic fracturing is a key process in petroleum and mining engineering. In this process, fluid is pumped into a rock fracture at ultra-high pressure in order to extend it. If the encompassing formation is permeable then some proportion of the injected fluid will escape at the fracture walls into the formation. Furthermore, if the fracturing fluid is water then the process is called hydrofracturing [17]. Fractures can occur as a result of a natural process or can be man-made. Kilometres-long volcanic dikes driven by magma can be considered as natural examples while hydraulic fractures initiated to extracting shale gas or improving well productivity in reservoir rocks with low permeability are considered examples of man-made fractures [4, 83]. When the process of hydraulic fracturing was introduced in the 1940s, it was just a timid technology. Its proliferation took place in the 1950s [16]. Over the years, this technology became more important due to its application in geothermal projects and shale gas exploitation [94]. Other applications of hydraulic fracturing include tunnel and dam construction, carbon sequestration, rock burst mitigation, block cave mining, groundwater remediation, and water well development [5]. It is estimated that seventy percent (70%) of gas wells and fifty percent (50%) of oil wells that have been drilled in North America since the 1950s have been hydraulically fractured [88].

In general, the hydraulic fracturing process consists of the following main phases: fracture initiation (in a case of zero-initial length fracture), fracture propagation, the flow of fluid through the channel and fluid leak-off into the formation [71]. During this process, four different types of mechanics are involved, namely, rock, fracture, fluid, and thermal. The rock mechanics describes the deformation of the surrounding rock due to fluid pressure; fracture mechanics describes the mechanisms of failure and parting that occur near the fracture tip; fluid mechanics describes the flow of fluid inside the fracture; and thermal mechanics describes the interaction and the exchange of heat between the formation and the fracturing fluid [16]. The combination of these mechanics results in the study of fracture propagation [88]. Analytical models to describe each of the responses have been developed.

According to Adachi et al. [4], the basic mathematical equations governing the hydraulic fracturing process are: (i) the elasticity equation; (ii) the fluid flow equation; (iii) the leak-off term; (iv) the proppant transport equation; and (v) the fracture growth condition. In this thesis, we will utilize these equations to describe the evolution of the hydraulic fracture propagation.

1.3 LITERATURE REVIEW

Since the introduction of hydraulic fracturing into the reservoir stimulating practice, several introductory and key papers focusing on hydraulic fracture modelling have been published. These papers formed the foundation of hydraulic fracture modelling. The first two-dimensional fracture model was developed in the work of Khristianovich and Zheltov [44]. Carter [9, 16] neglected both solid mechanics and fluid viscosity and focused on leak-off when investigating the hydraulic fracture problem. His work resulted in the most widely used leak-off model. Perkins and Kern [16, 66] assumed that fracture mechanics was negligible and concentrated on fluid flow. An extensive review of existing fracture models is given in [69].

Smirnov and Tagirova [77] obtained self-similar solution to the problem of hydraulic fracture formation in a permeable medium. They modeled the elasticity of the rock using the PKN formulation and the fluid leak-off through the fracture walls using Darcy's law. Self-similar solutions were determined when either the fluid flow rate or the net-fluid pressure was specified at the fracture entrance. Emerman et al. [17] presented similarity solutions for laminar and turbulent fluid fracture. They showed that flow resistance of the fluid is more important than the fracture resistance of the solid for most geological problems.

Fitt et al. [27] obtained similarity solution for a pre-existing hydraulic fracture embedded in an impermeable rock. Fareo and Mason [21] modified the model to a fluid-driven fracture propagating in a permeable rock with 1D fluid leak-off at the fracture walls. Fareo and Mason [21] showed that when the fracture half-width is proportional to the leak-off velocity, there exists some regions where there is extraction of the fluid at the fracture entrance and inflow of fluid at the fracture walls. Fareo and Mason [22, 23] investigated a fracture problem in which the fracturing fluid is non-Newtonian. A review of magma-filled fractures is given by Rubin [72].

Dontsov [14] investigated a penny-shaped fluid-driven fracture that accounts for fluid viscosity, fracture toughness, and leak-off. He obtained a closed-form approximate solution for the penny-shaped hydraulic fracture. Kanaun [42] investigated the propagation of hydraulic fracture crack in an elastic medium with varying fracture toughness. A comparison study of the Khristianovic-Geertsma-de Klerk model (KGD), Perkins-Kern-Nordgren model and a modified pseudo-3D model was performed by Nasirisavadkouhi [59].

Nchabeleng and Fareo [61, 62] derived group invariant and numerical solutions for a two-dimensional fracture driven by a laminar incompressible Newtonian fluid in a permeable rock. The PKN approximation was used to close the model. A fracture problem in which the fluid is non-Newtonian and the Cauchy principal integral is used to model the elasticity equation is considered in [67] .

Spence and Turcotte [83] derived a similarity solution for a two-dimensional fracture propagating in an impermeable medium. They argued that their solution was in good agreement with numerical solutions obtained by Spence and Sharp [82]. The technique that was used by Spence and Sharp [82] when deriving the self-similar solutions for a elastohydrodynamic cavity flow was to expand the cavity height in terms of Chebyshev polynomials for which the elastic pressure distribution can be calculated in closed form. Subsequently, they minimized a quadratic functional that depends non-linearly on the coefficients of the polynomials to meet the boundary condition of lubrication theory. They augmented a Chebyshev expansion by a term having the right singular behaviour at the origin, which results in rapid convergence. Mitchell et al. [54] presented an asymptotic framework which describes interaction between fracture toughness, fluid viscosity and leak-off.

Fitt et al. [25] considered the propagation of a one-dimensional fluid-filled fracture in a hot dry rock geothermal energy reservoir. Two crack laws (a linear law and a hyperbolic law) are considered as well as two flow laws (a cubic law and a linear law). It was found after performing a perturbation analysis that for some law combinations, a strained-coordinate analysis is required, whilst for others a matched asymptotic approach is needed. In the latter case the problem may be reduced to that of solving a linear, non-homogeneous singular integrodifferential equation to determine the behaviour in the boundary layer.

Tvardvsky [86] investigated stress intensity factors for anisotropic layered composites. He analyzed the influence of isolated collinear cracks in every other layer of a laminate with three or more layers. He implemented Fourier transform to reduce the problem to a singular integral equation. He found stress intensity factors for different layer thickness ratio, fracture length and composite material properties. Hayes [33] investigated the origins of the stress intensity factor approach to fracture.

Stoeckhert et al. [85] investigated fracture initiation and propagation process for a highly anisotropic rock with a special interest in slate rock. He performed a series of tensile fracturing laboratory experiments under uniaxial loading. The experiments were repeated for triaxial loading. A test utilising the fairly isotropic bebertal sandstone as a somewhat isotropic rock was likewise performed for comparison. Tensile fractures were created using the sleeve cracking technique in which a polymer tube put inside the bore-hole is pressurized to create tensile fractures propagating from the bore-hole. In the uniaxial test arrangement, the loading was varied with a specific end goal to ascertain the transition from strength-dominated fracture propagating at low loading magnitudes to stress-dominated fracture propagation at high loading magnitudes.

In their study, Asadi et al. [8] examined the initiation and propagation of hydraulic fracturing with the use of laboratory and numerical methods. The results obtained were compared with analytical methods. They use a series of laboratory tests to determine the fracture mechanics parameters as input parameters for hydraulic fracture simulation calculations. The laboratory tests showed that heterogeneity of the specimens greatly affects the initiation and propagation of the fractures. Asadi et al. [8] extracted the stress intensity factor in order to investigate the manner in which fractures initiate and propagate. According to linear elastic fracture mechanics, when the stress intensity factor is equal to fracture toughness, the fracture will propagate. It was shown by comparison that the Numerical results and the experimental results had good relation. The stress distribution was compared with the theoretical solution near the tip of the fracture.

Sheibani and Olson [76] considered the determination of stress intensity factor of a three-dimensional fracture using the displacement discontinuity method. They investigated a numerical method to evaluate the stress intensity factor in Mode I, II and III at the tip of the fracture. The stress field near the crack tip controls fracture propagation. Linear elastic fracture mechanics was used to study the fracture development. Zeeb and Konietzky [95] and Zeeb, Wolgast and Konietzky [96] conducted three-dimensional numerical calculations by using the DEM-code 3DEC for hydraulic fracturing. Detailed reviews of various numerical methods applied in rock mechanics can be found in [40].

Mondal and Mandal [56] developed an analytical method for solving singular integral equations of the first kind with Cauchy kernel. They used Chebyshev polynomials of the first kind, $T_n(x)$, second kind, $U_n(x)$, third kind, $V_n(x)$, and fourth kind, $W_n(x)$, to obtain complete analytical solutions. Eshkuvatov et al. [18] studied approximate methods for solving Cauchy type singular integral equations of the first kind over a finite interval. They showed that the method of approximate solution gives an exact solution when the force function is linear. Similar conclusion is given by Chakrabarti and Berge [10].

Kim [45] solved Cauchy type singular integrals equations by using Gaussian quadrature and chose the zeros of Chebyshev polynomials of first and second kinds as the collocation and abscissa points. Srivastav and Zhang [84] solved the Cauchy type singular integral equations by using the general quadrature-collocation nodes. Abdulkawi [1] used differential method to obtain numerical solution of a singular integral equation of the first kind with Cauchy kernel.

In their paper, Seifi et al. [75] proposed a numerical method to solve Cauchy type Fredholm integral equations of the first kind. A collocation technique based on Bernstein polynomials was used to approximate the solution of several cases of Cauchy type Fredholm integrals. By transforming their problem into a system of linear algebraic equations,

Seifi et al. [75] showed that their approach is computationally simple and attractive.

1.4 THEORETICAL BACKGROUND

1.4.1 *Mechanics of hydraulic fracturing*

1.4.1.1 *Linear Elastic Fracture Mechanics and the stress intensity factor*

The use of fracture mechanics approach to hydraulic fracture criterion was introduced by Abou-Sayed et al. [2]. The approach is based on the linear elastic fracture mechanics assumptions. Linear elastic fracture mechanics is the basic theory of fracture. It was originally developed through the work of Griffith [29] and later completed by Irwin [39]. Linear elastic fracture mechanics deals explicitly with sharp cracks in elastic bodies and assumes that the material is isotropic and linearly elastic. The above-mentioned assumptions respectively implies that the material properties do not depend on direction, and these materials have only two independent elastic constants which are Young's modulus and Poisson's ratio. It should be noted that there exists a small zone termed plastic zone in which the linear theory of elasticity is invalid. This zone is also referred to as the inelastic zone or fracture process zone [24].

The introduction of the stress intensity factor was a significant achievement in the theoretical foundation of linear elastic fracture mechanics. The stress intensity factor K is a parameter that is used to predict the stress state near the tip of the fracture. This factor depends on the fracture shape, fracture size, loading and geometric boundaries. An important feature of the stress intensity factor is that it determines the stress field in the vicinity of the fracture tip. There are a number of publications on the results of calculations of stress intensity factors for different geometries and loading cases [85–87, 89]. Figure 1 depicts the three different types of loading that a crack in a body can be subjected to.

According to Rummel and Winter [73], hydraulic fracture will happen when the Mode I stress intensity factor (K_I) at tip of the fracture reaches a critical fracture toughness (K_{IC}), that is, when K_I is kept nearly equal to the critical stress intensity factor K_{IC}, the fracture will start to grow. The fracture toughness parameter illustrates the resistance force to fracture growth [73]. It should be mentioned that stress intensity factors also exists for Mode II and III. There are numerous approaches available to determine the stress intensity factor. The most commonly used methods are [8]: numerical methods, analytical methods, and experimental methods. Generally, the stress intensity factor

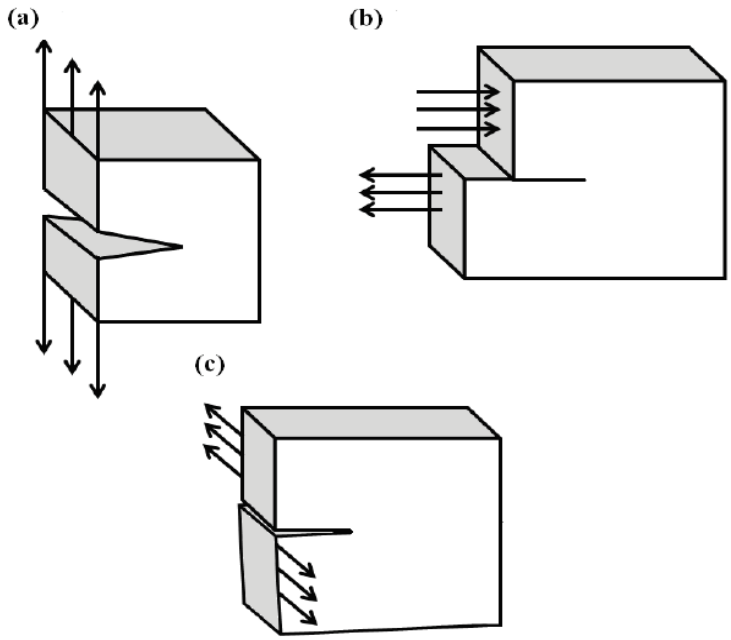

Figure 1: (a) Mode I (Opening) (b) Mode II (Sliding) and (c) Mode III (Tearing) deformations [6].

K_I for a simple case of a fracture in an infinite sheet is expressed in the form

$$K_I = \sigma\sqrt{\pi a}, \tag{1.4.1}$$

where a is a length scale characterising the fracture geometry and σ is the tensile stress perpendicular to the fracture. Expressions for the stress intensity factor for some additional geometries are given in Table 1.

Type of fracture	**Stress intensity factor,** K_I
Center fracture in an infinite plate with length $2a$	$\sigma\sqrt{\pi a}$
Edge fracture in a semi-infinite plate with length a	$1.12\sigma\sqrt{\pi a}$
Central penny-shaped fracture in an infinite plate with radius a	$2\sigma\sqrt{\frac{a}{\pi}}$
Center fracture in a plate of width W with length $2a$	$\sigma\sqrt{W\tan\left(\frac{\pi a}{W}\right)}$
2 symmetrical edge fractures in a plate of total width W, each with length a	$\sigma\sqrt{W\left[\tan\left(\frac{\pi a}{W}\right)+0.1\sin\left(\frac{2\pi a}{W}\right)\right]}$

Table 1: Stress intensity factors for different geometries.

1.4.2 *Fracture geometry models*

In the course of recent years, several models which can be broadly classified into two-dimensional and three-dimensional have been developed to study fracture propagation. These models form an integral part in the understanding and design of hydraulic fracture treatments. In this research, we restrict our discussion to two-dimensional models since we will be investigating a two-dimensional hydraulic fracture. The three most commonly used geometry models for describing the hydraulic fracture process are the KGD model [28], the PKN model [66], and the Penny-Shaped fracture model [49]. It is worth noting that both the PKN and KGD geometries are based on the plane strain assumption. A detailed history of hydraulic fracture models is given in [4].

1.4.2.1 *The Khristianovic-Geertsma-de Klerk model*

The KGD model is one of the classic two-dimensional hydraulic fracture models that has been dominant in the routine prediction of hydraulic fractures. This model, which is based on the assumptions of plane strain condition in horizontal planes, was first developed by Khristianaovic and Zheltov [44] in 1955. It was further developed by Geertsma and de Klerk [28] in 1969. The horizontal plain strain condition holds true only if the ratio of the height to length is near unity or less. The KGD [28] model takes into account the fracture mechanics of the fracture tip and also assumes that fluid flow inside the fracture as well as the frac-

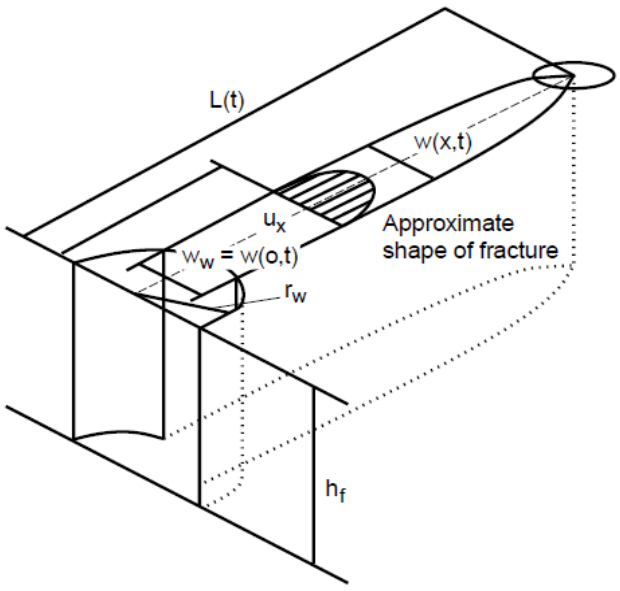

Figure 2: The KGD model [15].

ture propagation are one-dimensional. The fracture height is considered to be constant. The KGD geometry is depicted in Figure 2, where $w(x,t)$ represents the fracture width, h_f, the fracture height, $L(t)$, the fracture length and r_w is the wellbore radius.

1.4.2.2 *The Perkins-Kern-Nordgren model (PKN)*

Perkins and Kern [66] developed equations to calculate the fracture length and width for a fixed height fracture. In their work, Perkins and Kern [66] adapted the classic Sneddon plane strain crack solution to formulate the PK model [80]. The PK model was one of the groundbreaking achievement in this research area. Later Nordgren [63] improved this model by including the effects of fluid loss, hence, the model is now referred to as the PKN model. The PKN formulation is based on the assumption that fracture toughness is negligible, and that the fracture has a constant height and an elliptical cross-section. In addition to this, gravitational effects are not taken into account. The geometry of a PKN fracture is shown in Figure 3. Figure notations are the same as the KGD model. The specific assumptions for this model are given in [63, 93].

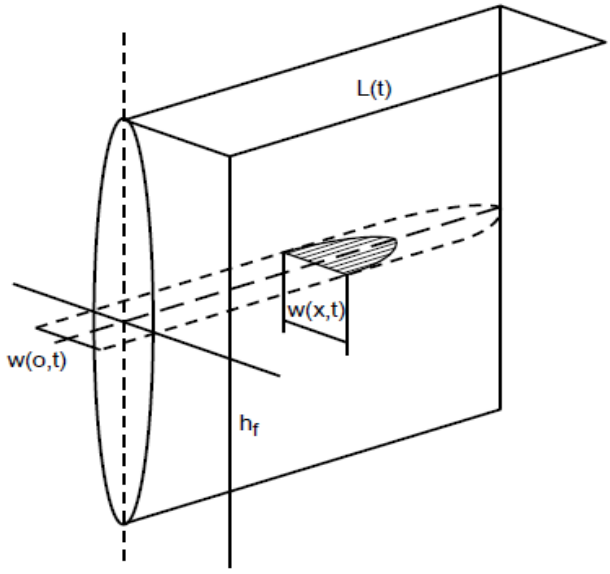

Figure 3: The PKN fracture model [69].

1.4.2.3 *The radial fracture model*

Radial fractures were considered by both Perkins and Kern [66] and Geertsma and de Klerk [28]. Their studies led to the development of the radial model. The radial model is relevant when there are no barriers constraining the growth of the fracture height or when a horizontal fracture is considered. The radial fracture model, also known as the

penny-shaped model, assumes that the fracture propagates within a given plane and that the geometry of the fracture is symmetrical with respect to the point at which fluid is injected (see Figure 4).

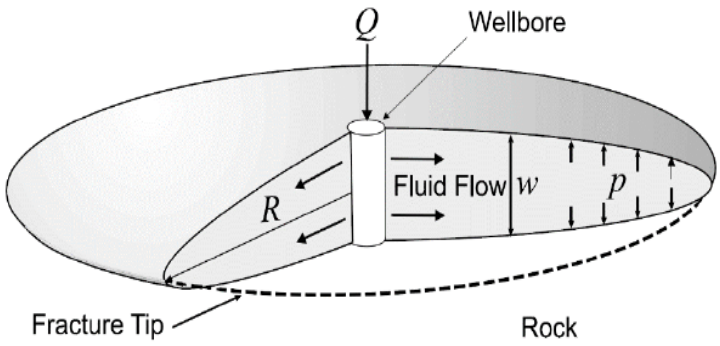

Figure 4: The Penny–Shaped model [28].

1.4.2.4 *Comparison between two-dimensional models*

The two-dimensional geometries discussed in the preceding sections contain a number of assumptions and properties. In Table 2, we give a comparison of these two-dimensional hydraulic fracture models.

Model	Assumptions	Shape	Suitable application
KGD	Fixed height, Horizontal plane strain, Fluid flow is one-dimensional along the fracture, Fracture propagation is dominated by the tip process	Rectangular cross section	Height $\gg$ length
PKN	Fixed height, Vertical plane strain, Fluid flow is one-dimensional along the fracture, Neglects fracture mechanics	Elliptical cross section	Height $\ll$ length
Radial	Propagates in a given plane, Symmetrical to the wellbore	Circular cross section	Radial

Table 2: Comparison between traditional two-dimensional hydraulic fracture models

1.4.3 *Darcy's law*

Leak-off phenomenon is common in permeable rock formations where some volume of the fracturing fluid is lost due to infiltration into the surrounding formation. There exists various leak-off models that can be

used to describe the flow of fluid in a porous medium each accounting for different effects and scenario settings. The most commonly used leak-off model was developed in the work of Carter [9] and it is given by

$$u_L = \frac{C_L}{\sqrt{t - t_{exp}}}, \tag{1.4.2}$$

where u_L is the leak-off velocity, C_L, the leak-off coefficient, t, the current time and t_{exp}, the time at which point u_L was exposed. Even though over the years the Carter's model has been the standard model in oil field applications, it is not without limitations. An important limitation of the Carter's leak-off model is that it requires the injection pressure to not propagate beyond the current extent of the fracture [65]. Hagoort et al. [30] showed that Carter's model overestimates the fracture propagation rate by a factor of two compared to the their three-dimensional numerical model. It was also shown in [46] that the particle velocity at the fracture tip becomes infinite if Carter's model is coupled with a non-local elasticity operator such as the KGD model. Moreover, the applicability of Carter's model is limited to short periods of time. In this research work, the flow of fluid through the interface into the rock formation will be modelled using Darcy's empirical flow law which is valid under a limited range of low velocities. The law resulted from experimental studies carried out by Henry Darcy in 1856. In his investigation, Darcy was concerned with the flow of water

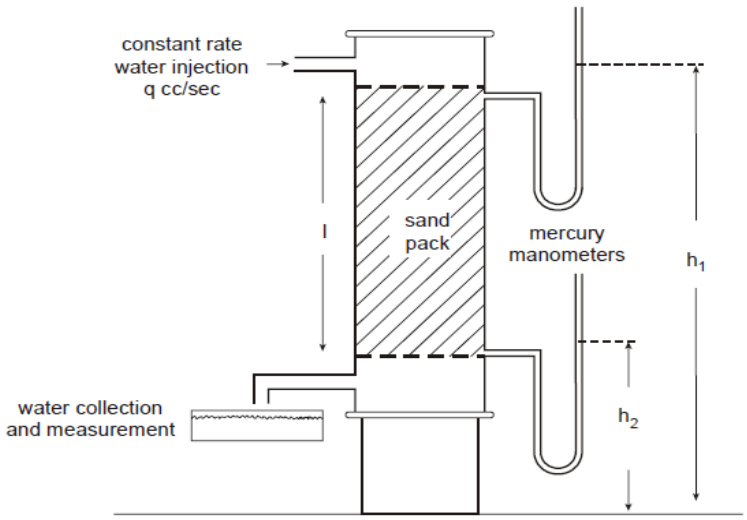

Figure 5: Schematic of Darcy's experimental equipment [13].

through unconsolidated sand filters for water purification. The filter that he designed to use for his experiments is shown in Figure 5. As a result of his experiments, Darcy provided an empirical equation that

related the flow of fluid through porous materials to the pressure gradient, which is given by

$$\frac{Q}{A} = -\frac{\kappa}{\mu}\nabla p_d, \tag{1.4.3}$$

where Q is the volume flow rate, A is the cross-sectional area, κ is the rock permeability, μ is the dynamic viscosity and p_d is the fluid pressure driving the fluid that has leaked-off through the interface. Hubbert [36] showed that it is possible to derive Darcy's law from Navier-Stokes equation of motion of a viscous fluid.

1.5 OUTLINE OF RESEARCH

In this thesis, we study two related hydraulic fracture problems. A two-dimensional hydraulic fracture propagating in a permeable rock under the influence of a Newtonian fluid injected into the fracture under high pressure is considered. Since the fluid-rock interface is permeable, fluid leaks through it into the surrounding rock formation in the direction normal to the interface, with velocity v_n. In the first problem, an equation involving v_n is not given apriori. A relationship between the leak-off velocity $v_n(t,x)$ and fracture half-width $h(t,x)$ is assumed. In the second problem, we consider a two-dimensional hydraulic fracture problem where Darcy's empirical flow model is used to describe the fluid leak-off through the permeable fluid-rock interface. The thesis consists of eight chapters and is divided into three parts. Part I is an introduction and a background. It consists of Chapter 1 and 2. Part II is concerned with mathematical preliminaries and models. It consists of Chapter 3 and 4. Part III contains the main results and conclusions. It consists of Chapter 5 to 8.

In Chapter 2, we review and give a detailed discussion on integral equations.

In Chapter 3, numerical methods for solving Cauchy-type singular integral equations are introduced. We start by solving a simple singular integral equation analytically subject to some prescribed boundary conditions. We then solve the same singular integral equation using four different numerical techniques. The analytical solution was used to evaluate the accuracy of the numerical solutions.

In Chapter 4, the mathematical model and governing equations are derived. We begin by introducing the problem and stating the general assumptions around the problem. The primary physical mechanisms involved are outlined and, finally, we derive the similarity solutions for the hydraulic fracture problem.

In Chapter 5, we solve the problem of a fluid-driven fracture propagating in a permeable rock when the leak-off velocity, v_n, is proportional to the half-width of the fracture, h, using numerical techniques developed in Chapter 3. The numerical solutions are presented and discussed.

In Chapter 6, a related problem of a fluid-driven fracture in permeable rock where the leak-off velocity is proportional to the gradient of the fluid-rock interface is considered. Numerical solutions are also obtained and discussed.

In Chapter 7, a two-dimensional fluid-driven fracture with Darcy flow through the fluid-rock interface and into the rock formation is considered. Numerical solutions for the governing equations are investigated.

Finally, conclusions drawn from the results are given in Chapter 8.

2

INTEGRAL EQUATIONS

2.1 INTRODUCTION

In this chapter, we will derive the mathematical model for a two-dimensional fluid-driven fracture propagating in a permeable rock and the Cauchy principal value integral derived from linear elastic fracture mechanics will be used to model the elasticity of the rock. The presence of the Cauchy principal value integral in the mathematical formulation poses a challenge in solving the mathematical problem. Thus, it is appropriate to introduce integral equations. Problems having Cauchy principal value integrals have been solved using a number of methods such as linear spline method, Chebyshev method, finite difference method, Galerkin method, etc. Several books on singular integral equations have been published. Worth mentioning is the book by Mushkelishvili [58]. We will begin this chapter by reviewing integral equations, in particular, singular integral equations; and their method of solution.

2.2 BACKGROUND TO INTEGRAL EQUATIONS

Integral equations are equations in which some unknown function $\psi(x)$ to be determined appears under one or several integral signs [70, 91, 92]. The name integral equation was first coined by du Bois-Reymond in 1888. More details about the origins of integral equations can be found in [19, 34, 74]. Integral equations arise in several fields of science; for example, in elasticity, potential theory, fluid mechanics, biomechanics, approximation theory, plasticity, game theory, queuing theory, medicine, acoustics, heat and mass transfer, economics [12]. Many physical problems can be described or stated mathematically using differential equations. These differential equations can be transformed into problems of solving some approximate integral equations. Specifically, initial value problems can be converted to Volterra integral equations or vice versa. Similarly, boundary value problems can be converted to Fredholm integral equations or vice versa [12].

A general form of an integral equation in $\psi(x)$ is [70, 92]

$$\delta(x)\psi(x) = f(x) + \lambda \int_{\alpha(x)}^{\beta(x)} K(x,t)\psi(t)\mathrm{d}t, \tag{2.2.1}$$

where $\delta(x)$ and $f(x)$ are forcing functions, $\alpha(x)$ and $\beta(x)$ are the limits of integration, λ is a constant parameter (nonzero, real or complex), $K(x,t)$ is the kernel of the integral equation, and $\psi(x)$ is the unknown function to be determined. It is important to state that the forcing func-

tions $\delta(x)$ and $f(x)$ together with the kernel function $K(x,t)$ are prescribed in advance. It can be easily seen in (2.2.1) that the unknown function $\psi(x)$ appears under the integral sign.

In what follows, we will review different types of integral equations and outline their basic definitions and properties.

2.3 CLASSIFICATION OF INTEGRAL EQUATIONS

There are many types of integral equations. The classification of integral equations depends on several factors such as the limits of integration, placement of the unknown function, nature of the forcing functions, the singular behaviour of the integral equation, linearity, homogeneity, the kind of the integral, etc. Similar to ordinary and partial differential equations, integral equations can be classified as linear or nonlinear; and also homogeneous or nonhomogeneous [12, 70, 92]. A linear integral equation is one in which the unknown function $\psi(x)$ under the integral sign is raised to the power of 1, i.e., it occurs linearly. However, an integral equation is called nonlinear if the unknown function $\psi(x)$ under the integral sign is raised to a power different from 1 or it is replaced by a nonlinear function such as $\sin\psi(x)$, $\sinh\psi(x)$, $e^{\psi(x)}$. On the other hand, an integral equation is said to be homogeneous if the forcing function $f(x) \equiv 0$. Otherwise the integral equation is said to be nonhomogeneous or inhomogeneous.

Let us now consider a standard form of a linear integral equation

$$\delta(x)\psi(x) = f(x) + \lambda \int_a^{\phi(x)} K(x,t)\psi(t)\mathrm{d}t, \quad a \in \mathbb{R}. \tag{2.3.1}$$

Table 3 gives a list of conditions that can be used to classify an integral equation.

No.	Type	Condition
1	First kind	$\delta(x) = 0$
2	Second kind	$\delta(x) = 1$
3	Third kind	$\delta(x) = \varphi(x)$
4	Homogeneous	$f(x) = 0$
5	Nonhomogeneous	$f(x) \neq 0$
6	Fredholm integral equations	$\phi(x) = b,\ b \in \mathbb{R}$
7	Volterra integral equations	$\phi(x) = x$

Table 3: Conditions for classifying integral equations.

A list of the types of integral equations is given below

1. Fredholm integral equations
2. Volterra integral equations

3. Singular integral equations
4. Volterra-Fredholm integral equations

The most frequently used linear integral equations are Fredholm and Volterra integral equations. Figure 6 illustrates the tree structure of these classes of linear integral equations.

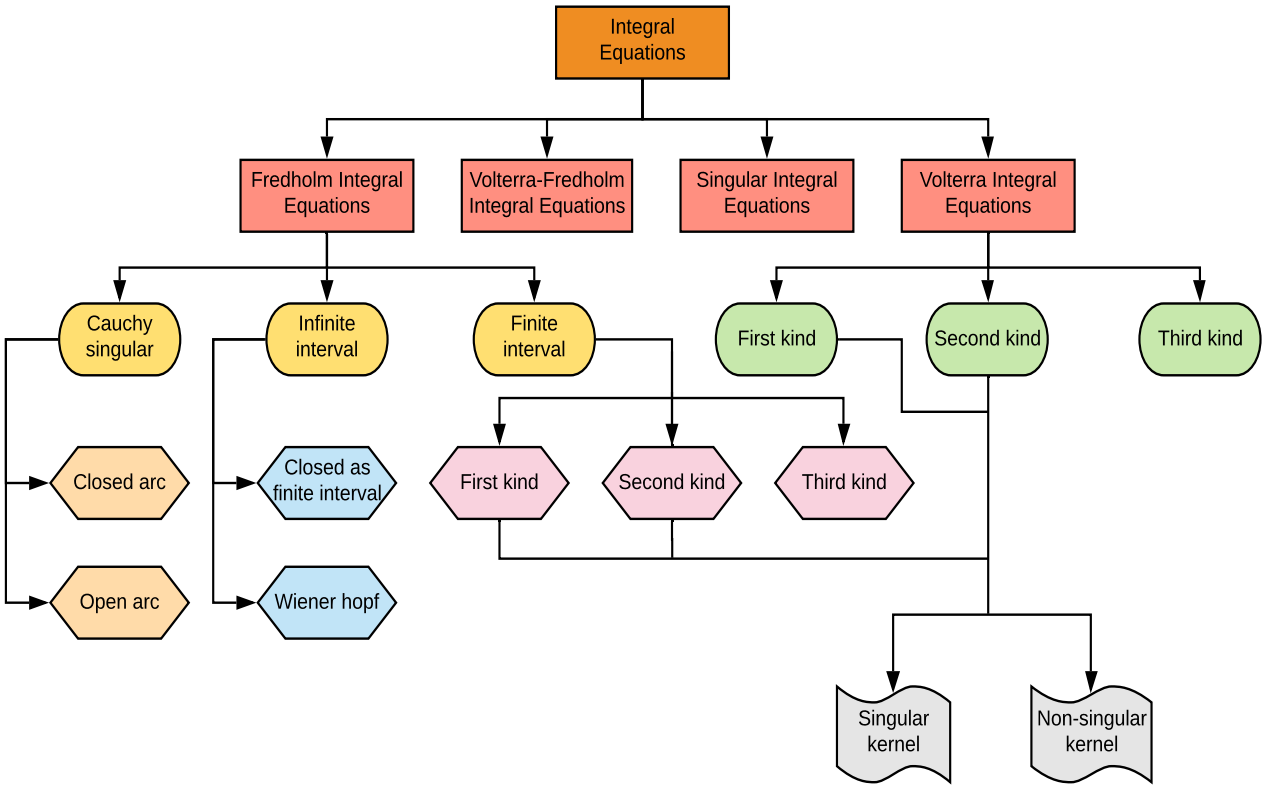

Figure 6: Structure of Fredholm and Volterra integral equations, adapted from [47].

We will outline the basic definitions and properties of each integral type.

2.3.1 *Fredholm integral equations*

The general form of a linear Fredholm integral equation is given by [70, 92]

$$\delta(x)\psi(x) = f(x) + \lambda \int_a^b K(x,t)\psi(t)\mathrm{d}t, \tag{2.3.2}$$

where the limits of integration a, b are fixed and the function $f(x)$ and the kernel $K(x,t)$ are prescribed in advance. Equation (2.3.2) is called a linear integral equation because the unknown function $\psi(x)$ appears linearly under the integral sign.

The value of the forcing function $\delta(x)$ gives the following kinds of Fredholm integral equations:

1. when $\delta(x) = 0$, equation (2.3.2) becomes

$$f(x) + \lambda \int_a^b K(x,t)\psi(t)\mathrm{d}t = 0, \tag{2.3.3}$$

and the resulting integral equation is termed Fredholm integral equation of the first kind.

2. when $\delta(x) = 1$, equation (2.3.2) becomes

$$\psi(x) = f(x) + \lambda \int_a^b K(x,t)\psi(t)\mathrm{d}t, \tag{2.3.4}$$

which is called Fredholm integral equation of the second kind.

3. when $\delta(x) = \varphi(x)$, equation (2.3.2) becomes

$$\varphi(x)\psi(x) = f(x) + \lambda \int_a^b K(x,t)\psi(t)\mathrm{d}t, \tag{2.3.5}$$

and in this case we obtain the general equation of Fredholm integral equation also called the Fredholm integral equation of the third kind. Integral equations of the second kind are the most important since the first and third kinds can often be reduced to the second kind.

Let us consider the problem of converting a boundary value problem to an equivalent Fredholm integral equation. In what follows, we give an illustrative example of converting a boundary value problems into Fredholm integral equation.

Example: consider the boundary value problem

$$y''(x) + y(x) = x,\ 0 \leqslant x \leqslant 1, \tag{2.3.6}$$

subject to boundary conditions

$$y(0) = 1,\ y(1) = 0. \tag{2.3.7}$$

We can solve equation (2.3.6) subject to (2.3.7) using standard methods to obtain

$$y(x) = x + \cos x - \cot\left(\frac{1}{2}\right)\sin x. \tag{2.3.8}$$

Now, in order to convert the differential equation (2.3.6) into Fredholm integral equation, we start by setting

$$y''(x) = \psi(x). \tag{2.3.9}$$

Integrating both sides of (2.3.9) twice from 0 to x and using the boundary condition at $x = 0$ gives

$$y(x) = 1 + xy'(0) + \int_0^x \left(\int_0^s \psi(t)\mathrm{d}t \right) \mathrm{d}s. \tag{2.3.10}$$

Integrating by parts with $u = \int_0^s \psi(t)\mathrm{d}t$ and $\mathrm{d}v = \mathrm{d}s$, we are able to reduce the multiple integrals in (2.3.10) into a single integral to get

$$y(x) = 1 + xy'(0) + x\int_0^x \psi(t)\mathrm{d}t + \int_0^x t\psi(t)\mathrm{d}t \tag{2.3.11}$$

Applying the boundary condition at $x = 1$, we obtain

$$\begin{aligned} y'(0) &= -1 - \int_0^1 (1-t)\psi(t)\mathrm{d}t \\ &= -1 - \int_0^x (1-t)\psi(t)\mathrm{d}t - \int_x^1 (1-t)\psi(t)\mathrm{d}t. \end{aligned} \tag{2.3.12}$$

Substituting (2.3.12) into (2.3.10) and expressing the multiple integrals as a single integral, we find

$$\begin{aligned} y(x) = 1 - x - \int_0^x x(1-t)\psi(t)\mathrm{d}t - \int_x^1 x(1-t)\psi(t)\mathrm{d}t \\ + \int_0^x (x-t)\psi(t)\mathrm{d}t. \end{aligned} \tag{2.3.13}$$

Using (2.3.9) and (2.3.13), (2.3.6) becomes

$$\psi(x) = x - y \tag{2.3.14}$$

$$= 2x - 1 + \int_0^x t(1-x)\psi(t)\mathrm{d}t + \int_x^1 x(1-t)\psi(t)\mathrm{d}t. \tag{2.3.15}$$

Equation (2.3.15) can be rewritten as

$$\psi(x) = 2x - 1 + \int_0^1 K(x,t)\psi(t)\mathrm{d}t, \tag{2.3.16}$$

where $f(x) = 2x - 1$ and the kernel $K(x,t)$ is given by

$$K(x,t) = \begin{cases} t(1-x), & 0 \leqslant t \leqslant x, \\ x(1-t), & x \leqslant t \leqslant 1. \end{cases} \tag{2.3.17}$$

This implies that equation (2.3.6) can be written as Fredholm integral equation.

Consider now the problem of converting Fredholm integral equation (2.3.16) to an equivalent boundary value problem. Differentiating both sides of equation (2.3.16) with respect to x and using the differentiation under the integral sign rule we find

$$\psi'(x) = 2 - \int_0^x t\psi(t)\mathrm{d}t + \int_x^1 (1-t)\psi(t)\mathrm{d}t. \tag{2.3.18}$$

We differentiate both sides of (2.3.18) again in order to remove of the integral signs. Generally, the differentiating process should be continued until a pure differential equation without the integral sign is obtained. From the second differentiation we obtain

$$\psi''(x) - \psi(x) = 0. \tag{2.3.19}$$

The related boundary conditions are obtained by substituting $x = 0$ and $x = 1$ into (2.3.15) to find that

$$\psi(0) = f(0) = -1, \ \psi(1) = f(1) = 1. \tag{2.3.20}$$

2.3.2 *Volterra integral equations*

The general form of a linear Volterra integral equation is given by [70, 92]

$$\delta(x)\psi(x) = f(x) + \lambda \int_a^x K(x,t)\psi(t)\mathrm{d}t, \tag{2.3.21}$$

where the kernel $K(x,t)$ and the function $f(x)$ are known and the unknown function $\psi(x)$ under the integral sign is linear. For Volterra equations, at least one of the limits of integration is a function of x or a variable.

Similarly, we have the following kinds of Volterra integral equations:

1. when $\delta(x) = 0$, equation (2.3.21) becomes

$$f(x) + \lambda \int_a^x K(x,t)\psi(t)\mathrm{d}t = 0, \tag{2.3.22}$$

   and the integral equation is called Volterra integral equation of the first kind.

2. when $\delta(x) = 1$, equation (2.3.21) becomes

$$\psi(x) = f(x) + \lambda \int_a^x K(x,t)\psi(t)\mathrm{d}t, \tag{2.3.23}$$

   and the integral equation is referred to as the Volterra integral equation of the second kind.

3. when $\delta(x) = \varphi(x)$, equation (2.3.21) becomes

$$\varphi(x)\psi(x) = f(x) + \lambda \int_a^x K(x,t)\psi(t)\mathrm{d}t, \tag{2.3.24}$$

   and the integral equation is called the Volterra integral equation of the third kind.

We will now give an illustrative example of how an initial value problem can be converted to a Volterra integral equation.

Example: consider the initial value problem

$$\psi'(x) = 6x\psi^2(x), \quad x \geqslant 0, \tag{2.3.25}$$

subject to the initial condition

$$\psi(0) = 1. \tag{2.3.26}$$

Solving equation (2.3.25) using the method of separation of variables subject to the initial condition, we obtain

$$\psi(x) = \frac{1}{1-3x^2}. \tag{2.3.27}$$

Now, integrating equation (2.3.25) with respect to x from 0 to x, we obtain

$$\int_0^x \psi'(t)\mathrm{d}t = \int_0^x 6t\psi^2(t)\mathrm{d}t, \tag{2.3.28}$$

and using the initial condition (2.3.26), (2.3.28) yields the following

$$\psi(x) = 1 + \int_0^x 6t\psi^2(t)\mathrm{d}t. \tag{2.3.29}$$

Equation (2.3.29) is a nonlinear Volterra integral equation of the second kind. It is nonlinear because the unknown function $\psi(t)$ under the integral sign is raised to the power of 2. In (2.3.29), we have $\delta(x) = f(x) = \lambda = 1$, $\alpha(x) = 0$, $\beta(x) = x$, and the kernel $K(x,t) = 6t$. Now, suppose we are given a Volterra integral equation as in (2.3.29) instead. In order to convert the Volterra integral equation to an equivalent ordinary differential equation, we will differentiate both sides of (2.3.29) and use the differentiation under the integral sign rule for differentiating an integral. Initial conditions can be determined by substituting $x = 0$ in the integral equation. Differentiating (2.3.29) with respect x and substituting $x = 0$ into (2.3.29) yields

$$\psi'(x) = 6x\psi^2(x), \ \psi(0) = 1. \tag{2.3.30}$$

Thus, the equivalent ordinary differential equation is the same as the one provided initially in equation (2.3.25) subject to the initial condition (2.3.26).

2.3.3 *Singular integral equations*

An integral equation may be called singular if the lower limit or the upper limit or both the limits of integration are infinite, or if the kernel function $K(x,t)$ is infinite at one or more points in the integration interval [19]. Specifically, integral equations of the first kind given by the form [70, 91, 92]

$$f(x) = \lambda \int_{\alpha(x)}^{\beta(x)} K(x,t)\psi(t)\mathrm{d}t, \tag{2.3.31}$$

or integral equations of the second kind given the form

$$\psi(x) = f(x) + \lambda \int_{\alpha(x)}^{\beta(x)} K(x,t)\psi(t)\mathrm{d}t, \tag{2.3.32}$$

are called singular if $\alpha(x)$, or $\beta(x)$, or both limits of integration are infinite. Moreover, the equation (2.3.31) or (2.3.32) is also called a singular integral equation if the kernel $K(x,t)$ contains a singularity, that is, $K(x,t) = \pm\infty$ at some points in the interval of integration. Examples of type-1 singular integral equations are

$$\psi(x) = 1 + \int_0^{\infty} K(x,t)\psi(t)\mathrm{d}t, \tag{2.3.33}$$

$$\mathcal{L}\{u(x)\} = \int_0^{\infty} e^{-\lambda x}\psi(x)\mathrm{d}x, \tag{2.3.34}$$

$$\mathcal{F}\{u(x)\} = \int_{-\infty}^{\infty} e^{-i\lambda x}\psi(x)\mathrm{d}x. \tag{2.3.35}$$

The integral equations (2.3.34) and (2.3.35) are the Laplace transform and the Fourier transform of the function $\psi(x)$ respectively. Examples of type-2 singular integral equations are

$$f(s) = \int_0^{s} \frac{1}{(s-t)^{\alpha}}\psi(t)\mathrm{d}t, \quad 0 < \alpha < 1, \tag{2.3.36}$$

$$f(s) = \int_0^{s} \frac{1}{\sqrt{s-t}}\psi(t)\mathrm{d}t, \tag{2.3.37}$$

$$\varphi(s) = 1 + \sqrt{s} - \int_0^{s} \frac{1}{\sqrt{s-t}}\varphi(t)\mathrm{d}t, \tag{2.3.38}$$

where the singular behaviour is attributed to the kernel function $K(s,t)$ becoming infinite as $t \to s$. It is important to highlight that integral equations such as (2.3.36) and (2.3.37) are called the generalized Abel's integral equations and Abel's problems respectively. Singular integral equations similar to (2.3.38) are called weakly-singular second kind Volterra integral equations.

In this thesis, we are concerned with singular integral equations where the kernel function $K(x,t)$ possess some sort of singularity at $t = x$. When a singularity of the kernel function $K(x,t)$ exists, it may be weak or strong. If the kernel function $K(x,t)$ is of the form

$$K(x,t) = \frac{F(x,t)}{|x-t|^{\alpha}}, \tag{2.3.39}$$

where the function $F(x,t)$ is bounded, and α is an arbitrary constant such that $0 < \alpha < 1$, and the kernel function is weakly singular, then the corresponding integral equation is called a weakly singular integral equation [51]. Abel's integral equation is an example of a weakly singular integral equation. However, if the kernel function $K(x,t)$ is of the form

$$K(x,t) = \frac{F(x,t)}{x-t}, \quad a < x < b, \tag{2.3.40}$$

where the function $F(x,t)$ is differentiable with $F(x,x) \neq 0$, then the kernel function $K(x,t)$ has a strong singularity at $t = x$ or equally put, it has a Cauchy type singularity at $t = x$, and the integral $\int_a^b K(x,t)\mathrm{d}t$ is taken to be a Cauchy principal value. The integral equation then is called a Cauchy type singular integral [51]. Cauchy singular integral equations are a special and important type of singular integral equations.

An example of a Cauchy singular integral kernel is

$$K(x,t) = \frac{1}{x-t}, \quad x \neq t. \tag{2.3.41}$$

If an integral equation contains additional derivatives of the unknown function $\psi(x)$ (inside or outside the integral), then the equation is called an integro-differential equation. The equation

$$\psi'(x) = f(x) + \int_a^b \frac{\psi(t)}{t-x}\mathrm{d}t, \quad a \leqslant x \leqslant b, \tag{2.3.42}$$

is an example of an integro-differential equation.

2.3.4 *Volterra-Fredholm integral equations*

In this section, we consider Volterra-Fredholm integral equations. These types of integral equations arise from parabolic boundary value problems, from the mathematical modelling of the spatio-temporal development of an epidemic, and from various physical and biological models [50, 90, 91]. The Volterra-Fredholm equations can appear in the following two forms, namely

$$\begin{aligned}\delta(x)\psi(x) = f(x) + \lambda_1 \int_0^{\gamma(x)} K_1(x,t)\psi(t)\mathrm{d}t + \\ \lambda_2 \int_a^b K_2(x,t)\psi(t)\mathrm{d}t,\end{aligned} \tag{2.3.43}$$

and the mixed form

$$\delta(x)\psi(x) = f(x) + \lambda \int_0^{\gamma(x)} \int_a^b K(s,t)\psi(t)\mathrm{d}t\mathrm{d}s, \tag{2.3.44}$$

where the functions $\delta(x)$, $\gamma(x)$ and $f(x)$ are known functions, the functions $K(x,t)$, $K_1(x,t)$ and $K_2(x,t)$ are known kernel functions, $\psi(x)$ is the unknown function and λ, λ_1 and λ_2 are constants. The integral equation (2.3.43) is considered to be a functional integral equation with proportional delay when $\gamma(x)$ is a first order polynomial. Examples of the two kinds of the Volterra-Fredholm integral equations are given by

$$\psi(x) = x^2 + 2 - \int_0^x \psi(t)\mathrm{d}t - \int_0^1 t\psi(t)\mathrm{d}t, \tag{2.3.45}$$

and

$$\psi(x) = 2x^2 + 6x + \int_0^x \int_0^1 \psi(t)\mathrm{d}t\mathrm{d}s. \tag{2.3.46}$$

2.4 STRUCTURE OF KERNEL

The nature of the kernel function plays a pivotal role when considering numerical techniques for solving an integral equation. Different types of kernel and singularities requires individual treatment. A Kernel function can take one of the following properties [81]:

1. A kernel function is considered to be symmetric or complex symmetric or Hermitian, if
   (i) $K(x,t) = K(t,x)$,
   (ii) $K(x,t) = \bar{K}(t,x)$ where $\bar{K}(t,x)$ is the complex conjugate of $K(x,t)$.

2. A kernel function is called a degenerate or seperable kernel if the kernel $K(x,t)$ can be expressed as

$$K(x,t) = \sum_{i=0}^{n} r_i(x)s_i(t). \tag{2.4.1}$$

3. A kernel function is said to be a difference kernel if $K(x,t) = K(x-t)$.

4. If the solution of the integral equation

$$\psi(x) = f(x) + \lambda \int_a^{\gamma(x)} K(x,t)\psi(t)\mathrm{d}t \tag{2.4.2}$$

   is of the form

$$\psi(x) = f(x) + \lambda \int_a^{\gamma(x)} \Gamma(x,t;\lambda)f(t)\mathrm{d}t. \tag{2.4.3}$$

   The kernel function $\Gamma(x,t;\lambda)$ is called the reciprocal or resolvent kernel.

Remarks

In summary, an integral equation is of the first kind if the unknown function $\psi(x)$ appears only under the integral sign. However, the integral equation is said to be of the second kind if the unknown function $\psi(x)$ appears inside and outside the integral sign. Lastly, the most general form of an integral equation is said to be the third kind.

The following basic characteristics are used to classify an integral:

1. Limits of integration
   - Both fixed: Fredholm equation.
   - One variable: Volterra equation.

2. Position of the unknown function $\psi(x)$
   - Inside the integral only: first kind.

- Inside and outside the integral: second kind.

3. Nature of the known function $f(x)$
   - Identically zero: Homogeneous.
   - Not identically zero: inhomogeneous.
4. Linearity
   - Linear integral equations.
   - Nonlinear integral equations.

A great deal of effort has been put into the development of numerical techniques for solving integral equations appearing in different forms. In Table 4 we present some of the frequently encountered integrals in scientific and engineering problems. Traditional methods such as the method of successive approximations and the method of successive substitutions are amongst the most commonly used methods for solving these types of integral equations. In fact, Ioakimidis [37] was first to apply the successive approximation method to the airfoil equation. Some singular integral equations, namely the Volterra type singular equations and Abel's equations, can easily be solved using the Laplace transform method. Newly developed methods, for example, the Adomian decomposition method and the modified decomposition method for solving nonlinear integral equations have attracted much attention from mathematicians and engineers, however, numerical methods still remain useful for solving highly complicated integral problems.

Name	**Form**
Fredholm integral equation - first kind	$f(x) = \lambda \int_a^b K(x,t)\psi(t)\mathrm{d}t$
Fredholm integral equation - second kind	$\psi(x) = f(x) + \lambda \int_a^b K(x,t)\psi(t)\mathrm{d}t$
Volterra integral equation - first kind	$f(x) = \lambda \int_a^x K(x,t)\psi(t)\mathrm{d}t$
Volterra integral equation - second kind	$\psi(x) = f(x) + \lambda \int_a^x K(x,t)\psi(t)\mathrm{d}t$
Abel equation	$\psi(x) = \int_a^x \frac{\psi(s)}{(x-s)^\alpha}\mathrm{d}s,\ 0 < \alpha < 1$
Cauchy-type integral equation	$\psi(x) = f(x) + \lambda \int_a^b \frac{\psi(s)}{x-s}\mathrm{d}s,$
Carleman equation	$\delta(x)\psi(x) = f(x) + \lambda \int_a^b \frac{\psi(s)}{x-s}\mathrm{d}s$
Integral equation of logarithmic kernel	$\int_a^b \ln\lvert x-t\rvert\, \psi(t)\mathrm{d}t = f(x)$
Wiener-Hopf integral equation	$\psi(x) = f(x) + \lambda \int_0^\infty K(x-t)\psi(t)\mathrm{d}t$

Table 4: Frequently encountered integral equations, λ is a parameter

2.5 CONCLUSION

In this chapter, we introduced integral equations, and a detailed review and discussion of singular integral equations was given.

In the next chapter, we outline numerical methods for solving singular integral equations. We consider a simple Cauchy integral equation that can be solved analytically to obtain a closed-form solution. We will then compare the numerical results to the analytical solution to evaluate the accuracy of the numerical methods. Matlab and Mathematica environment will be used to perform the numerical computations.

Part II

MATHEMATICAL PRELIMINARIES AND MODELS

3

SOME NUMERICAL TECHNIQUES AND SOLUTIONS FOR CAUCHY-TYPE SINGULAR INTEGRAL EQUATIONS OF THE FIRST KIND

3.1 INTRODUCTION

In this chapter, we introduce a number of numerical techniques that can be used to solve integro-differential equations. A simple and less complicated singular integral equation of the first kind with a Cauchy-type singular kernel for which an analytical solution exists will be presented. In addition, we will also compute numerical solutions for the simple singular integral equation using four different numerical methods and compare with the analytical solution to evaluate the accuracy of the numerical methods.

3.2 CAUCHY PRINCIPAL VALUE INTEGRALS

Let us first study singular integral equations containing Cauchy-type kernels before we introduce the simple singular integral equation that will be solved.

Suppose that $f(x)$ is unbounded in the neighbourhood of $x = c$ with $a < c < b$. The Cauchy principal value of the integral denoted

$$\fint_a^b f(x)\mathrm{d}x, \quad x \in \mathbb{R}$$

is defined by the limit

$$\fint_a^b f(x)\mathrm{d}x = \lim_{\alpha\to 0^+}\left[\int_a^{c-\alpha} f(x)\mathrm{d}x + \int_{c+\alpha}^b f(x)\mathrm{d}x\right]. \tag{3.2.1}$$

The Hilbert transform

$$\fint_a^b \frac{f(x)}{x-s}\mathrm{d}x = g(s), \quad -\infty \leqslant a < b \leqslant \infty, \quad a < s < b, \tag{3.2.2}$$

is an example of a principal value integral. A sufficient condition for the existence of this Cauchy principal value integral (3.2.2) is that $f(x)$ satisfy a Hölder condition in $[a,b]$. This means that there are constants $d > 0$ and $0 \leqslant \beta \leqslant 1$ such that for any two points x_1 and x_2 in $[a,b]$ we have

$$|f(x_1) - f(x_2)| \leqslant d\,|x_1 - x_2|^{\beta}. \tag{3.2.3}$$

The Hilbert transform (3.2.2) has a Cauchy singularity at $s = x$. Sometimes a singularity can be eliminated or avoided by a change of variable or a suitable transformation in the complex plane. Longman [48]

presented a simple method of evaluating Cauchy-type integrals by decomposing the integrand into its odd and even components and by noting that the integral of the former vanishes. He showed that the remaining integral can be approximated using any standard method for numerical integration since it does not contain a singularity. Monacella [55] proposed an alternative method whereby Cauchy principal value integrals can be approximated by simply ignoring the singularity. He showed that by ignoring the singularity, the problem of numerically approximating integrals of the form

$$\fint_a^b \frac{f(x)}{x-\xi}\mathrm{d}x, \quad a<\xi<b, \tag{3.2.4}$$

where $f(x)$ and its derivatives are continuous throughout interval of integration can be reduced to the numerical evaluation of the integral

$$I=\fint_{-a}^{a} \frac{f(x)}{x}\mathrm{d}x. \tag{3.2.5}$$

The integral in (3.2.5) can be rewritten as a

$$I=\int_{-a}^{a} \frac{f(x)-f(0)}{x}\mathrm{d}x+\fint_{-a}^{a} \frac{f(0)}{x}\mathrm{d}x. \tag{3.2.6}$$

The first integral in (3.2.6) is a proper integral and the second integral is singular and identically zero. Another method that can be used to numerically evaluate Cauchy principal values is the method of *subtracting out the singularity*. This method has been used widely [32]. With this method, we subtract the singularity so that we are left with some integral that can be integrated numerically using a Gaussian quadrature. The best-known example of this method is as follows. Assume $f(x)$ to be continuous at ξ. That is,

$$\begin{aligned} I=\fint_a^b \frac{f(x)}{x-\xi}\mathrm{d}x &= \int_a^b \frac{f(x)-f(\xi)}{x-\xi}\mathrm{d}x+f(\xi)\fint_a^b \frac{1}{x-\xi}\mathrm{d}x \\ &= \int_a^b \frac{f(x)-f(\xi)}{x-\xi}\mathrm{d}x+f(\xi)\log\frac{b-\xi}{\xi-a}. \end{aligned} \tag{3.2.7}$$

Note that for $a=-b$,

$$\lim_{b\to\infty}\log\frac{b-\xi}{\xi-a}=0. \tag{3.2.8}$$

If the derivative of $f(x)$ is also continuous at ξ, then the function

$$\phi(x)=\frac{f(x)-f(\xi)}{x-\xi}, \tag{3.2.9}$$

is defined at $x=\xi$ by

$$\phi(\xi)=\left.\frac{\mathrm{d}f}{\mathrm{d}x}\right|_{x=\xi}\equiv f'(\xi) \tag{3.2.10}$$

and is regular in the vicinity of ξ. Hence,

$$\int_a^b \phi(x)\mathrm{d}x \tag{3.2.11}$$

can be evaluated by any standard integration formula.

3.3 AN INVERSION TECHNIQUE USING PROPERTIES OF ABEL'S EQUATION

For the purpose of the study, we will consider one of the most basic Cauchy-type singular integral equations over a finite interval. Moreover, we restrict our discussion to Cauchy-type equations of the first kind on the real line.

Consider the singular integral equation

$$\int_a^b \frac{\Phi(t)\mathrm{d}t}{t-\sigma} = F(\sigma), \qquad a < \sigma < b, \tag{3.3.1}$$

where $F(\sigma)$ is a known function and the integral is understood in the principal value sense. As mentioned in Chapter 2, a kernel function of the form

$$K(t-\sigma) = \frac{1}{t-\sigma}, \tag{3.3.2}$$

is called a Cauchy kernel. Integral equations that contain this type of kernel are called Cauchy-type singular integral equations. It should be noted that the limits of integration a and b can be any real number. Moreover, it can easily be shown using the translations $t = a + (b-a)\xi$ and $\sigma = a + (b-a)x$ that equation (3.3.1) can be reduced to the case where $a = 0$ and $b = 1$ (see Appendix A for details). That is, equation (3.3.1) can be replaced by

$$\int_0^1 \frac{\psi(\xi)\mathrm{d}\xi}{\xi - x} = f(x), \qquad 0 < x < 1, \tag{3.3.3}$$

without loss of generality. To derive the solution for (3.3.3) we use a method due to Peters [68]. The left hand side of (3.3.3) can be written in the form

$$\begin{aligned}
\int_0^1 \frac{\psi(\xi)\mathrm{d}\xi}{\xi - x} &= \int_0^1 \left(\frac{1-\xi+x+\xi-x}{\xi-x}\right)\psi(\xi)\mathrm{d}\xi, \\
&= \int_0^1 \frac{\psi(\xi)\mathrm{d}\xi}{\xi-x} - \int_0^1 \frac{\xi\psi(\xi)\mathrm{d}\xi}{\xi-x} + x\int_0^1 \frac{\psi(\xi)\mathrm{d}\xi}{\xi-x} + \int_0^1 \psi(\xi)\mathrm{d}\xi, \\
&= f(x) - \int_0^1 \frac{\xi\psi(\xi)\mathrm{d}\xi}{\xi-x} + xf(x) + \int_0^1 \psi(\xi)\mathrm{d}\xi,
\end{aligned} \tag{3.3.4}$$

wherein (3.3.3) has been utilized. From (3.3.3) and (3.3.4), we obtain

$$\int_0^1 \frac{\xi\psi(\xi)\mathrm{d}\xi}{\xi - x} = xf(x) + c, \tag{3.3.5}$$

where

$$c = \int_0^1 \psi(\xi)\mathrm{d}\xi. \tag{3.3.6}$$

Multiplying both sides of equation (3.3.5) by $1/\sqrt{x}$ and integrating with respect to x gives

$$-\int_0^1 \ln\left|\frac{\sqrt{\xi}-\sqrt{x}}{\sqrt{\xi}+\sqrt{x}}\right| \sqrt{\xi}\psi(\xi)\mathrm{d}\xi = \int_0^x \sqrt{\theta} f(\theta)\mathrm{d}\theta + 2c\sqrt{x}. \quad (3.3.7)$$

The kernel function can be expressed as

$$-\ln\left|\frac{\sqrt{\xi}-\sqrt{x}}{\sqrt{\xi}+\sqrt{x}}\right| = \begin{cases} \int_0^\xi \frac{\mathrm{d}s}{\sqrt{\xi-s}\sqrt{x-s}}, & \xi < x, \\ \int_0^x \frac{\mathrm{d}s}{\sqrt{\xi-s}\sqrt{x-s}}, & \xi > x. \end{cases} \quad (3.3.8)$$

Therefore,

$$-\sqrt{\xi}\psi(\xi)\ln\left|\frac{\sqrt{\xi}-\sqrt{x}}{\sqrt{\xi}+\sqrt{x}}\right| = \begin{cases} \sqrt{\xi}\psi(\xi)\int_0^\xi \frac{\mathrm{d}s}{\sqrt{\xi-s}\sqrt{x-s}}, & \xi < x, \\ \sqrt{\xi}\psi(\xi)\int_0^x \frac{\mathrm{d}s}{\sqrt{\xi-s}\sqrt{x-s}}, & \xi > x. \end{cases} \quad (3.3.9)$$

If we substitute this representation into (3.3.7), we find

$$\int_0^x \sqrt{\xi}\psi(\xi)\int_0^\xi \frac{\mathrm{d}s}{\sqrt{\xi-s}\sqrt{x-s}}\mathrm{d}\xi + \int_x^1 \sqrt{\xi}\psi(\xi)\int_0^x \frac{\mathrm{d}s}{\sqrt{\xi-s}\sqrt{x-s}}\mathrm{d}\xi = \int_0^x \sqrt{\theta} f(\theta)\mathrm{d}\theta + 2c\sqrt{x}. \quad (3.3.10)$$

Next, we change the order of integration for each of the integrals on the left hand side of (3.3.10) to obtain

$$\int_0^x \frac{1}{\sqrt{x-s}}\int_s^x \frac{\sqrt{\xi}\psi(\xi)\mathrm{d}\xi}{\sqrt{\xi-s}}\mathrm{d}s + \int_0^x \frac{1}{\sqrt{x-s}}\int_x^1 \frac{\sqrt{\xi}\psi(\xi)\mathrm{d}\xi}{\sqrt{\xi-s}}\mathrm{d}s = \int_0^x \sqrt{\theta} f(\theta)\mathrm{d}\theta + 2c\sqrt{x}, \quad (3.3.11)$$

which is equivalent to

$$\int_0^x \frac{1}{\sqrt{x-s}}\int_s^1 \frac{\sqrt{\xi}\psi(\xi)\mathrm{d}\xi}{\sqrt{\xi-s}}\mathrm{d}s = \int_0^x \sqrt{\theta} f(\theta)\mathrm{d}\theta + 2c\sqrt{x}. \quad (3.3.12)$$

Equation (3.3.12) can be transformed into Abel's integral equation

$$\int_0^x \frac{\phi(s)}{\sqrt{x-s}}\mathrm{d}s = \omega(x), \quad (3.3.13)$$

where

$$\phi(s) = \int_s^1 \frac{\sqrt{\xi}\psi(\xi)\mathrm{d}\xi}{\sqrt{\xi-s}}\mathrm{d}s. \quad (3.3.14)$$

Equation (3.3.13) has the solution

$$\phi(x) = \frac{1}{\pi}\frac{\mathrm{d}}{\mathrm{d}x}\int_0^s \frac{\omega(s)\mathrm{d}s}{\sqrt{x-s}}, \tag{3.3.15}$$

and if $\omega(s)$ is differentiable, then

$$\phi(x) = \frac{1}{\pi}\left[\frac{\omega(0)}{\sqrt{x}} + \int_0^x \frac{\omega_s(s)\mathrm{d}s}{\sqrt{x-s}}\right]. \tag{3.3.16}$$

Applying this result in (3.3.12) leads to

$$\int_s^1 \frac{\sqrt{\xi}\psi(\xi)\mathrm{d}\xi}{\sqrt{\xi-s}} = \frac{1}{\pi}\int_0^s \frac{\sqrt{x}f(x)}{\sqrt{s-x}}\mathrm{d}x + c. \tag{3.3.17}$$

Similarly, the solution of the integral equation

$$\int_s^1 \frac{\varphi(\xi)\mathrm{d}\xi}{\sqrt{\xi-s}} = g(s) \tag{3.3.18}$$

can be derived from Abel's equation (3.3.13) as

$$\varphi(\xi) = -\frac{1}{\pi}\frac{\mathrm{d}}{\mathrm{d}\xi}\int_\xi^1 \frac{g(s)\mathrm{d}s}{\sqrt{s-\xi}}. \tag{3.3.19}$$

Therefore, (3.3.17) leads to

$$\sqrt{\xi}\psi(\xi) = \frac{c}{\pi\sqrt{1-\xi}} - \frac{1}{\pi^2}\frac{\mathrm{d}}{\mathrm{d}\xi}\int_\xi^1 \frac{1}{\sqrt{s-\xi}}\int_0^\sigma \frac{\sqrt{x}f(x)\mathrm{d}x}{\sqrt{x-s}}\mathrm{d}s. \tag{3.3.20}$$

Equation (3.3.20) is the formula for the solution of (3.3.3) but it is not the standard one. To obtain the standard formula, we change the order of integration in the second term on the right hand side of equation (3.3.20) and perform further manipulation (see Appendix A) to get

$$\psi(\xi) = \frac{c}{\pi\sqrt{\xi(1-\xi)}} - \frac{1}{\pi^2\sqrt{\xi(1-\xi)}}\int_0^1 \frac{\sqrt{x(1-x)}f(x)\mathrm{d}x}{x-\xi}, \tag{3.3.21}$$

where c is an arbitrary constant arising from inversion of the singular integral. This is the standard formula.

Let us consider a very special case of (3.3.3) where the forcing function $f(x)$ is set equal to 1, i.e.,

$$\int_0^1 \frac{\psi(\xi)\mathrm{d}\xi}{\xi-x} = 1. \tag{3.3.22}$$

Using the standard formula (3.3.21), the solution for (3.3.22) is given by

$$\psi(\xi) = \frac{c}{\pi\sqrt{\xi(1-\xi)}} - \frac{1}{\pi^2\sqrt{\xi(1-\xi)}}\int_0^1 \frac{\sqrt{x(1-x)}\mathrm{d}x}{x-\xi}. \tag{3.3.23}$$

Solving the integral term on the right hand side of (3.3.23), we obtain

$$⨍_0^1 \frac{\sqrt{x(1-x)}\mathrm{d}x}{x-\xi} = \frac{\pi}{2}(1-2\xi). \tag{3.3.24}$$

The integration was done with the help of a built–in integration function within Mathematica. We specified within the integration function that the supplied definite integral must be taken to be a Cauchy principal value integral. Now, using this result, equation (3.3.23) becomes

$$\psi(\xi) = \frac{c-\frac{1}{2}+\xi}{\pi\sqrt{\xi(1-\xi)}}. \tag{3.3.25}$$

3.4 A SURVEY OF SOME NUMERICAL METHODS FOR SINGULAR INTEGRAL EQUATIONS

Our aim in this section is to derive and study solutions of a simple integral differential equation.

Consider the problem of solving the singular integral equation given by

$$\frac{1}{\pi}\frac{\mathrm{d}}{\mathrm{d}x}\left(⨍_0^1 \frac{h_{\tilde{\xi}}(\xi)\mathrm{d}\xi}{\xi-x}\right) = 1, \qquad 0 \leqslant x \leqslant 1, \tag{3.4.1}$$

subject to the boundary conditions

$$h_x(0) = 0, \quad h(1) = 0. \tag{3.4.2a-b}$$

This problem was considered in [57]. In the sequel, we will solve (3.4.1) subject to (3.4.2a-b) both analytically and numerically. The analytical solution will be used to check the accuracies of numerical methods.

3.4.1 *Analytical solution*

We begin by integrating (3.4.1) with respect to x to obtain the characteristic singular integral equation

$$\int_0^1 \frac{h_{\tilde{\xi}}(\xi)\mathrm{d}\xi}{\xi-x} = \pi x + A, \tag{3.4.3}$$

where A is an arbitrary constant. We will utilize the standard inversion formula we derived in the previous section. In relation to the current problem, the unknown function $\psi(x)$ and forcing function $f(x)$ are given by $\psi(x) = h_x(x)$ and $f(x) = \pi x + A$ respectively. Thus, the inverse of (3.4.3) is given by

$$h_x(x) = \frac{c}{\sqrt{x(1-x)}} - \frac{1}{\pi^2\sqrt{x(1-x)}}⨍_0^1 \frac{\sqrt{\xi(1-\xi)}}{\xi-x}(\pi\xi + A)\mathrm{d}\xi.$$

(3.4.4)

We will proceed by solving the integral equation in (3.4.4) with the use of a built–in integration function within Mathematica. We obtained the following results

$$\int_0^1 \frac{\sqrt{\xi(1-\xi)}}{\xi - x} d\xi = \frac{\pi}{2}(1-2x), \tag{3.4.5}$$

$$\int_0^1 \frac{\xi\sqrt{\xi(1-\xi)}}{\xi - x} d\xi = \frac{\pi}{8}(1+4x-8x^2). \tag{3.4.6}$$

Using (3.4.5) and (3.4.6), (3.4.4) becomes

$$h_x(x) = \frac{c}{\sqrt{x(1-x)}} - \frac{1+4x-8x^2}{8\sqrt{x(1-x)}} - \frac{A(1-2x)}{2\pi\sqrt{x(1-x)}}. \tag{3.4.7}$$

Integration of (3.4.7) yields

$$h(x) = 2c\sin^{-1}(\sqrt{x}) - \left(\frac{x}{2} + \frac{1}{4} + \frac{A}{\pi}\right)\sqrt{x(1-x)} + B, \tag{3.4.8}$$

where A, B and c are unknown constants. The solution in (3.4.8) contains three unknown constants. We will therefore need three conditions to solve for the three unknowns. We will now assume

$$h(0) = \frac{3\pi}{8}. \tag{3.4.9}$$

Using the boundary conditions (3.4.2b) and (3.4.9), we find

$$h(1) = \pi c + B = 0, \quad \text{and} \quad h(0) = B = \frac{3\pi}{8}, \tag{3.4.10}$$

which gives $B = 3\pi/8$ and $c = -3/8$. Equation (3.4.8) becomes

$$h(x) = -\frac{3}{4}\sin^{-1}(\sqrt{x}) - \left(\frac{x}{2} + \frac{1}{4} + \frac{A}{\pi}\right)\sqrt{x(1-x)} + \frac{3\pi}{8}. \tag{3.4.11}$$

Consider now equation (3.4.7) in the following rearranged form

$$h_x(x) = \frac{1}{\sqrt{x(1-x)}}\left(c - \frac{1}{8} - \frac{A}{2\pi}\right) + \frac{1}{\sqrt{x(1-x)}}\left(\frac{Ax}{\pi} - 4x + 8x^2\right). \tag{3.4.12}$$

From the slope condition (3.4.2a), as $x \to 0$ we have $h_x(x) \to 0$. The slope condition is satisfied only if

$$c - \frac{1}{8} - \frac{A}{2\pi} = 0, \tag{3.4.13}$$

which, after solving, gives $A = -\pi$. Hence, the analytical solution for (3.4.1) is

$$h(x) = -\frac{3}{4}\sin^{-1}(\sqrt{x}) + \left(\frac{3}{4} - \frac{x}{2}\right)\sqrt{x(1-x)} + \frac{3\pi}{8}. \tag{3.4.14}$$

Equation (3.4.14) corresponds to the solution stated in [57]. Alternatively from (3.4.7), we rewrite

$$\int \frac{1}{\sqrt{-x^2+x}}\mathrm{d}x = \int \frac{1}{\sqrt{-\left(x-\frac{1}{2}\right)^2+\frac{1}{4}}}\mathrm{d}x. \tag{3.4.15}$$

Integrating the right side of (3.4.15) yields

$$\int \frac{1}{\sqrt{-\left(x-\frac{1}{2}\right)^2+\frac{1}{4}}}\mathrm{d}x = \sin^{-1}(2x-1)+c_2, \tag{3.4.16}$$

where c_2 is the constant of integration. The solution is then given by

$$h_2(x) = c\sin^{-1}(2x-1) - \left(\frac{x}{2}+\frac{1}{4}+\frac{A}{\pi}\right)\sqrt{x(1-x)}+B. \tag{3.4.17}$$

where A, B, and c are constants. In this case, applying the boundary conditions (3.4.2a-b) yields $A=-\pi$, $B=3\pi/16$ and $c=-3/8$, and the analytical solution is given by

$$h(x) = -\frac{3}{8}\sin^{-1}(2x-1) + \left(\frac{3}{4}-\frac{x}{2}\right)\sqrt{x(1-x)}+\frac{3\pi}{16}. \tag{3.4.18}$$

3.4.2 *Approximate analytical solution*

According to Chakrabarti and Berge [10], the approximation method for solving Cauchy-type singular integral equations of the first kind using polynomial approximation of degree n gives an exact solution when the force function is linear. In this section, we derive the approximate solution for the Cauchy integral equation given by (3.4.1). As an initial step, we introduce the following variables

$$h(x) = H(y), \qquad \text{where} \qquad y = 2x-1, \tag{3.4.19}$$

to transform the Cauchy integral equation into some form that will allow us to use some properties of Chebyshev polynomials. Substituting (3.4.19) into (3.4.1), we find

$$\frac{\mathrm{d}}{\mathrm{d}y}\left(\int_{-1}^{1}\frac{H_s(s)\mathrm{d}s}{s-y}\right) = \frac{\pi}{4}, \tag{3.4.20}$$

and the corresponding boundary conditions are given by

$$H(-1) = \frac{3\pi}{8},\ H(1)=0,\ \text{and}\ H_y(-1)=0. \tag{3.4.21}$$

For mathematical convenience, we set $\varphi(s)=H_s(s)$ and as a result

$$\frac{\mathrm{d}}{\mathrm{d}y}\left(\int_{-1}^{1}\frac{\varphi(s)\mathrm{d}s}{s-y}\right) = \frac{\pi}{4}. \tag{3.4.22}$$

Let the unknown function φ in (3.4.22) be approximated by the polynomial function φ_n

$$\varphi_n(y) = w(y)\sum_{i=0}^{n}\beta_i T_i(y), \tag{3.4.23}$$

where β_i, $i = 0,1,2,\ldots,n$, are unknown coefficients, $w(y)$ is the weight function given by

$$w(y) = \frac{1}{\sqrt{1-y^2}}, \tag{3.4.24}$$

and $T_i(y)$ is the Chebyshev polynomials of the first kind defined by

$$T_i(y) = \cos\left[i\cos^{-1}(y)\right], \quad i = 0,1,2,\ldots,n. \tag{3.4.25}$$

Substituting the approximate solution (3.4.23) into (3.4.22) yields

$$\frac{\mathrm{d}}{\mathrm{d}y}\left(\sum_{i=0}^{n}\beta_i\int_{-1}^{1}\frac{w(s)T_i(s)}{s-y}\mathrm{d}s\right) = \frac{\pi}{4}. \tag{3.4.26}$$

Rewrite equation (3.4.26) as

$$\frac{\mathrm{d}}{\mathrm{d}y}\left(\sum_{i=0}^{n}\beta_i r_i(y)\right) = \frac{\pi}{4}, \tag{3.4.27}$$

where

$$r_i(y) = \int_{-1}^{1}\frac{w(s)T_i(s)}{s-y}\mathrm{d}y = \int_{-1}^{1}\frac{T_i(s)}{\sqrt{1-s^2}(s-y)}\mathrm{d}y. \tag{3.4.28}$$

Let x_k be a zero of the Chebyshev polynomials of the second kind

$$U_{i-1}(x) = \frac{\sin\left[i\cos^{-1}(x)\right]}{\sin\left[\cos^{-1}(x)\right]}, \quad i = 0,1,2,\ldots,n. \tag{3.4.29}$$

Then,

$$x_k = \cos\left(\frac{k\pi}{i+1}\right), \quad k = 1,2,\ldots,n. \tag{3.4.30}$$

It is well known (see [52]) that

$$\int_{-1}^{1}\frac{T_i(s)}{\sqrt{1-s^2}(s-y)}\mathrm{d}y = \pi U_{i-1}(y), \tag{3.4.31}$$

where $U_i(y)$ is Chebyshev polynomial of the second kind. Equation (3.4.27) becomes, after using (3.4.31),

$$\frac{\mathrm{d}}{\mathrm{d}y}\left(\sum_{i=0}^{n}\beta_i U_{i-1}(y)\right) = \frac{1}{4}. \tag{3.4.32}$$

	i=0	i=1	i=2	i=3	i=4	i=5
$U_{i-1}(x)$	0	1	$2x$	$4x^2-1$	$8x^3-4x$	$16x^4-12x^2+1$

Table 5: Chebyshev polynomials of the Second kind ($n=5$).

We set $n=5$ so that we can solve the problem by hand calculations. Table 5 shows the first few Chebyshev polynomials of the second kind. Using the first five Chebyshev polynomials, equation (3.4.32) becomes

$$\frac{\mathrm{d}}{\mathrm{d}y}\left[\beta_1+2\beta_2 y+\beta_3(4y^2-1)+\beta_4(8y^3-4y)+\beta_5(16y^4-12y^2+1)\right]=\frac{1}{4}. \tag{3.4.33}$$

Taking the derivative with respect to y gives

$$2\beta_2+\beta_5\left(64y^3-24y\right)+\beta_4\left(24y^2-4\right)+8\beta_3 y=\frac{1}{4}. \tag{3.4.34}$$

We seek to determine the coefficients β_i, $i=0,1,2,\ldots,5$. Equating the coefficients of various powers of y from both sides of (3.4.34), we find $\beta_2=1/8, \beta_3=\beta_4=\beta_5=0$. The unknown function can now be expressed as

$$\varphi_5(y)=\frac{1}{\sqrt{1-y^2}}\left[\beta_0+\beta_1 y+\frac{1}{8}(2y^2-1)\right]. \tag{3.4.35}$$

This implies

$$H_y(y)=\frac{1}{\sqrt{1-y^2}}\left[\beta_0+\beta_1 y+\frac{1}{8}(2y^2-1)\right]. \tag{3.4.36}$$

Integrating (3.4.36) gives

$$H(y)=\beta_0\sin^{-1}(y)-\sqrt{1-y^2}\left(\frac{y}{8}+\beta_1\right)+c_3. \tag{3.4.37}$$

Next, using the boundary conditions, we obtain

$$H(-1)=-\frac{\pi}{2}\beta_0+c_3=\frac{3\pi}{8}, \tag{3.4.38}$$

$$H(1)=\frac{\pi}{2}\beta_0+c_3=0. \tag{3.4.39}$$

Solving for β_0 and c_3 we get $\beta_0=-3/8$ and $c_3=3\pi/16$. Hence, (3.4.37) becomes

$$H(y)=-\frac{3}{8}\sin^{-1}(y)-\sqrt{1-y^2}\left(\frac{y}{8}+\beta_1\right)+\frac{3\pi}{16}. \tag{3.4.40}$$

It is now left to determine the value of β_1. Equation (3.4.36) shows that as $y\to-1$,

$$H_y(y)\sim\frac{1}{\sqrt{1-y^2}}\left[\beta_0-\beta_1+\frac{1}{8}\right]=0, \tag{3.4.41}$$

which implies that $\beta_1 = -\frac{1}{4}$. Then,

$$H(y) = -\frac{3}{8}\sin^{-1}(y) - \sqrt{1-y^2}\left(\frac{y}{8} - \frac{1}{4}\right) + \frac{3\pi}{16}. \tag{3.4.42}$$

Reverting back to $h(x)$, we get

$$h(x) = -\frac{3}{8}\sin^{-1}(2x-1) + \left(\frac{3}{4} - \frac{x}{2}\right)\sqrt{x(1-x)} + \frac{3\pi}{16}. \tag{3.4.43}$$

Equation (3.4.43) is identical to equation (3.4.18) which is the analytical solution. For any choice of $n \geqslant 3$, $\beta_2 = 1/8$ and $\beta_i = 0$ for $i = 3, \ldots, n$.

3.4.3 *Finite difference method*

In this section, we will use finite difference approaches to solve the simple Cauchy integral equation. Finite difference approaches are generally employed to find solutions to differential equations by using approximate spatial and temporal derivatives that are based on discrete values at spatial grid points and discrete time levels [41]. It is important to note that the values of the grid spacing Δx and time step Δt affects the accuracy and behaviour of the solution, i.e., small values of Δx and Δt leads to small error values. Before we start using the finite difference approach, let us first derive the finite difference scheme that is appropriate for solving singular integral equations such as (3.4.1). We will use forward and backward Taylor series expansion to derive the finite difference approximations of the derivatives.

3.4.3.1 *Central difference at midpoints*

Taylor series expansion of a real function around a point $x_j = j\Delta$ for a uniform grid, as shown in Figure 7, is

$$f_{j+k} = f_j + \sum_{m=1}^{\infty} \frac{(k\Delta)^m}{m!} f_j^{(m)}, \tag{3.4.44}$$

where $k = \pm 1/2, \pm 3/2, \ldots, (2n-1)/2$ and $n \in \mathbb{Z}^+$. Equation (3.4.44) will be used to derive the numerical approximations for the derivatives.

The Taylor series expansion when $k = \pm 1/2$ is

$$f_{j+\frac{1}{2}} = f_j + \frac{1}{2}\Delta f_j' + \frac{1}{8}\Delta^2 f_j'' + \frac{1}{48}\Delta^3 f_j''' + \frac{1}{384}\Delta^4 f_j^{(4)} + \ldots \tag{3.4.45}$$

$$f_{j-\frac{1}{2}} = f_j - \frac{1}{2}\Delta f_j' + \frac{1}{8}\Delta^2 f_j'' - \frac{1}{48}\Delta^3 f_j''' + \frac{1}{384}\Delta^4 f_j^{(4)} - \ldots \tag{3.4.46}$$

Taking the difference between (3.4.45) and (3.4.46) yields

$$f_{j+\frac{1}{2}} - f_{j-\frac{1}{2}} = \Delta f_j' + \frac{1}{24}\Delta^3 f_j''' + \mathcal{O}(\Delta^5). \tag{3.4.47}$$

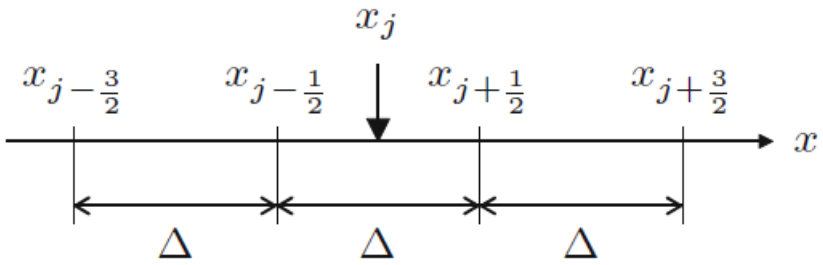

Figure 7: Central difference at midpoints on uniform grid [41].

However, if we take the sum of the two Taylor series, we find

$$f_{j+\frac{1}{2}} + f_{j-\frac{1}{2}} = 2f_j + \frac{1}{4}\Delta^2 f_j'' + \mathcal{O}(\Delta^4). \tag{3.4.48}$$

From (3.4.47) and (3.4.48), we obtain the finite difference formula for f_j and f_j' as

$$f_j = \frac{f_{j+\frac{1}{2}} + f_{j-\frac{1}{2}}}{2} - \frac{1}{8}\Delta^2 f_j'' + \mathcal{O}(\Delta^4), \tag{3.4.49}$$

$$f_j' = \frac{f_{j+\frac{1}{2}} - f_{j-\frac{1}{2}}}{\Delta} - \frac{1}{24}\Delta^2 f_j''' + \mathcal{O}(\Delta^4). \tag{3.4.50}$$

To derive the second-derivative approximation, we widen the stencil to include two additional points of $j \pm 3/2$ (see Figure 7). Expanding the Taylor series for $k = \pm 3/2$ we obtain

$$f_{j+\frac{3}{2}} = f_j + \frac{3}{2}\Delta f_j' + \frac{9}{8}\Delta^2 f_j'' + \frac{9}{16}\Delta^3 f_j''' + \frac{27}{128}\Delta^4 f_j^{(4)} + \dots \tag{3.4.51}$$

$$f_{j-\frac{3}{2}} = f_j - \frac{3}{2}\Delta f_j' + \frac{9}{8}\Delta^2 f_j'' - \frac{9}{16}\Delta^3 f_j''' + \frac{27}{128}\Delta^4 f_j^{(4)} - \dots \tag{3.4.52}$$

Taking the sum of the two Taylor series yields

$$f_{j+\frac{3}{2}} + f_{j-\frac{3}{2}} = 2f_j + \frac{9}{4}\Delta^2 f_j'' + \frac{27}{64}\Delta^4 f_j^{(4)} + \mathcal{O}(\Delta^6). \tag{3.4.53}$$

Using the finite difference approximation for f_j, the finite difference formula for f_j'' is given by

$$f_j'' = \frac{f_{j-\frac{3}{2}} - f_{j+\frac{1}{2}} - f_{j-\frac{1}{2}} + f_{j+\frac{3}{2}}}{2\Delta^2} - \frac{27}{128}\Delta^2 f^{(4)} + \mathcal{O}(\Delta^4). \tag{3.4.54}$$

3.4.3.2 *A conventional finite difference approach*

In this section, we are interested in solving equation (3.4.1) subject to the boundary conditions (3.4.2) using the finite difference method. The

first step is to partition the interval of integration $[0,1]$ into n equally spaced sub-intervals $[\xi_j, \xi_{j+1}]$ of length $h = 1/n$ where $0 \leqslant j \leqslant n-1$.

Let $P(x)$ be defined as

$$P = \fint_0^1 \frac{h_\xi(\xi)\mathrm{d}\xi}{\xi - x}, \tag{3.4.55}$$

then (3.4.1) becomes

$$\frac{\mathrm{d}P}{\mathrm{d}x} = \pi. \tag{3.4.56}$$

We will use finite differences to approximate $\mathrm{d}P/\mathrm{d}x$ and evaluate P at mid-grid points where it can be evaluated (see for example Smith, 1994) [78]. Using the central finite difference approximations, equation (3.4.1) becomes

$$\frac{P_{i+\frac{1}{2}} - P_{i-\frac{1}{2}}}{\xi_{i+\frac{1}{2}} - \xi_{i-\frac{1}{2}}} = \pi, \quad 1 \leqslant i \leqslant n-1, \tag{3.4.57}$$

where $P_{i\pm\frac{1}{2}}$ and $\xi_{i\pm\frac{1}{2}}$ are respectively given by

$$P_{i\pm\frac{1}{2}} = \fint_0^1 \frac{h_\xi(\xi)\mathrm{d}\xi}{\xi - \xi_{i\pm\frac{1}{2}}}, \tag{3.4.58}$$

$$\xi_{i\pm\frac{1}{2}} = \frac{i \pm \frac{1}{2}}{n}. \tag{3.4.59}$$

Assuming that the slope is constant in each sub-interval and by approximating $h_\xi(\xi)$ using forward differences, we obtain

$$P_{i-\frac{1}{2}} = \sum_{\substack{j=0 \\ j\neq i-1}}^{n-1} \left(\frac{h_{j+1} - h_j}{\xi_{j+1} - \xi_j}\right) \int_{\xi_j}^{\xi_{j+1}} \frac{\mathrm{d}\xi}{\xi - \xi_{i-\frac{1}{2}}} + \left(\frac{h_{j+1} - h_j}{\xi_{j+1} - \xi_j}\right) \fint_{\xi_{i-1}}^{\xi_i} \frac{\mathrm{d}\xi}{\xi - \xi_{i-\frac{1}{2}}}, \tag{3.4.60}$$

$$P_{i+\frac{1}{2}} = \sum_{\substack{j=0 \\ j\neq i}}^{n-1} \left(\frac{h_{j+1} - h_j}{\xi_{j+1} - \xi_j}\right) \int_{\xi_j}^{\xi_{j+1}} \frac{\mathrm{d}\xi}{\xi - \xi_{i+\frac{1}{2}}} + \left(\frac{h_{j+1} - h_j}{\xi_{j+1} - \xi_j}\right) \fint_{\xi_i}^{\xi_{i+1}} \frac{\mathrm{d}\xi}{\xi - \xi_{i+\frac{1}{2}}}. \tag{3.4.61}$$

By definition of the Cauchy principal value, the second integral in (3.4.60) is given by

$$\begin{aligned} \fint_{\xi_{i-1}}^{\xi_i} \frac{\mathrm{d}\xi}{\xi - \xi_{i-\frac{1}{2}}} &= \lim_{\alpha\to 0^+} \left[\int_{\xi_{i-1}}^{\xi_{i-\frac{1}{2}}-\alpha} \frac{\mathrm{d}\xi}{\xi - \xi_{i-\frac{1}{2}}} + \int_{\xi_{i-\frac{1}{2}}+\alpha}^{\xi_i} \frac{\mathrm{d}\xi}{\xi - \xi_{i-\frac{1}{2}}} \right] \\ &= \lim_{\alpha\to 0^+} \left[\ln\left|\xi - \xi_{i-\frac{1}{2}}\right|_{\xi_{i-1}}^{\xi_{i-\frac{1}{2}}-\alpha} + \ln\left|\xi - \xi_{i-\frac{1}{2}}\right|_{\xi_{i-\frac{1}{2}}+\alpha}^{\xi_i} \right]. \end{aligned} \tag{3.4.62}$$

Evaluating the terms in brackets, we get

$$\ln\left|\xi-\xi_{i-\frac{1}{2}}\right|_{\xi_{i-1}}^{\xi_{i-\frac{1}{2}}-\alpha}=\ln|-\alpha|-\ln\left|\xi_{i-1}-\xi_{i-\frac{1}{2}}\right|, \tag{3.4.63}$$

$$\ln\left|\xi-\xi_{i-\frac{1}{2}}\right|_{\xi_{i-\frac{1}{2}}+\alpha}^{\xi_i}=\ln\left|\xi_i-\xi_{i-\frac{1}{2}}\right|-\ln|\alpha|. \tag{3.4.64}$$

Thus,

$$\begin{aligned}\lim_{\alpha\to0^+}\left[\ln\left|\xi-\xi_{i-\frac{1}{2}}\right|_{\xi_{i-1}}^{\xi_{i-\frac{1}{2}}-\alpha}+\ln\left|\xi-\xi_{i-\frac{1}{2}}\right|_{\xi_{i-\frac{1}{2}}+\alpha}^{\xi_i}\right]&=\ln\left|\frac{\xi_i-\xi_{i-\frac{1}{2}}}{\xi_{i-1}-\xi_{i-\frac{1}{2}}}\right|\\&=\ln\left|\frac{\xi_{j+1}-\xi_{i-\frac{1}{2}}}{\xi_j-\xi_{i-\frac{1}{2}}}\right|,\end{aligned} \tag{3.4.65}$$

since $j=i-1$. Hence,

$$⨍_{\xi_{i-1}}^{\xi_i}\frac{\mathrm{d}\xi}{\xi-\xi_{i-\frac{1}{2}}}=\ln\left|\frac{\xi_{j+1}-\xi_{i-\frac{1}{2}}}{\xi_j-\xi_{i-\frac{1}{2}}}\right|. \tag{3.4.66}$$

Similarly, we find that

$$⨍_{\xi_{i-1}}^{\xi_i}\frac{\mathrm{d}\xi}{\xi-\xi_{i+\frac{1}{2}}}=\ln\left|\frac{\xi_{j+1}-\xi_{i+\frac{1}{2}}}{\xi_j-\xi_{i+\frac{1}{2}}}\right|. \tag{3.4.67}$$

Also,

$$⨍_{\xi_j}^{\xi_{j+1}}\frac{1}{\xi-\xi_{i\pm\frac{1}{2}}}\mathrm{d}\xi=\ln\left|\frac{\xi_{j+1}-\xi_{i\pm\frac{1}{2}}}{\xi_j-\xi_{i\pm\frac{1}{2}}}\right|. \tag{3.4.68}$$

This means

$$P\left(\xi_{i\pm\frac{1}{2}}\right)=\sum_{j=0}^{n-1}\left(\frac{h_{j+1}-h_j}{\xi_{j+1}-\xi_j}\right)\ln\left|\frac{\xi_{j+1}-\xi_{i\pm\frac{1}{2}}}{\xi_j-\xi_{i\pm\frac{1}{2}}}\right|. \tag{3.4.69}$$

Substituting (3.4.69) into (3.4.57) and rearranging, we find

$$\sum_{j=0}^{n-1}\frac{h_{j+1}-h_j}{(\xi_{i+\frac{1}{2}}-\xi_{i-\frac{1}{2}})(\xi_{j+1}-\xi_j)}\left[\ln\left|\frac{\xi_{j+1}-\xi_{i+\frac{1}{2}}}{\xi_j-\xi_{i+\frac{1}{2}}}\right|-\ln\left|\frac{\xi_{j+1}-\xi_{i-\frac{1}{2}}}{\xi_j-\xi_{i-\frac{1}{2}}}\right|\right]=\pi. \tag{3.4.70}$$

Equation (3.4.70) becomes

$$\sum_{j=0}^{n-1}(h_{j+1}-h_j)\ln\left|\frac{(2j-2i+1)^2}{(2j-2i+3)(2j-2i-1)}\right|=\frac{\pi}{n^2}, \tag{3.4.71}$$

where $\xi_{i+\frac{1}{2}}-\xi_{i-\frac{1}{2}}=\xi_{j+1}-\xi_j=\frac{1}{n}$. This can be equivalently written as

$$\sum_{j=0}^{n-1}(h_{j+1}-h_j)a_{i,j}=\frac{\pi}{n^2}, \tag{3.4.72}$$

where

$$a_{i,j} = \ln \left| \frac{(2j-2i+1)^2}{(2j-2i+3)(2j-2i-1)} \right|.$$

Expanding the summation and evaluating the resulting equation at $i = 1, 2, \ldots, n-1$ generates a system of $n-1$ linear equations in $n-1$ unknowns since $h(x_0) = h_0$ is known and $h_n = 0$ according to (3.4.2a-b). If we impose the boundary condition $h_x(0) = 0$, we are able to determine one unknown to get an $n-1$ system in $n-2$ unknowns. As a result we have an over-determined system. Any $n-2$ equations and not $n-1$ is therefore sufficient to determine the unknowns. We can choose, for example, index i, such that $1 \leqslant i \leqslant n-2$ or $2 \leqslant i \leqslant n-1$ or any $n-2$ systems. To illustrate this idea, we set $n = 5$.

Equation (3.4.72) becomes

$$\sum_{j=0}^{4} (h_{j+1} - h_j) a_{i,j} = \frac{\pi}{25}. \tag{3.4.73}$$

If $2 \leqslant i \leqslant 4$, we have the linear system given by

$$(a_{2,1} - a_{2,2})h_2 + (a_{2,2} - a_{2,3})h_3 + (a_{2,3} - a_{2,4})h_4 = \frac{\pi}{25} + a_{2,1}h_1, \tag{3.4.74}$$

$$(a_{3,1} - a_{3,2})h_2 + (a_{3,2} - a_{3,3})h_3 + (a_{3,3} - a_{3,4})h_4 = \frac{\pi}{25} + a_{3,1}h_1, \tag{3.4.75}$$

$$(a_{4,1} - a_{4,2})h_2 + (a_{4,2} - a_{4,3})h_3 + (a_{4,3} - a_{4,4})h_4 = \frac{\pi}{25} + a_{4,1}h_1, \tag{3.4.76}$$

The system of equations (3.4.74)-(3.4.76) consists of 3 unknowns. Figure 8 illustrates the results for the combination of equations involving the point $i = n-1$. It can be noted that when the point $P_{n-1/2}$ is involved in the computations the margin of error is quite big. However, if $1 \leqslant i \leqslant 3$, we have the linear system as

$$(a_{1,1} - a_{1,2})h_2 + (a_{1,2} - a_{1,3})h_3 + (a_{1,3} - a_{1,4})h_4 = \frac{\pi}{25} + a_{1,1}h_1, \tag{3.4.77}$$

$$(a_{2,1} - a_{2,2})h_2 + (a_{2,2} - a_{2,3})h_3 + (a_{2,3} - a_{2,4})h_4 = \frac{\pi}{25} + a_{2,1}h_1, \tag{3.4.78}$$

$$(a_{3,1} - a_{3,2})h_2 + (a_{3,2} - a_{3,3})h_3 + (a_{3,3} - a_{3,4})h_4 = \frac{\pi}{25} + a_{3,1}h_1, \tag{3.4.79}$$

Similarly, the system of equations (3.4.77)-(3.4.79) consists of 3 unknowns. Figure 9 illustrates the results for the combination of equations excluding the point $i = n-1$ for various values of n. It is clear that the exclusion of the point $P_{n-1/2}$ leads to very small error margins.

(i)

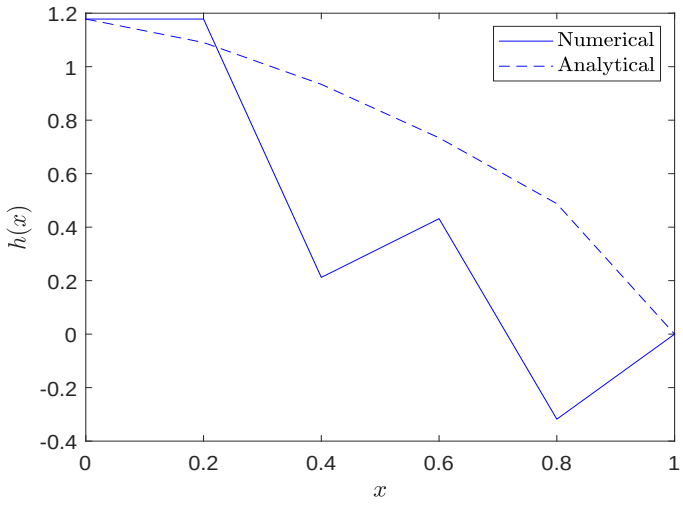

(ii)

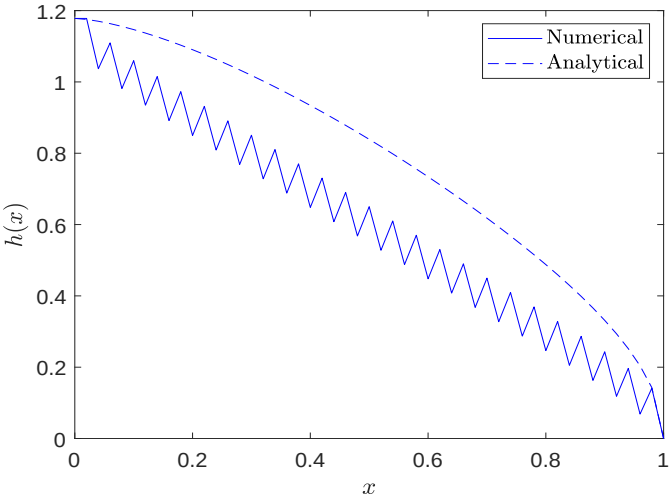

(iii)

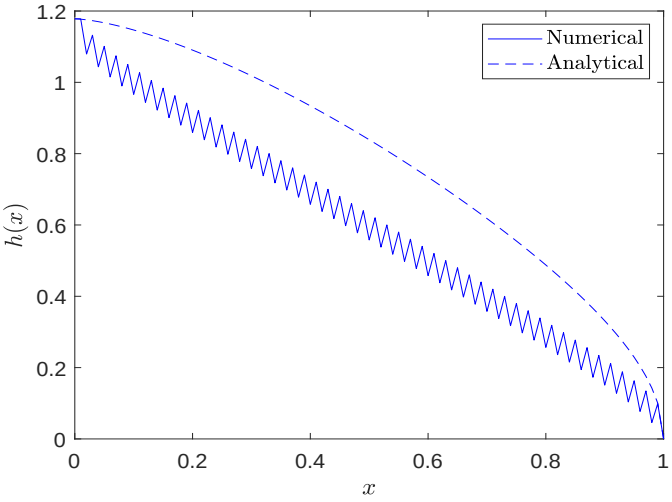

Figure 8: Graph of $h(x)$ plotted against x for (i) $n = 5$, (ii) $n = 50$ and (iii) $n = 100$ when $2 \leqslant i \leqslant n-1$, using the conventional finite difference approach.

We can now resolve that the current method is unstable for solving the underlying problem. It is in fact standard practice to exclude the tip when solving problems of this form. The best approach is to isolate the tip behaviour and that is why we need to progress from this method to a new method where we now use the tip behaviour as a variable. In the next section, we review and apply this new method to solve the underlying problem.

3.4.3.3 *An approach using transformation*

In this section, we present an alternative approach to the conventional approach in Section 3.4.3.2 whose accuracy depends on using the right combination of equations. We want a method that will work regardless of the choice of linear system. It is clear from the analytical solution (3.4.14) that $h(x) \to 0$ like $\sqrt{1-x}$ as $x \to 1$. Therefore, there is singularity in the slope of $h(x)$ near $x = 1$, i.e., $h_x(x) \to \infty$ as $x \to 1$. It is this singularity at $x = 1$ which disrupts the numerical scheme used in the preceding section. In order to address this, we consider the following transformation [57]

$$h(x) = F(y) \quad \text{where} \quad y = \sqrt{1-x}. \tag{3.4.80}$$

Under this transformation equation (3.4.1) becomes

$$\frac{1}{\pi}\left(\fint_0^1 \frac{F_\eta(\eta)\mathrm{d}\eta}{y^2-\eta^2}\right)_y = 2y, \tag{3.4.81}$$

subject to the boundary conditions

$$F(0) = 0, \quad F_y(1) = 0, \quad F(1) = \frac{3\pi}{8}. \tag{3.4.82a-c}$$

Similarly, the finite differences were used to approximate P_y, where

$$P = \fint_0^1 \frac{F_\eta(\eta)\mathrm{d}\eta}{y^2-\eta^2},$$

so that

$$\frac{\mathrm{d}P}{\mathrm{d}y} = 2\pi y.$$

Using finite differences, we have

$$\frac{P_{i+\frac{1}{2}} - P_{i-\frac{1}{2}}}{\eta_{i+\frac{1}{2}} - \eta_{i-\frac{1}{2}}} = \frac{2\pi i}{n}, \tag{3.4.83}$$

where $P_{i+1/2}$ and $\eta_{i+1/2}$ are respectively given by

$$P_{i\pm\frac{1}{2}} = \fint_0^1 \frac{F_\eta(\eta)\mathrm{d}\eta}{\eta_{i\pm\frac{1}{2}}^2 - \eta^2},$$

(i)

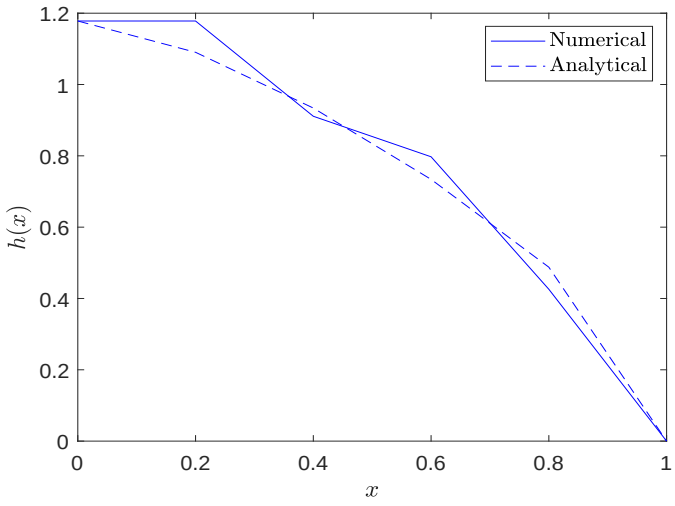

(ii)

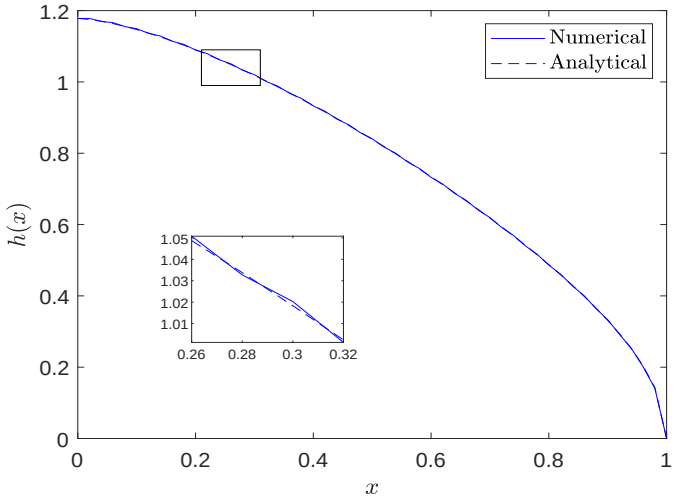

(iii)

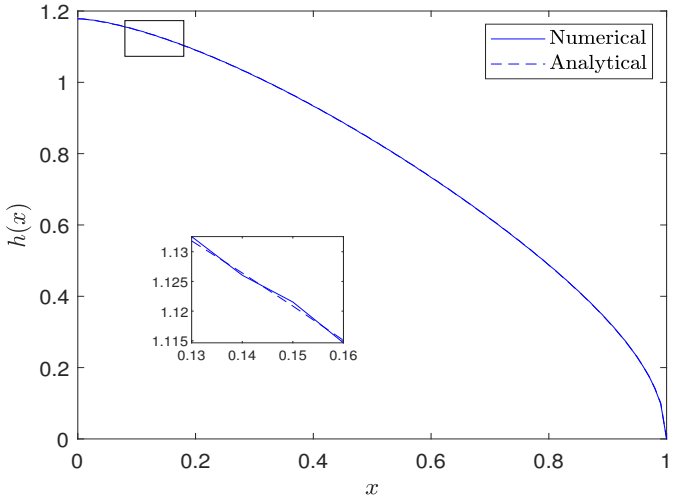

Figure 9: Graph of $h(x)$ plotted against x for (i) $n = 5$, (ii) $n = 50$ and (iii) $n = 100$ when $1 \leqslant i \leqslant n-2$, using the conventional finite difference approach.

$$\eta_{i\pm\frac{1}{2}} = \frac{i \pm \frac{1}{2}}{n}.$$

Assuming that the slope $\mathrm{d}F/\mathrm{d}\eta$ is constant in each interval, we obtain

$$P_{i-\frac{1}{2}} = \sum_{\substack{j=0 \\ j\neq i-1}}^{n-1} \left(\frac{F_{j+1}-F_j}{\eta_{j+1}-\eta_j}\right) \int_{\eta_j}^{\eta_{j+1}} \frac{\mathrm{d}\eta}{\eta_{i-\frac{1}{2}}^2 - \eta^2} + \left(\frac{F_i - F_{i-1}}{\eta_i - \eta_{i-1}}\right) \fint_{\eta_{i-1}}^{\eta_i} \frac{\mathrm{d}\eta}{\eta_{i-\frac{1}{2}}^2 - \eta^2}, \tag{3.4.84}$$

$$P_{i+\frac{1}{2}} = \sum_{\substack{j=0 \\ j\neq i-1}}^{n-1} \left(\frac{F_{j+1}-F_j}{\eta_{j+1}-\eta_j}\right) \int_{\eta_j}^{\eta_{j+1}} \frac{\mathrm{d}\eta}{\eta_{i+\frac{1}{2}}^2 - \eta^2} + \left(\frac{F_i - F_{i-1}}{\eta_i - \eta_{i-1}}\right) \fint_{\eta_{i-1}}^{\eta_i} \frac{\mathrm{d}\eta}{\eta_{i+\frac{1}{2}}^2 - \eta^2}. \tag{3.4.85}$$

Using the definition of a Cauchy's principal value, the singular integral equation in (3.4.84) can be expressed as

$$\begin{aligned}
\fint_{\eta_{i-1}}^{\eta_i} \frac{\mathrm{d}\eta}{\eta_{i-\frac{1}{2}}^2 - \eta^2} &= \lim_{\alpha\to 0^+} \left[\int_{\eta_{i-1}}^{\eta_{i-\frac{1}{2}}-\alpha} \frac{\mathrm{d}\eta}{\eta_{i-\frac{1}{2}}^2 - \eta^2} + \int_{\eta_{i-\frac{1}{2}}+\alpha}^{\eta_i} \frac{\mathrm{d}\eta}{\eta_{i-\frac{1}{2}}^2 - \eta^2} \right] \\
&= \lim_{\alpha\to 0^+} \left[\frac{1}{2\eta_{i-\frac{1}{2}}} \ln\left|\frac{\eta_{i-\frac{1}{2}}+\eta}{\eta_{i-\frac{1}{2}}-\eta}\right|_{\eta_{i-1}}^{\eta_{i-\frac{1}{2}}-\alpha} \right. \\
&\qquad \left. + \frac{1}{2\eta_{i-\frac{1}{2}}} \ln\left|\frac{\eta_{i-\frac{1}{2}}+\eta}{\eta_{i-\frac{1}{2}}-\eta}\right|_{\eta_{i-\frac{1}{2}}+\alpha}^{\eta_i} \right].
\end{aligned} \tag{3.4.86}$$

Evaluating the first term in brackets we get

$$\begin{aligned}
\ln\left|\frac{\eta_{i-\frac{1}{2}}+\eta}{\eta_{i-\frac{1}{2}}-\eta}\right|_{\eta_{i-1}}^{\eta_{i-\frac{1}{2}}-\alpha} &= \ln\left|\frac{2\eta_{i-\frac{1}{2}}-\alpha}{\alpha}\right| - \ln\left|\frac{\eta_{i-\frac{1}{2}}+\eta_{i-1}}{\eta_{i-\frac{1}{2}}-\eta_{i-1}}\right| \\
&= \ln\left|\frac{\left(2\eta_{i-\frac{1}{2}}-\alpha\right)\left(\eta_{i-\frac{1}{2}}-\eta_{i-1}\right)}{\alpha\left(\eta_{i-\frac{1}{2}}+\eta_{i-1}\right)}\right|.
\end{aligned} \tag{3.4.87}$$

The second term in brackets gives

$$\begin{aligned}
\ln\left|\frac{\eta_{i-\frac{1}{2}}+\eta}{\eta_{i-\frac{1}{2}}-\eta}\right|_{\eta_{i-\frac{1}{2}}+\alpha}^{\eta_i} &= \ln\left|\frac{\eta_{i-\frac{1}{2}}+\eta_i}{\eta_{i-\frac{1}{2}}-\eta_i}\right| - \ln\left|\frac{2\eta_{i-\frac{1}{2}}+\alpha}{-\alpha}\right| \\
&= \ln\left|\frac{-\alpha\left(\eta_{i-\frac{1}{2}}+\eta_i\right)}{\left(\eta_{i-\frac{1}{2}}-\eta_i\right)\left(2\eta_{i-\frac{1}{2}}+\alpha\right)}\right|.
\end{aligned} \tag{3.4.88}$$

Using (3.4.87) and (3.4.88) in (3.4.86), we get

$$\begin{aligned}\int_{\eta_{i-1}}^{\eta_i} \frac{\mathrm{d}\eta}{\eta_{i-\frac{1}{2}}^2 - \eta^2} &= \lim_{\alpha\to 0^+} \left[\frac{1}{2\eta_{i-\frac{1}{2}}} \ln \left| \frac{\left(2\eta_{i-\frac{1}{2}} - \alpha\right)\left(\eta_{i-\frac{1}{2}} - \eta_{i-1}\right)\left(\eta_{i-\frac{1}{2}} + \eta_i\right)}{\left(2\eta_{i-\frac{1}{2}} + \alpha\right)\left(\eta_{i-\frac{1}{2}} + \eta_{i-1}\right)\left(\eta_{i-\frac{1}{2}} - \eta_i\right)} \right| \right] \\ &= \frac{1}{2\eta_{i-\frac{1}{2}}} \ln \left| \frac{\left(\eta_{i-\frac{1}{2}} - \eta_{i-1}\right)\left(\eta_{i-\frac{1}{2}} + \eta_i\right)}{\left(\eta_{i-\frac{1}{2}} + \eta_{i-1}\right)\left(\eta_{i-\frac{1}{2}} - \eta_i\right)} \right|. \end{aligned} \tag{3.4.89}$$

Similarly,

$$\int_{\eta_{i-1}}^{\eta_i} \frac{\mathrm{d}\eta}{\eta_{i+\frac{1}{2}}^2 - \eta^2} = \frac{1}{2\eta_{i+\frac{1}{2}}} \ln \left| \frac{\left(\eta_{i+\frac{1}{2}} - \eta_{i-1}\right)\left(\eta_{i+\frac{1}{2}} + \eta_i\right)}{\left(\eta_{i+\frac{1}{2}} + \eta_{i-1}\right)\left(\eta_{i+\frac{1}{2}} - \eta_i\right)} \right|. \tag{3.4.90}$$

Since $j = i - 1$, we have

$$P_{i-\frac{1}{2}} = \sum_{j=0}^{n-1} \left(\frac{F_{j+1} - F_j}{\eta_{j+1} - \eta_j} \right) \frac{1}{2\eta_{i-\frac{1}{2}}} \ln \left| \frac{\left(\eta_{i-\frac{1}{2}} - \eta_j\right)\left(\eta_{i-\frac{1}{2}} + \eta_{j+1}\right)}{\left(\eta_{i-\frac{1}{2}} + \eta_j\right)\left(\eta_{i-\frac{1}{2}} - \eta_{j+1}\right)} \right|, \tag{3.4.91}$$

$$P_{i+\frac{1}{2}} = \sum_{j=0}^{n-1} \left(\frac{F_{j+1} - F_j}{\eta_{j+1} - \eta_j} \right) \frac{1}{2\eta_{i+\frac{1}{2}}} \ln \left| \frac{\left(\eta_{i+\frac{1}{2}} - \eta_j\right)\left(\eta_{i+\frac{1}{2}} + \eta_{j+1}\right)}{\left(\eta_{i+\frac{1}{2}} + \eta_j\right)\left(\eta_{i+\frac{1}{2}} - \eta_{j+1}\right)} \right|. \tag{3.4.92}$$

Substituting (3.4.91) and (3.4.92) into (3.4.83) and expressing the results in terms of i and j, we obtain

$$\begin{aligned}\sum_{j=0}^{n-1} (F_{j+1} - F_j) \left[\frac{1}{2i+1} \ln \left| \frac{(2i+2j+3)(2i-2j+1)}{(2i+2j+1)(2i-2j-1)} \right| - \right. \\ \left. \frac{1}{2i-1} \ln \left| \frac{(2i+2j+1)(2i-2j-1)}{(2i+2j-1)(2i-2j-3)} \right| \right] = \frac{2\pi i}{n^4}. \end{aligned} \tag{3.4.93}$$

If we evaluate (3.4.93) for any n and impose the boundary conditions (3.4.2) we obtain a system of $(n-1) \times (n-2)$ linear equations. The resulting system can be solved using any combination of equations since the transformation removed the singularity in $h_x(x)$ at $x = 1$. The results plotted in Figure 10 for the current numerical scheme compares well with the analytical results.

3.4.3.4 *Integral approximation approach*

In this section, we are interested in using a simple integral approximation method to estimate the integral in (3.4.1). To do this, composite integration rules will be used. For example, the interval of integration

(i)

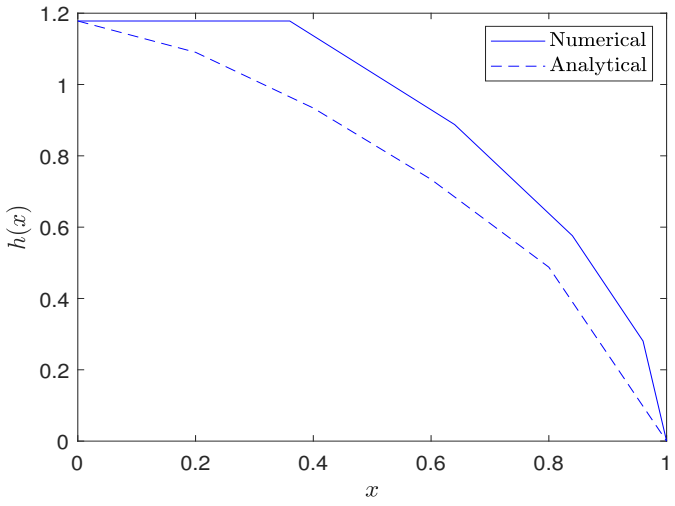

(ii)

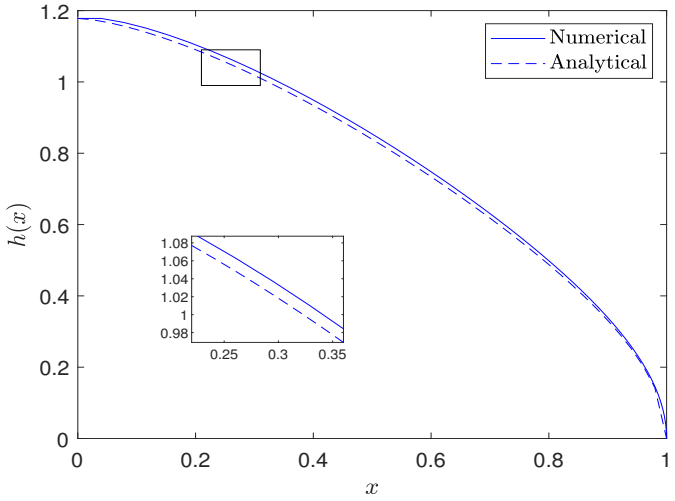

(iii)

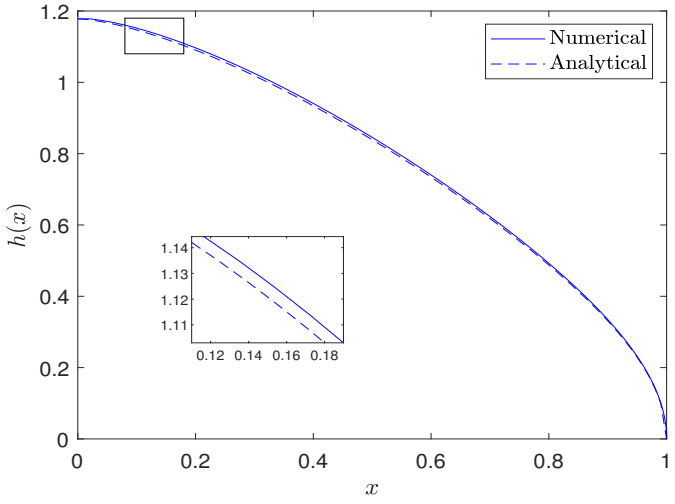

Figure 10: Graph of $h(x)$ plotted against x for (i) $n = 5$, (ii) $n = 50$ and (iii) $n = 100$, using the transformation method

will be divided into equal sub-intervals and an integration rule will be applied in each sub-interval. In relation to the paradigm problem (3.4.1), the function $f(\xi, x)$ has singularities at $\xi = x$. As a result, the values of ξ at which the integral is evaluated cannot be the mid-points of the sub-interval but edge-points of the sub-interval. One of the simplest methods of approximating an integral is the left-end point rule and it is given by

$$\int_{\xi_j}^{\xi_{j+1}} f(\xi, x)\mathrm{d}\xi = hf(\xi_j, x). \tag{3.4.94}$$

We now implement this technique in our problem. Let us first split the interval of integration $[0, 1]$ into n equal-sized sub-intervals and then represent the integral as a sum of the integrals in each sub-interval. That is, the expression for P given in (3.4.55) at mid-points can be written in the form

$$P_{i\pm\frac{1}{2}} = \int_0^1 \frac{h_{\tilde{\xi}}(\xi)\mathrm{d}\xi}{\xi - \xi_{i\pm\frac{1}{2}}} = \sum_{j=0}^{n-1} \int_{\xi_j}^{\xi_{j+1}} \frac{h_{\tilde{\xi}}(\xi)}{\xi - \xi_{i\pm\frac{1}{2}}}\mathrm{d}\xi. \tag{3.4.95}$$

Using the left-end point rule, we have

$$\sum_{j=0}^{n-1} \int_{\xi_j}^{\xi_{j+1}} \frac{h_{\tilde{\xi}}}{\xi - \xi_{i\pm\frac{1}{2}}}\mathrm{d}\xi \approx \sum_{j=0}^{n-1} h\frac{h_{\tilde{\xi}}}{\xi_j - \xi_{i\pm\frac{1}{2}}} = \sum_{j=0}^{n-1} \frac{h_{j+1} - h_j}{\xi_j - \xi_{i\pm\frac{1}{2}}}, \tag{3.4.96}$$

which implies that

$$P_{i\pm\frac{1}{2}} \approx \sum_{j=0}^{n-1} \frac{h_{j+1} - h_j}{\xi_j - \xi_{i\pm\frac{1}{2}}}. \tag{3.4.97}$$

Substituting (3.4.97) into (3.4.57), we find

$$\sum_{j=0}^{n-1} \frac{h_{j+1} - h_j}{\xi_j - \xi_{i+\frac{1}{2}}} - \sum_{j=0}^{n-1} \frac{h_{j+1} - h_j}{\xi_j - \xi_{i-\frac{1}{2}}} = \left(\xi_{i+\frac{1}{2}} - \xi_{i-\frac{1}{2}}\right)\pi = \frac{\pi}{n}, \tag{3.4.98}$$

since $\xi_{i+1/2} - \xi_{i-1/2} = h = 1/n$ and $1 \leqslant i \leqslant n-1$. Imposing the slope condition, equation (3.4.98) can be expressed as

$$\sum_{j=1}^{n-1} (h_{j+1} - h_j) f_{i,j} = \frac{\pi}{2n^2}, \tag{3.4.99}$$

where

$$f_{i,j} = \frac{1}{2j - 2i - 1} - \frac{1}{2j - 2i + 1}.$$

For any choice of n and assuming we know h_0 and $h'(x_0)$, equation (3.4.99) will result in a system of $n-1$ equations and $n-2$ unknowns. We will then have a over-determined system and any combination of $n-2$ equations can be used to solve for the $n-2$ unknowns. We demonstrate this idea with a small value of n. Setting $n = 5$, (3.4.99)

(i)

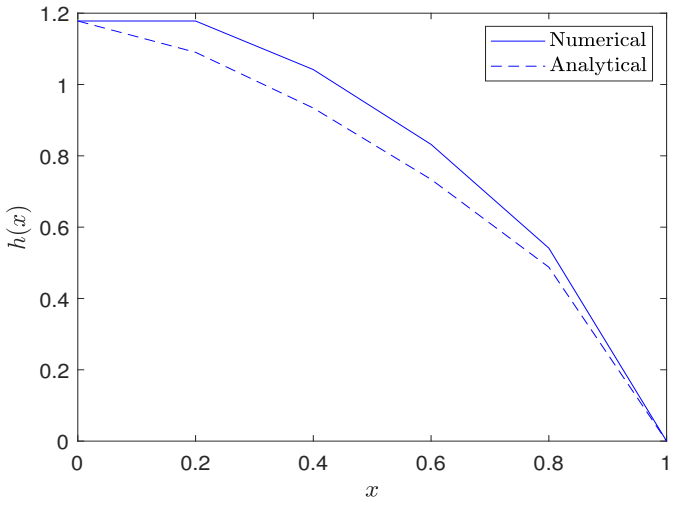

(ii)

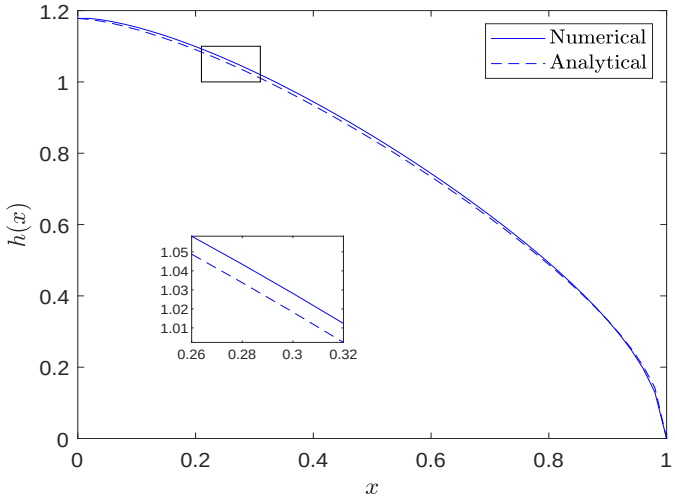

(iii)

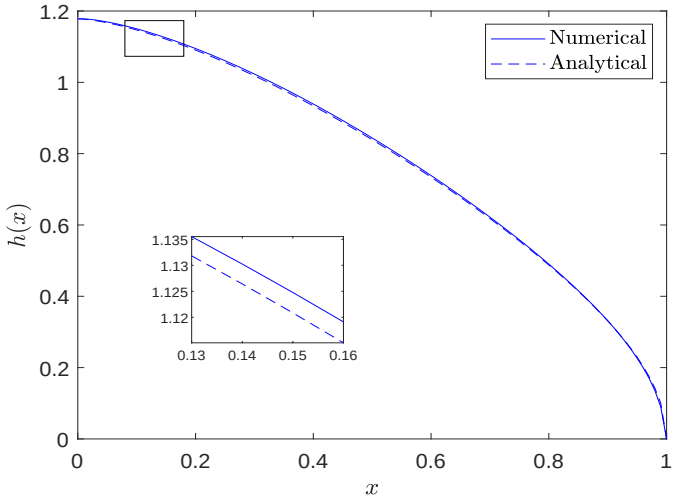

Figure 11: Graph of $h(x)$ plotted against x for (i) $n = 5$, (ii) $n = 50$ and (iii) $n = 100$, using the integral approximation approach.

yields

$$(f_{i,1}-f_{i,2})h_2+(f_{i,2}-f_{i,3})h_3+(f_{i,3}-f_{i,4})h_4=\frac{\pi}{50}+f_{i,1}h_1. \quad (3.4.100)$$

Here, we will evaluate (3.4.100) for $1 \leqslant i \leqslant 3$ and represent the resulting system of linear equations in matrix form

$$\begin{bmatrix}(f_{1,1}-f_{1,2}) & (f_{1,2}-f_{1,3}) & (f_{1,3}-f_{1,4})\\ (f_{2,1}-f_{2,2}) & (f_{2,2}-f_{2,3}) & (f_{2,3}-f_{2,4})\\ (f_{3,1}-f_{3,2}) & (f_{3,2}-f_{3,3}) & (f_{3,3}-f_{3,4})\end{bmatrix}\begin{bmatrix}h_2\\h_3\\h_4\end{bmatrix}=\begin{bmatrix}\frac{\pi}{50}+f_{11}h_1\\ \frac{\pi}{50}+f_{21}h_1\\ \frac{\pi}{50}+f_{31}h_1\end{bmatrix}.$$

The solution of the system is shown in Figure 11 where graphs of $h(x)$ plotted against x for $n = 5, 50, 100$. It can be seen that we did not lose much accuracy by approximating the integral by the left-end point rule.

3.4.4 *Spline method*

Spline methods such as the linear spline, quadratic splines, cubic splines, etc., can be used to solve equations such as (3.4.1) subject to (3.4.2). We will restrict our discussion to the linear spline method. Given a function $f(x)$ defined on $[a, b]$ and a set of nodes $a = x_0 < x_1 < \cdots < x_n = b$, a linear spline interpolant $s(x)$ for $f(x)$ is a function satisfying

- $s(x)$ is a linear polynomial (see Figure 12), denoted $s_i(x)$, in the sub-interval $[x_i, x_{i+1}]$ for each $i = 0, 1, \ldots, n-1$;
- Each linear spline passes through two consecutive points and agrees with the function $f(x)$ at a set of known points $x_0, x_1, \ldots, x_n$. For example $s_i(x_i) = f(x_i)$ and $s_{i+1}(x_{i+1}) = f(x_{i+1})$ for each $i = 0, 1, \ldots, n-1$;
- Two successive linear splines are continuous at their common interior points i.e. $s_i(x_{i+1}) = s_{i+1}(x_{i+1})$ for each $i = 0, 1, \ldots, n-2$.

The splines are given by

$$s_i(x) = a_i x + b_i, \quad x_i \leqslant x \leqslant x_{i+1},$$

where $i = 0, 1, \ldots, n-1$ and there are $2n$ unknown coefficients a_i and b_i, $i = 0, 1, \ldots, n-1$. To find the $2n$ unknowns, we need to set up $2n$ equations and then solve them simultaneously.

Consider now equations (3.4.1) and (3.4.2). Since $h(x) \to 0$ like $\sqrt{1-x}$ as $x \to 1$, we extract this tip behaviour and represent the remaining part of $h(x)$ using a linear spline. Furthermore, we divide the interval $[0, 1]$ into n sub-intervals of equal sizes such that in each sub-interval $[\xi_i, \xi_{i+1}]$, $h(x)$ takes the form

$$h_i(\xi) = (1-\xi)^{\frac{1}{2}} s_i(\xi), \quad (3.4.101)$$

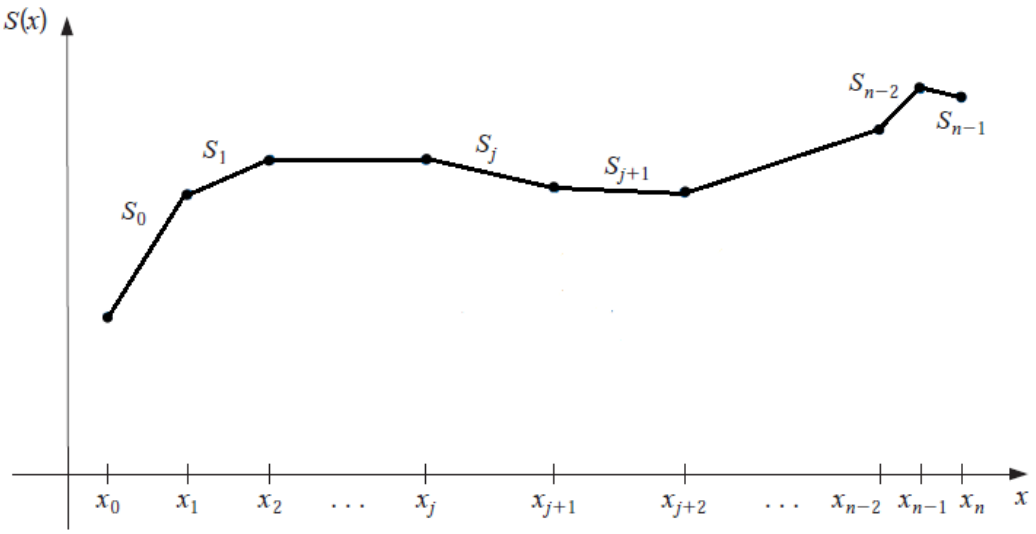

Figure 12: Linear spline interpolant $s(x)$.

where $s_i(\xi)$ is a piece-wise linear function given by

$$s_i(\xi) = a_i\xi + b_i.$$

Then,

$$\frac{\mathrm{d}h_i}{\mathrm{d}\xi} = a_i(1-\xi)^{\frac{1}{2}} - \frac{1}{2\sqrt{1-\xi}}\left(a_i\xi + b_i\right). \tag{3.4.102}$$

Using (3.4.102), we can write the expression for P given in (3.4.55) at mid-points as

$$P_{j\pm\frac{1}{2}} = \sum_{i=0}^{n-1} \int_{\xi_i}^{\xi_{i+1}} \left[\frac{(2-3\xi)a_i - b_i}{2\sqrt{1-\xi}\left(\xi - \xi_{j\pm\frac{1}{2}}\right)}\right] \mathrm{d}\xi. \tag{3.4.103}$$

Equation (3.4.103) can be rewritten as

$$P_{j-\frac{1}{2}} = \sum_{\substack{i=0 \\ i\neq j-1}}^{n-1} \int_{\xi_i}^{\xi_{i+1}} \left[\frac{(2-3\xi)a_i - b_i}{2\sqrt{1-\xi}\left(\xi - \xi_{j-\frac{1}{2}}\right)}\right] \mathrm{d}\xi + \int_{\xi_{j-1}}^{\xi_j} \left[\frac{(2-3\xi)a_{j-1} - b_{j-1}}{2\sqrt{1-\xi}\left(\xi - \xi_{j-\frac{1}{2}}\right)}\right] \mathrm{d}\xi, \tag{3.4.104}$$

and

$$P_{j+\frac{1}{2}} = \sum_{\substack{i=0 \\ i\neq j}}^{n-1} \int_{\xi_i}^{\xi_{i+1}} \left[\frac{(2-3\xi)a_i - b_i}{2\sqrt{1-\xi}\left(\xi - \xi_{j+\frac{1}{2}}\right)}\right] \mathrm{d}\xi + \int_{\xi_j}^{\xi_{j+1}} \left[\frac{(2-3\xi)a_j - b_j}{2\sqrt{1-\xi}\left(\xi - \xi_{j+\frac{1}{2}}\right)}\right] \mathrm{d}\xi. \tag{3.4.105}$$

Define

$$R_{i,j\pm\frac{1}{2}} = \int_{\xi_i}^{\xi_{i+1}} \frac{2-3\xi}{2\sqrt{1-\xi}\left(\xi-\xi_{j\pm\frac{1}{2}}\right)}\mathrm{d}\xi, \tag{3.4.106}$$

$$R^*_{i,j\pm\frac{1}{2}} = \int\!\!\!\!\!\!-_{\xi_i}^{\xi_{i+1}} \frac{2-3\xi}{2\sqrt{1-\xi}\left(\xi-\xi_{j\pm\frac{1}{2}}\right)}\mathrm{d}\xi, \tag{3.4.107}$$

$$Q_{i,j\pm\frac{1}{2}} = \int_{\xi_i}^{\xi_{i+1}} \frac{1}{2\sqrt{1-\xi}\left(\xi-\xi_{j\pm\frac{1}{2}}\right)}\mathrm{d}\xi, \tag{3.4.108}$$

$$Q^*_{i,j\pm\frac{1}{2}} = \int\!\!\!\!\!\!-_{\xi_i}^{\xi_{i+1}} \frac{1}{2\sqrt{1-\xi}\left(\xi-\xi_{j\pm\frac{1}{2}}\right)}\mathrm{d}\xi, \tag{3.4.109}$$

where $i = j-1$ in (3.4.107) and $i = j$ in (3.4.109). The integrals $R^*_{i,j\pm1/2}$ and $Q^*_{i,j\pm1/2}$ are Cauchy principal value integrals and we will use (3.2.1) and the method of *subtracting out the singularity* to deal with the singularity. Thus,

$$\begin{aligned} I &= \int\!\!\!\!\!\!-_{\xi_i}^{\xi_{i+1}} \frac{2-3\xi}{2\sqrt{1-\xi}\left(\xi-\xi_{j+\frac{1}{2}}\right)}\mathrm{d}\xi = I_- + I_+ \\ &= \lim_{\alpha\to 0}\left[\int_{\xi_i}^{\xi_{i+\frac{1}{2}}-\alpha} \frac{2-3\xi}{2\sqrt{1-\xi}\left(\xi-\xi_{j\pm\frac{1}{2}}\right)}\mathrm{d}\xi\right. \\ &\qquad \left. + \int_{\xi_{j+\frac{1}{2}}+\alpha}^{\xi_{i+1}} \frac{2-3\xi}{2\sqrt{1-\xi}\left(\xi-\xi_{j+\frac{1}{2}}\right)}\mathrm{d}\xi\right]. \end{aligned} \tag{3.4.110}$$

Setting $f(\xi) = 2-3\xi$ and subtracting the singularity, we obtain

$$\begin{aligned} I_- &= \int_{\xi_i}^{\xi_{i+\frac{1}{2}}-\alpha} \frac{f(\xi)-f\left(\xi_{j+\frac{1}{2}}\right)}{2\sqrt{1-\xi}\left(\xi-\xi_{j+\frac{1}{2}}\right)}\mathrm{d}\xi + f\left(\xi_{j+\frac{1}{2}}\right)\int_{\xi_i}^{\xi_{i+\frac{1}{2}}-\alpha} \frac{\mathrm{d}\xi}{2\sqrt{1-\xi}\left(\xi-\xi_{j+\frac{1}{2}}\right)} \\ &\approx \int_{\xi_i}^{\xi_{i+\frac{1}{2}}-\alpha} \frac{f'(\xi)\mathrm{d}\xi}{2\sqrt{1-\xi}} + f_{j+\frac{1}{2}}\int_{\xi_i}^{\xi_{i+\frac{1}{2}}-\alpha} \frac{\mathrm{d}\xi}{2\sqrt{1-\xi}\left(\xi-\xi_{j+\frac{1}{2}}\right)}. \end{aligned} \tag{3.4.111}$$

Similarly,

$$\begin{aligned} I_+ &= \int_{\xi_{i+\frac{1}{2}}+\alpha}^{\xi_{i+1}} \frac{f(\xi)-f\left(\xi_{j+\frac{1}{2}}\right)}{2\sqrt{1-\xi}\left(\xi-\xi_{j+\frac{1}{2}}\right)}\mathrm{d}\xi + f_{j+\frac{1}{2}}\int_{\xi_{i+\frac{1}{2}}+\alpha}^{\xi_{i+1}} \frac{\mathrm{d}\xi}{2\sqrt{1-\xi}\left(\xi-\xi_{j+\frac{1}{2}}\right)} \\ &\approx \int_{\xi_{i+\frac{1}{2}}+\alpha}^{\xi_{i+1}} \frac{f'(\xi)\mathrm{d}\xi}{2\sqrt{1-\xi}} + f_{j+\frac{1}{2}}\int_{\xi_{i+\frac{1}{2}}+\alpha}^{\xi_{i+1}} \frac{\mathrm{d}\xi}{2\sqrt{1-\xi}\left(\xi-\xi_{j+\frac{1}{2}}\right)}. \end{aligned}$$

(3.4.112)

The whole integral can now be written as

$$I = \int_{\xi_i}^{\xi_{i+\frac{1}{2}}} \frac{f'(\xi)\mathrm{d}\xi}{2\sqrt{1-\xi}} + \int_{\xi_{i+\frac{1}{2}}}^{\xi_{i+1}} \frac{f'(\xi)\mathrm{d}\xi}{2\sqrt{1-\xi}} + \frac{f_{j+\frac{1}{2}}}{2} \int_{\xi_i}^{\xi_{i+1}} \frac{\mathrm{d}\xi}{\sqrt{1-\xi}\left(\xi - \xi_{j+\frac{1}{2}}\right)}. \tag{3.4.113}$$

The last integral in (3.4.113) is a Cauchy principal value integral and when evaluated gives

$$\int_{\xi_i}^{\xi_{i+1}} \frac{\mathrm{d}\xi}{\sqrt{1-\xi}\left(\xi - \xi_{j+\frac{1}{2}}\right)} = \frac{1}{\sqrt{1-\xi_{j+\frac{1}{2}}}} \ln \left| \frac{\sqrt{1-\xi_i} + \sqrt{1-\xi_{j+\frac{1}{2}}}}{\sqrt{1-\xi_i} - \sqrt{1-\xi_{j+\frac{1}{2}}}} \frac{\sqrt{1-\xi_{i+1}} - \sqrt{1-\xi_{j+\frac{1}{2}}}}{\sqrt{1-\xi_{i+1}} + \sqrt{1-\xi_{j+\frac{1}{2}}}} \right|. \tag{3.4.114}$$

The remaining integrals contain weak singularities at $\xi = 1$. To overcome this singularities, we will numerically compute the integrals using the Matlab built-in function *quadgk* which can handle functions that have end point singularities. It should be noted that we can directly evaluate the integral in (3.4.103) using the *quadgk* function. The above analysis of handling a Cauchy principal value integral is also applied to $R_{i,j-1/2}$.

Using the result in (3.4.114), we get

$$Q^*_{i,j\pm\frac{1}{2}} = \frac{1}{\sqrt{1-\xi_{j\pm\frac{1}{2}}}} \ln \left| \frac{\sqrt{1-\xi_i} + \sqrt{1-\xi_{j\pm\frac{1}{2}}}}{\sqrt{1-\xi_i} - \sqrt{1-\xi_{j\pm\frac{1}{2}}}} \frac{\sqrt{1-\xi_{i+1}} - \sqrt{1-\xi_{j\pm\frac{1}{2}}}}{\sqrt{1-\xi_{i+1}} + \sqrt{1-\xi_{j\pm\frac{1}{2}}}} \right|. \tag{3.4.115}$$

Equation (3.4.104) and (3.4.105) becomes, respectively

$$P_{j-\frac{1}{2}} = \sum_{\substack{i=0 \\ i\neq j-1}}^{n-1} \left(a_i R_{i,j-\frac{1}{2}} - b_i Q_{i,j-\frac{1}{2}} \right) + a_{j-1} R^*_{j-1,j-\frac{1}{2}} - b_{j-1} Q^*_{j-1,j-\frac{1}{2}}, \tag{3.4.116}$$

$$P_{j+\frac{1}{2}} = \sum_{\substack{i=0 \\ i\neq j}}^{n-1} \left(a_i R_{i,j+\frac{1}{2}} - b_i Q_{i,j+\frac{1}{2}} \right) + a_j R^*_{j,j+\frac{1}{2}} - b_j Q^*_{j,j+\frac{1}{2}}. \tag{3.4.117}$$

Substituting (3.4.116) and (3.4.117) into (3.4.57), yields

$$\sum_{\substack{i=0 \\ i\neq j}}^{n-1} \left(a_i R_{i,j+\frac{1}{2}} - b_i Q_{i,j+\frac{1}{2}} \right) + a_j R^*_{j,j+\frac{1}{2}} - b_j Q^*_{j,j+\frac{1}{2}}$$

$$- \sum_{\substack{i=0 \\ i\neq j-1}}^{n-1} \left(a_i R_{i,j-\frac{1}{2}} - b_i Q_{i,j-\frac{1}{2}} \right) - a_{j-1} R^*_{j-1,j-\frac{1}{2}} + b_{j-1} Q^*_{j-1,j-\frac{1}{2}} = \frac{\pi}{n},$$

(3.4.118)

where $1 \leqslant j \leqslant n-1$. The current task is to solve for $\{a_i, b_i\}$ in each sub-interval. There are n such sub-intervals, and therefore, we have $2n$ unknowns. Equation (3.4.118) will generate a system of $n-1$ linear equations which leads to an under-determined system. Consequently, additional equations are required to solve for all the unknowns.

Consider now the continuity of $s_i(\xi)$ at interior points, i.e., at $\xi = \xi_i$, $s_i(\xi_i) = s_{i-1}(\xi_i)$. Since,

$$s_i(\xi_i) = a_i\xi_i + b_i, \quad \text{and} \quad s_{i-1}(\xi_i) = a_{i-1}\xi_i + b_{i-1}. \tag{3.4.119a-b}$$

The continuity at $\xi_i = i/n$ implies that

$$a_i\xi_i + b_i = a_{i-1}\xi_i + b_{i-1}. \tag{3.4.120}$$

That is,

$$(a_i - a_{i-1})\xi_i + (b_i - b_{i-1}) = 0, \quad \text{for} \quad 1 \leqslant i \leqslant n-1. \tag{3.4.121}$$

Using (3.4.121), we get an additional $n-1$ equations, i.e.,

$$\begin{aligned}
&i = 1: \quad (a_1 - a_0)\xi_1 + (b_1 - b_0) = 0,\\
&i = 2: \quad (a_2 - a_1)\xi_2 + (b_2 - b_1) = 0,\\
&i = 3: \quad (a_3 - a_2)\xi_3 + (b_3 - b_2) = 0,\\
&\quad\vdots \qquad\qquad \vdots \qquad\qquad \vdots\\
&i = n-1: \quad (a_{n-1} - a_{n-2})\xi_3 + (b_{n-1} - b_{n-2}) = 0.
\end{aligned} \tag{3.4.122}$$

From (3.4.118) and (3.4.121), we get a total of $2n-2$ equations. Using the $2n-2$ equations and the boundary conditions (3.4.2b-c), we are able to solve for all the unknowns.

For $n = 5$, the splines are given by

$$\begin{aligned}
s_0 &= a_0\xi + b_0, \qquad \xi_0 \leqslant \xi \leqslant \xi_1,\\
s_1 &= a_1\xi + b_1, \qquad \xi_1 \leqslant \xi \leqslant \xi_2,\\
s_2 &= a_2\xi + b_2, \qquad \xi_2 \leqslant \xi \leqslant \xi_3,\\
s_3 &= a_3\xi + b_3, \qquad \xi_3 \leqslant \xi \leqslant \xi_4,\\
s_4 &= a_4\xi + b_4, \qquad \xi_4 \leqslant \xi \leqslant \xi_5.
\end{aligned} \tag{3.4.123}$$

We now need to find the coefficients a_i and b_i of the linear splines. There are 10 unknowns coefficients in total to be determined. This means that we need 10 equations to determine these coefficients. Using the boundary conditions (3.4.2b-c), we obtain respectively

$$a_0 = \frac{3\pi}{16}, \text{ and } b_0 = \frac{3\pi}{8}. \tag{3.4.124}$$

We are now left to determine the remaining 8 unknown coefficients. Since each linear spline goes through two consecutive points, we require the splines to be continuous at interior points, which gives 4 continuity equations

$$\begin{aligned} a_0\xi_1 + b_0 - a_1\xi_1 - b_1 &= 0, \\ a_1\xi_2 + b_1 - a_2\xi_2 - b_2 &= 0, \\ a_2\xi_3 + b_2 - a_3\xi_3 - b_3 &= 0, \\ a_3\xi_4 + b_3 - a_4\xi_4 - b_4 &= 0. \end{aligned} \tag{3.4.125}$$

Also, we evaluate equation (3.4.118) for $1 \leqslant j \leqslant 4$ to obtain 4 additional equations

$$\begin{aligned} a_0R^*_{0,1} + b_0Q^*_{0,1} + a_1R^*_{1,1} + b_1Q^*_{1,1} + a_2R_{2,1} + b_2Q_{2,1} + a_3R_{3,1} \\ + b_3Q_{3,1} + a_4R_{4,1} + b_4Q_{4,1} = \frac{\pi}{5}, \end{aligned} \tag{3.4.126}$$

$$\begin{aligned} a_0R_{0,2} + b_0Q_{0,2} + a_1R^*_{1,2} + b_1Q^*_{1,2} + a_2R^*_{2,2} + b_2Q^*_{2,2} + a_3R_{3,2} \\ + b_3Q_{3,2} + a_4R_{4,2} + b_4Q_{4,2} = \frac{\pi}{5}, \end{aligned} \tag{3.4.127}$$

$$\begin{aligned} a_0R_{0,3} + b_0Q_{0,3} + a_1R_{1,3} + b_1Q_{1,3} + a_2R^*_{2,3} + b_2Q^*_{2,3} + a_3R^*_{3,3} \\ + b_3Q^*_{3,3} + a_4R_{4,3} + b_4Q_{4,3} = \frac{\pi}{5}, \end{aligned} \tag{3.4.128}$$

$$\begin{aligned} a_0R_{0,4} + b_0Q_{0,4} + a_1R_{1,4} + b_1Q_{1,4} + a_2R_{2,4} + b_2Q_{2,4} + a_3R^*_{3,4} \\ + b_3Q^*_{3,4} + a_4R^*_{4,4} + b_4Q^*_{4,4} = \frac{\pi}{5}, \end{aligned} \tag{3.4.129}$$

where $R_{i,j} = R_{i,j+1/2} - R_{i,j-1/2}$, $Q_{i,j} = Q_{i,j-1/2} - Q_{i,j+1/2}$, $R^*_{i,j} = R^*_{i,j+1/2} - R_{i,j-1/2}$ or $R^*_{i,j} = R_{i,j+1/2} - R^*_{i,j-1/2}$ and $Q^*_{i,j} = Q^*_{i,j-1/2} - Q_{i,j+1/2}$ or $Q^*_{i,j} = Q_{i,j-1/2} - Q^*_{i,j+1/2}$. The set of equations (3.4.124)-(3.4.129) can be written in matrix form as

$$\begin{bmatrix} 1 & 0 & 0 & 0 & 0 & 0 & 0 & 0 & 0 & 0 \\ 0 & 0 & 0 & 0 & 0 & 1 & 0 & 0 & 0 & 0 \\ \xi_1 & -\xi_1 & 0 & 0 & 0 & 1 & -1 & 0 & 0 & 0 \\ 0 & \xi_2 & -\xi_2 & 0 & 0 & 0 & 1 & -1 & 0 & 0 \\ 0 & 0 & \xi_3 & -\xi_3 & 0 & 0 & 0 & 1 & -1 & 0 \\ 0 & 0 & 0 & \xi_4 & -\xi_4 & 0 & 0 & 0 & 1 & -1 \\ R^*_{0,1} & R^*_{1,1} & R_{2,1} & R_{3,1} & R_{4,1} & Q^*_{0,1} & Q^*_{1,1} & Q_{2,1} & Q_{3,1} & Q_{4,1} \\ R_{0,2} & R^*_{1,2} & R^*_{2,2} & R_{3,2} & R_{4,2} & Q_{0,2} & Q^*_{1,2} & Q^*_{2,2} & Q_{3,2} & Q_{4,2} \\ R_{0,3} & R_{1,3} & R^*_{2,3} & R^*_{3,3} & R_{4,3} & Q_{0,3} & Q_{1,3} & Q^*_{2,3} & Q^*_{3,3} & Q_{4,3} \\ R_{0,4} & R_{1,4} & R_{2,4} & R^*_{3,4} & R^*_{4,4} & Q_{0,4} & Q_{1,4} & Q_{2,4} & Q^*_{3,4} & Q^*_{4,4} \end{bmatrix} \begin{bmatrix} a_0 \\ a_1 \\ a_2 \\ a_3 \\ a_4 \\ b_0 \\ b_1 \\ b_2 \\ b_3 \\ b_4 \end{bmatrix} = \begin{bmatrix} \frac{3\pi}{16} \\ \frac{3\pi}{8} \\ 0 \\ 0 \\ 0 \\ 0 \\ \frac{\pi}{5} \\ \frac{\pi}{5} \\ \frac{\pi}{5} \\ \frac{\pi}{5} \end{bmatrix}.$$

Since we have a linear system $\boldsymbol{Ax} = \boldsymbol{b}$, we can easily compute the inverse of $\boldsymbol{A}$ and then calculate the solution as $\boldsymbol{x} := \boldsymbol{A}^{-1}\boldsymbol{b}$. Figure 13 shows graphs of $h(x)$ plotted against x for $n = 5$, 50, 100. Once again, it can be noted that the margin of error is reasonably small for large n values.

(i)

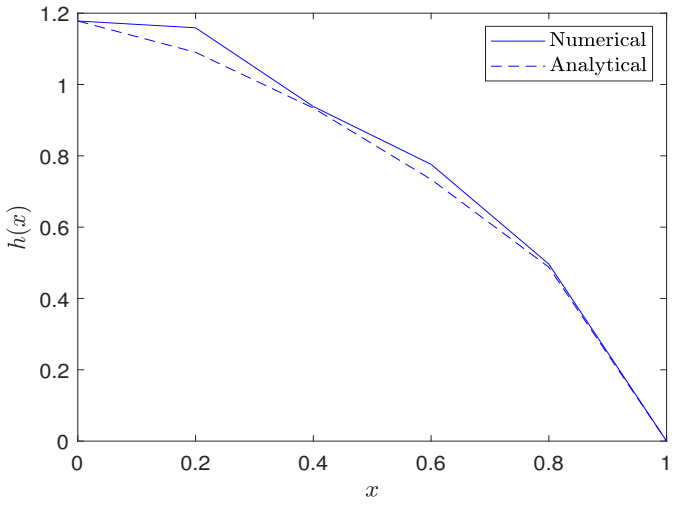

(ii)

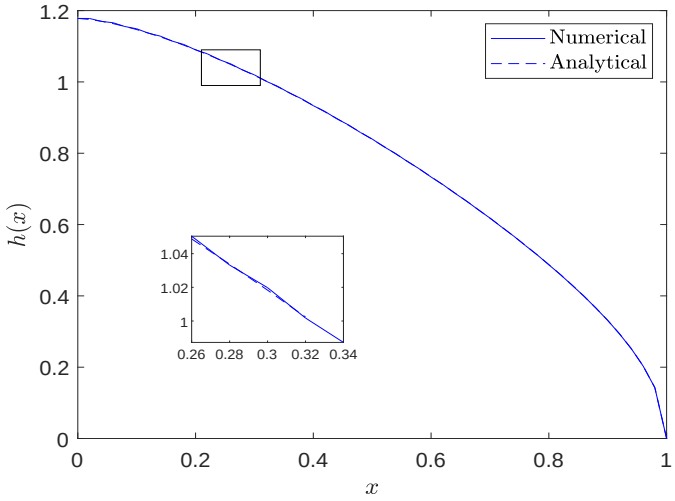

(iii)

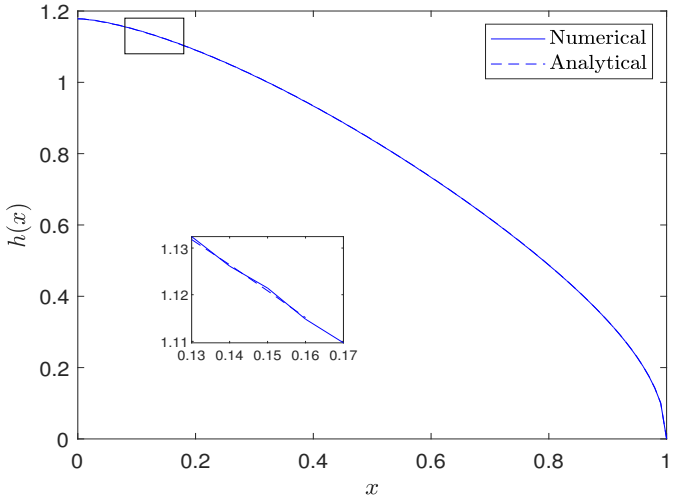

Figure 13: Graph of $h(x)$ plotted against x for (i) $n = 5$, (ii) $n = 50$ and (iii) $n = 100$, using the spline method.

(i)

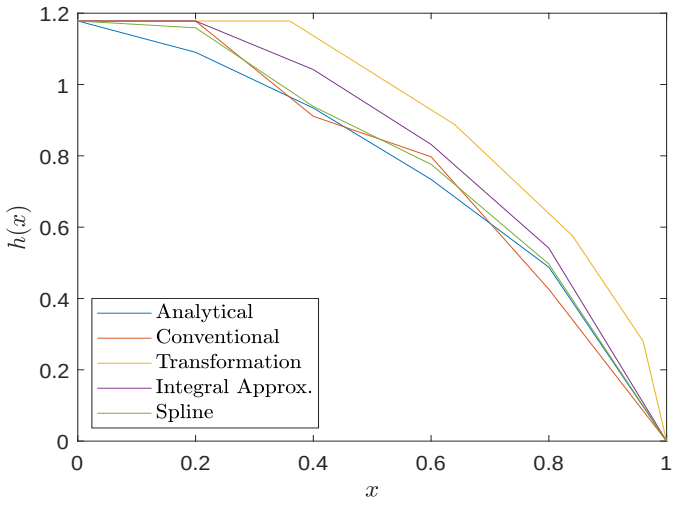

(ii)

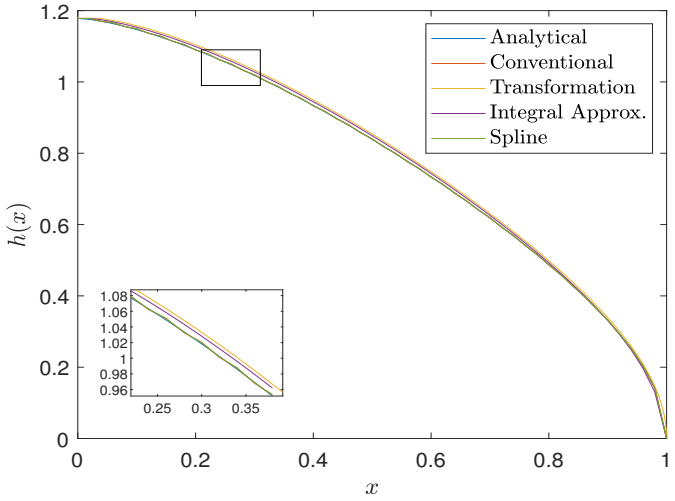

(iii)

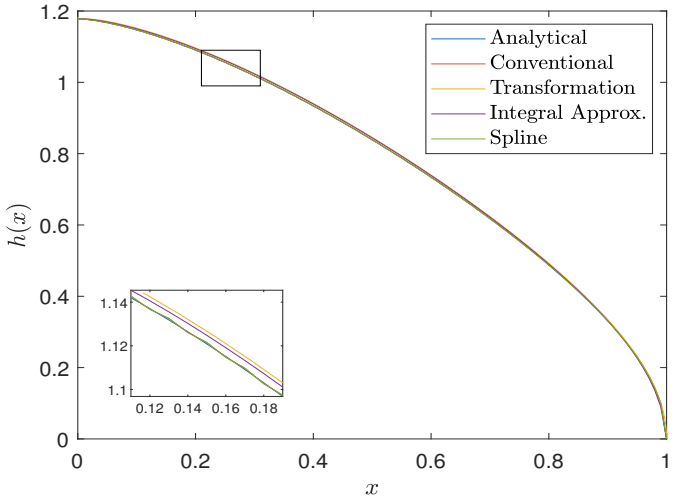

Figure 14: Graph of $h(x)$ plotted against x for (i) $n = 5$, (ii) $n = 50$ and (iii) $n = 100$.

(i)

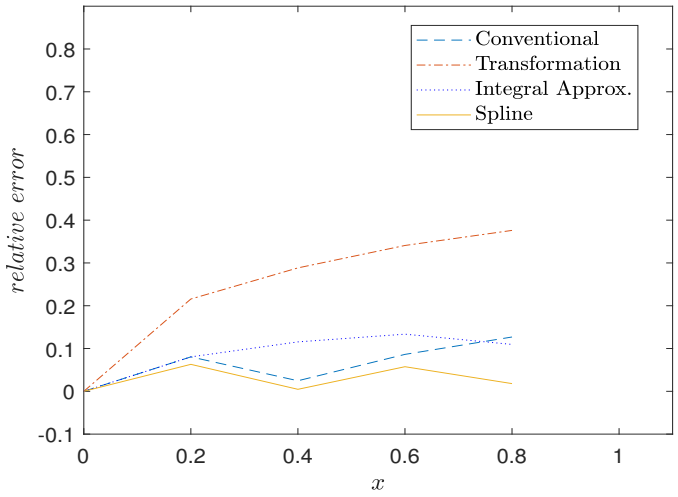

(ii)

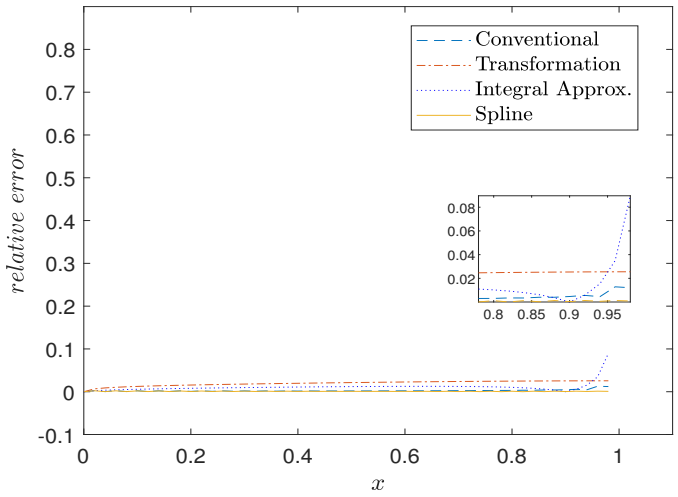

(iii)

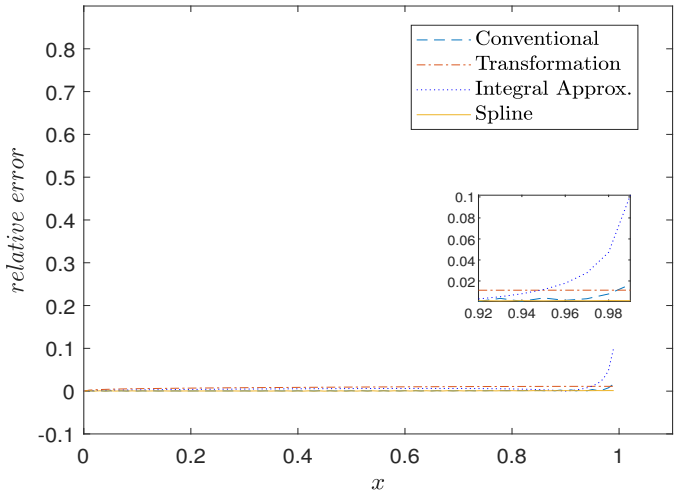

Figure 15: Plots of the relative error for (i) $n = 5$, (ii) $n = 50$ and (iii) $n = 100$.

3.4.5 *Comparison of the numerical methods*

In this section, we compare the results obtained from solving equation (3.4.1) using all the numerical methods presented in the previous subsections. Figure 14 shows the graphs of $h(x)$ plotted against x for all the numerical methods when $n = 5, 50, 100$. All the numerical methods compare well with the analytical solution. The conventional finite difference approach and the spline method showed a much better agreement with the analytical solution (see subplots in Figure 14 (ii) and (iii)) and were faster in terms of convergence. We also investigated these numerical methods in more detail by plotting the relative error, which is the ratio of the difference between exact and numerical solution to the exact solution, i.e., $error = (exact - numerics)/exact$. As n increases in Figure 15, we see the errors for all the numerical methods except the transformation method are decreasing. In particular, we see that the linear spline method did well in approximating the solution at $x = 1$, which was expected since the expression for $h(x)$ includes the $\sqrt{1-x}$ tip behaviour. The errors from the integral approximation approach are larger towards $x = 1$ than the errors from the other numerical methods, however, the results are still acceptable (see Figure 14).

3.5 CONCLUSION

In this chapter the method of solution for Cauchy-type singular integral equations were investigated. We started the chapter by deriving the standard formula for the solution of a singular integral equation of the first kind with a Cauchy kernel. Afterwards, we introduced a simple singular integral equation that can be solved both analytically and numerically. The standard formula was used to obtain the analytical solution of the simple integral equation. We then derived the approximate analytical solution of the singular integral equation and showed that it is the exact solution. The reason behind this was that the force function was a polynomial of degree one. It was also shown in [10, 18, 56] that for a Cauchy-type singular integral equation of the first kind with a linear force function the method of approximate solution gives an exact solution. Numerical solutions were then computed using four different techniques and the results were plotted against the analytical solution to evaluate the accuracy of the numerical methods. Plots showing errors from the numerical methods are also presented (see Figure 15). The most interesting observation that was made in this chapter was that the singularity in $h(x)$ at $x = 1$ disrupts the numerical schemes. To avoid this disruption, we select discrete points away from the point $x = 1$. It is important to highlight that some of the numerical schemes such as the linear spline method were able to handle this singularity.

4

MATHEMATICAL MODELS AND GOVERNING EQUATIONS

4.1 INTRODUCTION

In this chapter, we derive the mathematical model for a two-dimensional fluid-driven fracture propagating in a permeable medium. The Cauchy principal value integral derived from linear elastic fracture mechanics is used to close the model. The model is then non-dimesionalized and similarity solutions are derived.

4.2 PROBLEM DESCRIPTION

We consider a two-dimensional hydraulic fracture propagating in a permeable rock. The two-dimensional hydraulic fracture is a pre-existing fracture and a viscous incompressible Newtonian fluid is injected at sufficiently high pressure to propagate it. A proportion of the driving fluid infiltrates the rock formation through the fracture interface. The fracturing fluid causes the fracture to extend along the negative and positive x-direction, perpendicular to the compressive stress. The surrounding rock–mass is characterized by its Young's modulus E and Poison ratio ν. The flow of fluid inside the thin fracture is laminar and will be modelled using lubrication theory [3]. A detailed review of hydraulic fracture modelling is given in [53].

4.3 GOVERNING EQUATIONS

In this section, we derive the thin fluid-film equations for the flow of Newtonian fluid inside the two-dimensional fracture. The coordinate system and nomenclature are illustrated in Figure 16. The fracture is fully filled by a Newtonian fluid injected at the fracture centre $x = 0$ at a rate $Q(t,0)$. The fracture evolves under plane strain and it is symmetrical about the x-axis. The x-axis is defined along the length of the fracture and the z-axis along the width of the fracture. The flow of fluid is symmetrical about the plane $z = 0$. All the quantities are independent of y. The fracture is bounded by $z = h(t,x)$ above and $z = -h(t,x)$ below where $-L(t) \leqslant x \leqslant L(t)$ and $t \geqslant 0$. Since the fracture is symmetric with respect to $x = 0$, we restrict our analysis to one of the symmetrical parts of the fracture $x \in [0, L(t)]$. The body force due to gravity is neglected. The flow of fluid inside the fracture

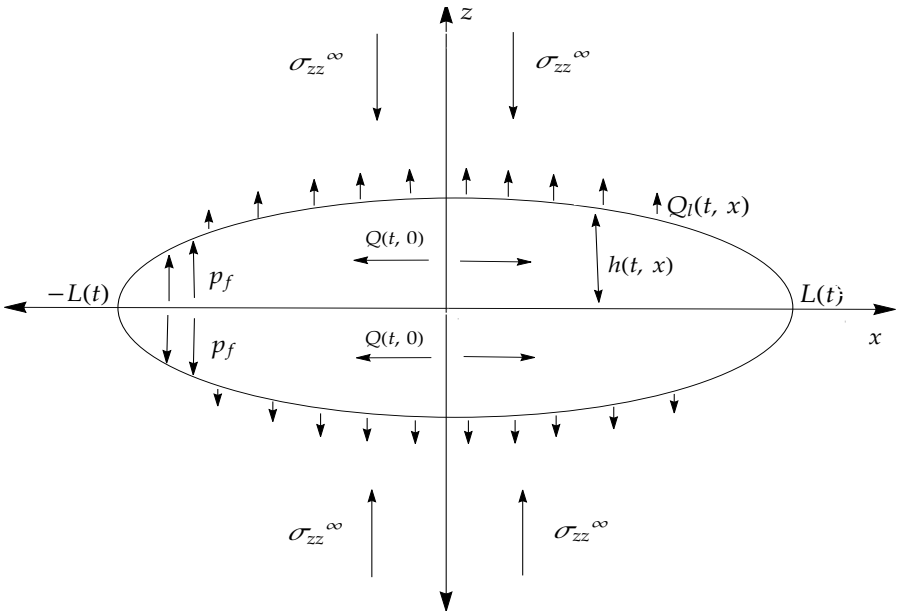

Figure 16: A pre-existing two-dimensional fluid-driven fracture propagating in a permeable rock where $h(t,x)$ represents the fracture half-width and $L(t)$ the fracture length.

satisfies the Navier-Stokes and conservation of mass equations for an incompressible fluid,

$$\frac{\partial \mathbf{v}}{\partial t} + (\mathbf{v}\cdot\nabla)\mathbf{v} = -\frac{1}{\rho}\nabla p + \nu\nabla^2\mathbf{v}, \quad \nabla.\mathbf{v} = 0, \tag{4.3.1a-b}$$

where $\mathbf{v} = (v_x(t,x,z), 0, v_z(t,x,z))$ denotes the fluid velocity, $p(t,x,z)$, the fluid pressure, ρ, the fluid density and μ, the fluid shear viscosity. In order to simplify equation (4.3.1a-b) for a fracture whose length is much greater than its height, we impose the lubrication approximation on the fracturing fluid. The thin film approximation of lubrication theory, given by

$$\epsilon = \frac{H}{L_0} \ll 1, \quad \epsilon^2 Re \ll 1, \tag{4.3.2a-b}$$

will be used in this work. In (4.3.2a-b), H is the characteristic fracture half-width, L_0 is the characteristic fracture length, and $Re = UL_0/\nu$ is the Reynolds number. We proceed to compare the order of magnitude of the terms in the conservation of mass equation and the Navier-Stokes equation. Let us first introduce the remaining characteristic quantities:

- the characteristic fluid velocity along the x-direction U
- the characteristic fluid velocity along the z-direction $W = \frac{UH}{L_0}$
- the characteristic fluid pressure $P = \frac{\mu U L_0}{H^2}$

- the characteristic time $T = \frac{L_0}{U}$.

We now give a justification for these quantities. We begin with the expression for the characteristic velocity along the z-direction. The conservation of mass equation written in cartesian coordinates is

$$\frac{\partial v_x}{\partial x} + \frac{\partial v_z}{\partial z} = 0. \tag{4.3.3}$$

Equation (4.3.3) becomes, after substituting the characteristic quantities,

$$\frac{U}{L_0} + \frac{W}{H} \sim 0, \tag{4.3.4}$$

and therefore,

$$W \sim \frac{UH}{L_0}. \tag{4.3.5}$$

We now justify the expression for the characteristic fluid pressure. Consider the x-component of the Navier-Stokes equation

$$\rho \frac{Dv_x}{Dt} = -\frac{\partial p}{\partial x} + \mu \left[\frac{\partial^2 v_x}{\partial x^2} + \frac{\partial^2 v_x}{\partial z^2} \right] \tag{4.3.6}$$

which can be expressed in terms of the characteristic quantities as

$$\rho \frac{U}{T} \sim -\frac{P}{L_0} + \mu \left(\frac{U}{L_0^2} + \frac{U}{H^2} \right). \tag{4.3.7}$$

Since (4.3.2a) is satisfied, we have

$$\frac{U}{L_0^2} \ll \frac{U}{H^2}. \tag{4.3.8}$$

The viscous term is approximated to be $\mu U / H^2$ and (4.3.7) becomes

$$\rho \frac{U}{T} \sim -\frac{P}{L_0} + \frac{\mu U}{H^2}. \tag{4.3.9}$$

Now

$$\frac{\text{inertial term}}{\text{viscous term}} = \frac{\rho U}{T} \div \frac{\mu U}{H^2} = \epsilon^2 Re \ll 1. \tag{4.3.10}$$

Therefore, equation (4.3.9) reduces to

$$P \sim \frac{\mu U L_0}{H^2}, \tag{4.3.11}$$

which is the characteristic fluid pressure. We will now non-dimensionalise the conservation of mass equation and each component of the Navier-Stokes equation using the following non-dimensional variables:

$$\begin{aligned} &\bar{L} = \frac{L}{L_0},\ \bar{x} = \frac{x}{L_0},\ \bar{z} = \frac{z}{H},\ \bar{t} = \frac{t}{T},\ \bar{h} = \frac{h}{H},\ \bar{b} = \frac{b}{B}, \\ &\bar{v}_x = \frac{v_x}{U},\ \bar{v}_z = \frac{v_z L_0}{UH},\ \bar{p} = \frac{H^2 p}{\mu U L_0},\ \overline{V} = \frac{V}{HL_0}, \end{aligned} \tag{4.3.12}$$

where, as described above, $L_0 = L(0)$, is the characteristic fracture length, and $H = h(0,0)$, is the characteristic fracture half-width. A new length scale, denoted by B, is the characteristic length scale for fluid leak-off. The conservation of mass equation and the x and z components of the Navier-Stokes equation in dimensionless form are

$$\frac{\partial \bar{v}_x}{\partial \bar{x}} + \frac{\partial \bar{v}_z}{\partial \bar{z}} = 0, \tag{4.3.13}$$

$$\begin{aligned} Re\left(\frac{H}{L_0}\right)^2\left(\frac{\partial \bar{v}_x}{\partial \bar{t}} + \bar{v}_x\frac{\partial \bar{v}_x}{\partial \bar{x}} + \bar{v}_z\frac{\partial \bar{v}_x}{\partial \bar{z}}\right) &= -\frac{\partial \bar{p}}{\partial \bar{x}} \\ &\quad + \left(\frac{H}{L_0}\right)^2\frac{\partial^2 \bar{v}_x}{\partial \bar{x}^2} + \frac{\partial^2 \bar{v}_x}{\partial \bar{z}^2}, \end{aligned} \tag{4.3.14}$$

$$\begin{aligned} Re\left(\frac{H}{L_0}\right)^4\left(\frac{\partial \bar{v}_z}{\partial \bar{t}} + \bar{v}_x\frac{\partial \bar{v}_z}{\partial \bar{x}} + \bar{v}_z\frac{\partial \bar{v}_z}{\partial \bar{z}}\right) &= -\frac{\partial \bar{p}}{\partial \bar{z}} + \left(\frac{H}{L_0}\right)^4\frac{\partial^2 \bar{v}_z}{\partial \bar{x}^2} \\ &\quad + \left(\frac{H}{L_0}\right)^2\frac{\partial^2 \bar{v}_z}{\partial \bar{z}^2}. \end{aligned} \tag{4.3.15}$$

Imposing the thin fluid-film approximation and dropping the overhead bars, the conservation of mass and Navier-Stokes equations in dimensionless form become

$$\frac{\partial v_x}{\partial x} + \frac{\partial v_z}{\partial z} = 0, \tag{4.3.16}$$

$$\frac{\partial p}{\partial x} = \frac{\partial^2 v_x}{\partial z^2}, \tag{4.3.17}$$

$$\frac{\partial p}{\partial z} = 0. \tag{4.3.18}$$

Note that the conservation of mass equation is unaltered after the application of the thin fluid-film approximation.

4.4 BOUNDARY EQUATIONS

We now specify the boundary and initial conditions for the underlying fracture problem. The boundary conditions for the lower surface $z = -h(t,x)$ and upper surface $z = h(t,x)$ are the no-slip condition and leak-off for a viscous fluid. Since the rock is permeable, the leak-off condition is imposed. The boundary conditions are as follows:

No-slip condition

$$z = h(t,x): \quad v_x(t,x,h(t,x)) = 0, \tag{4.4.1}$$

$$z = -h(t,x): \quad v_x(t,x,-h(t,x)) = 0. \tag{4.4.2}$$

Leak-off condition:

$$z = h(t,x): \quad v_z(t,x,h) = \frac{\partial h}{\partial t} + v_x(t,x,h)\frac{\partial h}{\partial x} + v_n(t,x) \\ = \frac{\partial h}{\partial t} + v_n(t,x), \tag{4.4.3}$$

$$z = -h(t,x): \quad v_z(t,x,-h) = -\frac{\partial h}{\partial t} - v_x(t,x,-h)\frac{\partial h}{\partial x} - v_n(t,x) \\ = -\left(\frac{\partial h}{\partial t} + v_n(t,x)\right), \tag{4.4.4}$$

since $v_x(t,x,\pm h) = 0$ from the no slip boundary condition (4.4.1) and (4.4.2).
Initial conditions

$$t = 0, \qquad L(0) = 1, \quad h(0,0) = 1. \tag{4.4.5}$$

The rock has a pre-existing fracture, hence

$$t = 0: \qquad h(0,x) = h_0(x), \quad 0 \leqslant x \leqslant L(t). \tag{4.4.6}$$

At the fracture tip

$$x = L(t): \qquad h(t,L(t)) = 0. \tag{4.4.7}$$

The half-width of the fracture vanishes at the fracture tip. It should be noted that the fracture tip condition (4.4.7) is a moving boundary condition since the fracture length $L(t)$ increases as the fracture propagates.

The mathematical formulation in dimensionless form is given as follows:
Governing equations

$$\frac{\partial v_x}{\partial x} + \frac{\partial v_z}{\partial z} = 0, \tag{4.4.8}$$

$$\frac{\partial p}{\partial x} = \frac{\partial^2 v_x}{\partial z^2}, \tag{4.4.9}$$

$$\frac{\partial p}{\partial z} = 0. \tag{4.4.10}$$

Boundary conditions

$$z = h(t,x): \quad v_x(t,x,h(t,x)) = 0, \tag{4.4.11}$$

$$z = -h(t,x): \quad v_x(t,x,-h(t,x)) = 0. \tag{4.4.12}$$

Leak-off condition:

$$z = h(t,x): \quad v_z(t,x,h(t,x)) = \frac{\partial h}{\partial t} + v_n(t,x), \tag{4.4.13}$$

$$z = -h(t,x): \quad v_z(t,x,-h(t,x)) = -\left(\frac{\partial h}{\partial t} + v_n(t,x)\right). \tag{4.4.14}$$

Initial conditions

$$t = 0: \quad L(0) = 1, \quad h(0,0) = 1, \tag{4.4.15}$$

$$t = 0: \quad h(0,x) = h_0(x), \quad 0 \leqslant x \leqslant L(t). \tag{4.4.16}$$

Fracture tip conditions

$$x = L(t): \ h(t,L(t)) = 0. \tag{4.4.17}$$

4.5 SOLID MECHANICS EQUATIONS

As the fracture propagation takes place in the rock, equations governing the flow of fluid inside the fracture are coupled with solid mechanics equations. Elasticity theory is used to define the relation between the fracture half-width and the net fluid pressure. In this work, we are concerned with the problem of a fluid-driven pre-existing hydraulic fracture propagating in a permeable rock where the elasticity of the rock is modelled using the Cauchy principal value integral derived from linear elastic fracture mechanics.

4.5.1 *Cauchy principal value integral*

At the fracture wall $z = h(t,x)$, from Cauchy's formula relating the stress vector to the stress tensor, we have

$$\sigma_{zz} = -p_f(t,x) + 2\mu\frac{\partial v_z}{\partial z} \qquad \text{on} \qquad z = h(t,x). \tag{4.5.1}$$

Since

$$p_f \sim \frac{\mu U L_0}{H^2} \tag{4.5.2}$$

and

$$\mu\frac{\partial v_z}{\partial z} \sim \mu\frac{U}{L_0}, \tag{4.5.3}$$

the ratio of their order of magnitude gives

$$\mu\frac{U}{L_0} \div \frac{\mu U L_0}{H^2} = \left(\frac{H}{L_0}\right)^2 \ll 1. \tag{4.5.4}$$

Thus,

$$\sigma_{zz}(t,x,z) = -p_f(t,x), \tag{4.5.5}$$

in dimensional form. The normal stress at the fracture wall is supported fully by the fluid pressure $p_f(t,x)$. In [61, 62], the fluid-driven fracture problem was considered, in which the PKN elasticity equation was employed. In this research work, we will describe the elasticity equation using the relation due to Spence and Sharp [82]:

$$\sigma_{zz} - \sigma_{zz}^{\infty} = \frac{2G}{\pi(1-\nu)} \int_0^{L(t)} \frac{\partial h(t,s)}{\partial s} \frac{s}{(s^2 - x^2)} \mathrm{d}s, \tag{4.5.6}$$

where σ_{zz} is the elastic normal stress along the fracture walls, σ_{zz}^{∞} is the normal stress at infinity within the rock-mass, G is the elastic shear modulus, ν is the Poisson's ratio and $G/(1-\nu)$ is defined as the elastic stiffness of the rock, a measure of resistance of rock to deformation. The bar on the integral sign represents the Cauchy principal value. The fracture will only extend when the net pressure of the fluid

$$p = p_f + \sigma_{zz}^{\infty} \tag{4.5.7}$$

is positive. Using (4.5.5) and (4.5.7), (4.5.6) becomes

$$p(t,x) = -\frac{2G}{\pi(1-\nu)} \int_0^{L(t)} \frac{\partial h(t,s)}{\partial s} \frac{s}{(s^2 - x^2)} \mathrm{d}s. \tag{4.5.8}$$

Substituting the dimensionless variables into (4.5.8) yields

$$P\bar{p}(\bar{t},\bar{x}) = -\frac{2GH}{\pi(1-\nu)L_0} \int_0^{\bar{L}(\bar{t})} \frac{\partial \bar{h}(\bar{t},\bar{s})}{\partial \bar{s}} \frac{\bar{s}}{\bar{s}^2 - \bar{x}^2} \mathrm{d}\bar{s}. \tag{4.5.9}$$

Suppressing the overhead bars, in dimensionless form, equation (4.5.9) becomes

$$p(t,x) = -\frac{2}{\pi} \int_0^{L(t)} \frac{\partial h}{\partial s} \frac{s}{s^2 - x^2} \mathrm{d}s, \tag{4.5.10}$$

where

$$P = \frac{GH}{(1-\nu)L_0} \tag{4.5.11}$$

is another scale for pressure. Equating (4.3.11) and (4.5.11) for the characteristic pressure, we find that characteristic velocity is

$$U = \frac{GH^3}{\mu(1-\nu)L_0^2}. \tag{4.5.12}$$

4.5.2 *Fracture propagation criterion and the stress intensity factor*

Early pioneers of fracture mechanics have published a lot of works on fracture propagation criterion for solid materials. These works laid a solid foundation for research in this area. Griffith [29] used an energy-balance approach on brittle materials to develop a model that can accurately predict the relationship between critical stress and the crack size.

However, his model failed when applied to metals. This was due to the assumption that the surface energy is the sole cause of fracture growth, which is only applicable for brittle materials. The failure was later corrected, at least in part, through the work of Irwin [38] and Orowan [64]. Irwin [38] proposed a similar energy approach to fracture propagation criterion. He presented the concept of energy release rate $\mathcal{G}$ which is the measure of energy release required for an increment of fracture extension. He suggested that the fracture will propagate when $\mathcal{G}$ reaches a critical value $\mathcal{G}_c$ where $\mathcal{G}_c$ is taken to be the critical strain energy release rate or fracture toughness. In plane stress the modified Griffith equation is:

$$\sigma_f = \sqrt{\frac{E\mathcal{G}_c}{\pi a}}, \tag{4.5.13}$$

where σ_f is the stress level, E the Young's modulus and a the fracture length. While the energy-balance approach proposed by both Griffith [29] and Irwin [38] provides a great deal of insight into the fracturing process, an alternative approach that considers the stress state near the fracture tip has proven to be extremely useful in engineering. This approach is characterized by a constant K that describes the behaviour of a linear elastic material at the fracture tip. In this research, we will use the stress intensity factor approach for fracture propagation criterion. The stress intensity factor, K, is defined by [39]

$$-p(t,x) \to \frac{K}{[2(x-L(t))]^{\frac{1}{2}}} \quad \text{as} \quad x \to L(t)^+. \tag{4.5.14}$$

Substituting the dimensionless variables into (4.5.14) yields

$$-P\bar{p}(\bar{t},\bar{x}) \to \frac{[K]\gamma}{[2L_0(\bar{x}-\bar{L}(\bar{t}))]^{\frac{1}{2}}} \quad \text{as} \quad x \to L^+ \tag{4.5.15}$$

where $P = GH/(1-\nu)L_0$. Dropping the overhead bars, in dimensionless form, equation (4.5.15) becomes

$$-p(t,x) \to \frac{\gamma}{[2(x-L(t))]^{\frac{1}{2}}}, \quad \text{as} \quad x \to L^+ \tag{4.5.16}$$

where $[K] = GH/(1-\nu)\sqrt{L_0}$ and γ is taken to be the dimensionless stress intensity factor.

4.6 NONLINEAR DIFFUSION EQUATION WITH LEAK-OFF VELOCITY TERM

In this section, we will derive the nonlinear diffusion equation governing the evolution of the hydraulic fracture half-width. The resulting partial differential equation will relate the fracture half-width $h(t,x)$ to the fluid pressure $p(t,x)$ and the leak-off velocity $v_n(t,x)$.

As a result of equation (4.4.10), we find that $p = p(t,x)$. We now integrate the mass conservation equation across the fracture width to obtain

$$v_z(t,x,h) - v_z(t,x,-h) + \int_{-h}^{h} \frac{\partial v_x(t,x,z)}{\partial x} \mathrm{d}z = 0. \tag{4.6.1}$$

Imposing the boundary conditions (4.4.13) and (4.4.14), (4.6.1) becomes

$$2\left(\frac{\partial h}{\partial t} + v_n(t,x)\right) + \int_{-h}^{h} \frac{\partial v_x(t,x,z)}{\partial x} \mathrm{d}z = 0. \tag{4.6.2}$$

Using the differentiation under the integral sign (see Appendix C) in conjunction with the boundary conditions (4.4.11) and (4.4.12), the integral term in (4.6.2) can be written as

$$\int_{-h}^{h} \frac{\partial v_x(t,x,z)}{\partial x} dz = \frac{\partial}{\partial x} \int_{-h}^{h} v_x(t,x,z) \mathrm{d}z. \tag{4.6.3}$$

Consequently, equation (4.6.2) becomes

$$2\left(\frac{\partial h}{\partial t} + v_n(t,x)\right) + \frac{\partial}{\partial x} \int_{-h}^{h} v_x(t,x,z) \mathrm{d}z = 0. \tag{4.6.4}$$

Now, in order to derive the expression for the fluid velocity along the fracture $v_x(t,x)$, we integrate (4.4.9) subject to the boundary conditions (4.4.11) and (4.4.12) to obtain

$$v_x(t,x,z) = \frac{1}{2}\frac{\partial p}{\partial x}\left[z^2 - h^2\right]. \tag{4.6.5}$$

The fluid-driven fracture is long and thin, and therefore, as shown in (4.4.10), the fluid pressure does not vary along the z-direction. It is therefore reasonable to define the fluid flow in the fracture in terms of the average fluid velocity $v_x^*(t,x)$ which is independent of the z coordinate and given by

$$v_x^*(t,x) = \frac{1}{2h} \int_{-h}^{h} v_x(t,x,z) \mathrm{d}z. \tag{4.6.6}$$

In terms of the average fluid velocity, $v_x^*(t,x)$, the total flux of fluid along the fracture is given by

$$Q(t,x) = 2\int_{-h}^{h} v_x(t,x,z) \mathrm{d}z = 4h(t,x) v_x^*(t,x). \tag{4.6.7}$$

Thus, $v_x^*(t,x)$ is the velocity of propagation of the flux of fluid. Substituting (4.6.5) into (4.6.6) and integrating the resulting expression with respect to z from $z = -h$ to $z = h$ yields

$$v_x^* = -\frac{h^2}{3}\frac{\partial p}{\partial x}. \tag{4.6.8}$$

Using (4.6.6) and (4.6.8), (4.6.4) becomes

$$\frac{\partial h}{\partial t} - \frac{1}{3}\frac{\partial}{\partial x}\left(h^3 \frac{\partial p}{\partial x}\right) + v_n = 0. \tag{4.6.9}$$

Equation (4.6.9) is a nonlinear diffusion equation for the fracture half-width containing the leak-off velocity v_n. The fluid pressure is related to the fracture half-width by

$$p(t,x) = -\frac{2}{\pi}\int_0^L \frac{\partial h}{\partial s}\frac{s}{s^2 - x^2}\mathrm{d}s. \tag{4.6.10}$$

Equations (4.6.9) and (4.6.10) are to be solved subject to the boundary conditions

$$h(0,0) = 1, \quad h_x(t,0) = 0, \quad h(L(t),t) = 0, \tag{4.6.12a-c}$$

where

$$-p(t,x) \to \frac{\gamma}{[2(x - L(t))]^{\frac{1}{2}}} \quad \text{as} \quad x \to L^+. \tag{4.6.13}$$

The final condition that can be obtained is the global mass balance equation. The balance law states that the rate of change of the total volume of the fracture must be equal to the difference of the fluid flow into the fracture at the entry and the volume of fluid that has leaked-off at the fracture walls. The balance law can be expressed as

$$\frac{\mathrm{d}V}{\mathrm{d}t} = Q(t,0) - Q_\ell(t,x), \tag{4.6.14}$$

where $\mathrm{d}V/\mathrm{d}t$ is the rate of change of the total volume of the fracture, Q the total volume flux of fluid in the x-direction along the fracture and Q_ℓ the flow rate of the leaked-off fluid. The volume of the fracture, $V(t)$, is

$$V(t) = 4\int_0^{L(t)} h(t,x)\mathrm{d}x, \tag{4.6.15}$$

and the flux of fluid leaving the fracture at the interface, Q_ℓ, is

$$Q_\ell(t,x) = 4\int_0^{L(t)} v_n(t,x,z)\mathrm{d}x. \tag{4.6.16}$$

Using (4.6.8), the volume flux of the fluid in the x-direction along the fracture becomes

$$Q(t,x) = 4\int_0^{h(t,x)} v_x(t,x,z)\mathrm{d}z = 4h(t,x)v_x^*(t,x) = -\frac{4}{3}h^3\frac{\partial p}{\partial x}. \tag{4.6.17}$$

At the fracture entry, $x = 0$, the rate of fluid flow into the fracture

$$Q(t,0) = 4\int_0^{h(t,0)} v_x(t,0,z)\mathrm{d}z = -\frac{4}{3}h^3(t,0)\frac{\partial p(t,0)}{\partial x}. \tag{4.6.18}$$

The global mass balance equation can be equivalently expressed as

$$\begin{aligned}\frac{\mathrm{d}V}{\mathrm{d}t} &= -\frac{4}{3}h^3(t,0)\frac{\partial p(t,0)}{\partial x} - 4\int_0^{L(t)} v_n(t,x)\mathrm{d}x,\\ &= 4h(t,0)v_x^*(t,0) - 4\int_0^{L(t)} v_n(t,x)\mathrm{d}x.\end{aligned} \tag{4.6.19}$$

Substituting the dimensionless variables in (4.3.12) into (4.6.19), we obtain, given that $v_n \sim [v_n]$

$$\frac{HL_0}{T}\frac{\mathrm{d}\overline{V}}{\mathrm{d}\bar{t}} = 4UH\bar{h}(\bar{t},0)\overline{v}_x^*(\bar{t},0) - 4[v_n]L_0\int_0^{\bar{L}(\bar{t})}\overline{v}_n(\bar{t},\bar{x})\mathrm{d}\bar{x}. \tag{4.6.20}$$

Multiplying through by $1/UH$ and dropping the overhead bars, we obtain

$$\frac{\mathrm{d}V}{\mathrm{d}t} = 4h(t,0)v_x^*(t,0) - 4\int_0^{L(t)} v_n(t,x)\mathrm{d}x, \tag{4.6.21}$$

where $v_n \sim UH/L_0$.

Similarity Solution

A transformation which reduces a partial differential equation to an ordinary differential equation is called a similarity transformation. The resulting solution to the partial differential equation obtained by a similarity transformation is called a similarity solution. In this section, we derive the similarity solution for equations (4.6.9) to (4.6.13). We introduce the independent similarity variable $\xi = x/L(t)$ and seek the solution of the form

$$h(t,x) = a(t)f(\xi), \quad v_n(t,x) = r(t)g(\xi), \quad \eta = \frac{s}{L(t)}. \tag{4.6.22a-c}$$

The functions $a(t)$, $r(t)$ and $L(t)$ have to be determined. Substituting (4.6.22a) into (4.6.10), we obtain

$$p(t,x) = -\frac{1}{\pi}\frac{a(t)}{L(t)}\int_0^1 \frac{\mathrm{d}f}{\mathrm{d}\eta}\frac{\eta}{\eta^2-\xi^2}\mathrm{d}\eta, \tag{4.6.23}$$

where η is a similarity variable. If we define

$$p(t,x) = \frac{a(t)}{L(t)}P(\xi), \tag{4.6.24}$$

then

$$P(\xi) = -\frac{2}{\pi}\int_0^1 \frac{\mathrm{d}f}{\mathrm{d}\eta}\frac{\eta}{\eta^2-\xi^2}\mathrm{d}\eta. \tag{4.6.25}$$

Substituting (4.6.22a-c) into (4.6.9) yields

$$-\frac{L^2(t)}{a^3(t)}\frac{\mathrm{d}L}{\mathrm{d}t}\xi\frac{\mathrm{d}f}{\mathrm{d}\xi} + \frac{L^3(t)}{a^4(t)}\frac{\mathrm{d}a}{\mathrm{d}t}f(\xi) - \frac{1}{3}\frac{\mathrm{d}}{\mathrm{d}\xi}\left(f^3\frac{\mathrm{d}P}{\mathrm{d}\xi}\right) + \frac{r(t)L^3(t)}{a^4(t)}g(\xi) = 0.$$

(4.6.26)

In order for the similarity solution to exist it is necessary that (4.6.26) does not depend on variable t. Therefore,

$$\frac{L^2(t)}{a^3(t)}\frac{\mathrm{d}L}{\mathrm{d}t} = c_1, \quad \frac{L^3(t)}{a^4(t)}\frac{\mathrm{d}a}{\mathrm{d}t} = c_2, \quad \frac{r(t)L^3(t)}{a^4(t)} = c_3, \tag{4.6.27a-c}$$

where c_1, c_2,and c_3 are constants. Thus,

$$-c_1\xi\frac{\mathrm{d}f}{\mathrm{d}\xi} + c_2 f(\xi) - f^2\frac{\mathrm{d}f}{\mathrm{d}\xi}\frac{\mathrm{d}P}{\mathrm{d}\xi} - \frac{1}{3}f^3\frac{\mathrm{d}^2P}{\mathrm{d}\xi^2} + c_3 g(\xi) = 0. \tag{4.6.28}$$

We now consider the equation describing the stress intensity factor. Using (4.6.22a-c) and (4.6.24), (4.6.13) becomes

$$-P(\xi) \to \frac{\gamma}{[2(\xi-1)]^{\frac{1}{2}}}\frac{L^{\frac{1}{2}}(t)}{a(t)} \quad \text{as} \quad \xi \to 1^+. \tag{4.6.29}$$

That is,

$$-P(\xi) \to \frac{\gamma}{[2(\xi-1)]^{\frac{1}{2}}} \quad \text{as} \quad \xi \to 1^+, \tag{4.6.30}$$

where

$$a(t) = L^{\frac{1}{2}}(t). \tag{4.6.31}$$

Substituting (4.6.31) into (4.6.27a) and using the boundary condition $L(0) = 1$, yield

$$L(t) = \left(\frac{3}{2}c_1 t + 1\right)^{\frac{2}{3}}. \tag{4.6.32}$$

Then, it follows directly that

$$a(t) = \left(\frac{3}{2}c_1 t + 1\right)^{\frac{1}{3}}, \tag{4.6.33}$$

$$r(t) = c_3 L^{-1}(t) = c_3\left(\frac{3}{2}c_1 t + 1\right)^{-\frac{2}{3}}. \tag{4.6.34}$$

Similarly, using $L(t)$ and $a(t)$ in (4.6.27b), we get that

$$c_1 = 2c_2. \tag{4.6.35}$$

The boundary value problem for the integro-differential system is given by

$$c_2 f(\xi) - 2c_2\xi\frac{\mathrm{d}f}{\mathrm{d}\xi} - \frac{1}{3}\frac{\mathrm{d}}{\mathrm{d}\xi}\left(f^3\frac{\mathrm{d}P}{\mathrm{d}\xi}\right) + c_3 g(\xi) = 0, \tag{4.6.36}$$

$$P(\xi) = -\frac{2}{\pi}\int_0^1 \frac{\mathrm{d}f}{\mathrm{d}\eta}\frac{\eta}{\eta^2-\xi^2}\mathrm{d}\eta, \tag{4.6.37}$$

$$f(0) = 1, \quad f'(0) = 0, \quad f(1) = 0, \tag{4.6.38a-c}$$

where

$$-P(\xi) \to \frac{\gamma}{[2(\xi-1)]^{\frac{1}{2}}} \quad \text{as} \quad \xi \to 1^{+}. \tag{4.6.39}$$

The similarity solutions are given by

$$L(t) = (3c_2 t + 1)^{\frac{2}{3}}, \tag{4.6.40}$$

$$h(t,x) = L^{\frac{1}{2}}(t) f(\xi), \tag{4.6.41}$$

$$v_n(t,x) = c_3 L^{-1}(t) g(\xi), \tag{4.6.42}$$

$$p(t,x) = L^{-\frac{1}{2}}(t) P(\xi). \tag{4.6.43}$$

Substituting (4.6.41) into (4.6.15) where $\xi = x/L(t)$, we obtain

$$V(t) = V_0(3c_2 t + 1), \tag{4.6.44}$$

where

$$V_0 = 4\int_0^1 f(\xi)\mathrm{d}\xi. \tag{4.6.45}$$

From (4.6.41) and (4.6.43),

$$h^3 \frac{\partial p}{\partial x} = f^3 \frac{\mathrm{d}P}{\mathrm{d}\xi}, \tag{4.6.46}$$

so that

$$Q(t,x) = -\frac{4}{3} f^3(\xi) \frac{\mathrm{d}P(\xi)}{\mathrm{d}\xi}. \tag{4.6.47}$$

The fluid flux at the fracture entry, $Q(t,0)$, becomes

$$Q(t,0) = -\frac{4}{3} f^3(0) \frac{\mathrm{d}P(0)}{\mathrm{d}\xi}. \tag{4.6.48}$$

The fluid flux at the fracture entry will therefore be a constant, say Q_0, for the boundary value problem (4.6.36)-(4.6.38a-c) to admit a similarity solution. Substituting (4.6.42) into (4.6.16) gives the fluid leak-off flux at the interface given by

$$Q_\ell = 4c_3 \int_0^1 g(\xi)\mathrm{d}\xi. \tag{4.6.49}$$

Thus, the mass balance equation is then given by

$$12c_2 \int_0^1 f(\xi)\mathrm{d}\xi = -\frac{4}{3} f^3(0) \frac{\mathrm{d}P(0)}{\mathrm{d}\xi} - 4c_3 \int_0^1 g(\xi)\mathrm{d}\xi. \tag{4.6.50}$$

4.7 CONCLUSION

In this chapter, we have considered a mathematical model for a two-dimensional pre-existing fracture propagating in a permeable rock. The governing equations for the flow of the Newtonian fluid in the two-dimensional fracture are the continuity and momentum balance equations. Since the fracture half-width is assumed to vary slowly along its length, such that the ratio of the fracture half-width to the fracture length is sufficiently small, lubrication theory holds. As a result, the governing equations - the continuity and momentum balance equations are simplified using lubrication theory. The Cauchy principal value integral derived from linear elastic fracture mechanics was used to describe the elasticity equation relating the fluid pressure to the fracture half-width. The stress intensity condition given by (4.6.13) is then imposed at the fracture tip.

Using similarity transformation, the system of partial differential equations was reduced to a system ordinary differential equations. The boundary conditions were also expressed in terms of the similarity variables. The integro-differential system has two equations but three unknown dependent variables $f(\xi), P(\xi)$ and $g(\xi)$ to solve for. The system also has two parameters c_2 and c_3 to determine. In Chapter 5 and 6, a form of $g(\xi)$ will be specified in terms of $f(\xi)$ and $f'(\xi)$ respectively, in order to fully solve the integro-differential system. Because the similarity transformation had to satisfy the stress intensity condition (4.6.13), the similarity solution of exponential time dependence was not possible, as previously reported in literature. With the aid of the initial condition $L(0) = 1$, pre-existing solutions are obtained for $L(t), h(t,x), V(t)$ and $p(t,x)$.

Part III

MAIN RESULTS AND CONCLUSIONS

5

LEAK-OFF FLUID VELOCITY PROPORTIONAL TO FRACTURE HALF-WIDTH

5.1 INTRODUCTION

In Chapter 3, we introduced a number of numerical techniques that can be used to solve equations containing Cauchy-type singular integrals. The finite difference method and the spline method gave a better accuracy than the other numerical techniques considered for solving the simple singular integral equation that was used to discuss the numerical methods. Moreover, we observed rapid convergence when using the conventional finite difference approach and the spline method. In this chapter, we will use the finite difference method and the spline method to solve the boundary value problem for the system of integral equations (4.6.36)-(4.6.43). However, in order to solve this system of equations we need to either specify $g(\xi)$ or state a relation between $g(\xi)$ and $f(\xi)$. In this chapter, we begin by specifying a form for $g(\xi)$ which is in direct proportion to $f(\xi)$.

5.2 LEAK-OFF FLUID VELOCITY PROPORTIONAL TO FRACTURE HALF-WIDTH

Consider a relationship between $g(\xi)$ and $f(\xi)$ of the form

$$g(\xi) = \bar{\beta}_1 f(\xi) \quad \text{where} \quad \bar{\beta}_1 = \frac{1}{c_3}\beta_1, \quad \bar{\beta}_1 \in \mathbb{R}. \tag{5.2.1}$$

It follows directly from (4.6.41) and (4.6.42) that

$$v_n(t,x) = \beta_1 \frac{h(t,x)}{L^{\frac{3}{2}}(t)}. \tag{5.2.2}$$

This means that the leak-off velocity is proportional to the fracture half-width, for which $\beta_1 \geqslant 0$. When $\beta_1 > 0$, there is fluid leak-off into the surrounding rock formation. When $\beta_1 = 0$, the rock mass is impermeable and no fluid leaks into the surrounding rock formation. The differential equation (4.6.36) becomes

$$(c_2 + \beta_1) f(\xi) - 2c_2\xi \frac{\mathrm{d}f}{\mathrm{d}\xi} - \frac{1}{3}\frac{\mathrm{d}}{\mathrm{d}\xi}\left(f^3 \frac{\mathrm{d}P}{\mathrm{d}\xi}\right) = 0, \tag{5.2.3}$$

where pressure P is given by equation (4.6.37) and the leak-off fluid velocity in terms of ξ is

$$v_n(t,x) = \beta_1 \frac{f(\xi)}{L(t)}. \tag{5.2.4}$$

Using (5.2.1), the mass balance equation (4.6.50) becomes

$$(12c_2 + 4\beta_1)\int_0^1 f(\xi)\mathrm{d}\xi = -\frac{4}{3}f^3(0)\frac{\mathrm{d}P(0)}{\mathrm{d}\xi}. \tag{5.2.5}$$

The expression for the fluid flux at the fracture entry, Q_0, given by (4.6.48), can be derived in terms of c_2, β_1 and $f(\xi)$. Integrating (5.2.3) with respect to η from ξ to 1, we obtain

$$-f^3(\xi)\frac{\mathrm{d}P}{\mathrm{d}\xi} = (9c_2 + 3\beta_1)\int_\xi^1 f(\eta)\mathrm{d}\eta + 6c_2\xi f(\xi). \tag{5.2.6}$$

When $\xi = 0$,

$$-f^3(0)\frac{\mathrm{d}P(0)}{\mathrm{d}\xi} = (9c_2 + 3\beta_1)\int_0^1 f(\xi)\mathrm{d}\xi. \tag{5.2.7}$$

Multiplying (5.2.7) by 4/3 and using (4.6.48), the fluid flux at the fracture entry in terms of c_2 and β_1 is given by

$$Q_0 = (12c_2 + 4\beta_1)\int_0^1 f(\xi)\mathrm{d}\xi. \tag{5.2.8}$$

Since we know that $f(0) = 1$ and $f(1) = 0$ and that $f(\xi)$ decreases monotonically, we have that

$$\int_0^1 f(\xi)\mathrm{d}\xi < 1, \tag{5.2.9}$$

which implies that

$$Q_0 < 12c_2 + 4\beta_1. \tag{5.2.10}$$

Thus, Q_0, the fluid flux at $x = 0$ is bounded. From (5.2.6), the gradient of the net pressure is given by

$$-\frac{\mathrm{d}P}{\mathrm{d}\xi} = \frac{1}{f^3(\xi)}\left[(9c_2 + 3\beta_1)\int_\xi^1 f(\eta)\mathrm{d}\eta + 6c_2\xi f(\xi)\right]. \tag{5.2.11}$$

Now, the problem is to solve for $f(\xi)$ and $P(\xi)$, the integro-differential system of equations

$$(c_2 + \beta_1)f(\xi) - 2c_2\xi\frac{\mathrm{d}f}{\mathrm{d}\xi} - \frac{1}{3}\frac{\mathrm{d}}{\mathrm{d}\xi}\left(f^3\frac{\mathrm{d}P}{\mathrm{d}\xi}\right) = 0, \tag{5.2.12}$$

$$P(\xi) = -\frac{2}{\pi}\int_0^1 \frac{\mathrm{d}f}{\mathrm{d}\eta}\frac{\eta}{\eta^2 - \xi^2}\mathrm{d}\eta, \tag{5.2.13}$$

subject to

$$f(0) = 1, \quad f'(0) = 0, \quad f(1) = 0, \tag{5.2.14a-c}$$

where

$$P(\xi) \to -\frac{\gamma}{\sqrt{2(\xi - 1)}} \quad \text{as} \quad \xi \to 1^+. \tag{5.2.15}$$

Once $f(\xi)$ and $P(\xi)$ are obtained, $L(t)$, $V(t)$, $h(t,x)$, $v_n(t,x)$ and $p(t,x)$ take the form

$$L(t) = (3c_2t+1)^{\frac{2}{3}}, \tag{5.2.16}$$

$$V(t) = V_0(3c_2t+1), \quad V_0 = 4\int_0^1 f(\xi)\mathrm{d}\xi, \tag{5.2.17}$$

$$h(t,x) = L^{\frac{1}{2}}(t)f(\xi), \tag{5.2.18}$$

$$v_n(t,x) = \beta_1 L^{-1}(t)f(\xi), \tag{5.2.19}$$

$$p(t,x) = L^{-\frac{1}{2}}(t)P(\xi). \tag{5.2.20}$$

The solutions of the integro-differential system depend on the leak-off parameter β_1, the constant c_2, the dimensionless stress intensity factor γ and the fluid flux specified at the fracture entry, Q_0. The values of β_1, γ and Q_0 will be specified prior to the numerical computations while c_2 will be obtained as part of the solution such that equation (5.2.8) is satisfied. It is important to note that for the fracture to grow, it is required that $c_2 > 0$. Then, by rearranging (5.2.8) we have that

$$c_2 = \frac{1}{12}\left[Q_0\left[\int_0^1 f(\xi)\mathrm{d}\xi\right]^{-1} - 4\beta_1\right] > 0. \tag{5.2.21}$$

That is,

$$4\beta_1 < Q_0\left[\int_0^1 f(\xi)\mathrm{d}\xi\right]^{-1}. \tag{5.2.22}$$

Since $f'(0) = 0$, we have that

$$\frac{1}{2} < \int_0^1 f(\xi)\mathrm{d}\xi < 1. \tag{5.2.23}$$

It follows directly that

$$1 < \left[\int_0^1 f(\xi)\mathrm{d}\xi\right]^{-1} < 2. \tag{5.2.24}$$

Hence,

$$4\beta_1 < Q_0\left[\int_0^1 f(\xi)\mathrm{d}\xi\right]^{-1} < 2Q_0, \tag{5.2.25}$$

which implies that

$$\beta_1 \ll \frac{Q_0}{2}. \tag{5.2.26}$$

5.3 TIP ASYMPTOTICS AND THE VELOCITY RATIO

In [20], Fareo and Mason considered the velocity ratio $v_x^*(t,x)/L'(t)$ for a fluid-driven fracture in PKN theory. They found that the velocity ratio function behaves approximately linearly along the fracture, and proceeded to obtaining approximate analytical solution. We will investigate the asymptotic solutions at the fracture tip as well as the behaviour of the velocity ratio at the fracture tip. Later in the chapter, the behaviour of the velocity ratio across the fracture will also be investigated as was done in PKN theory [20]. The velocity ratio is given by

$$\frac{v_x^*(t,x)}{L'(t)} = -\frac{1}{6c_2} f^2(\xi) P'(\xi). \tag{5.3.1}$$

At the tip, we have

$$\frac{v_x^*(t,L(t))}{L'(t)} = -\frac{1}{6c_2} f^2(1) P'(1). \tag{5.3.2}$$

We now seek to determine $f^2(1)P'(1)$.

In Spence and Sharp [82], the asymptotic behaviour for $f(\xi)$ and $P(\xi)$ near the fracture tip were derived for the case $\gamma = 0$ and $\gamma > 0$ for a fracture evolving from a point source. We will determine the asymptotic behaviour for $f(\xi), g(\xi)$ and $P(\xi)$ as $\xi \to 1$ for the case $\gamma = 0$ and $\gamma > 0$ for a pre-existing fracture. When $\gamma > 0$, the evolution of the fracture is analysed in the framework of linear elastic fracture mechanics and it corresponds to toughness driven regime of the KGD model. When $\gamma = 0$, the fracture is said to propagate in the viscosity-dominated regime which corresponds to the PKN and the viscosity driven variant of KGD.

Case: $\gamma = 0$

The asymptotic behaviour of $f(\xi)$ as $\xi \to 1$ is given by

$$f(\xi) \sim \alpha(1-\xi)^r, \tag{5.3.3}$$

where α and r are constants. This asymptotic behaviour satisfies the boundary condition $f(1) = 0$. We now rewrite (5.2.13) as

$$P(\xi) = -\frac{1}{\pi} \fint_{-1}^{1} \frac{\mathrm{d}f}{\mathrm{d}\eta} \frac{\mathrm{d}\eta}{\eta - \xi}. \tag{5.3.4}$$

for simplicity. Differentiating $f(\xi)$ and substituting into (5.3.4), we obtain

$$P(\xi) \sim -\frac{\alpha r}{\pi} \int_{-1}^{1} \frac{(1-\eta)^{r-1}\mathrm{d}\eta}{\eta - \xi} \quad \text{as} \quad \xi \to 1. \tag{5.3.5}$$

On setting $\eta = 1 - (1-\xi)u$, equation (5.3.5) becomes

$$P(\xi) \sim -\frac{\alpha r}{\pi}(1-\xi)^{r-1} \int_0^{\infty} \frac{u^r \mathrm{d}u}{u^2 - u} = \alpha r \cot(\pi r)(1-\xi)^{r-1}, \tag{5.3.6}$$

as $\xi \to 1$. The values for α and γ will be derived from equation (5.2.12). Substituting (5.3.3) and (5.3.6) into (5.2.12), we obtain

$$\begin{aligned}\alpha(c_2+\beta_1)(1-\xi)^r + 2\alpha r c_2(1-\xi)^{r-1} - 2\alpha r c_2(1-\xi)^r \\ -\frac{1}{3}\alpha^4 r(r-1)(4r-2)\cot(\pi r)(1-\xi)^{4r-3} \sim 0,\end{aligned} \tag{5.3.7}$$

as $\xi \to 1$. The balance of dominant terms in (5.3.7) requires that

$$4r-3 = r-1, \tag{5.3.8}$$

which after solving yields $r = 2/3$. Substituting the value of r into (5.3.7) and solving for α, we find

$$\alpha = 3\left(\sqrt{3}c_2\right)^{\frac{1}{3}}.$$

Then the limiting behaviour of $f(\xi), g(\xi)$ and $P(\xi)$ as $\xi \to 1$ are

$$f(\xi) \sim 3\left(\sqrt{3}c_2\right)^{\frac{1}{3}}(1-\xi)^{\frac{2}{3}}, \tag{5.3.9}$$

$$g(\xi) \sim 3\left(\sqrt{3}c_2\right)^{\frac{1}{3}}\bar{\beta}_1(1-\xi)^{\frac{2}{3}}, \tag{5.3.10}$$

$$P(\xi) \sim -\left(\frac{8c_2}{3}\right)^{\frac{1}{3}}(1-\xi)^{-\frac{1}{3}}. \tag{5.3.11}$$

The asymptotic solution for $f(\xi)$ and $P(\xi)$ near $\xi = 1$ depends on the parameter c_2, while the asymptotic behaviour for $g(\xi)$ depends on c_2 and the leak-odd parameter $\bar{\beta}_1$. The parameter c_2 is a measure of the rate of change of fracture volume as given in (5.2.17). From (5.3.9) and (5.3.11), we obtain $f^2(1)P'(1) = -6c_2$. Hence, the velocity ratio at the fracture tip is

$$\frac{v_x^*(t, L(t))}{L'(t)} = 1. \tag{5.3.12}$$

Therefore, the fluid velocity equals the speed of fracture propagation at the fracture tip.

Case: $\gamma > 0$

We seek asymptotic solutions for $f(\xi)$ and $P(\xi)$ as $\xi \to 1$ when the stress intensity factor $\gamma > 0$. The limiting behavior of $f(\xi)$ as $\xi \to 1$ when $\gamma > 0$ is given by the first term of (B.1.21)

$$f(\xi) \sim \gamma(1-\xi^2)^{\frac{1}{2}}. \tag{5.3.13}$$

From (5.2.11), it can be seen that as $\xi \to 1$

$$P'(\xi) \sim -\frac{6c_2}{f^2(\xi)}. \tag{5.3.14}$$

Substituting (5.3.13) into (5.3.14), we find that the pressure gradient as $\xi \to 1$ exhibits the following behaviour

$$P'(\xi) \sim -\Lambda_1 (1-\xi^2)^{-1}, \tag{5.3.15}$$

where

$$\Lambda_1 = \frac{6c_2}{\gamma^2}. \tag{5.3.16}$$

Thus, the asymptotic solutions for $f(\xi)$ and $P(\xi)$ as $\xi \to 1$, which are true for $\gamma > 0$ are

$$f(\xi) \sim \gamma (1-\xi^2)^{\frac{1}{2}}, \tag{5.3.17}$$

$$g(\xi) \sim \gamma \bar{\beta}_1 (1-\xi^2)^{\frac{1}{2}}, \tag{5.3.18}$$

$$P(\xi) \sim \frac{1}{2}\Lambda_1 \ln \left| \frac{1-\xi}{1+\xi} \right|. \tag{5.3.19}$$

Similarly, when $\gamma > 0$ we get that $f^2(1)P'(1) = -6c_2$ and the velocity ratio at the tip is again given by (5.3.12).

Thus for $\gamma \geqslant 0$, the fluid velocity equals the fracture propagation speed at the fracture tip. There is therefore no fluid leak-off and no fluid lag at the fracture tip. Fluid lag is a condition in which the fluid front lags behind the fracture tip as the fracture propagates.

It is important to note that equation (5.3.12) holds for $\gamma \geqslant 0$ since the fluid leak-off vanishes at the fracture tip, for $v_n \propto h$ and at $x = L(t)$, $h = 0$ for which $v_n = 0$. Using (5.3.9) and (5.3.11) for the case $\gamma = 0$ and (5.3.17) and (5.3.19) for $\gamma > 0$, it can be shown that

$$f^3 \frac{\mathrm{d}P}{\mathrm{d}\xi} \sim 2c_2 (3\sqrt{3})^{\frac{2}{3}} f(\xi) \to 0, \tag{5.3.20}$$

and

$$f^3 \frac{\mathrm{d}P}{\mathrm{d}\xi} \sim -\Lambda_1 \gamma^2 f(\xi) \to 0, \tag{5.3.21}$$

as $\xi \to 1$, respectively. The flux of fluid given by (4.6.47) therefore vanishes at the fracture tip. That is

$$Q(t, L(t)) = -\frac{4}{3} f^3(1) \frac{\mathrm{d}P(1)}{\mathrm{d}\xi} = 0. \tag{5.3.22}$$

Equation (5.3.20) and (5.3.21) above can also be verified using (5.2.6). The lubrication approximation however, breaks down at the tip of the fracture for $\gamma \geqslant 0$ since as $\xi \to 1$,

$$\frac{\mathrm{d}f}{\mathrm{d}\xi} = \begin{cases} -(8\sqrt{3}c_2)^{\frac{1}{3}}(1-\xi)^{-\frac{1}{3}}, & \gamma = 0, \\ \frac{-\gamma\xi}{(1-\xi^2)^{\frac{1}{2}}}, & \gamma > 0, \end{cases} \tag{5.3.23}$$

and hence from

$$\frac{\partial h}{\partial x} = L^{-\frac{1}{2}}(t)\frac{\mathrm{d}f}{\mathrm{d}\xi} \to -\infty \quad \text{as} \quad x \to L(t). \tag{5.3.24}$$

The lubrication theory (4.3.2) given by

$$\epsilon = \frac{H}{L_0} \ll 1, \quad \epsilon^2 Re \ll 1, \tag{5.3.25a-b}$$

therefore does not hold near the fracture tip.

5.4 FINITE DIFFERENCE METHOD

The integro-differential system (5.2.12)-(5.2.13) cannot be solved to obtain exact analytical solutions. The finite difference method is first employed to solve the integro-differential system (5.2.12)-(5.2.13) subject to the boundary conditions (5.2.14a-c) where as $\xi \to 1^+$ the fluid pressure satisfies (5.2.15). The parameters c_2 and β_1 in (5.2.12) are such that a value for $\beta_1 > 0$ will be chosen, while c_2 will be solved for as part of the solution using a shooting method. As will be seen, the finite difference method appears to fail to produce a smooth function $f(\xi)$, the reason of which is attributed to the slope of $f(\xi)$ at the tip. To solve, we partition the domain [0, 1] into n-equal sub-intervals given by $[\xi_j, \xi_{j+1}]$, where $\xi_j = j/n$ are the mesh points and $0 \leqslant j \leqslant n-1$. Here, j specifies the jth interval. We use the finite differences to approximate $\mathrm{d}P/\mathrm{d}\xi$ and $\mathrm{d}^2P/\mathrm{d}\xi^2$ such that the points for P are at the midpoints of the underlying mesh points ξ_j. Thus,

$$\frac{\mathrm{d}P}{\mathrm{d}\xi} = \frac{P_{i+\frac{1}{2}} - P_{i-\frac{1}{2}}}{\xi_{i+\frac{1}{2}} - \xi_{i-\frac{1}{2}}} \tag{5.4.1}$$

and

$$\frac{\mathrm{d}^2P}{\mathrm{d}\xi^2} = \frac{P_{i-\frac{3}{2}} - P_{i-\frac{1}{2}} - P_{i+\frac{1}{2}} + P_{i+\frac{3}{2}}}{2\left[\xi_{i+\frac{1}{2}} - \xi_{i-\frac{1}{2}}\right]^2}. \tag{5.4.2}$$

As can be seen in (5.2.13), we position the pressure P at mid-mesh points in order to avoid the singularity at the mesh points. Discretising (5.2.12), we obtain

$$\begin{aligned}(c_2+\beta)f_i - 2c_2 i(f_{i+1} - f_i) - nf_i^2(f_{i+1} - f_i)\left[\frac{P_{i+\frac{1}{2}} - P_{i-\frac{1}{2}}}{\xi_{i+\frac{1}{2}} - \xi_{i-\frac{1}{2}}}\right] \\ - \frac{1}{3}f_i^3\left[\frac{P_{i-\frac{3}{2}} - P_{i-\frac{1}{2}} - P_{i+\frac{1}{2}} + P_{i+\frac{3}{2}}}{2\left[\xi_{i+\frac{1}{2}} - \xi_{i-\frac{1}{2}}\right]^2}\right] = 0,\end{aligned} \tag{5.4.3}$$

where the pressure $P(\xi)$ is descritised as

$$P_{i\pm\alpha} = P(\xi_{i\pm\alpha}) = -\frac{2}{\pi}\int_0^1 \frac{\mathrm{d}f}{\mathrm{d}\eta}\frac{\eta}{\eta^2-\xi_{i\pm\alpha}^2}\mathrm{d}\eta, \quad \alpha = \pm\frac{1}{2}, \pm\frac{3}{2}. \tag{5.4.4}$$

By approximating the integral in (5.4.4) to be the sum of integrals in each sub-interval $[\xi_j, \xi_{j+1}]$ yields

$$P_{i\pm\alpha} = -\frac{2}{\pi}\sum_{j=0}^{n-1}\int_{\xi_j}^{\xi_{j+1}} \frac{\mathrm{d}f}{\mathrm{d}\eta}\frac{\eta}{\eta^2-\xi_{i\pm\alpha}^2}\mathrm{d}\eta. \tag{5.4.5}$$

Assuming that $\mathrm{d}f/\mathrm{d}\eta$ is constant in each sub-interval $[\xi_j, \xi_{j+1}]$ and using forward difference to approximate $\mathrm{d}f/\mathrm{d}\eta$ yields

$$P_{i\pm\alpha} = -\frac{1}{\pi}\sum_{j=0}^{n-1}\left(\frac{f_{j+1}-f_j}{\eta_{j+1}-\eta_j}\right)\int_{\xi_j}^{\xi_{j+1}} \frac{2\eta}{\eta^2-\xi_{i\pm\alpha}^2}\mathrm{d}\eta. \tag{5.4.6}$$

The Cauchy principal value integral in (5.4.6) when evaluated gives

$$\int_{\xi_j}^{\xi_{j+1}} \frac{2\eta\mathrm{d}\eta}{\eta^2-\xi_{i\pm\alpha}^2} = \ln\left|\frac{\xi_{j+1}^2-\xi_{i\pm\alpha}^2}{\xi_j^2-\xi_{i\pm\alpha}^2}\right|, \tag{5.4.7}$$

hence,

$$P_{i\pm\alpha} = -\frac{n}{\pi}\sum_{j=0}^{n-1}(f_{j+1}-f_j)\ln\left|\frac{\xi_{j+1}^2-\xi_{i\pm\alpha}^2}{\xi_j^2-\xi_{i\pm\alpha}^2}\right|. \tag{5.4.8}$$

Using (5.4.8), the first and second derivatives of the pressure become

$$\frac{\mathrm{d}P}{\mathrm{d}\xi} = \frac{P_{i+\frac{1}{2}}-P_{i-\frac{1}{2}}}{\xi_{i+\frac{1}{2}}-\xi_{i-\frac{1}{2}}} = \frac{n^2}{\pi}\sum_{j=0}^{n-1}(f_{j+1}-f_j)r_{i,j}, \tag{5.4.9}$$

$$\frac{\mathrm{d}^2P}{\mathrm{d}\xi^2} = \frac{P_{i-\frac{3}{2}}-P_{i-\frac{1}{2}}-P_{i+\frac{1}{2}}+P_{i+\frac{3}{2}}}{2\left[\xi_{i+\frac{1}{2}}-\xi_{i-\frac{1}{2}}\right]^2} = \frac{n^3}{2\pi}\sum_{j=0}^{n-1}(f_{j+1}-f_j)s_{i,j}, \tag{5.4.10}$$

where

$$r_{i,j} = \ln\left|\frac{(2j-2i+3)(2j+2i+1)^2(2j-2i-1)}{(2j+2i-1)(2j-2i+1)^2(2j+2i+3)}\right|, \tag{5.4.11}$$

and

$$s_{i,j} = \ln\left|\frac{(2j+2i+3)^2(2j-2i+3)^2(2j-2i-3)(2j+2i-3)}{(2j-2i-1)^2(2j+2i-1)^2(2j+2i+5)(2j-2i+5)}\right|. \tag{5.4.12}$$

Equation (5.4.3) then becomes

$$\begin{aligned}(c_2+\beta)f_i - 2c_2 i(f_{i+1}-f_i) - \frac{n^3}{\pi}f_i^2(f_{i+1}-f_i)\sum_{j=0}^{n-1}(f_{j+1}-f_j)r_{i,j} \\ - \frac{n^3}{6\pi}f_i^3\sum_{j=0}^{n-1}(f_{j+1}-f_j)s_{i,j} = 0.\end{aligned} \tag{5.4.13}$$

Equation (5.4.13) is only valid for $2 \leqslant i \leqslant n-2$ for which we have $n-3$ equations. After imposing boundary conditions, there will be $n-2$ unknowns to solve for. An extra equation is needed to uniquely determine the solutions and this equation is obtained at the $(n-1)^{\text{th}}$ node. When $i = n-1$, the second derivative of the pressure is given by

$$\frac{\mathrm{d}^2 P}{\mathrm{d}\xi^2} = \frac{P_{n-\frac{5}{2}} - P_{n-\frac{3}{2}} - P_{n-\frac{1}{2}} + P_{n+\frac{1}{2}}}{2\left(\xi_{n-\frac{1}{2}} - \xi_{n-\frac{3}{2}}\right)^2}. \tag{5.4.14}$$

It can be seen that the node $\xi_{n+1/2}$ lies outside the interval $[0, 1]$. As a remedy, we impose the pressure condition just outside the crack tip given by

$$-P\left(\xi_{n+\frac{1}{2}}\right) \sim \frac{\gamma}{\left[2\left(\xi_{n+\frac{1}{2}} - 1\right)\right]^{\frac{1}{2}}} = \gamma\sqrt{n}\,, \tag{5.4.15}$$

since $\xi_{n+1/2} = 1 + 1/2n$, where γ is the dimensionless stress intensity factor. Equation (5.2.12) for $n-1$ becomes

$$\begin{aligned}(c_2+\beta_1)f_{n-1} - 2c_2(n-1)(f_n - f_{n-1}) - \frac{n^3 f_{n-1}^2 (f_n - f_{n-1})}{\pi}\sum_{j=0}^{n-1}(f_{j+1}-f_j)r_{n-1,j} \\ - \frac{f_{n-1}^3}{3}\left[\frac{n^3}{2\pi}\sum_{j=0}^{n-1}(f_{j+1}-f_j)c_{n-1,j} - \frac{\gamma n^{\frac{1}{2}}}{2}\right] = 0,\end{aligned} \tag{5.4.16}$$

where

$$c_{i,j} = \ln\left|\frac{(2j-2i+3)^2(2j+2i-3)(2j+2i+3)}{(2j+2i-1)^2(2j-2i-1)(2j-2i+5)}\right|. \tag{5.4.17}$$

Now, for any choice of $n \geqslant 4$, we will have the following system of nonlinear equations

$$\begin{aligned}i = 2: \quad & (c_2+\beta_1)f_2 - 4c_2(f_3 - f_2) \\ & - \frac{n^3}{\pi} f_2^2 (f_3 - f_2)\sum_{j=1}^{n-1}(f_{j+1}-f_j)r_{2,j} \\ & - \frac{n^3}{6\pi} f_2^3 \sum_{j=1}^{n-1}(f_{j+1}-f_j)s_{2,j} = 0,\end{aligned} \tag{5.4.18}$$

$$\begin{aligned}i = 3: \quad & (c_2+\beta_1)f_3 - 6c_2(f_4 - f_3) \\ & - \frac{n^3}{\pi} f_3^2 (f_4 - f_3)\sum_{j=1}^{n-1}(f_{j+1}-f_j)r_{3,j} \\ & - \frac{n^3}{6\pi} f_3^3 \sum_{j=1}^{n-1}(f_{j+1}-f_j)s_{3,j} = 0,\end{aligned} \tag{5.4.19}$$

$$
\begin{aligned}
&\vdots \qquad\qquad \vdots \qquad\qquad \vdots \\
&i = n-2 : (c_2+\beta_1)f_{n-2} - 2c_2(n-2)(f_{n-1}-f_{n-2}) \\
&\qquad - \frac{n^3 f_{n-2}^2 (f_{n-1}-f_{n-2})}{\pi} \sum_{j=0}^{n-1} (f_{j+1}-f_j) r_{n-2,j} \\
&\qquad - \frac{n^3}{6\pi} f_{n-2}^3 \sum_{j=1}^{n-1} (f_{j+1}-f_j) s_{n-2,j} = 0,
\end{aligned}
\tag{5.4.20}
$$

$$
\begin{aligned}
&i = n-1 : (c_2+\beta_1)f_{n-1} - 2c_2(n-1)(f_n-f_{n-1}) \\
&\qquad - \frac{n^3 f_{n-1}^2 (f_n-f_{n-1})}{\pi} \sum_{j=0}^{n-1} (f_{j+1}-f_j) r_{n-1,j} \\
&\qquad - \frac{f_{n-1}^3}{3} \left[\frac{n^3}{2\pi} \sum_{j=0}^{n-1} (f_{j+1}-f_j) c_{n-1,j} - \frac{\gamma n^{\frac{1}{2}}}{2} \right] = 0.
\end{aligned}
\tag{5.4.21}
$$

To this point, we have managed to set up the system of nonlinear equations that will be solved for f_i, $i = 2, 3, \ldots, n-1$. In the next section, we outline and discuss the Newton-Raphson method for solving a system of nonlinear equations.

5.5 THE NEWTON-RAPHSON METHOD FOR A SYSTEM OF EQUATIONS

The Newton-Raphson formula for a single-equation can be easily derived from the first-order Taylor series expansion of $f(x)$ about x:

$$f(x_{i+1}) = f(x_i) + (x_{i+1} - x_i) f'(x_i) \tag{5.5.1}$$

where x_i is the initial guess of the solution or root and x_{i+1} is the improved solution. If x_{i+1} is the root of $f(x) = 0$, then equation (5.5.1) becomes

$$0 = f(x_i) + (x_{i+1} - x_i) f'(x_i), \tag{5.5.2}$$

which after solving for x_{i+1} gives

$$x_{i+1} = x_i - \frac{f(x_i)}{f'(x_i)}. \tag{5.5.3}$$

Equation (5.5.3) is the Newton-Raphson formula for a single-equation. We will now derive the Newton-Raphson formula for a system of equations in the same fashion to the single-equation form.

Let us consider an n-dimensional problem given by

$$
\begin{aligned}
&f_1(x_1, x_2, \ldots, x_n) = 0, \\
&f_2(x_1, x_2, \ldots, x_n) = 0, \\
&\qquad \vdots \qquad\qquad \vdots \\
&f_n(x_1, x_2, \ldots, x_n) = 0.
\end{aligned}
\tag{5.5.4}
$$

The solution of (5.5.4) are the values of the x's that makes the system of equations equal to zero. Determining the values of these x's for the n simultaneous equations is a much more difficult task than that of finding the root of a single-equation problem. The most effective yet simple technique for determining the solution vector $\boldsymbol{x}$ is the Newton-Raphson method. In order to derive the multiple-equation form of the Newton-Raphson method, we first start by writing the first-order Taylor series expansion for each of the equations as

$$f_{1,i+1} = f_{1,i} + (x_{1,i+1} - x_{1,i})\frac{\partial f_{1,i}}{\partial x_1} + (x_{2,i+1} - x_{2,i})\frac{\partial f_{1,i}}{\partial x_2} + \cdots + (x_{n,i+1} - x_{n,i})\frac{\partial f_{1,i}}{\partial x_n} \tag{5.5.5}$$

$$f_{2,i+1} = f_{2,i} + (x_{1,i+1} - x_{1,i})\frac{\partial f_{2,i}}{\partial x_1} + (x_{2,i+1} - x_{2,i})\frac{\partial f_{2,i}}{\partial x_2} + \cdots + (x_{n,i+1} - x_{n,i})\frac{\partial f_{2,i}}{\partial x_n} \tag{5.5.6}$$

$$\vdots \qquad\qquad \vdots$$

$$f_{n,i+1} = f_{n,i} + (x_{1,i+1} - x_{1,i})\frac{\partial f_{n,i}}{\partial x_1} + (x_{2,i+1} - x_{2,i})\frac{\partial f_{n,i}}{\partial x_2} + \cdots + (x_{n,i+1} - x_{n,i})\frac{\partial f_{n,i}}{\partial x_n} \tag{5.5.7}$$

where

$$[f_{1,i}, \ldots, f_{n,i}] = [f_1(x_{1,i}, x_{2,i}, \ldots, x_{n,i}), \ldots, f_n(x_{1,i}, x_{2,i}, \ldots, x_{n,i})]. \tag{5.5.8}$$

If

$$\boldsymbol{x}_{i+1} = [x_{1,i+1}, x_{2,i+1}, \ldots, x_{n,i+1}]^T \tag{5.5.9}$$

is the solution vector then

$$\boldsymbol{f}_{i+1} = [f_{1,i+1}, f_{2,i+1}, \ldots, f_{n,i+1}]^T \tag{5.5.10}$$

will be equal to zero. In this case, the system of equations (5.5.5)-(5.5.7) becomes, after rearranging,

$$\frac{\partial f_{1,i}}{\partial x_1}x_{1,i+1} + \frac{\partial f_{1,i}}{\partial x_2}x_{2,i+1} + \cdots + \frac{\partial f_{1,i}}{\partial x_n}x_{n,i+1} = -f_{1,i} + x_{1,i}\frac{\partial f_{1,i}}{\partial x_1} + x_{2,i}\frac{\partial f_{1,i}}{\partial x_2} + \cdots + x_{n,i}\frac{\partial f_{1,i}}{\partial x_n} \tag{5.5.11}$$

$$\frac{\partial f_{2,i}}{\partial x_1}x_{1,i+1} + \frac{\partial f_{2,i}}{\partial x_2}x_{2,i+1} + \cdots + \frac{\partial f_{2,i}}{\partial x_n}x_{n,i+1} = -f_{2,i} + x_{1,i}\frac{\partial f_{2,i}}{\partial x_1} + x_{2,i}\frac{\partial f_{2,i}}{\partial x_2} + \cdots + x_{n,i}\frac{\partial f_{2,i}}{\partial x_n} \tag{5.5.12}$$

$$\begin{aligned}\frac{\partial f_{n,i}}{\partial x_1}x_{1,i+1}+\frac{\partial f_{n,i}}{\partial x_2}x_{2,i+1}+\cdots+\frac{\partial f_{n,i}}{\partial x_n}x_{n,i+1}&=-f_{n,i}\\ +x_{1,i}\frac{\partial f_{n,i}}{\partial x_1}+x_{2,i}\frac{\partial f_{n,i}}{\partial x_2}+\cdots+x_{n,i}\frac{\partial f_{n,i}}{\partial x_n}&\end{aligned} \tag{5.5.13}$$

The system of equations (5.5.11)-(5.5.13) can be expressed in terms of matrix notation as

$$\boldsymbol{J}(\boldsymbol{x})\boldsymbol{x}_{i+1}=-\boldsymbol{f}(\boldsymbol{x})+\boldsymbol{J}(\boldsymbol{x})\boldsymbol{x}_i, \tag{5.5.14}$$

or more compactly

$$\boldsymbol{J}(\boldsymbol{x})\Delta\boldsymbol{x}=-\boldsymbol{f}(\boldsymbol{x}), \tag{5.5.15}$$

where $\Delta\boldsymbol{x}=\boldsymbol{x}_{i+1}-\boldsymbol{x}_i$ and $J(\boldsymbol{x})$ is the Jacobian matrix consisting of the partial derivatives, i.e.,

$$\boldsymbol{J}(\boldsymbol{x})=\begin{bmatrix}\frac{\partial f_{1,i}}{\partial x_1} & \frac{\partial f_{1,i}}{\partial x_2} & \cdots & \frac{\partial f_{1,i}}{\partial x_n}\\ \frac{\partial f_{2,i}}{\partial x_1} & \frac{\partial f_{2,i}}{\partial x_2} & \cdots & \frac{\partial f_{2,i}}{\partial x_n}\\ \vdots & \vdots & \ddots & \vdots\\ \frac{\partial f_{n,i}}{\partial x_1} & \frac{\partial f_{n,i}}{\partial x_2} & \cdots & \frac{\partial f_{n,i}}{\partial x_n}\end{bmatrix}.$$

Equation (5.5.15) can be solved using the Gaussian elimination method. Alternatively, we can solve (5.5.14) by multiplying both sides of (5.5.14) with the inverse of the Jacobian to obtain

$$\boldsymbol{x}_{i+1}=\boldsymbol{x}_i-\boldsymbol{J}^{-1}(\boldsymbol{x})\boldsymbol{f}(\boldsymbol{x}). \tag{5.5.16}$$

The algorithm below outlines the steps for the Newton-Raphson method for simultaneous equations:

Algorithm 1 Algorithm to compute the Newton-Raphson method.

Step 1 Initialize the solution vector $\boldsymbol{x}$

Step 2 Evaluate $\boldsymbol{f}(\boldsymbol{x})$

Step 3 Compute the Jacobian matrix $\boldsymbol{J}(\boldsymbol{x})$

Step 4 Set up the simultaneous equations in (5.5.15) *and solve for* $\Delta\boldsymbol{x}$

Step 5 Let $\boldsymbol{x}\leftarrow\boldsymbol{x}+\Delta\boldsymbol{x}$ *and repeat step 2 to 5.*

The process should be continued until a stopping criteria is satisfied, e.g, $||\boldsymbol{x}_{i+1}-\boldsymbol{x}_i||_\infty/||\boldsymbol{x}_{i+1}||_\infty<\varepsilon$, where ε is the error tolerance. It must be noted that the success of the Newton-Raphson method depends mostly on the starting point, that is, a good initial estimate of $\boldsymbol{x}$ will converge to the root rapidly.

5.6 DISCUSSION ON NUMERICAL METHOD

The boundary value problem for an integro-differential system, given by (5.2.12)-(5.2.14a-c) may now be solved numerically. The problem was discretised in Section 5.4. We partitioned domain $[0, 1]$ into n equal sub-intervals given by $[\xi_j, \xi_{j+1}]$ for $0 \leqslant j \leqslant n-1$ on the interval [0, 1], where n is taken to be the number of sub-intervals. We then assumed that $f'(\xi)$ is constant in each sub-interval $[\xi_j, \xi_{j+1}]$ and can be approximated by finite differences. The first and second derivatives of $P(\xi)$ were also approximated by finite differences and positioned at the mid-grid points because of the singularity of the pressure at the grid points. It was noticed that when $i = n-1$, it was not possible to determine the second derivative of $P(\xi)$ using (5.4.8) since the node $\xi_{n+1/2}$ lies outside the interval $[0, 1]$. We imposed the stress intensity factor condition given by (5.2.15) to overcome this challenge.

The problem was then to solve the system of nonlinear algebraic equations (5.4.13) for $2 \leqslant i \leqslant n-2$ and (5.4.21) subject to the boundary conditions (5.2.14a-c). The system was solved iteratively for values of f at the nodes using the Newton-Raphson method with some specified tolerance. The accuracy of the results obtained were confirmed using a Matlab built-in nonlinear system solver *fsolve*. The Levenberg-Marquardt algorithm was specified within the *fsolve* optimization options. The Levenberg-Marquardt algorithm is a hybrid technique that uses both the steepest descent and the Gauss-Newton method to find the minimum of a function. The two numerical results showed close agreement. The initial solution was taken to be the function $f(\xi) = \sqrt[3]{1-\xi}$, for $\xi \in [0, 1]$. The leak-off parameter β_1, the fluid flux at the fracture entry Q_0 and the dimensionless stress intensity factor γ were prescribed such that $\beta_1 < Q_0/2$. The parameter c_2 is to be solved for as part of the solution. We iterate based on the bisection method by solving the nonlinear system with varying values of c_2 until a value of c_2 is obtained for which the condition (5.2.8) given by

$$Q_0 = (12c_2 + 4\beta_1) \int_0^1 f(\xi) \mathrm{d}\xi \tag{5.6.1}$$

is satisfied. Thus, the value of c_2 is obtained directly from the numerical solution. In order to check accuracy of the numerical results, $Q_0, f(\xi)$ and $\frac{\mathrm{d}P(\xi)}{\mathrm{d}\xi}$ at $\xi = 0$ satisfies

$$Q_0 = -\frac{4}{3} f^3(0) \frac{\mathrm{d}P(0)}{\mathrm{d}\xi}. \tag{5.6.2}$$

It was not possible to determine $P'(0)$ using (5.2.13) since the points for $P(\xi)$ are at the midpoints of the underlying mesh points and $P(0)$ could not be evaluated. The pressure gradient at $\xi = 0$ on the right hand side of (5.6.2) was obtained using (5.2.11) and the value of $f(0)$ from the solution of $f(\xi)$. It is worth mentioning that an attempt was

made to determine the pressure gradient at $\xi = 0$ by first obtaining the solution of $P(\xi)$ using equation (5.2.13). To do this, we first numerically differentiated $f(\xi)$ and then substituted into (5.2.13) to obtain the mid-point values of the pressure. Afterwards, we calculated the values of $P(\xi)$ at the grid points using a Matlab built-in interpolation function *interp1*. The values of $P(\xi)$ at the grid points can alternatively be obtained using the following finite difference approximation

$$P_i = \frac{P_{i+\frac{1}{2}} + P_{i-\frac{1}{2}}}{2}. \tag{5.6.3}$$

Once we obtained the grid points for $P(\xi)$, we then numerically differentiated $P(\xi)$ to obtain the pressure gradient. It was found that the value of the pressure gradient at $\xi = 0$ changed as we changed the interpolation method, i.e., $P'(0)$ obtained using linear interpolation was different from $P'(0)$ obtained using spline interpolation. As a result, this approach was only used for determining $P(\xi)$ and not the pressure gradient.

Once (5.6.2) was also satisfied, the solution of $f(\xi)$ was substituted into (5.2.18) and (5.2.19) to obtain functions $h(t,x)$ and $v_n(t,x)$, and the solution of $P(\xi)$ substituted into (5.2.20) to obtain $p(t,x)$.

Here, we illustrates the behaviour of $f(\xi)$ when plotted against ξ for a range of values of n given by $n = 50, 80, 100$ for the case where $\beta_1 = 0.01$, $Q_0 = 0.2$ and $\gamma = 0.5$. A variation in the value of any of these parameters did not affect the behaviour of $f(\xi)$. The solutions obtained are illustrated in Figure 17, in which the graph of $f(\xi)$ against ξ does not produce a smooth curve, for the values $n = 50, 80, 100$. This behaviour is however not surprising since from (5.3.9) and (5.3.17), the problem possesses a singularity in the slope of $f(\xi)$ as $f'(\xi) \to -\infty$ near $\xi = 1$. It is this singularity in $f'(\xi)$ at $\xi = 1$ which disrupts the finite difference method. We encountered a similar problem in Chapter 3 when solving a simple singular integral equation.

5.7 SPLINE METHOD

It is obvious from the asymptotic solutions (5.3.9) and (5.3.17) that there is a singularity in the slope of $f(\xi)$ as $f'(\xi) \to -\infty$ near $\xi = 1$. It is this singularity that led to non-smooth curves when using the finite difference method. As a remedy, we extract the tip behaviour of the similarity function $f(\xi)$, and then use a linear spline to represent the remaining part of $f(\xi)$. To do this, we partition [0, 1] into n equal sub-intervals and take $f(\xi)$ in each sub-interval to be of the form

$$f_i(\xi) = (1 - \xi^2)^{\frac{1}{2}} \Pi_i(\xi), \tag{5.7.1}$$

where $\Pi_i(\xi)$ is a piece-wise linear function given by

$$\Pi_i(\xi) = a_i \xi + b_i. \tag{5.7.2}$$

(i)

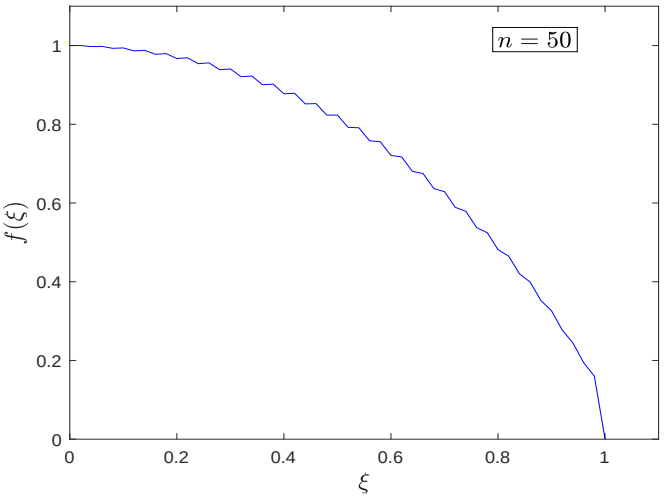

(ii)

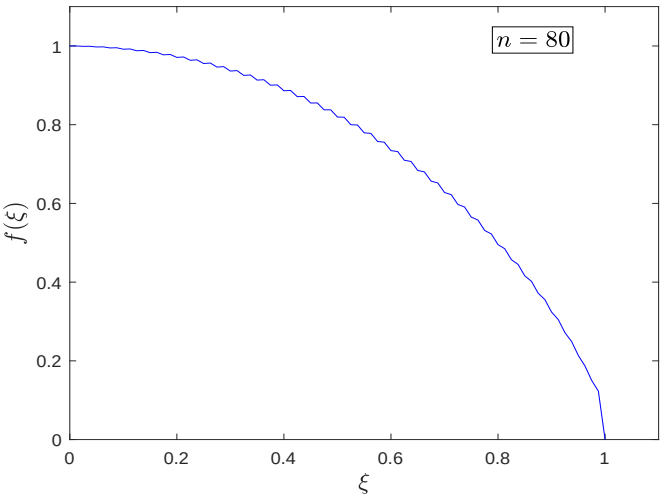

(iii)

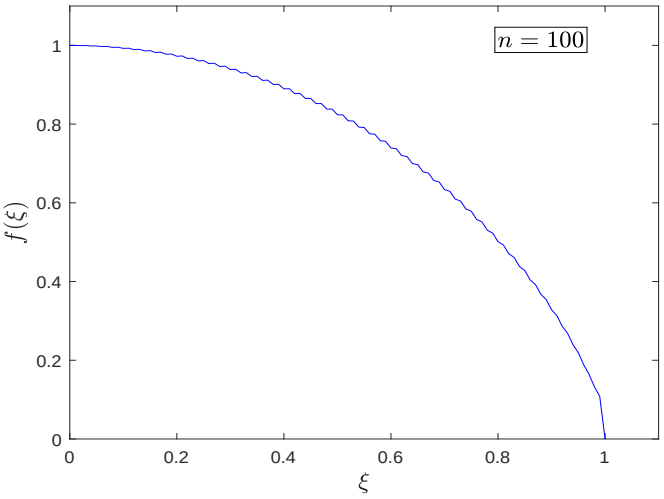

Figure 17: Graph of $f(\xi)$ plotted against ξ for $\beta_1 = 0.01$, $Q_0 = 0.2$, $\gamma = 0.5$ when (i) $n = 50$, (ii) $n = 80$ and (iii) $n = 100$.

Dividing the interval [0,1] into n sub-intervals $[\eta_j, \eta_{j+1}], j = 0, 1, \ldots, n-1$ and after substituting (5.7.1) into (5.2.13), we obtain

$$P_{i\pm\alpha} = -\frac{2}{\pi}\sum_{j=0}^{n-1}\left[\fint_{\eta_j}^{\eta_{j+1}} \frac{\eta(1-2\eta^2)a_j d\eta}{(\eta^2-\xi_{i\pm\alpha}^2)\sqrt{1-\eta^2}} - \fint_{\eta_j}^{\eta_{j+1}} \frac{\eta^2 b_j d\eta}{(\eta^2-\xi_{i\pm\alpha}^2)\sqrt{1-\eta^2}}\right], \tag{5.7.3}$$

where $\alpha = \pm 1/2, \pm 3/2$.

We now show how the Cauchy principal value integrals in (5.7.3) will be evaluated. Consider the first integral on the right hand side of (5.7.3). If we set

$$f_1(\eta, \tau) = \frac{\eta(1-2\eta^2)}{(\eta+\tau)}, \tag{5.7.4}$$

where $\tau = \xi_{j\pm\alpha}$, then

$$\fint_{\eta_j}^{\eta_{j+1}} \frac{\eta(1-2\eta^2)d\eta}{(\eta+\tau)(\eta-\tau)\sqrt{1-\eta^2}} = \fint_{\eta_j}^{\eta_{j+1}} \frac{f_1(\eta,\tau)\,d\eta}{(\eta-\tau)\sqrt{1-\eta^2}}. \tag{5.7.5}$$

We want to integrate

$$\begin{aligned} I &= \fint_{\eta_j}^{\eta_{j+1}} \frac{f_1(\eta,\tau)\,d\eta}{(\eta-\tau)\sqrt{1-\eta^2}} = I_- + I_+ \\ &= \lim_{\epsilon\to 0^+}\left[\int_{\eta_j}^{\tau-\epsilon} \frac{f_1(\eta,\tau)\,d\eta}{(\eta-\tau)\sqrt{1-\eta^2}} + \int_{\tau+\epsilon}^{\eta_{j+1}} \frac{f_1(\eta,\tau)\,d\eta}{(\eta-\tau)\sqrt{1-\eta^2}}\right]. \end{aligned} \tag{5.7.6}$$

To do so, we subtract the singularity so that we are left with some integral we can integrate numerically. We do so in the following way:

$$\begin{aligned} I_- &= \int_{\eta_j}^{\tau-\epsilon} \frac{f_1(\eta,\tau)-f_1(\tau,\tau)}{(\eta-\tau)\sqrt{1-\eta^2}}d\eta + f_1(\tau,\tau)\int_{\eta_j}^{\tau-\epsilon} \frac{d\eta}{(\eta-\tau)\sqrt{1-\eta^2}} \\ &\approx \int_{\eta_j}^{\tau-\epsilon} \frac{f_1'(\eta,\tau)\,d\eta}{\sqrt{1-\eta^2}} + f_1(\tau,\tau)\int_{\eta_j}^{\tau-\epsilon} \frac{d\eta}{(\eta-\tau)\sqrt{1-\eta^2}}. \end{aligned} \tag{5.7.7}$$

In a similar fashion, we get

$$\begin{aligned} I_+ &= \int_{\tau+\epsilon}^{\eta_{j+1}} \frac{f_1(\eta,\tau)-f_1(\tau,\tau)}{(\eta-\tau)\sqrt{1-\eta^2}}d\eta + f_1(\tau,\tau)\int_{\tau+\epsilon}^{\eta_{j+1}} \frac{d\eta}{(\eta-\tau)\sqrt{1-\eta^2}} \\ &\approx \int_{\tau+\epsilon}^{\eta_{j+1}} \frac{f_1'(\eta,\tau)\,d\eta}{\sqrt{1-\eta^2}} + f_1(\tau,\tau)\int_{\tau+\epsilon}^{\eta_{j+1}} \frac{d\eta}{(\eta-\tau)\sqrt{1-\eta^2}}. \end{aligned} \tag{5.7.8}$$

The whole integral is then given by

$$I = \int_{\eta_j}^{\tau} \frac{f_1'(\eta,\tau)\,d\eta}{\sqrt{1-\eta^2}} + \int_{\tau}^{\eta_{j+1}} \frac{f_1'(\eta,\tau)\,d\eta}{\sqrt{1-\eta^2}} + f_1(\tau,\tau)\fint_{\eta_j}^{\eta_{j+1}} \frac{d\eta}{(\eta-\tau)\sqrt{1-\eta^2}}.$$

(5.7.9)

When evaluated, the last integral in (5.7.9) gives

$$\fint_{\eta_j}^{\eta_{j+1}} \frac{\mathrm{d}\eta}{(\eta-\tau)\sqrt{1-\eta^2}} = \frac{1}{\sqrt{1-\tau^2}} \ln \left| \frac{1+\sqrt{1-\tau^2}\sqrt{1-\eta_j^2}-\tau\eta_j}{1+\sqrt{1-\tau^2}\sqrt{1-\eta_{j+1}^2}-\tau\eta_{j+1}} \right|. \tag{5.7.10}$$

Applying the above analysis on the second integral in (5.7.3), we get

$$\begin{aligned} \fint_{\eta_j}^{\eta_{j+1}} \frac{f_2(\eta,\tau)\mathrm{d}\eta}{(\eta-\tau)\sqrt{1-\eta^2}} = \int_{\eta_j}^{\tau} \frac{f_2'(\eta,\tau)\,\mathrm{d}\eta}{\sqrt{1-\eta^2}} + \int_{\tau}^{\eta_{j+1}} \frac{f_2'(\eta,\tau)\,\mathrm{d}\eta}{\sqrt{1-\eta^2}} \\ + f_2(\tau,\tau) \fint_{\eta_j}^{\eta_{j+1}} \frac{\mathrm{d}\eta}{(\eta-\tau)\sqrt{1-\eta^2}}, \end{aligned} \tag{5.7.11}$$

where

$$f_2(\eta,\xi) = \frac{\eta^2}{\eta+\xi}. \tag{5.7.12}$$

We will apply this analysis to the pressure expression given in (5.7.3) when evaluated at each value of α, that is, when the pressure is

$$\begin{aligned} P_{i-\frac{1}{2}} = -\frac{2}{\pi} \sum_{\substack{j=0 \\ j\neq i-1}}^{n-1} \left[\int_{\eta_j}^{\eta_{j+1}} \frac{\eta(1-2\eta^2)a_j\mathrm{d}\eta}{\left(\eta^2-\xi_{i-\frac{1}{2}}^2\right)\sqrt{1-\eta^2}} - \int_{\eta_j}^{\eta_{j+1}} \frac{\eta^2 b_j\mathrm{d}\eta}{\left(\eta^2-\xi_{i-\frac{1}{2}}^2\right)\sqrt{1-\eta^2}} \right] \\ - \frac{2}{\pi} \left[\fint_{\eta_{i-1}}^{\eta_i} \frac{\eta(1-2\eta^2)a_j\mathrm{d}\eta}{\left(\eta^2-\xi_{i-\frac{1}{2}}^2\right)\sqrt{1-\eta^2}} - \fint_{\eta_{i-1}}^{\eta_i} \frac{\eta^2 b_j\mathrm{d}\eta}{\left(\eta^2-\xi_{i-\frac{1}{2}}^2\right)\sqrt{1-\eta^2}} \right], \end{aligned} \tag{5.7.13}$$

$$\begin{aligned} P_{i+\frac{1}{2}} = -\frac{2}{\pi} \sum_{\substack{j=0 \\ j\neq i}}^{n-1} \left[\int_{\eta_j}^{\eta_{j+1}} \frac{\eta(1-2\eta^2)a_j\mathrm{d}\eta}{\left(\eta^2-\xi_{i+\frac{1}{2}}^2\right)\sqrt{1-\eta^2}} - \int_{\eta_j}^{\eta_{j+1}} \frac{\eta^2 b_j\mathrm{d}\eta}{\left(\eta^2-\xi_{i+\frac{1}{2}}^2\right)\sqrt{1-\eta^2}} \right] \\ - \frac{2}{\pi} \left[\fint_{\eta_i}^{\eta_{i+1}} \frac{\eta(1-2\eta^2)a_j\mathrm{d}\eta}{\left(\eta^2-\xi_{i+\frac{1}{2}}^2\right)\sqrt{1-\eta^2}} - \fint_{\eta_i}^{\eta_{i+1}} \frac{\eta^2 b_j\mathrm{d}\eta}{\left(\eta^2-\xi_{i+\frac{1}{2}}^2\right)\sqrt{1-\eta^2}} \right], \end{aligned} \tag{5.7.14}$$

$$P_{i-\frac{3}{2}} = -\frac{2}{\pi}\sum_{\substack{j=0\\ j\neq i-2}}^{n-1}\left[\int_{\eta_j}^{\eta_{j+1}}\frac{\eta(1-2\eta^2)a_j\mathrm{d}\eta}{\left(\eta^2-\xi_{i-\frac{3}{2}}^2\right)\sqrt{1-\eta^2}}-\int_{\eta_j}^{\eta_{j+1}}\frac{\eta^2 b_j\mathrm{d}\eta}{\left(\eta^2-\xi_{i-\frac{3}{2}}^2\right)\sqrt{1-\eta^2}}\right]$$
$$-\frac{2}{\pi}\left[\int_{\eta_{i-2}}^{\eta_{i-1}}\frac{\eta(1-2\eta^2)a_j\mathrm{d}\eta}{\left(\eta^2-\xi_{i-\frac{3}{2}}^2\right)\sqrt{1-\eta^2}}-\int_{\eta_{i-2}}^{\eta_{i-1}}\frac{\eta^2 b_j\mathrm{d}\eta}{\left(\eta^2-\xi_{i-\frac{3}{2}}^2\right)\sqrt{1-\eta^2}}\right], \tag{5.7.15}$$

$$P_{i+\frac{3}{2}} = -\frac{2}{\pi}\sum_{\substack{j=0\\ j\neq i+1}}^{n-1}\left[\int_{\eta_j}^{\eta_{j+1}}\frac{\eta(1-2\eta^2)a_j\mathrm{d}\eta}{\left(\eta^2-\xi_{i+\frac{3}{2}}^2\right)\sqrt{1-\eta^2}}-\int_{\eta_j}^{\eta_{j+1}}\frac{\eta^2 b_j\mathrm{d}\eta}{\left(\eta^2-\xi_{i+\frac{3}{2}}^2\right)\sqrt{1-\eta^2}}\right]$$
$$-\frac{2}{\pi}\left[\int_{\eta_{i+1}}^{\eta_{i+2}}\frac{\eta(1-2\eta^2)a_j\mathrm{d}\eta}{\left(\eta^2-\xi_{i+\frac{3}{2}}^2\right)\sqrt{1-\eta^2}}-\int_{\eta_{i+1}}^{\eta_{i+2}}\frac{\eta^2 b_j\mathrm{d}\eta}{\left(\eta^2-\xi_{i+\frac{3}{2}}^2\right)\sqrt{1-\eta^2}}\right]. \tag{5.7.16}$$

Discretising (5.2.12) and approximating the pressure terms using central difference, we obtain

$$\begin{aligned}&(c_2+\beta_1)\left(1-\xi^2\right)^{\frac{1}{2}}(a_i\xi+b_i)-\frac{2c_2\xi\left[(1-2\xi^2)a_i-\xi b_i\right]}{\sqrt{1-\xi^2}}\\&-(1-\xi^2)(a_i\xi+b_i)^2\left[\frac{(1-2\xi^2)a_i-\xi b_i}{\sqrt{1-\xi^2}}\right]\left[\frac{P_{i+\frac{1}{2}}-P_{i-\frac{1}{2}}}{\xi_{i+\frac{1}{2}}-\xi_{i-\frac{1}{2}}}\right]\\&-\frac{1}{3}(1-\xi^2)^{\frac{3}{2}}(a_i\xi+b_i)^3\left[\frac{P_{i-\frac{3}{2}}-P_{i-\frac{1}{2}}-P_{i+\frac{1}{2}}+P_{i+\frac{3}{2}}}{2\left(\xi_{i+\frac{1}{2}}-\xi_{i-\frac{1}{2}}\right)^2}\right]=0,\end{aligned} \tag{5.7.17}$$

where $1 \leqslant i \leqslant n-1$. The current task is to solve for $\{a_i, b_i\}$, $i = 1,2,\ldots,n-1$ in each sub-interval. There are n sub-intervals and $n+1$ grid points hence we have $2n$ unknowns in total. Equation (5.7.17) will generate a system of $n-1$ nonlinear equations.

Now, in each sub-interval there exist a linear spline of the form

$$\Pi_i(\xi) = a_i\xi + b_i, \tag{5.7.18}$$

and by the continuity condition two successive linear splines are continuous at their common interior points, that is

$$\Pi_i(\xi_i) = \Pi_{i-1}(\xi_i), \qquad i = 1,2,3,\ldots,n-1. \tag{5.7.19}$$

The continuity condition (5.7.19) gives an additional $n-1$ equations. We now have a total of $2n-2$ equations. We use the slope and boundary conditions to determine the values a_0 and b_0. As a result, the $2n-2$

equations are sufficient to solve the underlying system of nonlinear equations. We use an example to outline the procedure of solving the problem. For any choice of $n \geqslant 2$, we have n splines with $2n$ unknowns. The slope condition $f'(0) = 0$ implies that $a_0 = 0$ and the boundary condition at the fracture entry gives $b_0 = 1$, hence $f_0(\xi) = \sqrt{1-\xi^2}$. We now have a total of $2n-2$ unknowns. Equation (5.7.17) gives $n-1$ equations, for example

$$\begin{aligned} i=1: \quad & (c_2+\beta_1)\left(1-\xi^2\right)^{\frac{1}{2}}(a_1\xi+b_1) - \frac{2c_2\xi\left[(1-2\xi^2)a_1-\xi b_1\right]}{\sqrt{1-\xi^2}} \\ & - n(1-\xi^2)(a_1\xi+b_1)^2(P_{\frac{3}{2}}-P_{\frac{1}{2}})\left[\frac{(1-2\xi^2)a_1-\xi b_1}{\sqrt{1-\xi^2}}\right] \\ & - \frac{n^2}{6}(1-\xi^2)^{\frac{3}{2}}(a_1\xi+b_1)^3(P_{-\frac{1}{2}}-P_{\frac{1}{2}}-P_{\frac{3}{2}}+P_{\frac{5}{2}}) = 0, \end{aligned} \tag{5.7.20}$$

$$\begin{aligned} i=2: \quad & (c_2+\beta_1)\left(1-\xi^2\right)^{\frac{1}{2}}(a_2\xi+b_2) - \frac{2c_2\xi\left[(1-2\xi^2)a_2-\xi b_2\right]}{\sqrt{1-\xi^2}} \\ & - n(1-\xi^2)(a_2\xi+b_2)^2(P_{\frac{5}{2}}-P_{\frac{3}{2}})\left[\frac{(1-2\xi^2)a_2-\xi b_2}{\sqrt{1-\xi^2}}\right] \\ & - \frac{n^2}{6}(1-\xi^2)^{\frac{3}{2}}(a_2\xi+b_2)^3(P_{\frac{1}{2}}-P_{\frac{3}{2}}-P_{\frac{5}{2}}+P_{\frac{7}{2}}) = 0, \end{aligned} \tag{5.7.21}$$

$$\vdots \qquad\qquad \vdots$$

$$\begin{aligned} i=n-1: \quad & (c_2+\beta_1)\left(1-\xi^2\right)^{\frac{1}{2}}(a_{n-1}\xi+b_{n-1}) - \frac{2c_2\xi\left[(1-2\xi^2)a_{n-1}-\xi b_{n-1}\right]}{\sqrt{1-\xi^2}} \\ & - n(1-\xi^2)(a_{n-1}\xi+b_{n-1})^2\left(P_{n-\frac{1}{2}}-P_{n-\frac{3}{2}}\right)\left[\frac{(1-2\xi^2)a_{n-1}-\xi b_{n-1}}{\sqrt{1-\xi^2}}\right] \\ & - \frac{n^2}{6}(1-\xi^2)^{\frac{3}{2}}(a_{n-1}\xi+b_{n-1})^3\left(P_{n-\frac{5}{2}}-P_{n-\frac{3}{2}}-P_{n-\frac{1}{2}}+P_{n+\frac{1}{2}}\right) = 0. \end{aligned} \tag{5.7.22}$$

Similarly, we get $n-1$ equations from the continuity condition

$$i=1: \quad a_1\xi_1 + b_1 - b_0 = 0, \tag{5.7.23}$$

$$i=2: \quad (a_2-a_1)\xi_2 + b_2 - b_1 = 0, \tag{5.7.24}$$

$$\vdots \qquad\qquad \vdots$$

$$i=n-1: \quad (a_{n-1}-a_{n-2})\xi_{n-1} + b_{n-1} - b_{n-2} = 0. \tag{5.7.25}$$

Equations (5.7.20) and (5.7.22) contains two pressure terms $P_{-1/2}$ and $P_{n+1/2}$ which lie outside the interval $[0,\ 1]$. By symmetry, we have that $P_{-1/2} = P_{1/2}$. Consequently, (5.7.20) becomes

$$\begin{aligned}
&(c_2+\beta_1)\left(1-\xi^2\right)^{\frac{1}{2}}(a_1\xi+b_1) - \frac{2c_2\xi\left[(1-2\xi^2)a_1-\xi b_1\right]}{\sqrt{1-\xi^2}} \\
&- n(1-\xi^2)(a_1\xi+b_1)^2(P_{\frac{3}{2}}-P_{\frac{1}{2}})\left[\frac{(1-2\xi^2)a_1-\xi b_1}{\sqrt{1-\xi^2}}\right] \\
&- \frac{n^2}{6}(1-\xi^2)^{\frac{3}{2}}(a_1\xi+b_1)^3\left(P_{\frac{5}{2}}-P_{\frac{3}{2}}\right) = 0.
\end{aligned} \tag{5.7.26}$$

As shown previously, we approximate the term $P_{n+1/2}$ using the pressure condition which describes the behaviour of pressure near but just outside the fracture tip. Equation (5.7.22) then becomes

$$\begin{aligned}
&(c_2+\beta_1)\left(1-\xi^2\right)^{\frac{1}{2}}(a_{n-1}\xi+b_{n-1}) - \frac{2c_2\xi\left[(1-2\xi^2)a_{n-1}-\xi b_{n-1}\right]}{\sqrt{1-\xi^2}} \\
&- n(1-\xi^2)(a_{n-1}\xi+b_{n-1})^2\left(P_{n-\frac{1}{2}}-P_{n-\frac{3}{2}}\right)\left[\frac{(1-2\xi^2)a_{n-1}-\xi b_{n-1}}{\sqrt{1-\xi^2}}\right] \\
&- \frac{n^2}{6}(1-\xi^2)^{\frac{3}{2}}(a_{n-1}\xi+b_{n-1})^3\left(P_{n-\frac{5}{2}}-P_{n-\frac{3}{2}}-P_{n-\frac{1}{2}}-\gamma n^{\frac{1}{2}}\right) = 0.
\end{aligned} \tag{5.7.27}$$

In the next section, we discuss the approaches employed for solving the resulting system of nonlinear equations.

5.8 DISCUSSION ON NUMERICAL METHOD

The numerical scheme used to accurately solve the boundary value problem for the integro-differential system (5.2.12)-(5.2.14a-c) was based on the spline method. The discretisation and set up of the problem is outlined in the previous section. As shown, the remedy to the singularity challenge at the fracture tip was to extract the fracture tip behaviour and represent the remaining part of $f(\xi)$ as a piece-wise linear function, i.e., linear in each sub-interval $[\xi_i, \xi_{i+1}]$.

The resulting set of nonlinear algebraic equations were solved for the unknown coefficients $\boldsymbol{a} = [a_1, a_2, \ldots, a_{n-1}]$ and $\boldsymbol{b} = [b_1, b_2, \ldots, b_{n-1}]$ using the Matlab nonlinear system solver *fsolve*. The *fsolve* was preferred due to its implementation of an optimization procedure to determine the unknown coefficients. We used the Matlab function *rand* to obtain the initial guess for the unknown coefficients. The *rand* function generates uniformly distributed random numbers in the interval (0,1). The system was solved iteratively subject to the boundary conditions (5.2.14a-c). The parameters β_1, Q_0 and γ are prescribed. For fixed β_1, Q_0 and γ, we iterated based on the bisection method with varying values of c_2 until the condition (5.2.8) was satisfied. The value of c_2 was

obtained as part of the solution. Similarly, the accuracy of the numerical results was verified using equation (5.6.2). Once the solution for $f(\xi)$ and the value of c_2 are obtained, $L(t)$, $V(t)$, $h(t,x)$ and $v_n(t,x)$ are obtained from (5.2.16), (5.2.17), (5.2.18) and (5.2.19). Here, the mid-grid values for $P(\xi)$ were calculated using (5.7.3) and the Matlab function *interp1* was used to obtain grid points values of $P(\xi)$. The pressure gradient at $\xi = 0$ was obtained directly from (5.2.11).

We now illustrate the behaviour of $f(\xi)$ when plotted against ξ for the case where $\beta_1 = 0.01$, $Q_0 = 0.2$ and $\gamma = 0.5$. The solution for $f(\xi)$ obtained using the spline method is compared to the solution obtained in Section 5.6 using finite difference method. It is clear in Figure 18 that the solutions overlap and that the spline method produces a smooth curve.

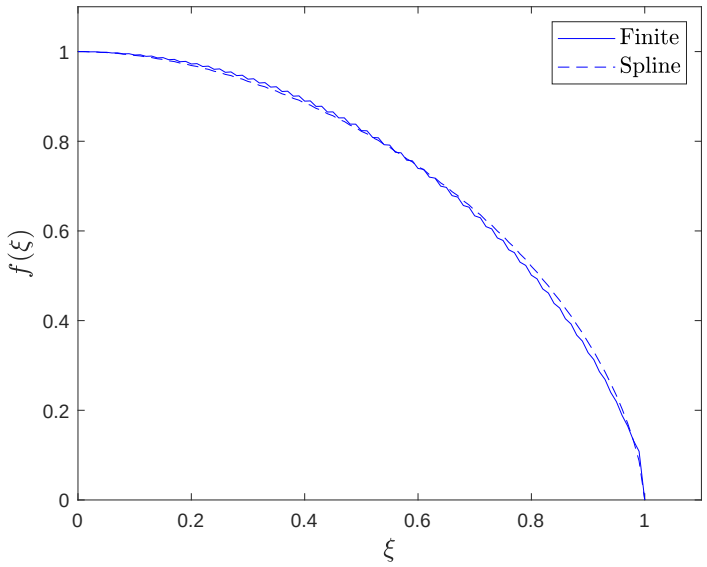

Figure 18: Comparison of the solution for the similarity function $f(\xi)$ obtained using the finite difference method and the spline method when $n = 100$.

5.9 NUMERICAL RESULTS AND DISCUSSIONS

This section will illustrate the behaviour of the fracture length, fracture volume, fracture half-width, leak-off fluid velocity and the fluid pressure for varied parameter values. We will also illustrate the relationship between the parameters $c_2, \beta_1, Q_0, \gamma$ in the model.

In Figure 19, $h(t,x)$ is plotted against x at $t = 0, 10, 20$ and 50 when $\beta_1 = 0, 0.01, 0.04$. As expected, $h(t,x)$ increases with time, and as β_1 increases, indicating increase in leak-off, the rate of increase of $h(t,x)$ is seen to decrease.

In Figure 20, the fracture half-width, $h(t,x)$, leak-off velocity, $v_n(t,x)$, and the net pressure, $p(t,x)$, are plotted against x for $\beta_1 = 0$, 0.005, 0.01, 0.04 when $\gamma = 0.5$ and $Q_0 = 0.2$. In Figure 20(i), the half-width of the fracture evolved the greatest when $\beta_1 = 0$ and the least when $\beta_1 = 0.04$. In Figure 20(ii), the graph of $v_n(t,x)$ reflects the assumption that the leak-off velocity is proportional to the fracture half-width. In Figure 20(iii), the fluid pressure is positive across fracture except near the fracture tip in agreement with (5.3.19).

In Figure 21, $h(t,x)$, $v_n(t,x)$ and $p(t,x)$ are plotted at time $t = 50$ for $Q_0 = 0.1, 0.15$, 0.2 and 0.25 when $\gamma = 0.5$ and $\beta_1 = 0.01$. It can be seen in Figure 21(i) that as Q_0 increases, the fracture half-width increases as expected, despite leak-off of fluid into the rock mass. The fracture half-width evolved the least when $Q_0 = 0.1$ and the greatest when $Q_0 = 0.25$.

In Figure 22, $h(t,x)$, $v_n(t,x)$ and $p(t,x)$ are plotted at time $t = 50$ for $\gamma = 0, 2$, 4 and 10 when $Q_0 = 0.2$ and $\beta_1 = 0.01$. When $\gamma = 0$, the pressure near but just outside the fracture tip is zero and equation (5.2.15) is satisfied. When $\gamma > 0$, the net pressure is negative and equation (5.2.15) is satisfied. Expectedly, an increase in γ did not lead to growth in the fracture half-width.

In Figure 23(i-iii), graphs of $L(t)$ are plotted against t for varied values of β_1, Q_0 and γ. The length of the fracture $L(t)$ is an increasing function of time and $L(t) \to \infty$ as $t \to \infty$. In Figure 23(i), $L(t)$ is plotted for $\beta_1 = 0, 0.005, 0.01$ and 0.04 when $\gamma = 0.5$ and $Q_0 = 0.2$. Fluid leak-off at the fluid-rock interface reduces the rate of growth of fracture length impacting on the extent of propagation of the fracture. The length of the fracture grew the strongest when $\beta_1 = 0$, as would intuitively be expected, and it grew the weakest when $\beta_1 = 0.04$. In Figure 23(ii), $L(t)$ is plotted for $Q_0 = 0.1, 0.15, 0.2$ and 0.25 when $\gamma = 0.5$ and $\beta_1 = 0.01$. The rate of growth of the fracture length was the weakest when $Q_0 = 0.1$ and the strongest when $Q_0 = 0.25$. In Figure 23(iii), $L(t)$ is plotted for $\gamma = 0, 2, 4$ and 10 when $\beta_1 = 0.01$ and $Q_0 = 0.2$. The graphs for the fracture length are indistinguishable for the different values of γ. It is can seen that γ has a slight effect on the rate of growth of the fracture length.

Figure 24(i-iii) shows the fracture volume evolution over time, as well as the plot of the velocity ratio and the dimensionless pressure gradient. In Figure 24(i), $V(t)$ is plotted for $\beta_1 = 0, 0.005, 0.01$ and 0.04 when $\gamma = 0.5$ and $Q_0 = 0.2$. The value of the initial fracture volume, V_0, was determined to be approximately 2.97. The fracture volume increases linearly with time. Therefore, $V'(t) > 0$ for all t and $V(t) \to \infty$ as $t \to \infty$. The fracture volume grew the least when $\beta_1 = 0.04$, for which fluid leak-off is highest, and the greatest when $\beta_1 = 0$. Figure 24(ii), illustrates the velocity ratio for different values of β_1. The graphs of the velocity ratio for the values of β_1 considered are not approximately straight lines as anticipated. Fareo and Mason [20]

(i)

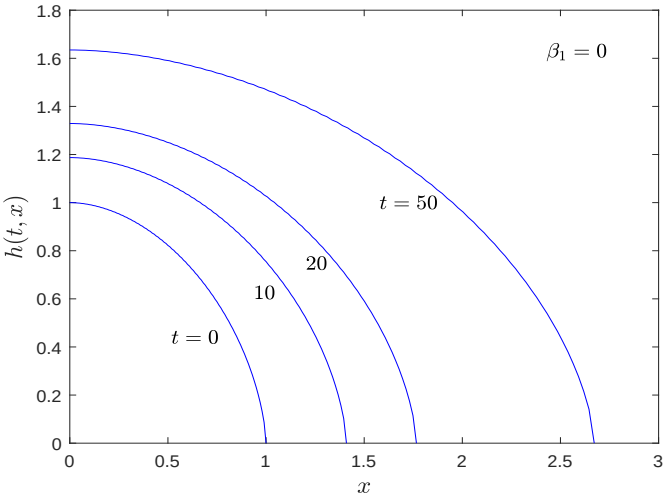

(ii)

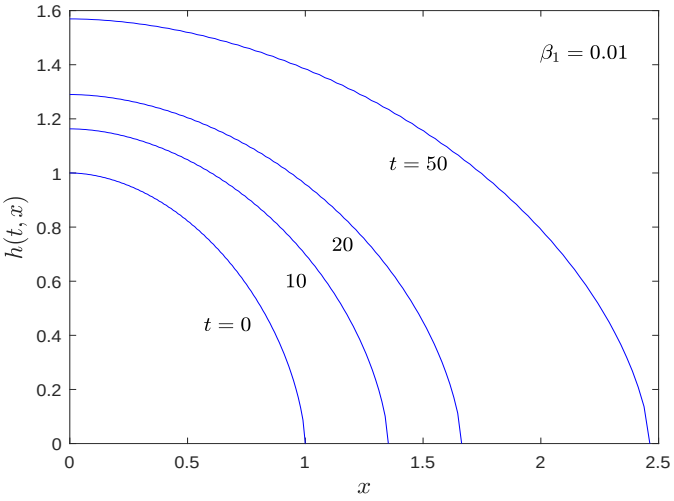

(iii)

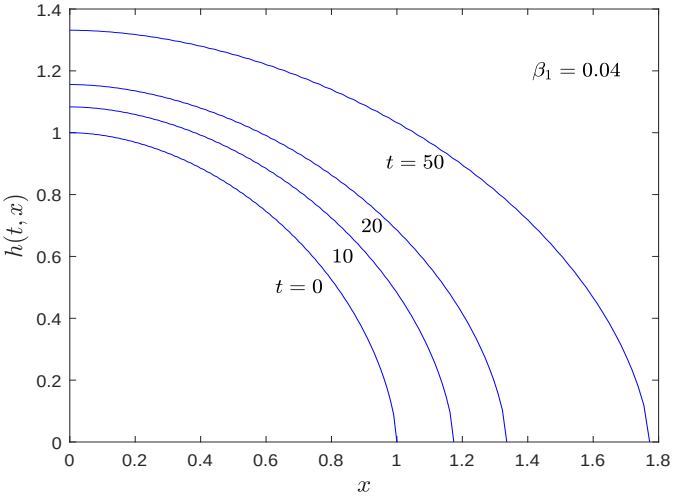

Figure 19: Graph of $h(t,x)$ plotted against x at times $t = 0, 10, 20, 50$ for $Q_0 = 0.2$, $\gamma = 0.5$ and for (i) $\beta_1 = 0$ and $c_2 = 0.022453$, (ii) $\beta_1 = 0.01$ and $c_2 = 0.019100$ and (iii) $\beta_1 = 0.04$ and $c_2 = 0.009068$.

(i)

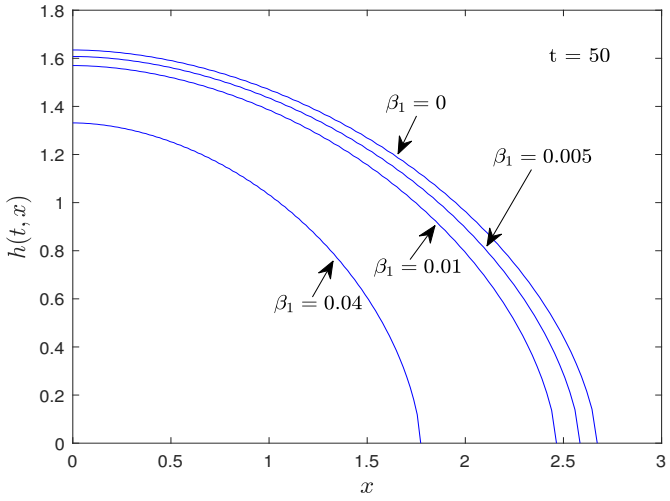

(ii)

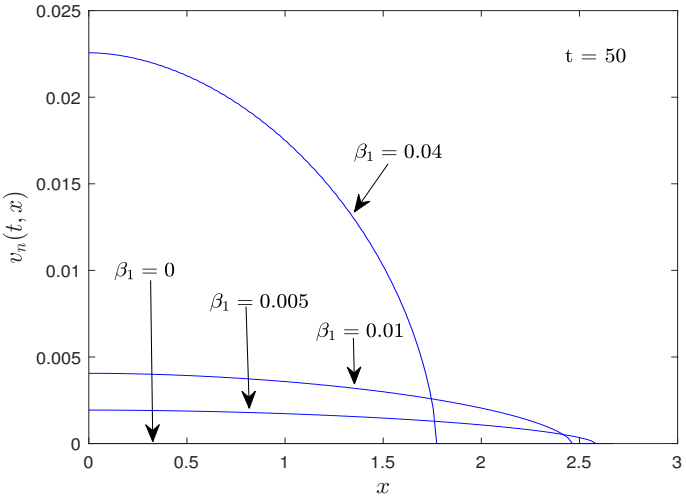

(iii)

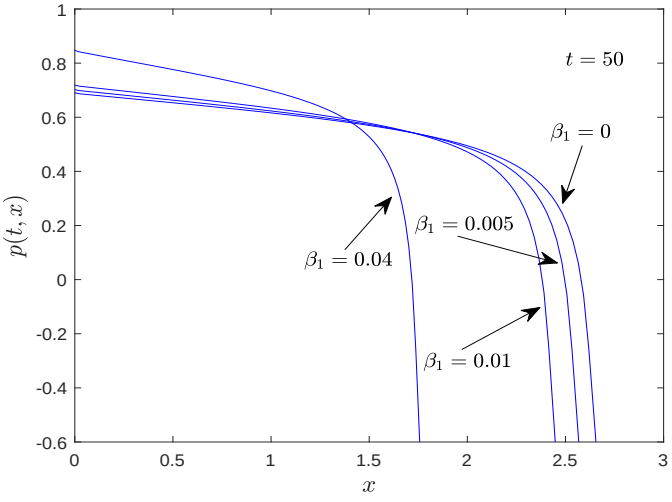

Figure 20: Graphs of (i) the fracture half-width $h(t,x)$, (ii) leak-off fluid velocity $v_n(t,x)$ and (iii) the net pressure $p(t,x)$, plotted against x for $\beta_1 = 0$, 0.005, 0.01, 0.04 when $Q_0 = 0.2$ and $\gamma = 0.5$ at $t = 50$.

(i)

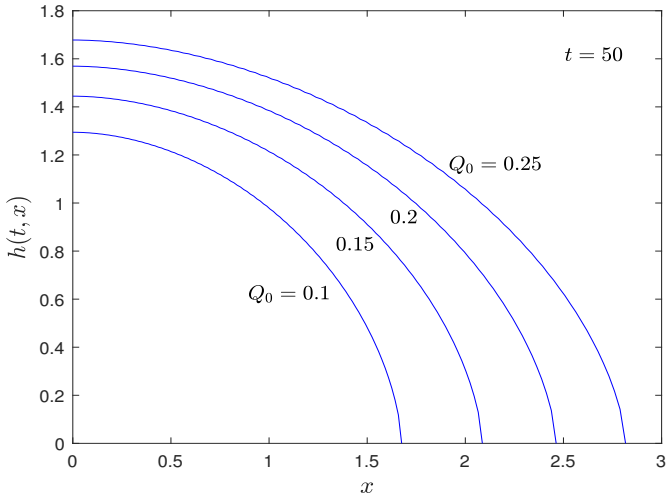

(ii)

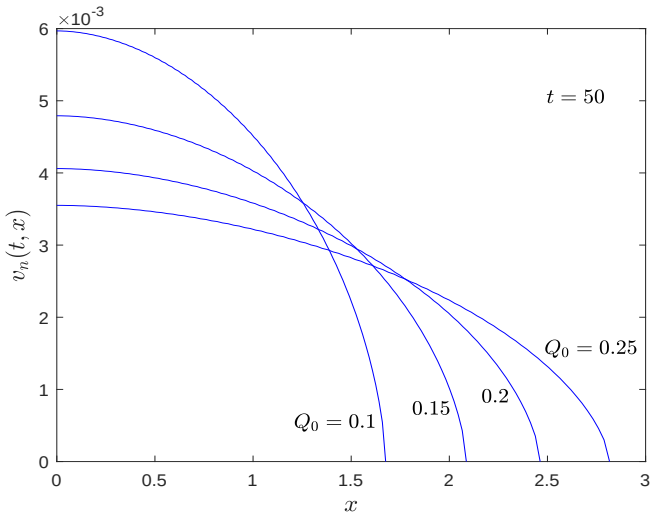

(iii)

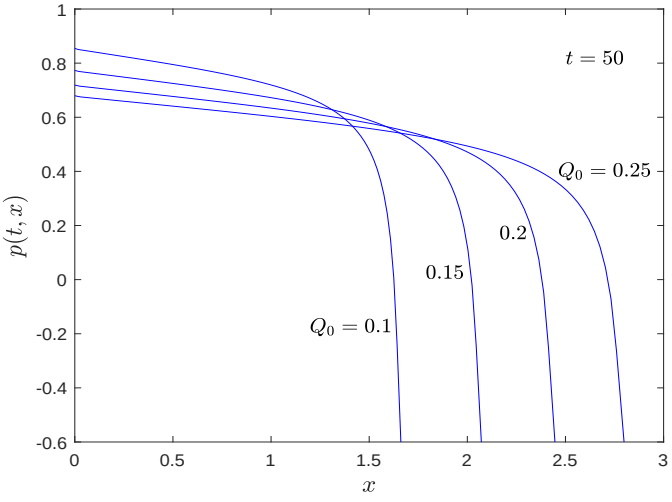

Figure 21: Graphs of (i) the fracture half-width $h(t,x)$, (ii) leak-off fluid velocity $v_n(t,x)$ and (iii) the net pressure $p(t,x)$, plotted against x for $Q_0 = 0.1, 0.15, 0.2, 0.25$ when $\gamma = 0.5$ and $\beta_1 = 0.01$ at $t = 50$.

(i)

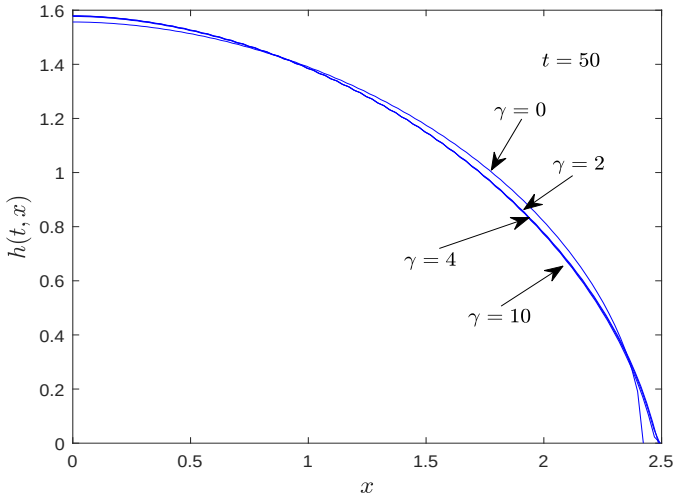

(ii)

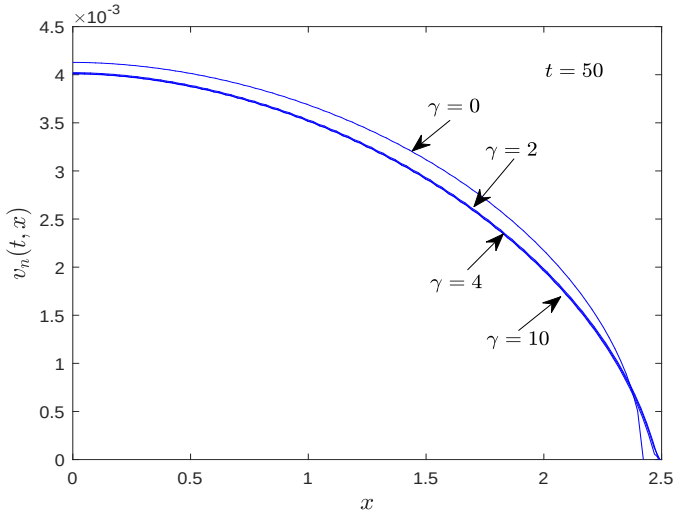

(iii)

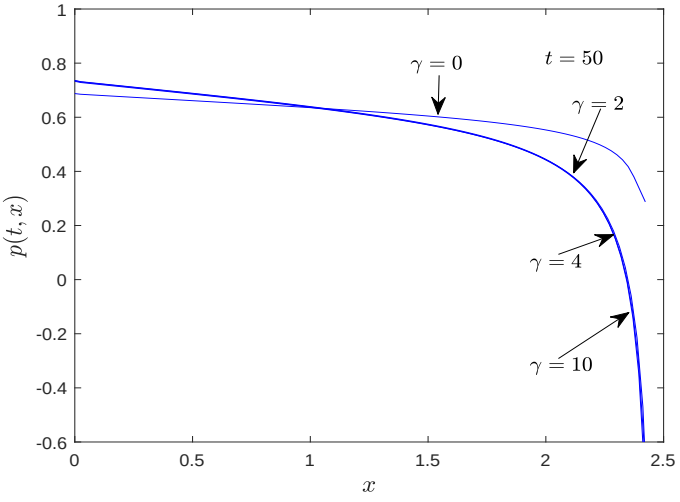

Figure 22: Graphs of (i) the fracture half-width $h(t,x)$, (ii) leak-off fluid velocity $v_n(t,x)$ and (iii) the net pressure $p(t,x)$, plotted against x for $\gamma = 0$, 2, 4, 10 when $Q_0 = 0.2$ and $\beta_1 = 0.01$ at $t = 50$.

(i)

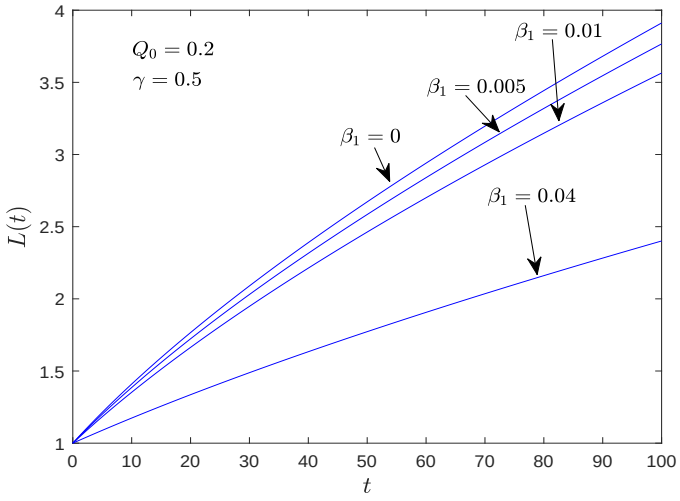

(ii)

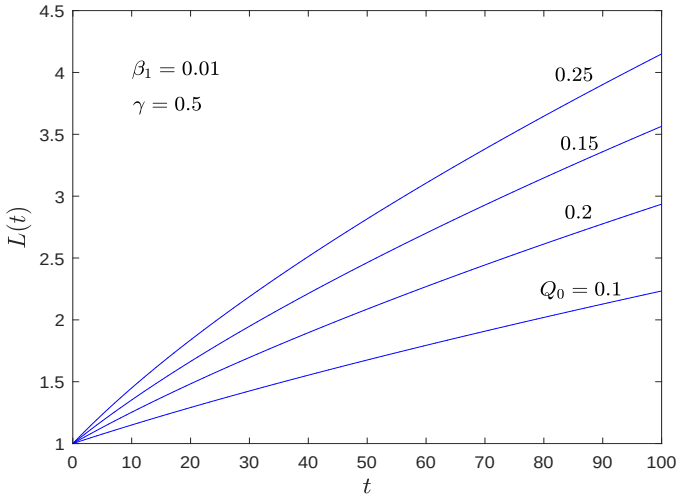

(iii)

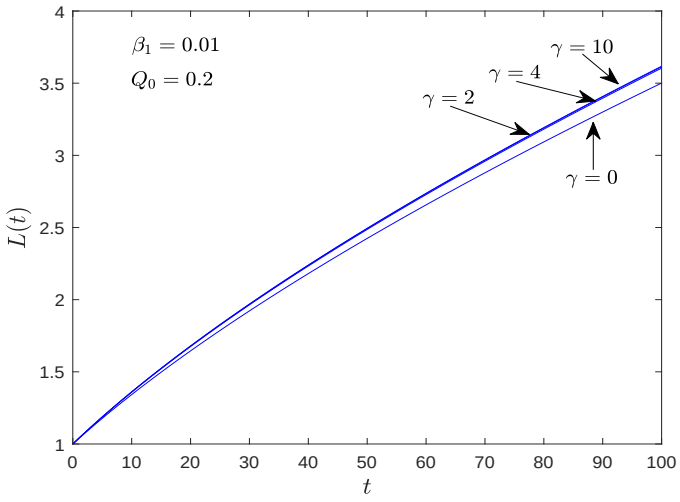

Figure 23: Fracture length plotted for various values of (i) β_1, (ii) Q_0, (iii) γ.

(i)

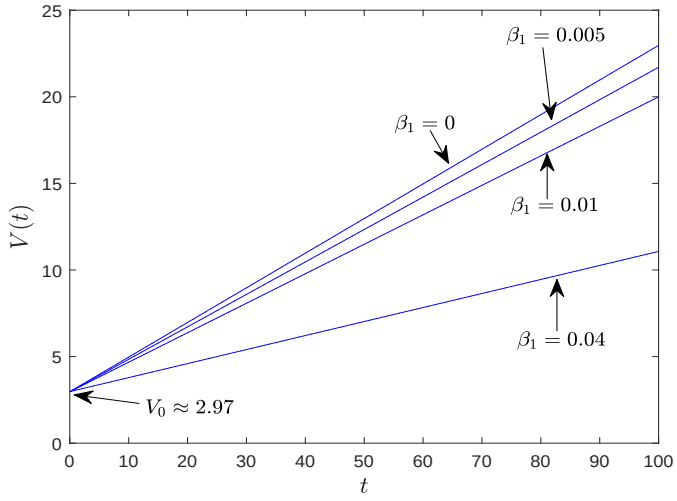

(ii)

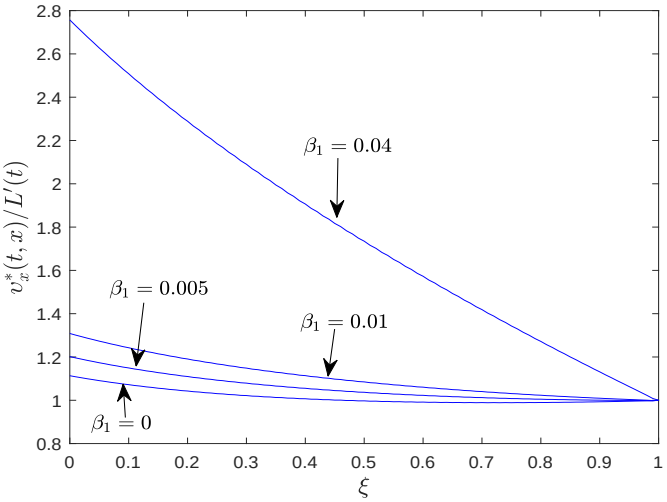

(iii)

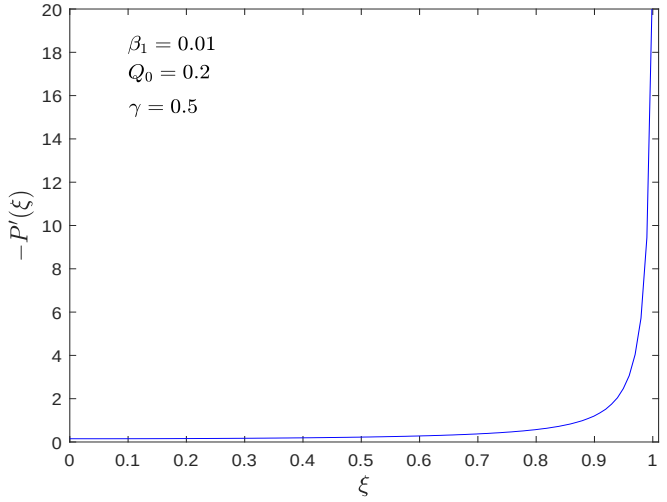

Figure 24: Graphs illustrating (i) fracture volume plotted against t for $\beta_1 = 0, 0.005, 0.01, 0.04$ when $Q_0 = 0.2$ and $\gamma = 0.5$, (ii) velocity ratio $v_x^*(t,x)/L'(t)$ plotted against ξ for $\beta_1 = 0, 0.005, 0.01, 0.04$ when $Q_0 = 0.2$ and $\gamma = 0.5$, (iii) dimensionless pressure gradient plotted against ξ for $Q_0 = 0.2$, $\gamma = 0.5$ and $\beta_1 = 0.01$.

(i)

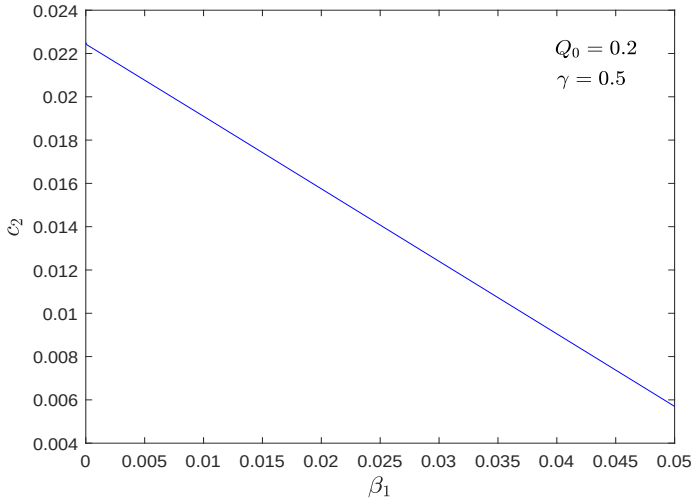

(ii)

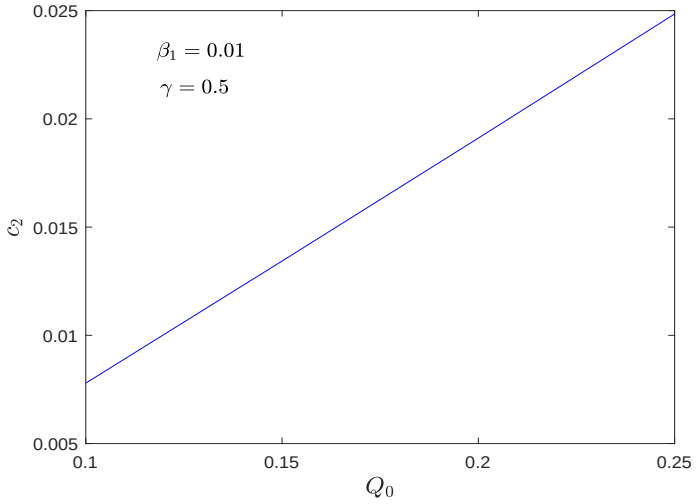

(iii)

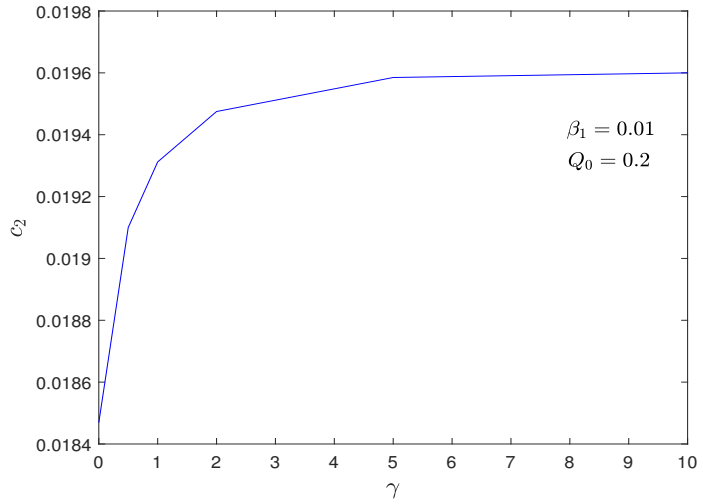

Figure 25: The constant c_2 plotted against (i) β_1, (ii) Q_0, (iii) γ.

investigated the behaviour of the velocity ratio $v_x^*(t,x)/L'(t)$ across the fracture in PKN theory. They found that the ratio behaves approximately linearly across the fracture which led to the obtaining of approximate solutions. In Figure 24(iii) the non-dimensional pressure gradient $P'(\xi)$ is plotted against ξ and the limiting behaviour of $P'(\xi)$ as $\xi \to 1$ proportional to $1/(1-\xi)^{-1}$ is displayed in the plot.

Figure 25 shows the relationship between c_2, β_1, Q_0 and γ in the model. In Figure 25(i), c_2 is plotted against the leak-off parameter β_1. It can be seen that c_2 is inversely proportional to β_1. In Figure 25(ii), c_2 is plotted against fluid flux at the fracture entry Q_0. It can be seen that c_2 increases as linear function of Q_0. In Figure 25(iii), c_2 is plotted against the dimensionless stress intensity factor γ. There is a rapid increase in the value of c_2 between $0 \leqslant \gamma \leqslant 3$ followed by a gradual increase and finally the graph seems to reach a plateau.

5.10 CONCLUSION

In this chapter, we investigated a two-dimensional pre-existing fracture propagating in a permeable rock when fracturing fluid of Newtonian rheology is injected under high pressure into the fracture. The governing equations which is the boundary value problem for the integro-differential system was derived in Chapter 4. It contains three dependent variables $f(\xi), g(\xi)$ and $P(\xi)$ to solve for, but two equations. In order to close the system, a linear relation between $g(\xi)$ and $f(\xi)$ of the form $g(\xi) = \bar{\beta}_1 f(\xi)$ had to be specified. The non-linear system contains four parameters c_2, β_1, Q_0 and γ, which all have to be specified except c_2. The constant c_2 was obtained as part of the solution. Numerical solutions to the system were obtained using the linear spline method. The finite difference method gave quite a similar solution, but the singularity in the slope of $f(\xi)$ at the tip made solutions for $h(x,t)$ to exhibit oscillations along x. The results obtained were as expected.

6

LEAK-OFF FLUID VELOCITY PROPORTIONAL TO GRADIENT OF FLUID-ROCK INTERFACE

6.1 INTRODUCTION

In this chapter, we consider the case in which $g(\xi)$ is proportional to $f'(\xi)$. This results in the leak-off velocity being proportional to the gradient of the fluid-rock interface. The resulting integro-differential system is then solved numerically using the linear spline method. A discussion of the numerical results is then provided. The numerical approach outlined in Section 5.8 also applies in this chapter.

6.2 LEAK-OFF FLUID VELOCITY PROPORTIONAL TO GRADIENT OF FLUID-ROCK INTERFACE

Consider the case where

$$g(\xi) = -\bar{\beta}_2 \xi \frac{\mathrm{d}f}{\mathrm{d}\xi} \quad \text{where} \quad \bar{\beta}_2 = \frac{1}{c_3}\beta_2, \quad \bar{\beta}_2 \in \mathbb{R}. \tag{6.2.1}$$

It follows from the similarity solution (4.6.42), given $\xi = x/L(t)$, that

$$v_n(t,x) = -\beta_2 \frac{x\frac{\partial h}{\partial x}}{L^{\frac{3}{2}}(t)}. \tag{6.2.2}$$

Hence, the leak-off velocity $v_n(t,x)$ is proportional to the gradient of the half-width of the fracture. The differential equation (4.6.36) becomes

$$c_2 f(\xi) - (2c_2 + \beta_2)\xi \frac{\mathrm{d}f}{\mathrm{d}\xi} - \frac{1}{3}\frac{\mathrm{d}}{\mathrm{d}\xi}\left(f^3 \frac{\mathrm{d}P}{\mathrm{d}\xi}\right) = 0. \tag{6.2.3}$$

Using (6.2.1), the mass balance equation (4.6.50) becomes

$$12c_2 \int_0^1 f(\xi)\mathrm{d}\xi = -\frac{4}{3}f^3(0)\frac{\mathrm{d}P(0)}{\mathrm{d}\xi} + 4\beta_2 \int_0^1 \xi \frac{\mathrm{d}f}{\mathrm{d}\xi}\mathrm{d}\xi. \tag{6.2.4}$$

By integrating by parts using the boundary condition $f(1) = 0$, we obtain

$$\int_0^1 \xi \frac{\mathrm{d}f}{\mathrm{d}\xi}\mathrm{d}\xi = -\int_0^1 f(\xi)\mathrm{d}\xi. \tag{6.2.5}$$

Equation (6.2.4) becomes

$$(12c_2 + 4\beta_2)\int_0^1 f(\xi)\mathrm{d}\xi = -\frac{4}{3}f^3(0)\frac{\mathrm{d}P(0)}{\mathrm{d}\xi}. \tag{6.2.6}$$

The expression for the fluid flux at the fracture entry, $Q_0(t)$, can be derived in terms of c_2, β_2 and $f(\xi)$. Integrating (6.2.3) with respect to η from ξ to 1, we obtain

$$-f^3\frac{\mathrm{d}P}{\mathrm{d}\xi} = (9c_2+3\beta_2)\int_\xi^1 f(\eta)\mathrm{d}\eta + (6c_2+3\beta_2)\xi f(\xi). \tag{6.2.7}$$

Evaluating (6.2.7) at $\xi = 0$, we find that

$$-f^3(0)\frac{\mathrm{d}P(0)}{\mathrm{d}\xi} = (9c_2+3\beta_2)\int_0^1 f(\xi)\mathrm{d}\xi. \tag{6.2.8}$$

Multiplying (6.2.8) by 4/3 and using (4.6.48), the fluid flux at the fracture entry can be expressed as

$$Q_0 = (12c_2+4\beta_2)\int_0^1 f(\xi)\mathrm{d}\xi. \tag{6.2.9}$$

From (6.2.7), we obtain the pressure gradient as

$$-\frac{\mathrm{d}P}{\mathrm{d}\xi} = \frac{1}{f^3(\xi)}\left[(9c_2+3\beta_2)\int_\xi^1 f(\eta)\mathrm{d}\eta + (6c_2+3\beta_2)\xi f(\xi)\right]. \tag{6.2.10}$$

The problem is to solve for $f(\xi)$ and $P(\xi)$, the system of differential equations

$$c_2 f(\xi) - 2c_2\left(1+\frac{\beta_2}{2c_2}\right)\xi\frac{\mathrm{d}f}{\mathrm{d}\xi} - \frac{1}{3}\frac{\mathrm{d}}{\mathrm{d}\xi}\left(f^3\frac{\mathrm{d}P}{\mathrm{d}\xi}\right) = 0, \tag{6.2.11}$$

$$P(\xi) = -\frac{2}{\pi}\int_0^1 \frac{\mathrm{d}f}{\mathrm{d}\eta}\frac{\eta}{\eta^2-\xi^2}\mathrm{d}\eta, \tag{6.2.12}$$

subject to

$$f(0) = 1, \quad f'(0) = 0, \quad f(1) = 0, \tag{6.2.13a-d}$$

where

$$P(\xi) \to -\frac{\gamma}{\sqrt{2(\xi-1)}} \quad \text{as} \quad \xi \to 1^+. \tag{6.2.14}$$

Once $f(\xi)$ and $P(\xi)$ are obtained, $L(t)$, $V(t)$, $h(t,x)$, $v_n(t,x)$ and $p(t,x)$ take the form

$$L(t) = (3c_2t+1)^{\frac{2}{3}}, \tag{6.2.15}$$

$$V(t) = V_0(3c_2t+1), \quad V_0 = 4\int_0^1 f(\xi)\mathrm{d}\xi, \tag{6.2.16}$$

$$h(t,x) = L^{\frac{1}{2}}(t)f(\xi), \tag{6.2.17}$$

$$v_n(t,x) = -\beta_2\xi L^{-1}(t)f'(\xi), \tag{6.2.18}$$

$$p(t,x) = L^{-\frac{1}{2}}(t)P(\xi). \tag{6.2.19}$$

The solutions of the system of differential equation depends on the constant c_2, the dimensionless stress intensity factor γ and the fluid flux specified at the fracture entry, Q_0. The values of γ and Q_0 will be specified before commencing the numerical computations and the constant c_2 will be obtained as part of the solution such that equation (6.2.9) is satisfied. Since, it is required that $c_2 > 0$ and (6.2.9) has the same form as (5.2.8), then we have that

$$\beta_2 \ll \frac{Q_0}{2}. \tag{6.2.20}$$

6.3 TIP ASYMPTOTICS AND THE VELOCITY RATIO

In this section, we will investigate the limiting behaviour of $f(\xi), g(\xi)$ and $P(\xi)$ at the fracture tip as well as the behaviour of the velocity ratio at the fracture tip.

Case: $\gamma = 0$

We seek the asymptotic behaviour for $f(\xi)$ and $P(\xi)$ as $\xi \to 1$. The asymptotic solutions are of the form

$$f(\xi) \sim \sigma(1-\xi)^{\rho} \quad \text{as} \quad \xi \to 1, \tag{6.3.1}$$

$$P(\xi) \sim \sigma\rho\cot(\pi\rho)(1-\xi)^{\rho-1} \quad \text{as} \quad \xi \to 1, \tag{6.3.2}$$

where σ and ρ are constants and since (6.3.1) has the same form as (5.3.3), (6.3.2) is then same as (5.3.6). Substituting (6.3.1) and (6.3.2) into (6.2.11), we obtain

$$\begin{aligned} &\sigma c_2(1-\xi)^{\rho} + (2c_2+\beta_2)\sigma\rho\xi(1-\xi)^{\rho-1} \\ &-\frac{1}{3}\sigma^4\rho(\rho-1)(4\rho-2)\cot(\pi\rho)(1-\xi)^{4\rho-3} \sim 0, \end{aligned} \tag{6.3.3}$$

as $\xi \to 1$. The dominant terms in (6.3.3) balance each other when

$$4\rho - 3 = \rho - 1, \tag{6.3.4}$$

which gives $\rho = 2/3$. Substituting the value of ρ into (6.3.3) we find that

$$\sigma = (27\sqrt{3}c_2)^{\frac{1}{3}}\left[1+\frac{\beta_2}{2c_2}\right]^{\frac{1}{3}}. \tag{6.3.5}$$

Therefore, the asymptotic solutions for $f(\xi), g(\xi)$ and $P(\xi)$ as $\xi \to 1$ are

$$f(\xi) \sim (27\sqrt{3}c_2)^{\frac{1}{3}}\left[1+\frac{\beta_2}{2c_2}\right]^{\frac{1}{3}}(1-\xi)^{\frac{2}{3}}, \tag{6.3.6}$$

$$g(\xi) \sim (8\sqrt{3}c_2)^{\frac{1}{3}}\left[1+\frac{\beta_2}{2c_2}\right]^{\frac{1}{3}}\bar{\beta}_2\xi(1-\xi)^{-\frac{1}{3}}, \tag{6.3.7}$$

$$P(\xi) \sim -\left(\frac{8c_2}{3}\right)^{\frac{1}{3}}\left[1+\frac{\beta_2}{2c_2}\right]^{\frac{1}{3}}(1-\xi)^{-\frac{1}{3}}. \tag{6.3.8}$$

The asymptotic solutions for $f(\xi), g(\xi)$ and $P(\xi)$ near $\xi = 1$ depend on parameter c_2 and the leak-off parameter β. The velocity ratio is given by

$$\frac{v_x^*(t,x,z)}{L'(t)} = -\frac{1}{6c_2} f^2(\xi) P'(\xi), \tag{6.3.9}$$

and at the fracture tip, we have

$$\frac{v_x^*(t,L(t))}{L'(t)} = -\frac{1}{6c_2} f^2(1) P'(1) = 1 + \frac{\beta_2}{2c_2}. \tag{6.3.10}$$

Therefore, due to leak-off, the fluid velocity is greater than the speed of fracture propagation at the fracture tip, for $\beta_2 > 0$ and $c_2 > 0$.

Case: $\gamma > 0$

Similarly, we seek the asymptotic behaviour for $f(\xi), g(\xi)$ and $P(\xi)$ as $\xi \to 1$ when the dimensionless stress intensity factor $\gamma > 0$. When $\gamma > 0$, the asymptotic behaviour of $f(\xi)$ as $\xi \to 1$ is given by the first term of (B.1.21)

$$f(\xi) \sim \gamma(1-\xi^2)^{\frac{1}{2}}. \tag{6.3.11}$$

It is clear that when $\xi \to 1$, the first term of equation (6.2.10) tends to zero so that

$$P'(\xi) \sim -\Lambda_2 (1-\xi^2)^{-1}, \tag{6.3.12}$$

where

$$\Lambda_2 = \frac{(6c_2 + 3\beta_2)}{\gamma^2}.$$

Hence, the asymptotic solutions of (6.2.11) as $\xi \to 1$, which are true for $\gamma > 0$ are

$$f(\xi) \sim \gamma(1-\xi^2)^{\frac{1}{2}}, \tag{6.3.13}$$

$$g(\xi) \sim \frac{\gamma\beta_2\xi^2}{(1-\xi^2)^{\frac{1}{2}}}, \tag{6.3.14}$$

$$P(\xi) \sim \frac{1}{2}\Lambda_2 \ln\left|\frac{1-\xi}{1+\xi}\right|, \tag{6.3.15}$$

where (6.3.15) is obtained by integrating (6.3.12). The velocity ratio is given by

$$\frac{v_x^*(t,x,z)}{L'(t)} = -\frac{1}{6c_2} f^2(\xi) P'(\xi), \tag{6.3.16}$$

and at the fracture tip, we have

$$\frac{v_x^*(t,L(t))}{L'(t)} = -\frac{1}{6c_2} f^2(1) P'(1) = 1 + \frac{\beta_2}{2c_2}. \tag{6.3.17}$$

Thus, for $\gamma \geqslant 0$, the fluid velocity is greater than the speed of fracture propagation at the fracture tip when $\beta_2 > 0$. For $\beta_2 = 0$, there is no fluid leak-off at the fracture tip and therefore, the fluid velocity at the tip equals the fracture propagation speed.

Equation (6.3.10) and (6.3.17) can be written as

$$v_x^*(t, L(t)) = L'(t) + \frac{\beta_2}{2c_2} L'(t), \tag{6.3.18}$$

for which the velocity of the fluid at the fracture tip equals the velocity of the fracture tip plus velocity of fluid leak-off relative to the tip. The velocity of leak-off at the fracture tip is then $\beta_2 L'(t)/2c_2$, for $0 \leqslant \beta_2 < \infty$.

Even though $v_n \propto h_x(t, x)$, it appears that the leak-off condition given by $v_z(t, x) = \pm h_t(t, x) \pm v_n$ breaks down at the fracture tip since fluid flow is horizontal there.

6.4 SPLINE METHOD

Similar to the preceding problem, we extract the tip behaviour of the similarity function $f(\xi)$ and then represent the remaining part of $f(\xi)$ using a linear spline. We divide the interval [0, 1] into n equally-spaced sub-intervals and then take $f(\xi)$ in each sub-interval to be of the form

$$f_i(\xi) = (1 - \xi^2)^{\frac{1}{2}} Y_i(\xi), \tag{6.4.1}$$

where $Y_i(\xi)$ is a piece-wise linear function given by

$$Y_i(\xi) = a_i \xi + b_i. \tag{6.4.2}$$

Dividing the interval [0,1] into n sub-intervals $[\eta_j, \eta_{j+1}], j = 0, 1, \ldots, n-1$ and after substituting (6.4.1) into (6.2.12), we obtain

$$P_{i\pm\alpha} = -\frac{2}{\pi} \sum_{j=0}^{n-1} \left[\fint_{\eta_j}^{\eta_{j+1}} \frac{\eta(1 - 2\eta^2) a_j \mathrm{d}\eta}{(\eta^2 - \xi_{i\pm\alpha}^2)\sqrt{1 - \eta^2}} - \fint_{\eta_j}^{\eta_{j+1}} \frac{\eta^2 b_j \mathrm{d}\eta}{(\eta^2 - \xi_{i\pm\alpha}^2)\sqrt{1 - \eta^2}} \right]. \tag{6.4.3}$$

where $\alpha = \pm 1/2, \pm 3/2$. Discretising (6.2.11) and approximating the pressure terms using central difference, we obtain

$$\begin{aligned} & c_2 \left(1 - \xi^2\right)^{\frac{1}{2}} (a_i \xi + b_i) - (2c_2 + \beta_2)\xi \left[\frac{(1 - 2\xi^2) a_i - \xi b_i}{\sqrt{1 - \xi^2}} \right] \\ & - (1 - \xi^2)(a_i \xi + b_i)^2 \left[\frac{(1 - 2\xi^2) a_i - \xi b_i}{\sqrt{1 - \xi^2}} \right] \left[\frac{P_{i+\frac{1}{2}} - P_{i-\frac{1}{2}}}{\xi_{i+\frac{1}{2}} - \xi_{i-\frac{1}{2}}} \right] \\ & - \frac{1}{3}(1 - \xi^2)^{\frac{3}{2}} (a_i \xi + b_i)^3 \left[\frac{P_{i-\frac{3}{2}} - P_{i-\frac{1}{2}} - P_{i+\frac{1}{2}} + P_{i+\frac{3}{2}}}{2\left(\xi_{i+\frac{1}{2}} - \xi_{i-\frac{1}{2}}\right)^2} \right] = 0, \end{aligned} \tag{6.4.4}$$

where $1 \leqslant i \leqslant n-1$. Since there are n sub-intervals, we will have $2n$ unknowns. The boundary condition (6.2.13a) and the slope condition (6.2.13b) are used to determine b_0 and a_0, respectively. As a result, there will be $2n-2$ unknowns remaining to be determined. We will obtain $n-1$ equations from (6.4.4) and an additional $n-1$ equations from the continuity condition. The continuity condition states that two successive linear splines are continuous at their common interior points, that is

$$Y_i(\xi_i) = Y_{i-1}(\xi_i), \qquad i = 1,2,3,\ldots,n-1. \tag{6.4.5}$$

Thus, for $n \geqslant 2$ we have

$$\begin{aligned} i=1: \quad & c_2\left(1-\xi^2\right)^{\frac{1}{2}}(a_1\xi+b_1) - (2c_2+\beta_2)\xi\left[\frac{(1-2\xi^2)a_1-\xi b_1}{\sqrt{1-\xi^2}}\right] \\ & - n(1-\xi^2)(a_1\xi+b_1)^2(P_{\frac{3}{2}}-P_{\frac{1}{2}})\left[\frac{(1-2\xi^2)a_1-\xi b_1}{\sqrt{1-\xi^2}}\right] \\ & - \frac{n^2}{6}(1-\xi^2)^{\frac{3}{2}}(a_1\xi+b_1)^3(P_{\frac{5}{2}}-P_{\frac{3}{2}}) = 0, \end{aligned} \tag{6.4.6}$$

$$\begin{aligned} i=2: \quad & c_2\left(1-\xi^2\right)^{\frac{1}{2}}(a_2\xi+b_2) - (2c_2+\beta_2)\xi\left[\frac{(1-2\xi^2)a_2-\xi b_2}{\sqrt{1-\xi^2}}\right] \\ & - n(1-\xi^2)(a_2\xi+b_2)^2(P_{\frac{5}{2}}-P_{\frac{3}{2}})\left[\frac{(1-2\xi^2)a_2-\xi b_2}{\sqrt{1-\xi^2}}\right] \\ & - \frac{n^2}{6}(1-\xi^2)^{\frac{3}{2}}(a_2\xi+b_2)^3(P_{\frac{1}{2}}-P_{\frac{3}{2}}-P_{\frac{5}{2}}+P_{\frac{7}{2}}) = 0, \end{aligned} \tag{6.4.7}$$

$$\vdots \qquad\qquad \vdots$$

$$\begin{aligned} i=n-1: \quad & c_2\left(1-\xi^2\right)^{\frac{1}{2}}(a_{n-1}\xi+b_{n-1}) - (2c_2+\beta_2)\xi\left[\frac{(1-2\xi^2)a_{n-1}-\xi b_{n-1}}{\sqrt{1-\xi^2}}\right] \\ & - n(1-\xi^2)(a_{n-1}\xi+b_{n-1})^2\left(P_{n-\frac{1}{2}}-P_{n-\frac{3}{2}}\right)\left[\frac{(1-2\xi^2)a_{n-1}-\xi b_{n-1}}{\sqrt{1-\xi^2}}\right] \\ & - \frac{n^2}{6}(1-\xi^2)^{\frac{3}{2}}(a_{n-1}\xi+b_{n-1})^3\left(P_{n-\frac{5}{2}}-P_{n-\frac{3}{2}}-P_{n-\frac{1}{2}}-\gamma n^{\frac{1}{2}}\right) = 0. \end{aligned} \tag{6.4.8}$$

Similarly, from the continuity condition we obtain

$$i=1: \quad a_1\xi_1 + b_1 - b_0 = 0, \tag{6.4.9}$$

$$i=2: \quad (a_2-a_1)\xi_2 + b_2 - b_1 = 0, \tag{6.4.10}$$

$$\vdots \qquad\qquad \vdots$$

$$i = n-1: \quad (a_{n-1} - a_{n-2})\xi_{n-1} + b_{n-1} - b_{n-2} = 0. \tag{6.4.11}$$

The resulting system of equations is solved for the unknown coefficients using a Matlab built-in function *fsolve*.

6.5 NUMERICAL RESULTS AND DISCUSSIONS

In this section, the numerical results for the fracture half-width, volume and length are shown, as well as the results for the leak-off fluid velocity and pressure. We also show the relationship between the parameters $c_2, \beta_2, Q_0, \gamma$ in the model.

Figure 26 illustrates the evolution of the fracture half-width, $h(t,x)$, over time for $\beta_2 = 0, 0.01, 0.04$ when $\gamma = 0.5$ and $Q_0 = 0.2$. When $\beta_2 = 0$, the rock is impermeable, while for $\beta_2 > 0$ there is fluid leak-off at the interface. The rate of growth for the fracture half-width can be seen to decrease with time, as β_2 increases.

In Figure 27, $h(t,x), v_n(t,x)$ and $p(t,x)$ are plotted for $\beta_2 = 0$, 0.005, 0.01 and 0.04 when $\gamma = 0.5$ and $Q_0 = 0.2$. As the parameter β_2 increases in Figure 27(i), the rate at which the fracture half-width evolves decreases. The half-width of the fracture evolves the least extent when $\beta_2 = 0.04$, for which the leak-off is highest and evolves the greatest when $\beta_2 = 0$, for which the rock is impermeable. In Figure 27 (ii), $v_n(t,x)$ is approximately zero at the interface near the fracture entry and $v_n \to \infty$ at the fracture tip for $\beta_2 > 0$. Therefore, there is fluid leak-off at the interface in the region $0 \leqslant x \leqslant L(t)$. In Figure 27(iii), $p(t,x)$ is positive along x except in the neighbourhood of the fracture tip where it drops off at a faster rate to negative values.

In Figure 28, $h(t,x), v_n(t,x)$ and $p(t,x)$ are plotted for $Q_0 = 0.1, 0.15$, 0.2 and 0.23 when $\gamma = 0.5$ and $\beta_2 = 0.01$. As the parameter Q_0 increases in Figure 28(i), the rate at which the half-width of the fracture evolves increases. The fracture half-width evolved the least when $Q_0 = 0.1$, for which the rate of fluid injection into the fracture at the fracture entry is low and evolved the greatest when $Q_0 = 0.23$, for which the rate of fluid injection at the fracture entry is high. In the neighbourhood of the fracture entry in Figure 28(ii), $v_n(t,x)$ is approximately zero and at the fracture tip, $v_n(t, L(t)) = \infty$. In Figure 28(iii), $p(t,x) > 0$ across the fracture except in the neighbourhood of the fracture tip.

In Figure 29, $h(t,x)$, $v_n(t,x)$ and $p(t,x)$ are plotted for $\gamma = 0, 0.5$, 1 and 2 when $Q_0 = 0.2$ and $\beta_2 = 0.01$. The half-width of the fracture and the velocity of fluid leak-off were slightly affected by the increase in γ as shown in Figure 29(i) and Figure 29(ii), respectively. When $\gamma = 0$, the pressure remained positive across the fracture and when $\gamma > 0$, the pressure is positive across the fracture except at the fracture tip where it tends to negative infinity.

(i)

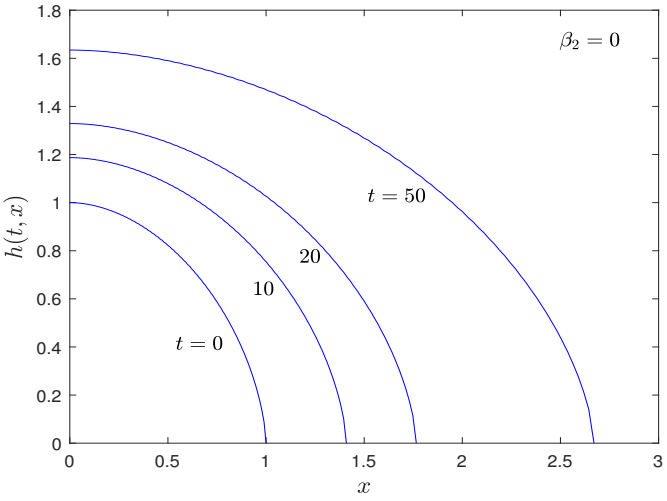

(ii)

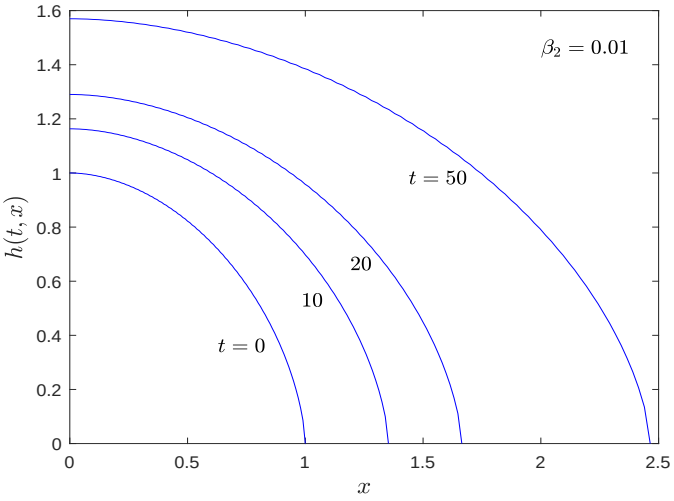

(iii)

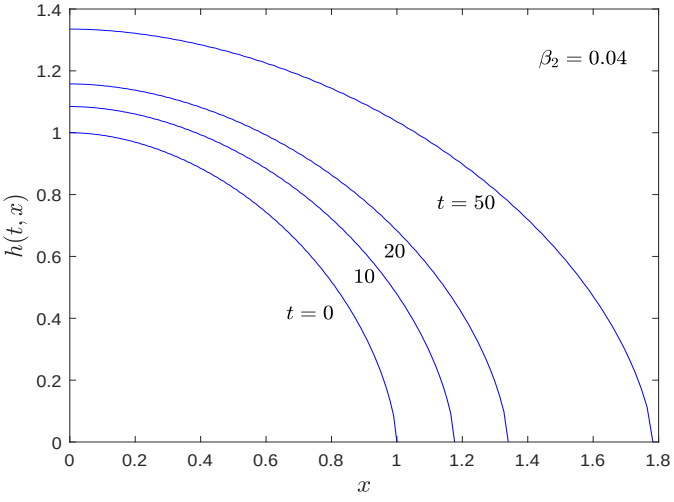

Figure 26: Graph of $h(t,x)$ plotted against x at times $t = 0, 10, 20, 50$ for $Q_0 = 0.2$, $\gamma = 0.5$ and for (i) $\beta_2 = 0$ and $c_2 = 0.022433$, (ii) $\beta_2 = 0.01$ and $c_2 = 0.019125$ and (iii) $\beta_2 = 0.04$ and $c_2 = 0.009200$.

(i)

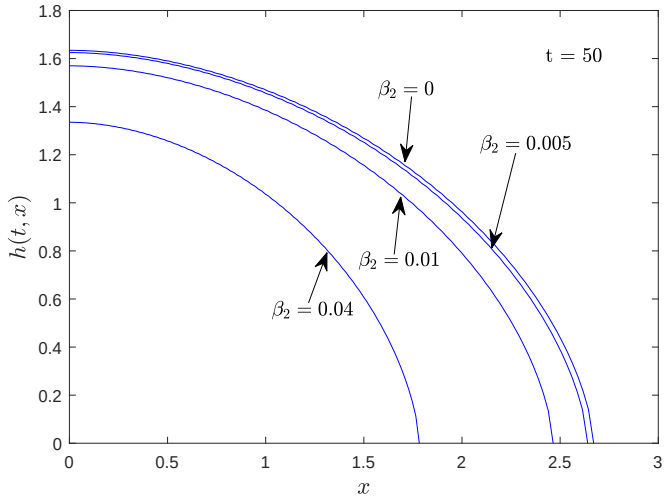

(ii)

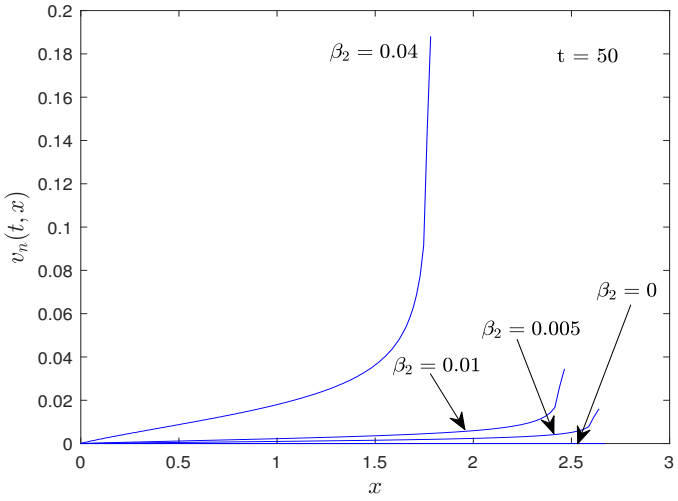

(iii)

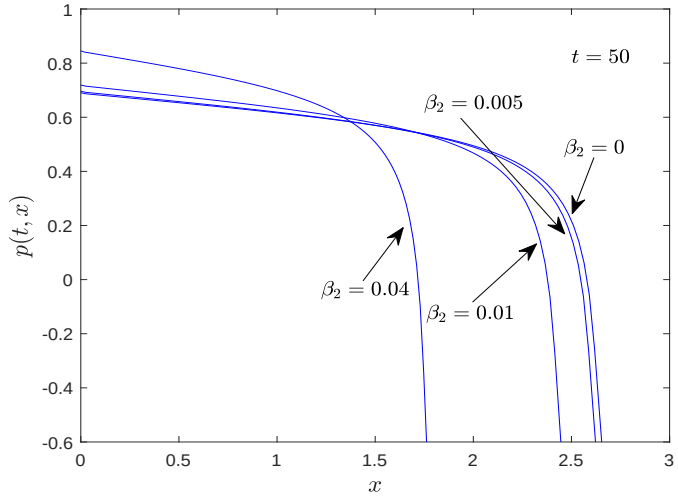

Figure 27: Graphs of (i) the fracture half-width $h(t,x)$, (ii) leak-off fluid velocity $v_n(t,x)$ and (iii) the fluid pressure $p(t,x)$, plotted against x for $\beta_2 = 0$, 0.005, 0.01, 0.04 when $Q_0 = 0.2$ and $\gamma = 0.5$ at $t = 50$.

(i)

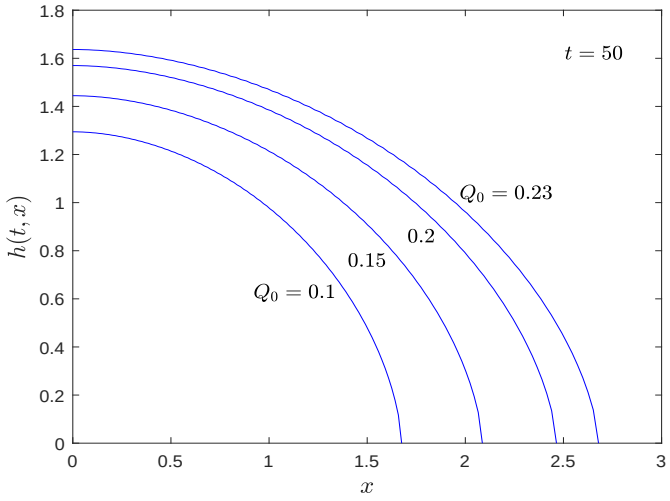

(ii)

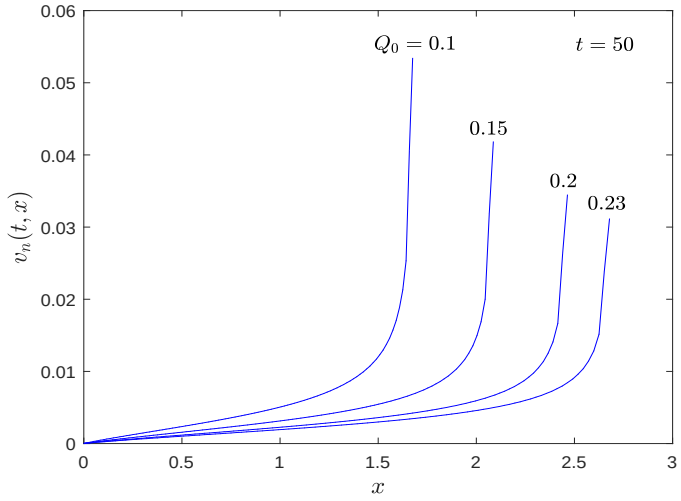

(iii)

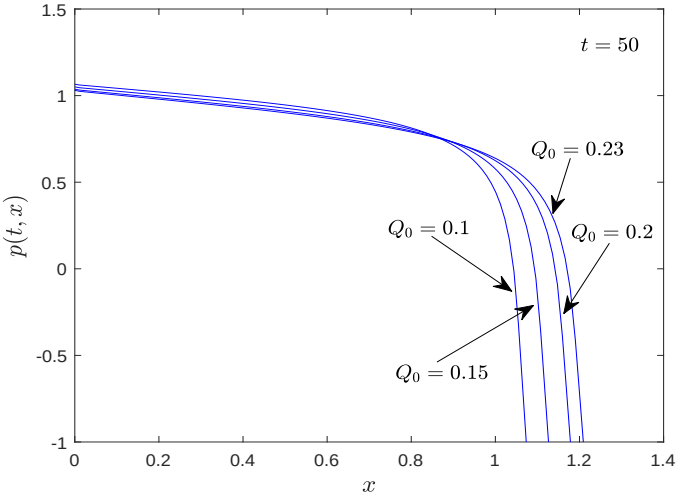

Figure 28: Graphs of (i) the fracture half-width $h(t,x)$, (ii) leak-off fluid velocity $v_n(t,x)$ and (iii) the fluid pressure $p(t,x)$, plotted against x for $Q_0 = 0.1, 0.15, 0.2, 0.23$ when $\gamma = 0.5$ and $\beta_2 = 0.01$ at $t = 50$.

(i)

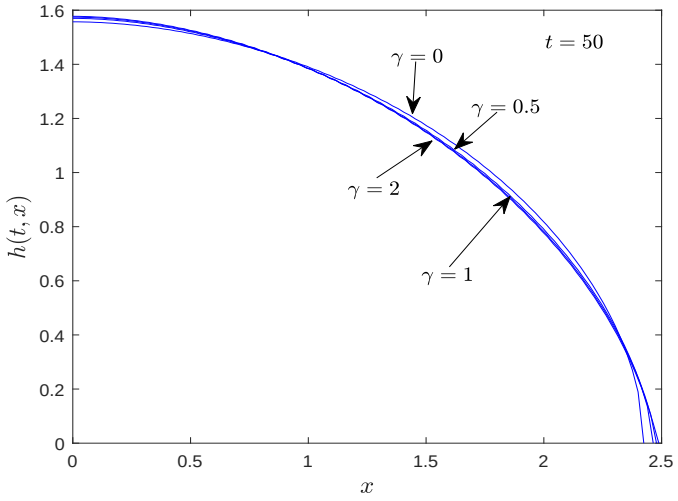

(ii)

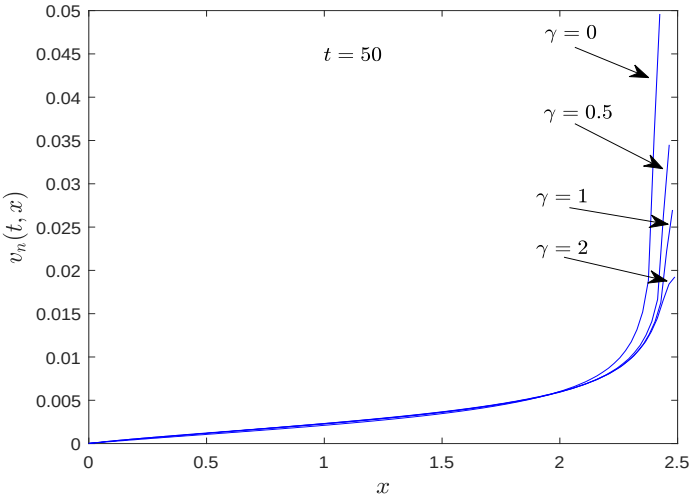

(iii)

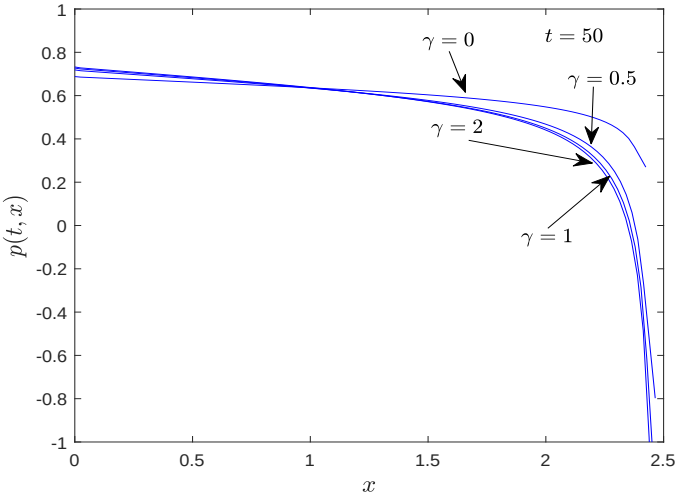

Figure 29: Graphs of (i) the fracture half-width $h(t,x)$, (ii) leak-off fluid velocity $v_n(t,x)$ and (iii) the fluid pressure $p(t,x)$, plotted against x for $\gamma = 0, 0.5, 1, 2$ when $Q_0 = 0.2$ and $\beta_2 = 0.01$ at $t = 50$.

(i)

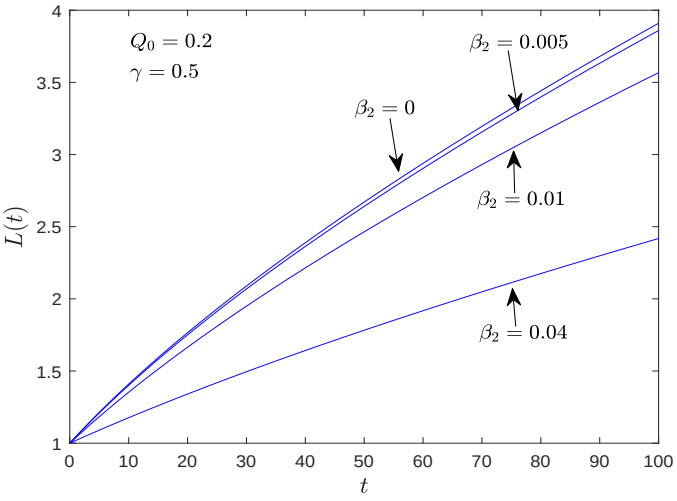

(ii)

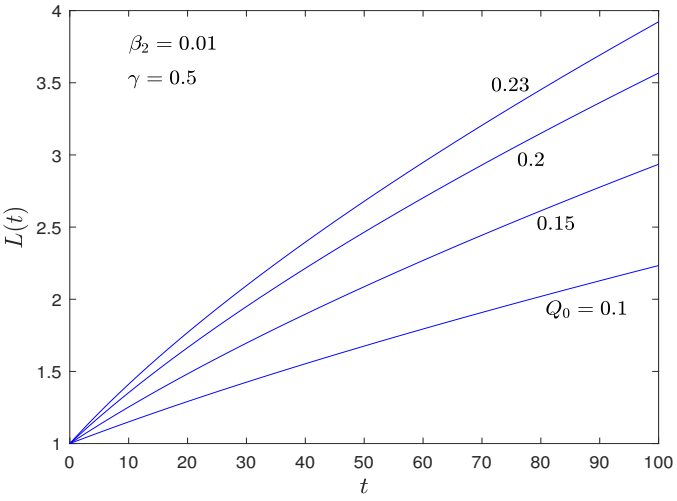

(iii)

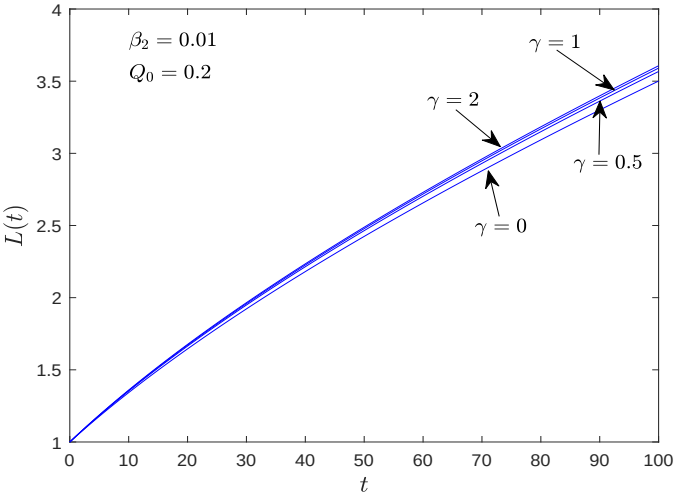

Figure 30: Fracture length plotted for various values of (i) β_2, (ii) Q_0, (iii) γ.

(i)

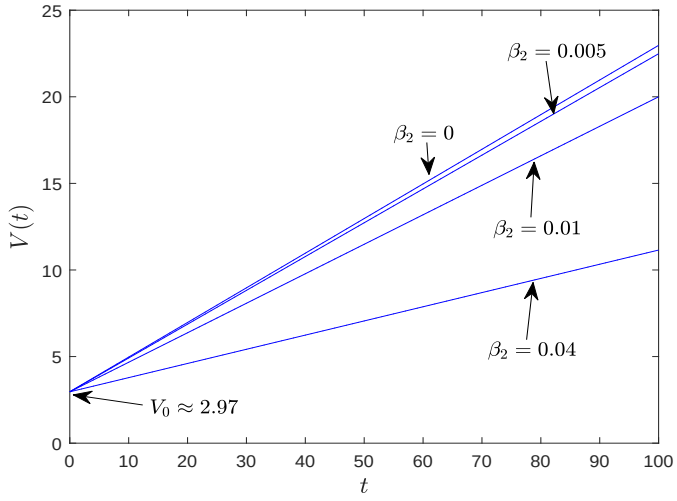

(ii)

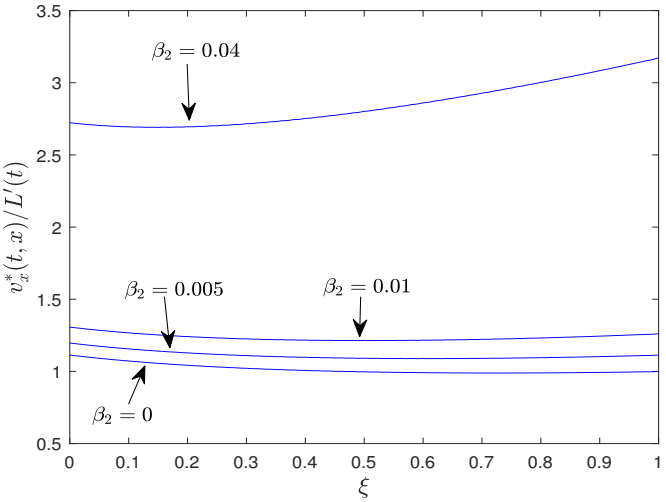

(iii)

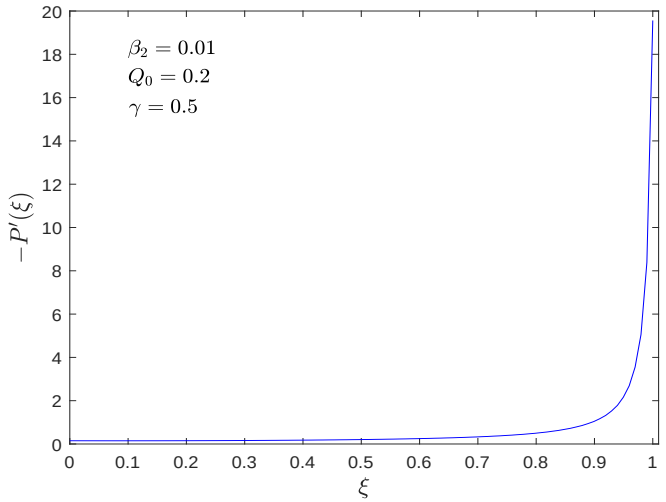

Figure 31: Graphs illustrating (i) fracture volume plotted against t for $\beta_2 = 0, 0.005, 0.01, 0.04$ when $Q_0 = 0.2$ and $\gamma = 0.5$ (ii) velocity ratio $v_x^*(t,x)/L'(t))$ plotted against ξ for $\beta_2 = 0, 0.005, 0.01, 0.04$ when $Q_0 = 0.2$ and $\gamma = 0.5$, (iii) dimensionless pressure gradient for $Q_0 = 0.2$, $\gamma = 0.5$ and $\beta_2 = 0.01$.

(i)

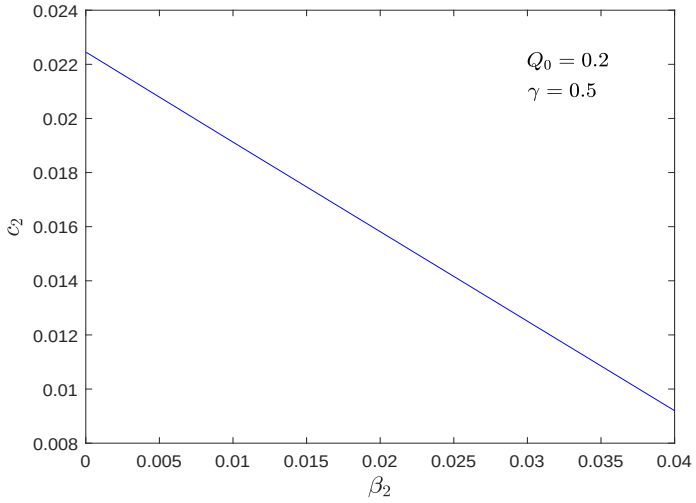

(ii)

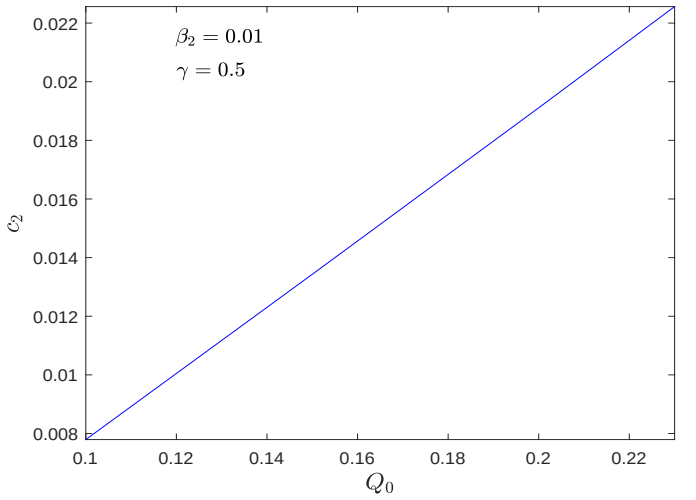

(iii)

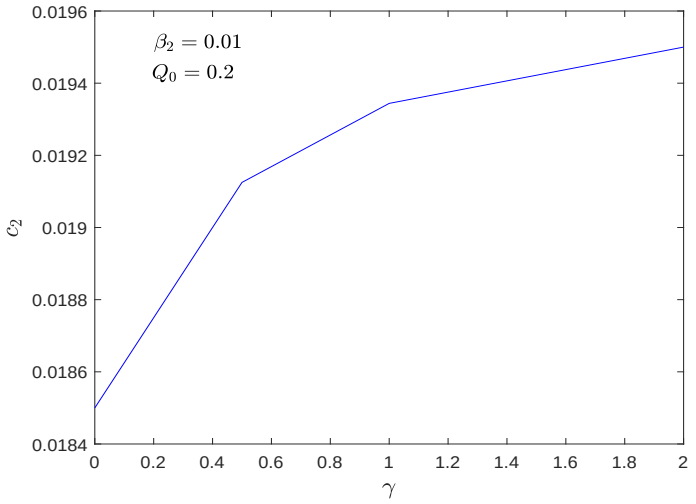

Figure 32: The constant c_2 plotted against (i) β_2, (ii) Q_0, (iii) γ.

In Figure 30(i-iii), the fracture length $L(t)$ is plotted against t for varied values of β_2, Q_0 and γ. The length of the fracture is an increasing function and $L(t) \to \infty$ as $t \to \infty$. In Figure 30(i), $L(t)$ is plotted against time t for $\beta_2 = 0, 0.005, 0.01$ and 0.4. It can be seen that the length of the fracture grows strongly when $\beta_2 = 0$, for which there is no fluid leak-off at the interface and it grows the weakest when $\beta_2 = 0,04$, fro which leak-off is the highest. Figure 30(ii) illustrates the graphs of the fracture length over time for $Q_0 = 0.1, 0.15$, 0.2 and 0.23 when $\gamma = 0.5$ and $\beta_2 = 0.01$. As expected, the fracture length $L(t)$ increases as Q_0 increases. In Figure 30(iii), $L(t)$ is plotted for $\gamma = 0, 0.5$, 1 and 2 when $Q_0 = 0.2$ and $\beta_2 = 0.01$. An increase in γ resulted in a slight increase in the rate of growth of the fracture length. The growth of $L(t)$ was stronger when $\gamma = 2$ and weaker when $\gamma = 0$.

Figure 31, illustrates the fracture volume over time, the velocity ratio and the non-dimensional pressure gradient. Figure 31 (i) shows that larger β_2 values imply smaller fracture volumes. In Figure 31(ii), the velocity ratio along the fracture is plotted against ξ for various values of β_2. For smaller β_2 values, the width-averaged velocity was slightly greater than the propagation speed of the fracture while for larger values of β_2 the width-averaged velocity was significantly greater than the propagation speed of the fracture. In Figure 31(iii), the dimensionless pressure gradient is plotted against ξ for $\beta_2 = 0.01$, $Q_0 = 0.2$ and $\gamma = 0.5$.

Figure 32 depicts the relationship between the parameters c_2, β_2, Q_0 and γ. In Figure 32(i-ii), it can be seen that c_2 decreases as a linear function of β_2 while the fluid flux at the fracture entry Q_0 is directly proportional to c_2. In Figure 32(iii), c_2 is plotted against the dimensionless stress intensity factor γ. For the values of γ considered, c_2 increases as a function of γ.

6.6 CONCLUSION

Numerical solutions have been presented to the boundary value problem for the integro-differential system derived in Chapter 4 when the permeability of the fluid-rock interface is such that the leak-off velocity is proportional to the gradient of the fluid-rock interface. The integro-differential system contained four parameters c_2, β_2, Q_0 and γ, which all had to be specified except c_2. The constant c_2 was obtained as part of the solution using a flux boundary condition.

Numerical solutions were found for the fracture volume, $V(t)$, fracture length, $L(t)$, fracture half-width, $h(t,x)$, leak-off velocity, $v_n(t,x)$ and fluid pressure, $p(t,x)$ for various values of the parameters.

For all the solutions obtained, $h_x(t,x) \to \pm\infty$, as $x \to \mp L(t)$, and as a result, the lubrication approximation breaks down near $x = L(t)$.

Finally, the velocity ratio at the fracture tip satisfies $v_x^*(t,x)/L'(t) > 0$, suggesting that the fluid velocity at the fracture tip is greater than

the speed of fracture propagation. This results is largely attributed to the fluid leak-off at the fracture tip, in the horizontal direction.

7

TWO-DIMENSIONAL FLUID-DRIVEN FRACTURE WITH DARCY FLOW IN PERMEABLE ROCK FORMATION

7.1 INTRODUCTION

In Chapter 5 and 6, a model for fluid leak-off was not prescribed. Instead, a relationship between the leak-off function $g(\xi)$ and the half-width function $f(\xi)$ was stated. This relationship involved a constant of proportionality β which played an important role in quantifying the leak-off extent. The higher β was, the more the fluid leak-off through the fluid-rock interface, which impacts on the growth rate of the fracture half-width. Darcy model will now be employed to model the fluid leak-off through the interface into the porous rock formation. In [60], a mathematical model was derived for a two-dimensional fracture in PKN theory, with fluid leak-off through the interface into the porous rock formation modelled using Darcy 's law.

7.2 FLUID LEAK-OFF INTO THE PERMEABLE MEDIUM

The flow of fluid through the fluid-rock interface into the porous rock matrix is taken to be one-dimensional, in the direction normal to the fracture interface $z = h(x,t)$ and obeys Darcy's law given by equation (1.4.3). Equation (1.4.3) in the z-direction, given that $Q/A = b_t(t,x)$, becomes

$$\frac{\partial p_d}{\partial z} = -\frac{\mu}{\kappa}\frac{\partial b}{\partial t}, \tag{7.2.1}$$

where $b(t,x)$ is the leak-off depth measured relative to the fracture interface and $b_t(t,x)$ is taken to be the velocity of the fluid that has leaked-off at the fracture interface. The leak-off velocity $b_t(t,x)$ is measured relative to the interface in the normal direction. Integrating (7.2.1) with respect to z from h to $h+b$, we get

$$p_d(t,x,h+b) - p_d(t,x,h) = -\frac{\mu}{\kappa} b \frac{\partial b}{\partial t}. \tag{7.2.2}$$

Using the pressure condition at the boundary given by

$$p_d(t,x,h+b) = 0 \qquad \text{and} \qquad p_d(t,x,h) = p(t,x), \tag{7.2.3}$$

equation (7.2.2) becomes

$$\frac{\partial b}{\partial t} = \frac{\kappa}{\mu}\frac{p}{b}. \tag{7.2.4}$$

Substituting the non-dimensional variables in (4.3.12) into (7.2.4), and using the fact that $P = \mu U L_0 / H^2$, we find

$$\frac{\partial \bar{b}}{\partial \bar{t}} = \kappa \frac{UTL_0}{H^2 B^2} \frac{\bar{p}}{\bar{b}}. \tag{7.2.5}$$

Thus, (7.2.5) in dimensionless form, after dropping the overhead bars, becomes

$$\frac{\partial b}{\partial t} = \frac{p}{b}, \tag{7.2.6}$$

where

$$B = \left[\frac{\kappa UTL_0}{H^2} \right]^{\frac{1}{2}}.$$

7.3 TWO-DIMENSIONAL FLUID-DRIVEN FRACTURE WITH DARCY FLOW MODEL

By writing $v_n = b_t(t,x)$, the nonlinear diffusion equation, in dimensionless form, is now given by

$$\frac{\partial h}{\partial t} - \frac{1}{3} \frac{\partial}{\partial x} \left(h^3 \frac{\partial p}{\partial x} \right) + \frac{\partial b}{\partial t} = 0. \tag{7.3.1}$$

Consider now the boundary conditions for the problem. The rock has a pre-existing fracture, hence

$$t = 0: \quad h(0,x) = h_0(x), \quad b(0,x) = b_0(x), \quad 0 \leqslant x \leqslant L(t). \tag{7.3.2}$$

The initial conditions are

$$t = 0: \quad L(0) = 1, \quad h(0,0) = 1. \tag{7.3.3}$$

We assume that the slope of the fracture and the slope of the leak-off depth are zero at $x = 0$ since we assume the fracture is symmetric with respect to $x = 0$ and smooth [26]

$$\left. \frac{\partial h}{\partial x} \right|_{x=0} = 0, \quad \text{and} \quad \left. \frac{\partial b}{\partial x} \right|_{x=0} = 0. \tag{7.3.4}$$

At the fracture tip

$$x = L(t): \qquad h(t, L(t)) = 0, \quad b(t, L(t)) = 0. \tag{7.3.5}$$

The fracture half-width together with the leak-off depth vanishes at the fracture tip.

The mathematical formulation for the two-dimensional hydraulic fracture with Darcy flow is summarized as follows:

$$\frac{\partial h}{\partial t} - \frac{1}{3}\frac{\partial}{\partial x}\left(h^3\frac{\partial p}{\partial x}\right) + \frac{\partial b}{\partial t} = 0, \tag{7.3.6}$$

$$\frac{\partial b}{\partial t} = \frac{p}{b}, \tag{7.3.7}$$

$$p(t,x) = -\frac{2}{\pi}\int_0^L \frac{\partial h}{\partial s}\frac{s}{s^2-x^2}\mathrm{d}s, \tag{7.3.8}$$

$$h(0,0) = 1,\ h_x(t,0) = 0,\ b_x(t,0) = 0,\ h(t,L(t)) = 0,\ b(t,L(t)) = 0, \tag{7.3.9a-e}$$

where

$$-p(t,x) \to \frac{\gamma}{[2(x-L(t))]^{\frac{1}{2}}} \quad \text{as} \quad x \to L^+. \tag{7.3.10}$$

The flux of fluid leaving the fracture at the interface becomes

$$Q_\ell = 4\int_0^{L(t)} \frac{\partial b(t,x)}{\partial t}\mathrm{d}x. \tag{7.3.11}$$

The global mass balance equation (4.6.21) becomes

$$\frac{\mathrm{d}V}{\mathrm{d}t} = 4h(t,0)v_x^*(t,0) - 4\int_0^{L(t)} \frac{\partial b}{\partial t}\mathrm{d}x. \tag{7.3.12}$$

Similarity Solution

We now reduce the system of partial differential equations (7.3.6)-(7.3.10) into a system of ordinary differential equations.

First, we introduce the similarity variable $\xi = x/L(t)$ and seek the solution of the system in the form

$$h(t,x) = a(t)f(\xi), \quad b(t,x) = r(t)g(\xi), \tag{7.3.13a-b}$$

where $a(t)$, $r(t)$ and $L(t)$ have to be determined. The similarity form of pressure derived in Section 4.6 is given by

$$p(t,x) = \frac{a(t)}{L(t)}P(\xi), \tag{7.3.14}$$

where

$$p(\xi) = -\frac{2}{\pi}\int_0^1 \frac{\mathrm{d}f}{\mathrm{d}\eta}\frac{\eta}{\eta^2-\xi^2}\mathrm{d}\eta. \tag{7.3.15}$$

Substituting (7.3.13a-b) and (7.3.14) into (7.3.6) and (7.3.7) gives

$$\left[-\frac{a(t)}{L(t)}\frac{\mathrm{d}L}{\mathrm{d}t}\xi\frac{\mathrm{d}f}{\mathrm{d}\xi} + \frac{\mathrm{d}a}{\mathrm{d}t}f(\xi)\right] - \frac{1}{3}\frac{a^4(t)}{L^3(t)}\frac{\mathrm{d}}{\mathrm{d}\xi}\left(f^3\frac{\mathrm{d}P}{\mathrm{d}\xi}\right) + \frac{a(t)}{r(t)L(t)}\frac{P(\xi)}{g(\xi)} = 0, \tag{7.3.16}$$

$$-\frac{r(t)}{L(t)}\frac{\mathrm{d}L}{\mathrm{d}t}\xi\frac{\mathrm{d}g}{\mathrm{d}\xi}+\frac{\mathrm{d}r}{\mathrm{d}t}g(\xi)=\frac{a(t)}{r(t)L(t)}\frac{P(\xi)}{g(\xi)}. \tag{7.3.17}$$

With further simplification, we obtain

$$\left[-\frac{L^2(t)}{a^3(t)}\frac{\mathrm{d}L}{\mathrm{d}t}\xi\frac{\mathrm{d}f}{\mathrm{d}\xi}+\frac{L^3(t)}{a^4(t)}\frac{\mathrm{d}a}{\mathrm{d}t}f(\xi)\right]-\frac{1}{3}\frac{\mathrm{d}}{\mathrm{d}\xi}\left(f^3\frac{\mathrm{d}P}{\mathrm{d}\xi}\right)+\frac{L^2(t)}{a^3(t)r(t)}\frac{P(\xi)}{g(\xi)}=0. \tag{7.3.18}$$

$$-\xi\frac{\mathrm{d}g}{\mathrm{d}\xi}+\frac{L(t)}{r(t)}\left(\frac{\mathrm{d}L}{\mathrm{d}t}\right)^{-1}\frac{\mathrm{d}r}{\mathrm{d}t}g(\xi)=\frac{a(t)}{r^2(t)}\left(\frac{\mathrm{d}L}{\mathrm{d}t}\right)^{-1}\frac{P(\xi)}{g(\xi)}. \tag{7.3.19}$$

For a similarity solution to exists it is necessary that we set

$$\begin{aligned}&\frac{L^2(t)}{a^3(t)}\frac{\mathrm{d}L}{\mathrm{d}t}=c_1,\quad \frac{L^3(t)}{a^4(t)}\frac{\mathrm{d}a}{\mathrm{d}t}=c_2,\quad \frac{L^2(t)}{a^3(t)r(t)}=c_3,\\ &\frac{L(t)}{r(t)}\frac{\mathrm{d}r}{\mathrm{d}t}\left(\frac{\mathrm{d}L}{\mathrm{d}t}\right)^{-1}=c_4,\quad \frac{a(t)}{r^2(t)}\left(\frac{\mathrm{d}L}{\mathrm{d}t}\right)^{-1}=c_5,\end{aligned} \tag{7.3.20a-e}$$

so that the system depends on the variable ξ only. Here c_1, c_2, c_3, c_4 and c_5 are constants. Then, we have that

$$\left[c_2f(\xi)-c_1\xi\frac{\mathrm{d}f}{\mathrm{d}\xi}\right]-\frac{1}{3}\frac{\mathrm{d}}{\mathrm{d}\xi}\left(f^3\frac{\mathrm{d}P}{\mathrm{d}\xi}\right)+c_3\frac{P(\xi)}{g(\xi)}=0, \tag{7.3.21}$$

$$c_4g(\xi)-\xi\frac{\mathrm{d}g}{\mathrm{d}\xi}=c_5\frac{P(\xi)}{g(\xi)}. \tag{7.3.22}$$

In order to proceed from here, we first solve for the functions $L(t)$, $a(t)$, and $r(t)$. We begin by rearranging the equations in (7.3.20a-e) as follows

$$\begin{aligned}&\frac{\mathrm{d}L}{\mathrm{d}t}=c_1\frac{a^3(t)}{L^2(t)},\quad \frac{\mathrm{d}a}{\mathrm{d}t}=c_2\frac{a^4(t)}{L^3(t)},\quad r(t)=\frac{1}{c_3}\frac{L^2(t)}{a^3(t)},\\ &\frac{\mathrm{d}r}{\mathrm{d}t}=c_4\frac{r(t)}{L(t)}\frac{\mathrm{d}L}{\mathrm{d}t},\quad r^2(t)=\frac{a(t)}{c_5}\left(\frac{\mathrm{d}L}{\mathrm{d}t}\right)^{-1}.\end{aligned} \tag{7.3.23a-e}$$

Now, consider the pressure near but just outside the fracture tip. In terms of similarity variables, (4.5.16) is expressed as

$$-P(\xi)\to\frac{\gamma}{[2(\xi-1)]^{\frac{1}{2}}}\frac{L^{\frac{1}{2}}(t)}{a(t)}\quad\text{as}\quad\xi\to1^+. \tag{7.3.24}$$

That is,

$$-P(\xi)\to\frac{\gamma}{[2(\xi-1)]^{\frac{1}{2}}}\quad\text{as}\quad\xi\to1^+, \tag{7.3.25}$$

where

$$a(t) = L^{\frac{1}{2}}(t). \tag{7.3.26}$$

Substituting (7.3.26) into (7.3.23a) and solving for $L(t)$ subject to the initial condition $L(0) = 1$ yields

$$L(t) = \left(\frac{3}{2}c_1 t + 1\right)^{\frac{2}{3}}. \tag{7.3.27}$$

Solving for $a(t)$ using (7.3.23b) gives

$$a(t) = (3c_2 t + k_2)^{\frac{1}{3}}. \tag{7.3.28}$$

Using (7.3.26) and (7.3.28), the length can be equivalently expressed as

$$L(t) = (3c_2 t + k_2)^{\frac{2}{3}}. \tag{7.3.29}$$

Equating (7.3.27) and (7.3.29) yields

$$c_1 = 2c_2 \quad \text{and} \quad k_2 = 1. \tag{7.3.30}$$

Therefore,

$$L(t) = (3c_2 t + 1)^{\frac{2}{3}} \tag{7.3.31}$$

$$a(t) = (3c_2 t + 1)^{\frac{1}{3}}. \tag{7.3.32}$$

The function $r(t)$ can be easily obtained as

$$r(t) = \frac{1}{c_3}\frac{(3c_2 t + 1)^{\frac{4}{3}}}{(3c_2 t + 1)} = \frac{1}{c_3}(3c_2 t + 1)^{\frac{1}{3}} = \frac{1}{c_3}a(t). \tag{7.3.33}$$

Taking the first derivative of both $L(t)$ and $r(t)$, we obtain

$$\frac{\mathrm{d}L}{\mathrm{d}t} = \frac{2c_2}{a(t)}, \quad \frac{\mathrm{d}r}{\mathrm{d}t} = \frac{c_2}{c_3 a^2(t)}. \tag{7.3.34a-b}$$

Using the functions $L(t)$, $r(t)$ and their derivatives given in (7.3.34a-b), equation (7.3.23d) gives

$$c_4 = \frac{1}{2}. \tag{7.3.35}$$

Substituting (7.3.33) and (7.3.34a) into (7.3.23e) yields

$$c_3^2 = 2c_2 c_5. \tag{7.3.36}$$

The mathematical formulation of the problem is summarized as follows

$$c_2\left[f(\xi) - 2\xi\frac{\mathrm{d}f}{\mathrm{d}\xi}\right] - \frac{1}{3}\frac{\mathrm{d}}{\mathrm{d}\xi}\left(f^3\frac{\mathrm{d}P}{\mathrm{d}\xi}\right) + c_3\frac{P(\xi)}{g(\xi)} = 0, \tag{7.3.37}$$

$$g(\xi) - 2\xi\frac{\mathrm{d}g}{\mathrm{d}\xi} = 2c_5\frac{P(\xi)}{g(\xi)}, \tag{7.3.38}$$

$$P(\xi) = -\frac{2}{\pi}\int_0^1 \frac{\mathrm{d}f}{\mathrm{d}\eta}\frac{\eta}{\eta^2 - \xi^2}\mathrm{d}\eta, \tag{7.3.39}$$

$$f(0) = 1,\ f'(0) = 0,\ g'(0) = 0,\ f(1) = 0,\ g(1) = 0, \tag{7.3.40a-e}$$

where

$$-P(\xi) \to \frac{\gamma}{[2(\xi-1)]^{\frac{1}{2}}} \quad \text{as} \quad \xi \to 1^{+}. \tag{7.3.41}$$

The similarity solutions are given by

$$L(t) = (3c_2 t + 1)^{\frac{2}{3}}, \tag{7.3.42}$$

$$h(t,x) = L^{\frac{1}{2}}(t) f(\xi), \tag{7.3.43}$$

$$b(t,x) = c_3^{-1} L^{\frac{1}{2}}(t) g(\xi), \tag{7.3.44}$$

$$v_n(t,x) = \frac{c_2}{c_3 L(t)} \left[g(\xi) - 2\xi g'(\xi) \right], \tag{7.3.45}$$

$$p(t,x) = L^{-\frac{1}{2}}(t) P(\xi), \tag{7.3.46}$$

$$c_1 = 2c_2, \quad c_1 c_5 = c_3^2. \tag{7.3.47a-b}$$

Equation $c_1 c_5 = c_3^2$ is satisfied when

$$c_1 = \frac{c_3}{\alpha} \quad \text{and} \quad c_5 = \alpha c_3, \quad \alpha \neq 0 \in \mathbb{R}. \tag{7.3.48a-b}$$

Using (7.3.48a-b), (7.3.37) and (7.3.38) can be expressed equivalently as

$$c_2 \left[f(\xi) - 2\xi \frac{\mathrm{d}f}{\mathrm{d}\xi} \right] - \frac{1}{3} \frac{\mathrm{d}}{\mathrm{d}\xi} \left(f^3 \frac{\mathrm{d}P}{\mathrm{d}\xi} \right) + 2\alpha c_2 \frac{P(\xi)}{g(\xi)} = 0, \tag{7.3.49}$$

$$g(\xi) - 2\xi \frac{\mathrm{d}g}{\mathrm{d}\xi} - 4\alpha^2 c_2 \frac{P(\xi)}{g(\xi)} = 0. \tag{7.3.50}$$

Differentiating (7.3.44) with respect to t and substituting into (7.3.11), we obtain

$$Q_\ell = 4 \frac{c_2}{c_3} \int_0^1 \left[g(\xi) - 2\xi \frac{\mathrm{d}g}{\mathrm{d}\xi} \right] \mathrm{d}\xi. \tag{7.3.51}$$

Integrating by parts and using the fact that $c_3 = 2\alpha c_2$, we obtain

$$Q_\ell = 6\alpha^{-1} \int_0^1 g(\xi) \mathrm{d}\xi. \tag{7.3.52}$$

The global mass balance equation is then given by

$$12 c_2 \int_0^1 f(\xi) \mathrm{d}\xi = -\frac{4}{3} f^3(0) \frac{\partial P(0)}{\partial \xi} - 6\alpha^{-1} \int_0^1 g(\xi) \mathrm{d}\xi. \tag{7.3.53}$$

Before we state the complete mathematical formulation of the problem, let us first derive the expression for the pressure gradient. Equation (7.3.49) can be rewritten as

$$\frac{\mathrm{d}}{\mathrm{d}\xi} \left(f^3 \frac{\mathrm{d}P}{\mathrm{d}\xi} \right) = 9c_2 f(\xi) - 6c_2 (\xi f(\xi))_\xi + \frac{9g(\xi)}{2\alpha} - \frac{3}{\alpha} (\xi g(\xi))_\xi. \tag{7.3.54}$$

Integrating (7.3.54) with respect to ξ from ξ to 1 gives

$$-f^3\frac{\mathrm{d}P}{\mathrm{d}\xi} = 9c_2\int_\xi^1 f(\eta)\mathrm{d}\eta + \frac{9}{2\alpha}\int_\xi^1 g(\eta)\mathrm{d}\eta + 6c_2\xi f(\xi) + \frac{3}{\alpha}\xi g(\xi). \tag{7.3.55}$$

Thus,

$$-\frac{\mathrm{d}P}{\mathrm{d}\xi} = \frac{1}{f^3(\xi)}\left[9c_2\int_\xi^1 f(\eta)\mathrm{d}\eta + \frac{9}{2\alpha}\int_\xi^1 g(\eta)\mathrm{d}\eta + 6c_2\xi f(\xi) + \frac{3}{\alpha}\xi g(\xi)\right]. \tag{7.3.56}$$

The pressure gradient at $\xi = 0$ is

$$-\left.\frac{\mathrm{d}P}{\mathrm{d}\xi}\right|_{\xi=0} = \frac{1}{f^3(0)}\left[9c_2\int_0^1 f(\xi)\mathrm{d}\xi + \frac{9}{2\alpha}\int_0^1 g(\xi)\mathrm{d}\xi\right]. \tag{7.3.57}$$

Using (7.3.57), the fluid flux at the fracture entry can be expressed as

$$Q_0 = -\frac{4}{3}f^3(0)\frac{\mathrm{d}P(0)}{\mathrm{d}\xi} = 12c_2\int_0^1 f(\xi)\mathrm{d}\xi + 6\alpha^{-1}\int_0^1 g(\xi)\mathrm{d}\xi. \tag{7.3.58}$$

The problem is to solve the integro-differential system:

$$c_2\left[f(\xi) - 2\xi\frac{\mathrm{d}f}{\mathrm{d}\xi}\right] - \frac{1}{3}\frac{\mathrm{d}}{\mathrm{d}\xi}\left(f^3\frac{\mathrm{d}P}{\mathrm{d}\xi}\right) + 2\alpha c_2\frac{P(\xi)}{g(\xi)} = 0, \tag{7.3.59}$$

$$g(\xi) - 2\xi\frac{\mathrm{d}g}{\mathrm{d}\xi} - 4\alpha^2 c_2\frac{P(\xi)}{g(\xi)} = 0, \tag{7.3.60}$$

$$P(\xi) = -\frac{2}{\pi}\int_0^1 \frac{\mathrm{d}f}{\mathrm{d}\eta}\frac{\eta}{\eta^2-\xi^2}\mathrm{d}\eta, \tag{7.3.61}$$

subject to

$$f(0) = 1,\ f'(0) = 0,\ g'(0) = 0,\ f(1) = 0,\ g(1) = 0, \tag{7.3.62a-e}$$

where

$$P(\xi) \to -\frac{\gamma}{[2(\xi-1)]^{\frac{1}{2}}} \quad \text{as} \quad \xi \to 1^+. \tag{7.3.63}$$

The fluid flux at the fracture entry satisfies

$$Q_0 = 12c_2\int_0^1 f(\xi)\mathrm{d}\xi + 6\alpha^{-1}\int_0^1 g(\xi)\mathrm{d}\xi. \tag{7.3.64}$$

Once $f(\xi)$, $g(\xi)$ and $P(\xi)$ are obtained, $L(t)$, $V(t)$, $h(t,x)$, $b(t,x)$, $v_n(t,x)$ and $p(t,x)$ take the form

$$L(t) = (3c_2t+1)^{\frac{2}{3}}, \tag{7.3.65}$$

$$V(t) = V_0(3c_2t+1), \quad V_0 = 4\int_0^1 f(\xi)\mathrm{d}\xi, \tag{7.3.66}$$

$$h(t,x) = L^{\frac{1}{2}}(t) f(\xi), \tag{7.3.67}$$

$$b(t,x) = \frac{1}{2\alpha c_2} L^{\frac{1}{2}}(t) g(\xi), \tag{7.3.68}$$

$$v_n(t,x) = \frac{g(\xi) - 2\xi g'(\xi)}{2\alpha L(t)}, \tag{7.3.69}$$

$$p(t,x) = L^{-\frac{1}{2}}(t) P(\xi). \tag{7.3.70}$$

We have now completed the mathematical formulation for a fluid-driven fracture in a permeable rock where the fluid flow inside the rock is described by Darcy's flow model. The solution here depends on α, c_2, γ and Q_0. The values of α, γ and Q_0 will be specified prior to the numerical computations while c_2 will be obtained as part of the solution using equation (7.3.64).

7.4 TIP ASYMPTOTICS AND THE VELOCITY RATIO

It was difficult to determine the asymptotic solutions for $f(\xi)$, $g(\xi)$ and $P(\xi)$ that satisfies the system of equations (7.3.59)-(7.3.61). As a result, we cannot determine the value of $f^2(1)P'(1)$ using the near tip asymptotics.

7.5 SPLINE METHOD

Since we cannot integrate (7.3.59)-(7.3.61) to obtain exact solutions, numerical solutions will be sought. As shown in Chapter 5 and 6, the remedy to the challenge presented by the singularity in the slope of $f(\xi)$ near $\xi = 1$ is to extract the tip behaviour of the function $f(\xi)$ and then represent the remaining part of $f(\xi)$ using a linear spline. In this chapter, we will adopt this idea for both the half-width function $f(\xi)$ and the leak-off depth function $g(\xi)$. To do this, we divide the interval $[0,1]$ into n equal sub-intervals and take $f(\xi)$ and $g(\xi)$ in each sub-interval to be of the form

$$f_i(\xi) = (1-\xi^2)^{\frac{1}{2}} M_i(\xi) \quad \text{and} \quad g_i(\xi) = (1-\xi^2)^{\frac{1}{2}} N_i(\xi), \tag{7.5.1a-b}$$

where $M_i(\xi)$ and $N_i(\xi)$ are piece-wise linear functions given by

$$M_i(\xi) = a_i\xi + b_i \quad \text{and} \quad N_i(\xi) = r_i\xi + s_i. \tag{7.5.2a-b}$$

Dividing the interval $[0,1]$ into n sub-intervals $[\eta_j, \eta_{j+1}], j = 0, 1, \ldots, n-1$ and after substituting (7.5.1a) into (7.3.61), we obtain

$$P_{i\pm\alpha} = -\frac{2}{\pi} \sum_{j=0}^{n-1} \left[\int_{\eta_j}^{\eta_{j+1}} \frac{\eta(1-2\eta^2) a_j \mathrm{d}\eta}{(\eta^2 - \xi_{i\pm\alpha}^2)\sqrt{1-\eta^2}} - \int_{\eta_j}^{\eta_{j+1}} \frac{\eta^2 b_j \mathrm{d}\eta}{(\eta^2 - \xi_{i\pm\alpha}^2)\sqrt{1-\eta^2}} \right]. \tag{7.5.3}$$

where $\alpha = \pm 1/2, \pm 3/2$. The pressure at the grid points is given by

$$P_i = \frac{P_{i+\frac{1}{2}} + P_{i-\frac{1}{2}}}{2}, \tag{7.5.4}$$

where $P_{i\pm 1/2}$ is given by (7.5.3). Discretising (7.3.59) and (7.3.60), and approximating the pressure terms using the central difference, we obtain

$$\begin{aligned} & c_2 \left[\left(1-\xi^2\right)^{\frac{1}{2}} (a_i\xi + b_i) - \frac{2\xi\left((1-2\xi^2)a_i - \xi b_i\right)}{\sqrt{1-\xi^2}} \right] \\ & - (1-\xi^2)(a_i\xi + b_i)^2 \left[\frac{(1-2\xi^2)a_i - \xi b_i}{\sqrt{1-\xi^2}} \right] \left[\frac{P_{i+\frac{1}{2}} - P_{i-\frac{1}{2}}}{\xi_{i+\frac{1}{2}} - \xi_{i-\frac{1}{2}}} \right] \\ & - \frac{1}{3}(1-\xi^2)^{\frac{3}{2}}(a_i\xi + b_i)^3 \left[\frac{P_{i-\frac{3}{2}} - P_{i-\frac{1}{2}} - P_{i+\frac{1}{2}} + P_{i+\frac{3}{2}}}{2\left(\xi_{i+\frac{1}{2}} - \xi_{i-\frac{1}{2}}\right)^2} \right] \\ & + \alpha c_2 \left[\frac{P_{i+\frac{1}{2}} + P_{i-\frac{1}{2}}}{\sqrt{1-\xi^2}\,(r_i\xi + s_i)} \right] = 0, \end{aligned} \tag{7.5.5}$$

$$\begin{aligned} & \left(1-\xi^2\right)^{\frac{1}{2}} (r_i\xi + s_i) - \frac{2\xi\left[(1-2\xi^2)r_i - \xi s_i\right]}{\sqrt{1-\xi^2}} \\ & - 2\alpha^2 c_2 \left[\frac{P_{i+\frac{1}{2}} + P_{i-\frac{1}{2}}}{\sqrt{1-\xi^2}\,(r_i\xi + s_i)} \right] = 0, \end{aligned} \tag{7.5.6}$$

where $1 \leqslant i \leqslant n-1$. The current problem is to solve for $\{a_i, b_i, r_i, s_i\}$, $i = 1, 2, \ldots, n-1$ in each sub-interval. There are n sub-intervals and $n+1$ mesh points hence we have $4n$ unknowns in total. Equation (7.5.5) and (7.5.6) will generate a system of $2n-2$ nonlinear equations. We obtain additional equations to solve for the unknowns from the continuity condition of two successive linear splines. That is,

$$M_i(\xi_i) = M_{i-1}(\xi_i), \tag{7.5.7}$$

$$N_i(\xi_i) = N_{i-1}(\xi_i), \tag{7.5.8}$$

where $i = 1, 2, 3, \ldots, n-1$. The continuity conditions (7.5.7) and (7.5.8) give an additional $2n-2$ equations. From equation (7.5.5)-(7.5.8), we obtain a total of $4n-4$ equations. Using the slope and boundary conditions at the fracture entry, we are able to determine the values of a_0, b_0 and r_0. We specified an initial value for s_0 and allowed its value to be updated through the calculations so that it is determined as part of the solution. Consequently, the system of $4n-4$ equations are sufficient to solve for the unknowns. We now outline the procedure for solving the underlying system of nonlinear equations. For any choice of $n \geqslant 2$, we have $2n$ splines with $4n$ unknowns. Applying the slope conditions $f'(0) = 0$ and $g'(0) = 0$ implies that $a_0 = 0$ and $r_0 = 0$. The boundary

condition at the fracture entry gives $b_0 = 1$, hence $f_0(\xi) = \sqrt{1-\xi^2}$ and $g_0(\xi) = s_0\sqrt{1-\xi^2}$. We now have a total of $4n-4$ unknowns and a system of $4n-4$ nonlinear equations. Evaluating (7.5.5)-(7.5.8) at $1 \leqslant i \leqslant n-1$, we obtain

$$\begin{aligned} i=1: \quad & c_2\left[\left(1-\xi^2\right)^{\frac{1}{2}}\left(a_1\xi+b_1\right)-\frac{2\xi\left((1-2\xi^2)a_1-\xi b_1\right)}{\sqrt{1-\xi^2}}\right] \\ & -n(1-\xi^2)(a_1\xi+b_1)^2\left[\frac{(1-2\xi^2)a_1-\xi b_1}{\sqrt{1-\xi^2}}\right]\left[P_{\frac{3}{2}}-P_{\frac{1}{2}}\right] \\ & -\frac{n^2}{6}(1-\xi^2)^{\frac{3}{2}}(a_1\xi+b_1)^3\left[P_{\frac{5}{2}}-P_{\frac{3}{2}}\right] \\ & +\alpha c_2\left[\frac{P_{\frac{3}{2}}-P_{\frac{1}{2}}}{\sqrt{1-\xi^2}\,(r_1\xi+s_1)}\right]=0, \end{aligned} \tag{7.5.9}$$

$$\begin{aligned} & \left(1-\xi^2\right)^{\frac{1}{2}}\left(r_1\xi+s_1\right)-\frac{2\xi\left[(1-2\xi^2)r_1-\xi s_1\right]}{\sqrt{1-\xi^2}} \\ & -2\alpha^2 c_2\left[\frac{P_{i+\frac{1}{2}}+P_{i-\frac{1}{2}}}{\sqrt{1-\xi^2}\,(r_1\xi+s_1)}\right]=0, \end{aligned} \tag{7.5.10}$$

$$\begin{aligned} i=2: \quad & c_2\left[\left(1-\xi^2\right)^{\frac{1}{2}}\left(a_2\xi+b_2\right)-\frac{2\xi\left((1-2\xi^2)a_2-\xi b_2\right)}{\sqrt{1-\xi^2}}\right] \\ & -n(1-\xi^2)(a_2\xi+b_2)^2\left[\frac{(1-2\xi^2)a_2-\xi b_2}{\sqrt{1-\xi^2}}\right]\left[P_{\frac{5}{2}}-P_{\frac{3}{2}}\right] \\ & -\frac{n^2}{6}(1-\xi^2)^{\frac{3}{2}}(a_2\xi+b_2)^3\left[P_{\frac{1}{2}}-P_{\frac{3}{2}}-P_{\frac{5}{2}}-P_{\frac{7}{2}}\right] \\ & +\alpha c_2\left[\frac{P_{\frac{5}{2}}-P_{\frac{3}{2}}}{\sqrt{1-\xi^2}\,(r_2\xi+s_2)}\right]=0, \end{aligned} \tag{7.5.11}$$

$$\begin{aligned} & \left(1-\xi^2\right)^{\frac{1}{2}}\left(r_2\xi+s_2\right)-\frac{2\xi\left[(1-2\xi^2)r_2-\xi s_2\right]}{\sqrt{1-\xi^2}} \\ & -2\alpha^2 c_2\left[\frac{P_{\frac{5}{2}}+P_{\frac{3}{2}}}{\sqrt{1-\xi^2}\,(r_2\xi+s_2)}\right]=0, \end{aligned} \tag{7.5.12}$$

$$\vdots \qquad\qquad \vdots$$

$$
\begin{aligned}
i = n-1: \quad & c_2 \left[\left(1-\xi^2\right)^{\frac{1}{2}} \left(a_{n-1}\xi + b_{n-1}\right) - \frac{2\xi\left((1-2\xi^2)a_{n-1} - \xi b_{n-1}\right)}{\sqrt{1-\xi^2}} \right] \\
& - n(1-\xi^2)(a_{n-1}\xi + b_{n-1})^2 \left[\frac{(1-2\xi^2)a_{n-1} - \xi b_{n-1}}{\sqrt{1-\xi^2}} \right] \left[P_{n-\frac{1}{2}} - P_{n-\frac{3}{2}} \right] \\
& - \frac{n^2}{6}(1-\xi^2)^{\frac{3}{2}}(a_{n-1}\xi + b_{n-1})^3 \left[P_{n-\frac{5}{2}} - P_{n-\frac{3}{2}} - P_{n-\frac{1}{2}} - \gamma n^{\frac{1}{2}} \right] \\
& + \alpha c_2 \left[\frac{P_{n-\frac{1}{2}} + P_{n-\frac{3}{2}}}{\sqrt{1-\xi^2}\,(r_{n-1}\xi + s_{n-1})} \right] = 0,
\end{aligned}
\tag{7.5.13}
$$

$$
\begin{aligned}
& \left(1-\xi^2\right)^{\frac{1}{2}} \left(r_{n-1}\xi + s_{n-1}\right) - \frac{2\xi\left[(1-2\xi^2)r_{n-1} - \xi s_{n-1}\right]}{\sqrt{1-\xi^2}} \\
& - 2\alpha^2 c_2 \left[\frac{P_{n-\frac{1}{2}} + P_{n-\frac{3}{2}}}{\sqrt{1-\xi^2}\,(r_{n-1}\xi + s_{n-1})} \right] = 0.
\end{aligned}
\tag{7.5.14}
$$

Similarly, we obtain $2n-2$ equations from the continuity conditions

$$
\begin{aligned}
i = 1: \quad & a_1\xi_1 + b_1 - b_0 = 0, && (7.5.15)\\
& r_1\xi_1 + s_1 - s_0 = 0, && (7.5.16)\\
i = 2: \quad & (a_2 - a_1)\xi_2 + b_2 - b_1 = 0, && (7.5.17)\\
& (r_2 - r_1)\xi_2 + s_2 - s_1 = 0, && (7.5.18)\\
& \vdots \qquad\qquad \vdots \\
i = n-1: \quad & (a_{n-1} - a_{n-2})\xi_{n-1} + b_{n-1} - b_{n-2} = 0, && (7.5.19)\\
& (r_{n-1} - r_{n-2})\xi_{n-1} + s_{n-1} - s_{n-2} = 0. && (7.5.20)
\end{aligned}
$$

The resulting system of nonlinear equations is solved for the unknown coefficients using Matlab function *fsolve*.

7.6 DISCUSSION ON NUMERICAL METHOD

We will follow the same numerical scheme outlined in Section 5.8 to derive the solution for the system of equations (7.3.59) to (7.3.61) subject to the boundary conditions (7.3.62a-e). The underlying boundary value problem was solved for certain limiting values of α, γ and Q_0. The unknown constant c_2 was determined using the mass balance law given by (7.3.64). The initial guesses for $\boldsymbol{a} = [a_1, a_2, \ldots, a_{n-1}]$ and $\boldsymbol{b} = [b_1, b_2, \ldots, b_{n-1}]$ were obtained using the Matlab function *rand*. It must be noted that we did not enforce any boundary condition on s_0

while doing the calculations. The value of s_0 was obtained from the numerical computations.

A check of accuracy was made using equation (5.6.2). Once (5.6.2) was satisfied, the corresponding solutions of $f(\xi), g(\xi)$ and the value c_2 were substituted into (7.3.65) to (7.3.70) in order to obtain $L(t)$, $V(t)$, $h(t,x)$, $b(t,x), v_n(t,x)$ and $p(t,x)$.

7.7 NUMERICAL RESULTS AND DISCUSSIONS

In Figure 33, $h(t,x)$ is plotted against x at $t = 0, 20, 50$ and 200 when $\alpha = 6, 18, 50$. As anticipated, $h(t,x)$ increases with time, and as α increases the rate of increase of $h(t,x)$ is seen to increase.

In Figure 34(i-iii), graphs of fracture half-width, $h(t,x)$, leak-off depth, $b(t,x)$, and the fluid pressure, $p(t,x)$, are plotted against x at time $t = 200$ for various values of α when $Q_0 = 0.25$ and $\gamma = 0.01$. An increase in the parameter α led to an increase in the growth of the fracture half-width as can be seen in Figure 34(i). In Figure 34(ii), it can be seen that the leak-off depth near the fracture entry decreases with increasing α. In Figure 34(iii), the graphs of $p(t,x)$ are indistinguishable.

Figure 35(i-iii) illustrates the effect of Q_0 on the $h(t,x)$, $b(t,x)$ and $p(t,x)$. As Q_0 is increased, corresponding to stronger fluid injection at the fracture entry, the extent of growth of the fracture half-width increased. The shape of leak-off depth and the fluid pressure are as expected.

In Figure 36(i-iii), graphs of $h(t,x), b(t,x)$ and $p(t,x)$ are plotted at time $t = 200$ for different values of γ when $Q_0 = 0.25$ and $\alpha = 8$. An increase in γ did not significantly affect $h(t,x)$ and $b(t,x)$. When analysing the graphs of $p(t,x)$ in Figure 36(iii), it can be seen that the average value of the pressure $p(t,x)$ is growing with an increase in γ.

In Figure 37(i-iii), $v_n(t,x)$ is plotted against x at time $t = 200$ for different values of α, Q_0 and γ. In Figure 37(i) it can be seen that an increase in α led to a slight increase in the leak-off velocity. An increase in the parameter Q_0 led to an increase in the leak-off velocity as can be seen in Figure 37(ii). In Figure 37(iii), the graphs of $v_n(t,x)$ are indistinguishable.

In Figure 38(i-iii), the fracture length $L(t)$ is plotted against t for varied values of α, Q_0 and γ. In Figure 38(i), the fracture length is plotted for various values of α. The fracture length grew the strongest when $\alpha = 50$ and the least when $\alpha = 6$. Figure 38(ii) shows how the fracture length evolved over time for different values Q_0. The fracture length increased with an increase in Q_0 and it was the highest when $Q_0 = 0.27$ and lowest when $Q_0 = 0.21$. Figure 38(iii) shows how the fracture length evolves over time for varied values of γ. The fracture lengths are indistinguishable.

(i)

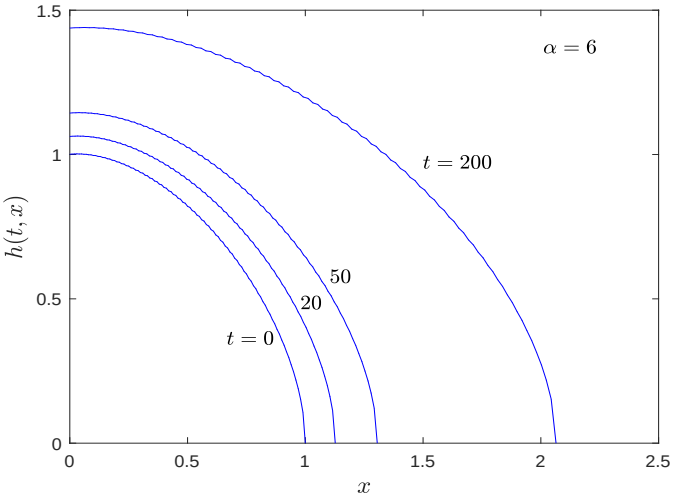

(ii)

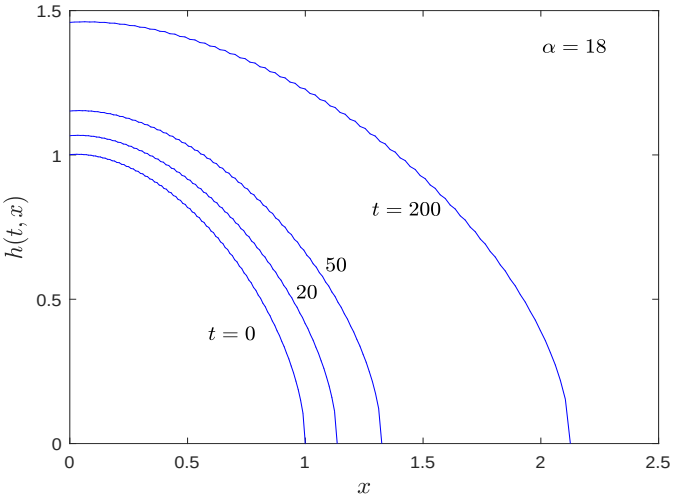

(iii)

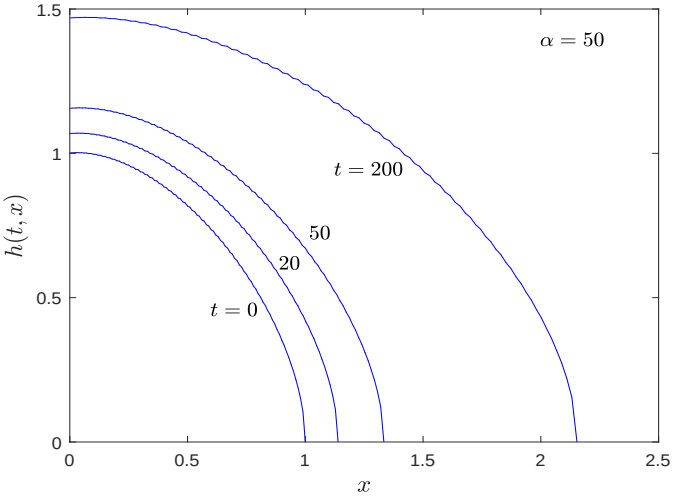

Figure 33: Graph of $h(t,x)$ plotted against x at times $t = 0, 20, 50, 200$ for $Q_0 = 0.25$, $\gamma = 0.01$ and for (i) $\alpha = 6$ and $c_2 = 0.003277$, (ii) $\alpha = 18$ and $c_2 = 0.0034975$ and (iii) $\alpha = 50$ and $c_2 = 0.003600$.

(i)

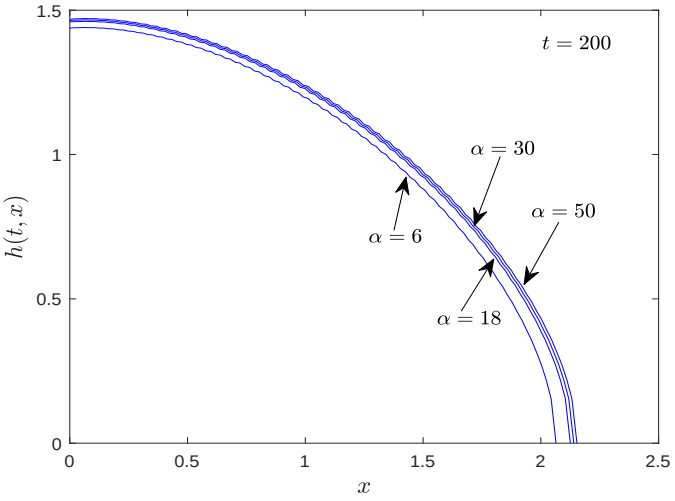

(ii)

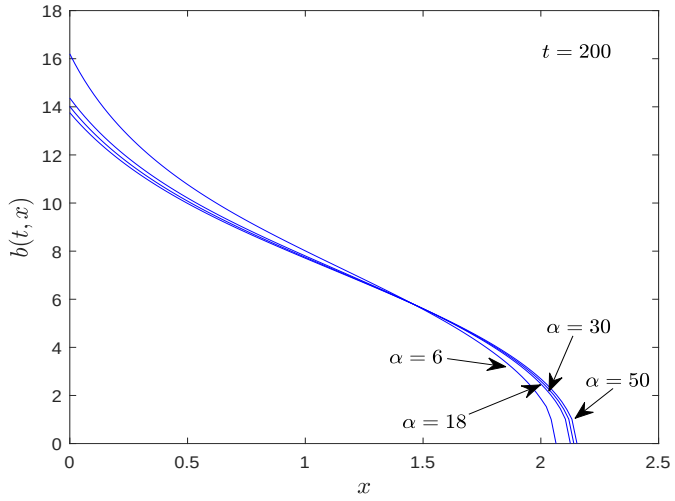

(iii)

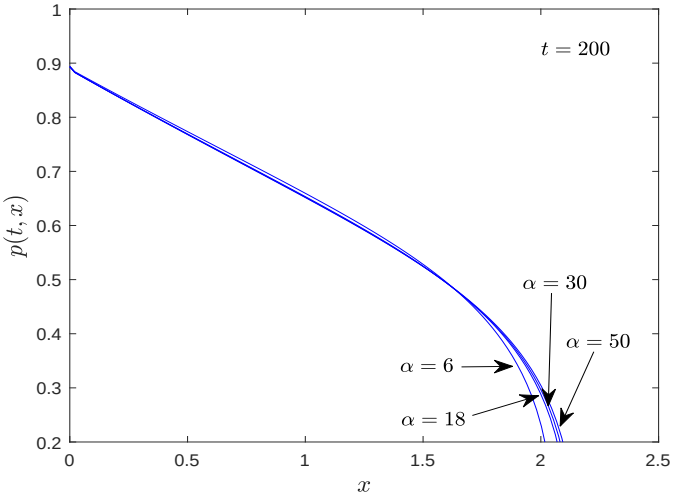

Figure 34: Graphs of (i) the fracture half-width $h(t,x)$, (ii) leak-off depth $b(t,x)$ and (iii) the fluid pressure $p(t,x)$, plotted against x for $\alpha = 6, 18, 30, 50$ when $Q_0 = 0.25$ and $\gamma = 0.5$ at $t = 200$.

(i)

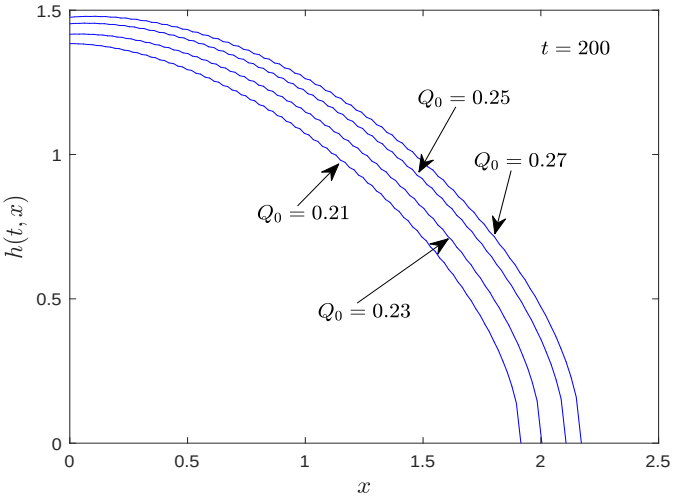

(ii)

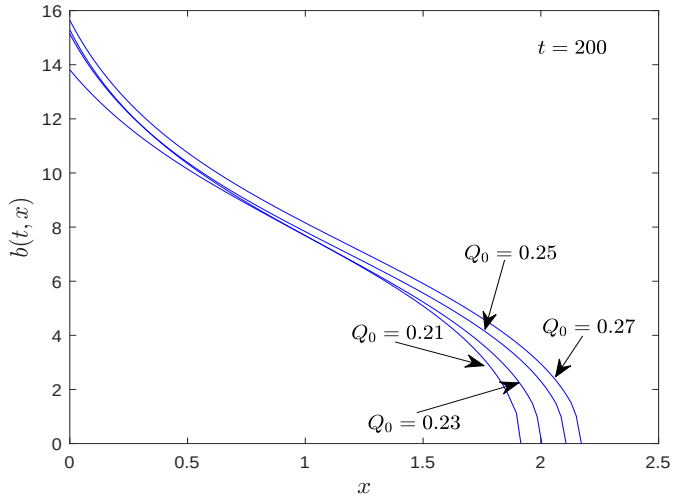

(iii)

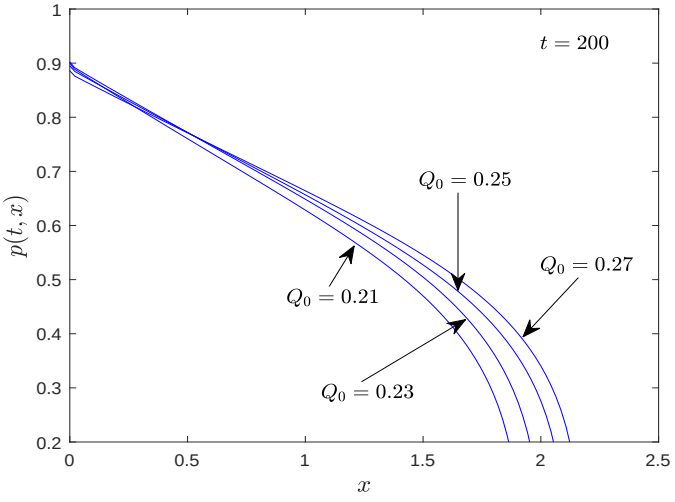

Figure 35: Graphs of (i) the fracture half-width $h(t,x)$, (ii) leak-off depth $b(t,x)$ and (iii) the fluid pressure $p(t,x)$, plotted against x for $Q_0 = 0.21, 0.23, 0.25, 0.27$ when $\gamma = 0.5$ and $\alpha = 8$ at $t = 200$.

(i)

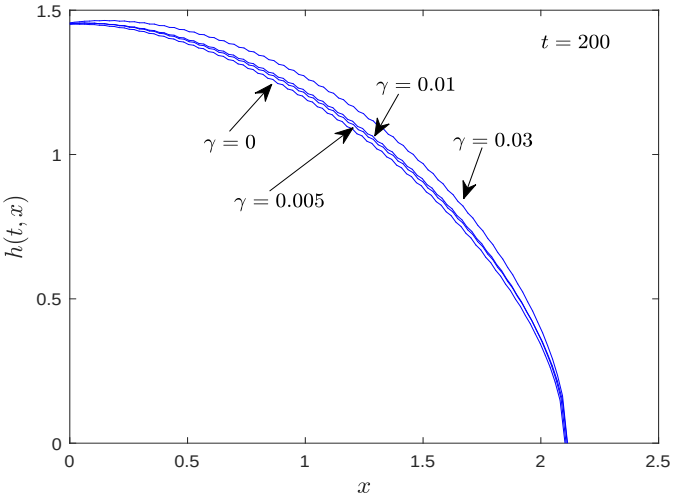

(ii)

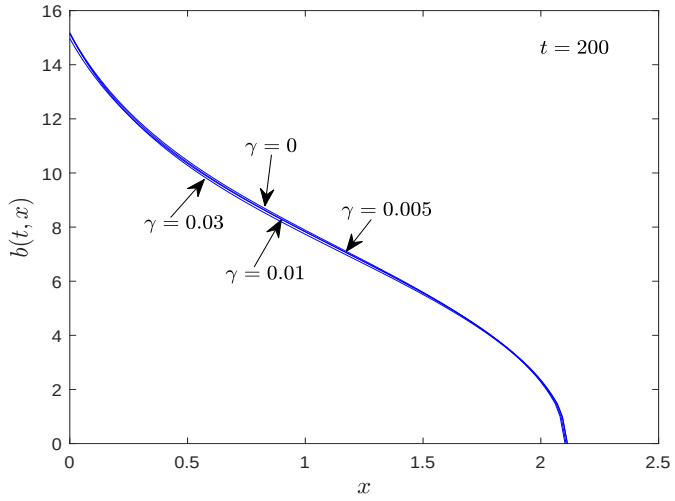

(iii)

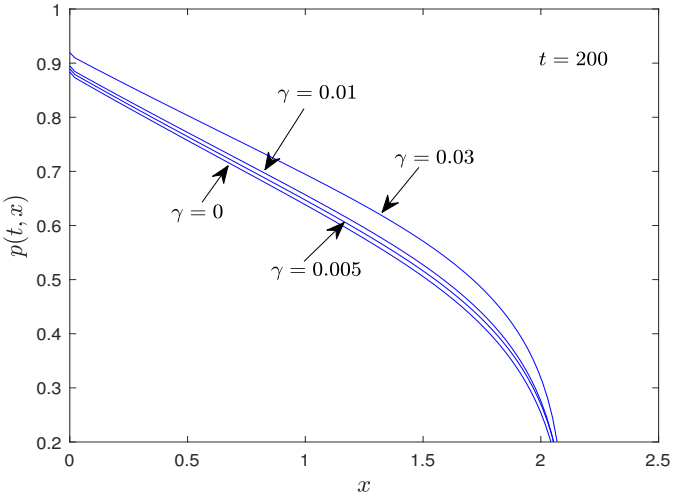

Figure 36: Graphs of (i) the fracture half-width $h(t,x)$, (ii) leak-off depth $b(t,x)$ and (iii) the fluid pressure $p(t,x)$, plotted against x for $\gamma = 0, 0.005, 0.01, 0.03$ when $Q_0 = 0.25$ and $\alpha = 8$ at $t = 200$.

(i)

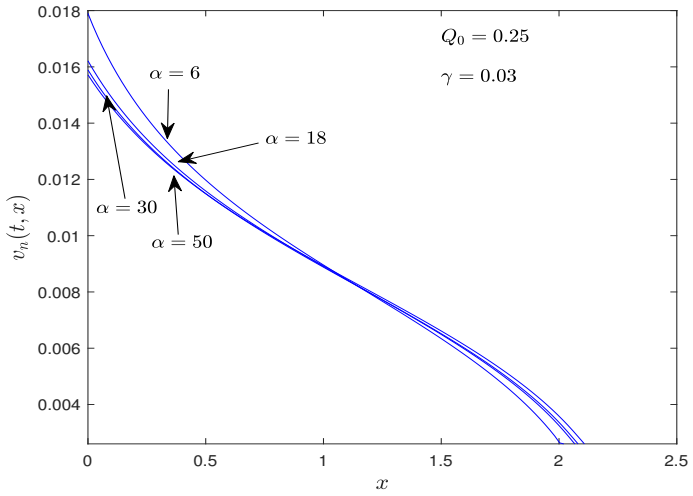

(ii)

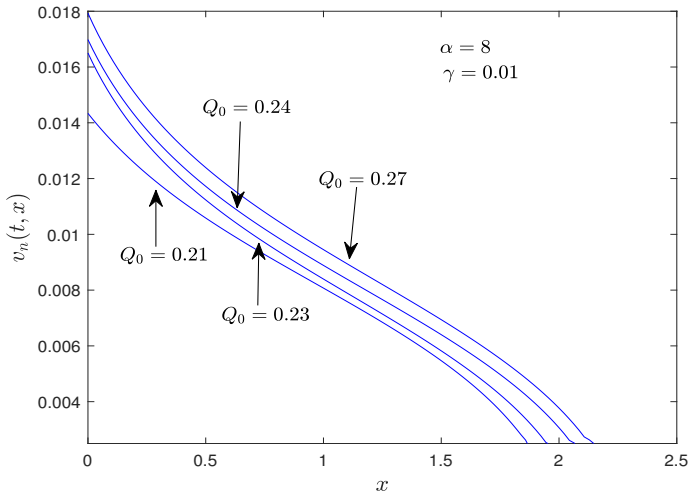

(iii)

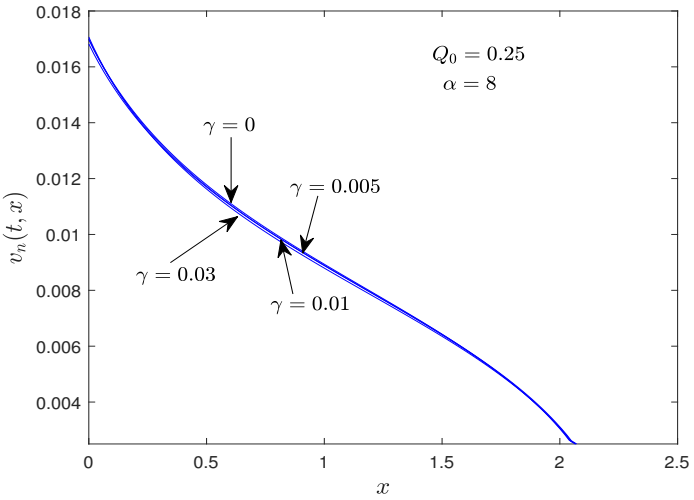

Figure 37: Leak-off velocity $v_n(t,x)$ plotted for various values of (i) α, (ii) Q_0, (iii) γ, at $t = 200$.

(i)

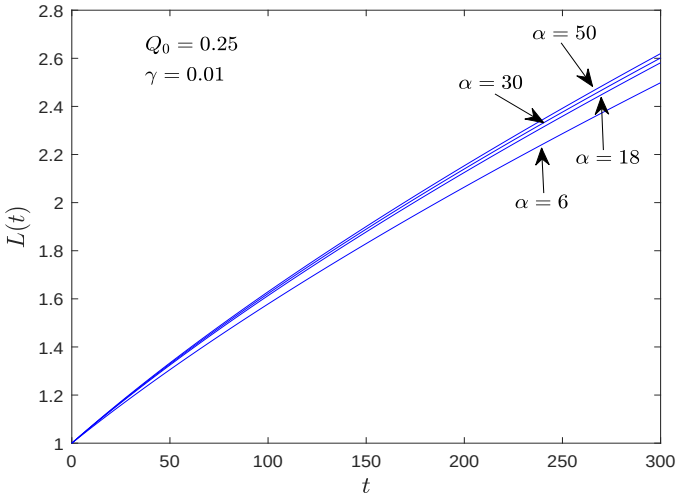

(ii)

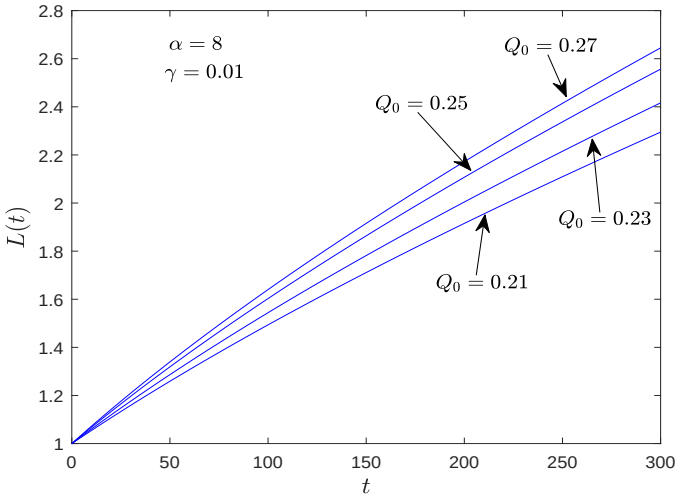

(iii)

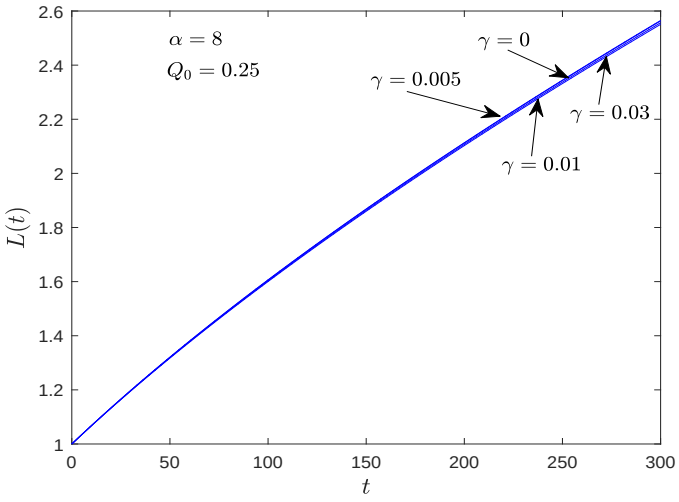

Figure 38: Fracture length plotted for various values of (i) α, (ii) Q_0, (iii) γ.

(i)

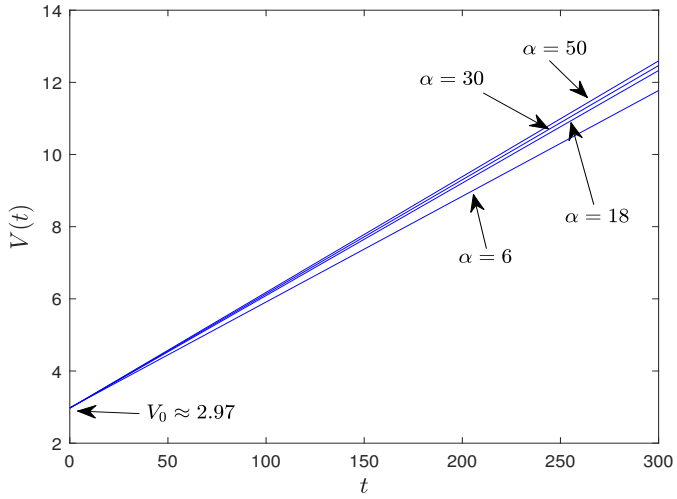

(ii)

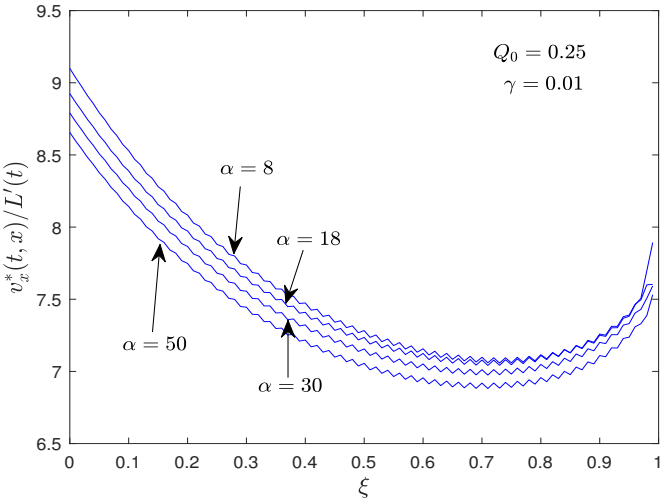

(iii)

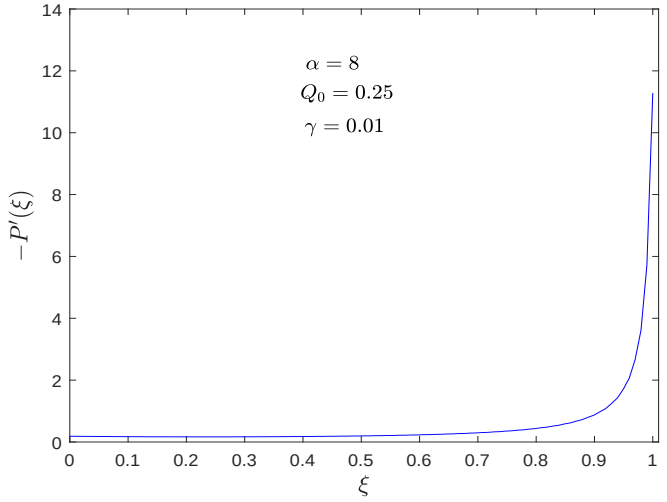

Figure 39: Graphs illustrating (i) the fracture volume plotted against t for $\alpha = 6$, 18,30, 50 when $Q_0 = 0.25$, and $\gamma = 0.01$, (ii) the dimensionless pressure gradient plotted against ξ for $\alpha = 8$, $Q_0 = 0.25$, and $\gamma = 0.01$.

(i)

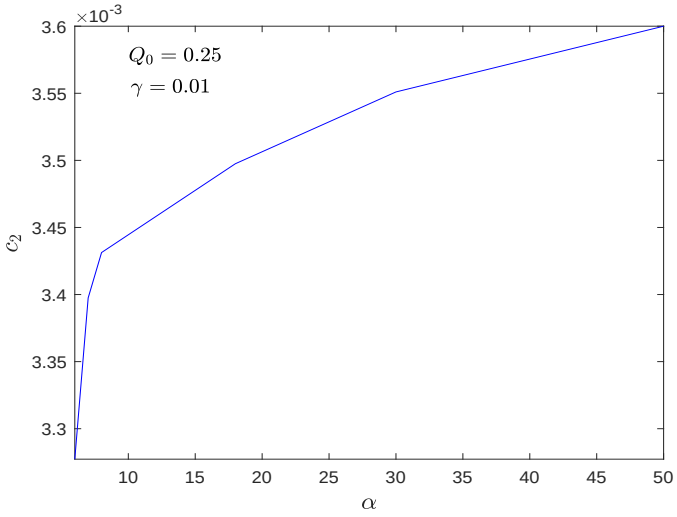

(ii)

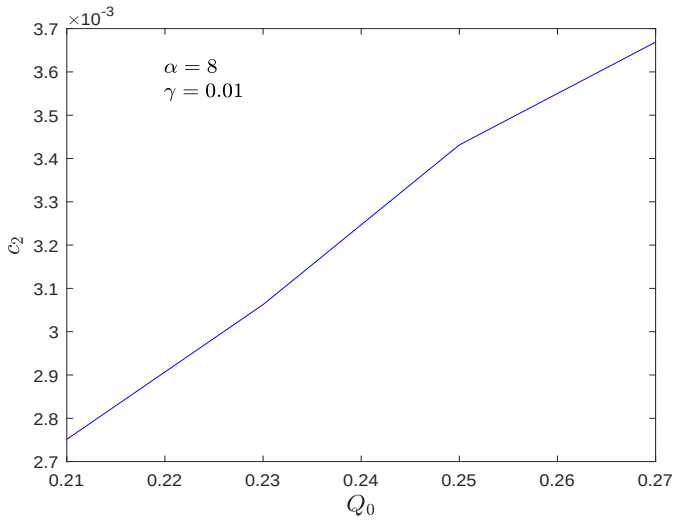

(iii)

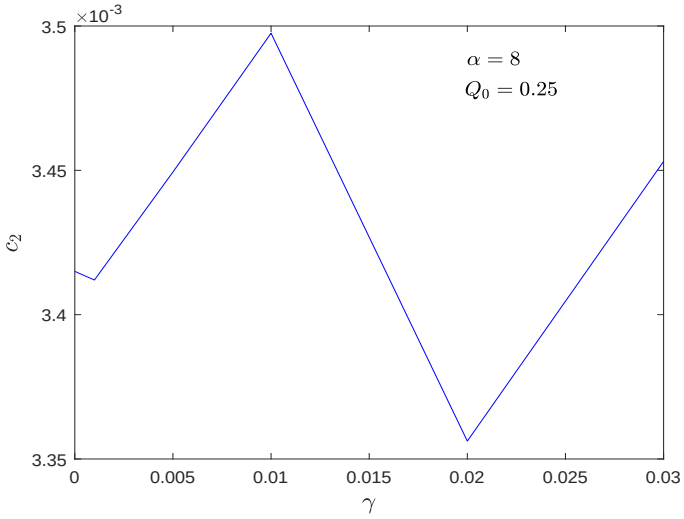

Figure 40: The constant c_2 plotted against (i) α, (ii) Q_0, (iii) γ.

Figure 39(i-iii) shows the fracture volume over time and the non-dimensional pressure gradient. In Figure 39(i), the volume of the fracture is plotted for $\alpha = 6, 18, 30$ and 50. It can be seen that an increase in α did not yield any significant changes in the volume of the fracture. Figure 39(ii), illustrates the velocity ratio $v_x^*/L'(t)$ for different values of α. The graphs of $v_x^*/L'(t)$ are not approximately straight lines as anticipated. In Figure 39(iii), the non-dimensional pressure gradient is plotted against ξ for $\alpha = 8$, $Q_0 = 0.25$ and $\gamma = 0.01$. The graph of the pressure gradient is taking the expected shape.

Figure 40 depicts the relationship between the parameters c_2, α, Q_0 and γ. In Figure 40(i) c_2 is plotted against α. It can be seen that c_2 is an increasing function of α. In Figure 40(ii) c_2 is plotted against Q_0. Again, c_2 is an increasing function Q_0. In Figure 40(iii) c_2 is plotted against γ. The graph exhibits an oscillatory behaviour.

7.8 CONCLUSION

In this Chapter, a two-dimensional, pre-existing, fluid-driven fracture propagating in a permeable rock was considered in which fluid seepage into the porous rock matrix is modelled using Darcy's law. We started the chapter by stating Darcy's flow model which relates the leak-off depth to the pressure gradient and non-dimesionalising it. By relating the rate of change of the leak-off depth $b(t,x)$ to the leak-off velocity $v_n(t,x)$, the integro-differential equation (4.6.36) derived in Chapter 4 for describing the evolution of the fracture half-width became (7.3.1). Equation (7.3.1) was then coupled with a first-order partial differential equation governing the leak-off depth $b(t,x)$ and the Cauchy principal value integral for the pressure. The boundary value problem for the integro-differential system contained three dependent variables $h(t,x), b(t,x)$ and $p(t,x)$ to solve for and three equations. Similarity solutions were derived for the integro-differential system. The resulting system of equations governing the physical mechanisms after the similarity transformation contained the constants c_2, c_3 and c_5. A proportionality constant α was introduced and used to relate c_2 to c_3 and c_5. The resulting integro-differential system then dependent on two parameters, namely, α and c_2. For this case, it was difficult to determine the near tip asymptotics that satisfies the system of equations (7.3.59)-(7.3.61). The spline method was used to solve the integro-differential system. It was found that larger values of α are associated with larger fracture lengths, volumes and half-widths. It was also found that the leak-off depth in the neighbourhood of the fracture entry decreased with increasing α and that the fluid pressure is not significantly affected by the change in α. Expectedly, large values of Q_0 resulted in an increase in the propagation rate of the fracture half-width and fracture length. An increase in γ did not have much effect on the fracture length and leak-off depth. A positive linear relationship between c_2 and

the parameters α and Q_0 was noted. No clear relationship was drawn between c_2 and γ.

8

CONCLUSION

The aim of this research was to study a two-dimensional fluid-driven fracture propagating in a permeable rock. The two-dimensional fracture is pre-existing and it is propagated by the injection of a high pressured viscous incompressible Newtonian fluid into it. Some proportion of the fracturing fluid infiltrates the encompassing rock-mass formation through the fracture walls. The mathematical model governing the propagation of the fracture was based on two main important assumptions. The first assumption is the lubrication approximation which was used to simplify the Navier-Stokes equation. The other assumption is that the elasticity theory is applied hence the rock elasticity is modelled using the Cauchy principal integral derived from linear elastic fracture mechanics. The presence of the Cauchy-type singular integral equation in the mathematical model necessitated a study of integral equations, in particular, singular integral equations and their method of solutions. In Chapter 2, we studied integral equations and gave a detailed review and discussion.

In Chapter 3, we studied the method of solution for Cauchy-type integral equations. We started the chapter by reviewing Cauchy-type integral equations and demonstrating the procedure of inverting a Cauchy integral equation of the first kind. A simple Cauchy-type singular integral equation over a finite interval was introduced and analytical, approximate and numerical techniques for solving the integral equation were investigated. The analytical solution for the integral equation was used as a benchmark solution against the numerical solutions. We achieved rapid convergence and high accuracy when using the conventional finite difference approach and the linear spline method. As a result, the linear spline method was preferred for solving the boundary value problem for the hydraulic fracture problem that was to be considered in this thesis.

In Chapter 4, we considered the problem of a two-dimensional, pre-existing, fluid-driven fracture propagating in a permeable rock in which fluid leak-off through the interface into the surrounding rock formation was described by a leak-off velocity term, $v_n(t,x)$. The mathematical formulation resulted in a system of partial differential equations relating the fracture half-width, leak-off velocity and the fluid pressure. Using a similarity transformation, the integro-differential system of equations was reduced to a system of ordinary differential equations. The resulting integro-differential system contained three dependent variables $f(\xi), g(\xi)$ and $P(\xi)$ to solve for, but two equations. The system also had two parameters c_2 and c_3 to determine.

In Chapter 5, we investigated the problem formulated in Chapter 4 for the case in which the leak-off velocity is proportional to the half-width of the fracture. The parameter β_1 was used as a proportionality constant and the resulting integro-differential system was then dependent on the parameters c_2 and β_1. The parameter β_1 was prescribed while c_2 was determined as part of the solution. When $\beta_1 = 0$, there is no leak-off at the interface and the rock is impermeable. When $\beta_1 > 0$, there is leak-off at the interface into the porous rock-matrix. It was found that small values of β_1 leads to higher rate of growth of the fracture half-width, fracture length and fracture volume while large β_1 values results in low rate of fracture propagation. We also saw from Figure 21(i) and Figure 23(ii) that an increase in the parameter Q_0 is associated with an increase in the propagation rate of the fracture half-width and length. An increase in γ led to marginal changes in the fracture half-width, length, leak-off velocity, and the fluid pressure. We also noted that c_2 is a decreasing linear function of β_1 and an increasing linear function of Q_0.

In Chapter 6, we investigated the problem formulated in Chapter 4 for the case in which the leak-off velocity is proportional to the gradient of the fracture interface. For this case, we used the parameter β_2 as the proportionality constant and the resulting integro-differential system was then dependent on the parameters c_2 and β_2. Similar to Chapter 5, the parameter β_2 was prescribed while c_2 was determined as part of the solution. It was found that small values of β_2 resulted in high growth rate of the fracture half-width, fracture length and fracture volume, as was expected, while large β_2 values resulted in low fracture propagation rate. It was also noted that an increase in the parameter Q_0 was associated with a high propagation rate of the fracture half-width and fracture length. Expectedly, an increase in γ led to marginal changes in fracture half-width, length, leak-off velocity, and the fluid pressure. Lastly, we noted that c_2 is a decreasing linear function of β_2 and an increasing linear function of Q_0.

In Chapter 7, we considered a fluid-driven fracture propagating in a permeable rock with Darcy fluid flow in the rock-mass formation. A mathematical model which is the boundary value problem for the integro-differential system of equations governing the evolution of the fracture was formulated. Using a similarity transformation, the system of partial differential equations was reduced to a system of ordinary differential equations and similarity solutions were obtained. The resulting integro-differential system contained three dependent variables $f(\xi), g(\xi)$ and $P(\xi)$ to solve for and three unknown constants c_2, c_3 and c_5. The constants were linked to each other by a proportionality constant α, .i.e., $c_3 = \alpha c_1$ and $c_5 = \alpha c_3$. As a result, the system then dependent on the parameters α and c_2. The parameter α was chosen to obtain different mathematical models which were solved numerically and the parameter c_2 was obtained as part of the solution. Numeri-

cal solutions were obtained for the fracture length, volume, half-width, leak-off depth and the fluid pressure. An increase in α led to marginal increase in the fracture length, volume, half-width, leak-off depth and the fluid pressure while an increase in the parameter Q_0 led to significant increase in the same variables. Marginal effects were also observed with an increase in γ. It was also found that the values c_2 for which the mass balance was satisfied in this problem were smaller compared to c_2 values obtained in Chapter 5 and Chapter 6.

This work gave an insight into understanding how fluid-driven fractures evolve over time when the elasticity of the rock is modeled using the Cauchy principal integral derived from linear elastic fracture mechanics and when the fluid inside the rock formation is modelled using either a leak-off velocity term or Darcy's flow model. Darcy model employed is based on moderate flow through porous media. As a result, future work could include a case in which there is high velocity flow through the fluid-rock interface in which case, a non-Darcy model such as the Forchheimer model is employed to describe fluid leak-off through the fluid-rock interface into the surrounding rock mass.

Part IV

APPENDIX

APPENDIX A

A.1 INVERSION OF A CAUCHY INTEGRAL EQUATION

There are many physical problems which can be reduced to the solution of the equation

$$\fint_a^b \frac{\Phi(t)\mathrm{d}t}{t-\sigma} = F(\sigma), \qquad a < \sigma < b, \tag{A.1.1}$$

where $F(\tau)$ is a known real function. Here, we seek a solution of a Cauchy-type singular integral equation of the first kind in the interval (0,1). To obtain the solution, we start by making the following translations

$$t = a + (b-a)\xi, \qquad t \in (a,b) \Rightarrow \xi \in (0,1), \tag{A.1.2}$$

$$\sigma = a + (b-a)x, \qquad \sigma \in (a,b) \Rightarrow x \in (0,1). \tag{A.1.3}$$

We also have that $t - \sigma = (b-a)(\xi - x)$. Using these translations, equation (A.1.1) becomes

$$\fint_0^1 \frac{\psi(\xi)\mathrm{d}\xi}{\xi - x} = f(x), \qquad 0 < x < 1, \tag{A.1.4}$$

where

$$\psi(\xi) = \Phi(a + (b-a)\xi), \; f(x) = F(a + (b-a)x). \tag{A.1.5}$$

The integral term in (A.1.4) can be written in the form

$$\begin{aligned}
\fint_0^1 \frac{\psi(\xi)\mathrm{d}\xi}{\xi - x} &= \fint_0^1 \left(\frac{1 - \xi + x + \xi - x}{\xi - x} \right) \psi(\xi)\mathrm{d}\xi, \\
&= \fint_0^1 \frac{\psi(\xi)\mathrm{d}\xi}{\xi - x} - \fint_0^1 \frac{\xi\psi(\xi)\mathrm{d}\xi}{\xi - x} + x\fint_0^1 \frac{\psi(\xi)\mathrm{d}\xi}{\xi - x} + \int_0^1 \psi(\xi)\mathrm{d}\xi, \\
&= f(x) - \fint_0^1 \frac{\xi\psi(\xi)\mathrm{d}\xi}{\xi - x} + xf(x) + \int_0^1 \psi(\xi)\mathrm{d}\xi,
\end{aligned} \tag{A.1.6}$$

Hence, equation (A.1.4) becomes

$$\fint_0^1 \frac{\xi\psi(\xi)\mathrm{d}\xi}{\xi - x} = xf(x) + c \tag{A.1.7}$$

where

$$c = \int_0^1 \psi(\xi)\mathrm{d}\xi. \tag{A.1.8}$$

Multiplying (A.1.7) with $\frac{1}{\sqrt{x}}$ and integrating with respect to x gives

$$\int_0^1 \left(\int_0^x \frac{\mathrm{d}x}{(\xi - x)\sqrt{x}} \right) \xi \psi(\xi) \mathrm{d}\xi = \int_0^x \sqrt{\lambda} f(\lambda) \mathrm{d}\lambda + 2c\sqrt{x}. \quad \text{(A.1.9)}$$

Consider now the inner integral on the left hand side of (A.1.9) without the interval of integration

Let $u = \sqrt{x} \Longrightarrow u^2 = x$. Then the inner integral can be written equivalently as

$$\int \frac{\mathrm{d}x}{(\xi - x)\sqrt{x}} = 2 \int \frac{\mathrm{d}u}{\xi - u^2}, \quad \text{(A.1.10)}$$

$$= -2 \int \frac{\mathrm{d}u}{(u - \sqrt{\xi})(u + \sqrt{\xi})}, \quad \text{(A.1.11)}$$

$$= -\frac{1}{\sqrt{\xi}} \left[\int \frac{\mathrm{d}u}{u - \sqrt{\xi}} - \int \frac{\mathrm{d}u}{u + \sqrt{\xi}} \right]. \quad \text{(A.1.12)}$$

Now, set $v_1 = u - \sqrt{\xi} \Longrightarrow \mathrm{d}u = \mathrm{d}v_1$. Then

$$\int \frac{\mathrm{d}u}{u - \sqrt{\xi}} = \int \frac{\mathrm{d}v_1}{v_1}. \quad \text{(A.1.13)}$$

This is a standard integral

$$\int \frac{\mathrm{d}v_1}{v_1} = \ln(v_1) = \ln(u - \sqrt{\xi}). \quad \text{(A.1.14)}$$

Similarly, set $v_2 = u + \sqrt{\xi} \Longrightarrow \mathrm{d}u = \mathrm{d}v_2$. Then

$$\int \frac{\mathrm{d}u}{u + \sqrt{\xi}} = \int \frac{\mathrm{d}v_2}{v_2} = \ln(v_2) = \ln(u + \sqrt{\xi}). \quad \text{(A.1.15)}$$

Substituting back into equation (A.1.12), we obtain

$$-\frac{1}{\sqrt{\xi}} \left[\int \frac{\mathrm{d}u}{u - \sqrt{\xi}} - \int \frac{\mathrm{d}u}{u + \sqrt{\xi}} \right] = -\frac{1}{\sqrt{\xi}} \ln \left(\frac{\sqrt{x} - \sqrt{\xi}}{\sqrt{x} + \sqrt{\xi}} \right). \quad \text{(A.1.16)}$$

Using (A.1.16), (A.1.9) becomes

$$-\int_0^1 \ln \left| \frac{\sqrt{\xi} - \sqrt{x}}{\sqrt{\xi} + \sqrt{x}} \right| \sqrt{\xi} \psi(\xi) \mathrm{d}\xi = \int_0^x \sqrt{\lambda} f(\lambda) \mathrm{d}\lambda + 2c\sqrt{x}. \quad \text{(A.1.17)}$$

Another result that we need is

$$-\ln \left| \frac{\sqrt{\xi} - \sqrt{x}}{\sqrt{\xi} + \sqrt{x}} \right| = \begin{cases} \int_0^\xi \frac{\mathrm{d}s}{\sqrt{\xi - s}\sqrt{x - s}}, & x > \xi, \\ \int_0^x \frac{\mathrm{d}s}{\sqrt{\xi - s}\sqrt{x - s}}, & x < \xi, \end{cases} \quad \text{(A.1.18)}$$

which is proved as follows. Let $u = x - s \Longrightarrow \mathrm{d}s = -\mathrm{d}u$, then we have

$$\int \frac{\mathrm{d}s}{\sqrt{\xi - s}\sqrt{x - s}} = -\int \frac{\mathrm{d}u}{\sqrt{u}\sqrt{u - x + \xi}}. \quad \text{(A.1.19)}$$

Again, let $v = \frac{\sqrt{u}}{\sqrt{x-\xi}} \implies \mathrm{d}u = 2\sqrt{x-\xi}\sqrt{u}\mathrm{d}v$. Then

$$-\int \frac{\mathrm{d}u}{\sqrt{u}\sqrt{u-x+\xi}} = -2\int \frac{\sqrt{x-\xi}\sqrt{u}\mathrm{d}v}{\sqrt{u}\sqrt{(x-\xi)v^2-(x-\xi)}}, \tag{A.1.20}$$

$$= -2\int \frac{\mathrm{d}v}{\sqrt{v^2-1}}. \tag{A.1.21}$$

We now introduce the following trigonometric substitution, $v = \sec\theta \implies \mathrm{d}v = \sec\theta\tan\theta\mathrm{d}\theta$ and $\theta = \operatorname{arcsec} v$. Then (A.1.21) becomes

$$\begin{aligned} -2\int \frac{\mathrm{d}v}{\sqrt{v^2-1}} &= -2\int \frac{\sec\theta\tan\theta\mathrm{d}\theta}{\sqrt{\sec^2\theta-1}}, \\ &= -2\int \sec\theta\mathrm{d}\theta, \\ &= -2\int \frac{\sec^2\theta+\sec\theta\tan\theta}{\sec\theta+\tan\theta}\mathrm{d}\theta. \end{aligned} \tag{A.1.22}$$

Setting

$$\psi = \sec\theta+\tan\theta \implies \mathrm{d}\theta = \frac{\mathrm{d}\psi}{\sec^2\theta+\sec\theta\tan\theta}, \tag{A.1.23}$$

we find

$$\int \frac{\sec^2\theta+\sec\theta\tan\theta}{\sec\theta+\tan\theta}\mathrm{d}\theta = \int \frac{\mathrm{d}\psi}{\psi} = \mathrm{In}(\psi). \tag{A.1.24}$$

Now,

$$\begin{aligned} \mathrm{In}(\psi) &= \mathrm{In}(\sec\theta+\tan\theta), \\ &= \mathrm{In}(\sec(\operatorname{arcsec} v)+\tan(\operatorname{arcsec} v)), \\ &= \mathrm{In}(\sqrt{v^2-1}+v), \\ &= \mathrm{In}\left(\sqrt{\frac{u}{x-\xi}-1}+\frac{\sqrt{u}}{\sqrt{x-\xi}}\right), \\ &= \mathrm{In}\left(\frac{\sqrt{\xi-s}+\sqrt{x-s}}{\sqrt{x-\xi}}\right). \end{aligned} \tag{A.1.25}$$

Substituting back, we get

$$\int \frac{\mathrm{d}s}{\sqrt{\xi-s}\sqrt{x-s}} = -2\mathrm{In}\left(\frac{\sqrt{\xi-s}+\sqrt{x-s}}{\sqrt{x-\xi}}\right)+c_1. \tag{A.1.26}$$

where c_1 is a constant. Putting the intervals of integration, we get

$$\begin{aligned} \int_0^{\xi} \frac{\mathrm{d}s}{\sqrt{\xi-s}\sqrt{x-s}} &= -2\,\mathrm{In}\left(\frac{\sqrt{\xi-s}+\sqrt{x-s}}{\sqrt{x-\xi}}\right)+c_1\Big|_0^{\xi}, \\ &= \mathrm{In}\left(\frac{\sqrt{x}+\sqrt{\xi}}{\sqrt{x}-\sqrt{\xi}}\right), \end{aligned} \tag{A.1.27}$$

for $x > \xi$. Similarly, when $x < \xi$ we have

$$\int_0^x \frac{\mathrm{d}s}{\sqrt{\xi - s}\sqrt{x - s}} = \mathrm{In}\left(\frac{\sqrt{\xi} + \sqrt{x}}{\sqrt{\xi} - \sqrt{x}}\right). \tag{A.1.28}$$

If the representation in (A.1.18) is substituted in (A.1.17), we find

$$\int_0^x \sqrt{\xi}\psi(\xi) \int_0^\xi \frac{\mathrm{d}s}{\sqrt{\xi - s}\sqrt{x - s}}\mathrm{d}\xi + \int_x^1 \sqrt{\xi}\psi(\xi) \int_0^x \frac{\mathrm{d}s}{\sqrt{\xi - s}\sqrt{x - s}}\mathrm{d}\xi = \int_0^x \sqrt{\lambda} f(\lambda)\mathrm{d}\lambda + 2c\sqrt{x}. \tag{A.1.29}$$

The double integration terms on the left hand side of (A.1.29) are written such that we first integrate with respect to s from 0 to ξ and then the resulting integrals are integrated with respect to ξ from 0 to x. The region of integration, therefore, is the triangle lying above the diagonal $\xi = s$. (see Figure 41) We now change the order of integration so that we start by integrating from $\xi = s$ to $\xi = x$ and afterwards in the s direction from $s = 0$ to $s = x$. Equation (A.1.29) then becomes

$$\int_0^x \frac{1}{\sqrt{x - s}} \int_s^x \frac{\sqrt{\xi}\psi(\xi)\mathrm{d}\xi}{\sqrt{\xi - s}}\mathrm{d}s + \int_0^x \frac{1}{\sqrt{x - s}} \int_x^1 \frac{\sqrt{\xi}\psi(\xi)\mathrm{d}\xi}{\sqrt{\xi - s}}\mathrm{d}s = \int_0^x \sqrt{\lambda} f(\lambda)\mathrm{d}\lambda + 2c\sqrt{x}. \tag{A.1.30}$$

which yields

$$\int_0^x \frac{1}{\sqrt{x - s}} \int_s^1 \frac{\sqrt{\xi}\psi(\xi)\mathrm{d}\xi}{\sqrt{\xi - s}}\mathrm{d}s = \int_0^x \sqrt{\lambda} f(\lambda)\mathrm{d}\lambda + 2c\sqrt{x}. \tag{A.1.31}$$

It is well known that the solution of Abel's equation

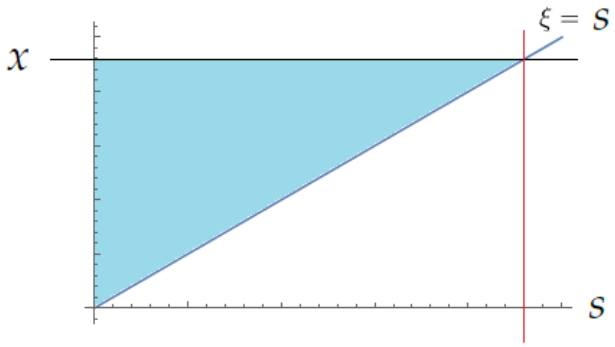

Figure 41: The region of integration (shaded area).

$$\int_0^x \frac{\phi(s)}{\sqrt{x - s}}\mathrm{d}s = \omega(x), \tag{A.1.32}$$

is

$$\phi(x) = \frac{1}{\pi}\frac{\mathrm{d}}{\mathrm{d}x}\int_0^x \frac{\omega(s)\mathrm{d}s}{\sqrt{x - s}}, \tag{A.1.33}$$

and if $\omega(x)$ is differentiable

$$\phi(x) = \frac{1}{\pi}\left[\frac{\omega(0)}{\sqrt{x}} + \int_0^x \frac{\omega_s(s)\mathrm{d}s}{\sqrt{x-s}}\right]. \tag{A.1.34}$$

Equation (A.1.33) can easily be obtained using Laplace transform method (see [70]). Leibnitz rule of differentiation cannot be used in (A.1.33). From (A.1.33), we have

$$\begin{aligned}
\phi(x) &= \frac{1}{\pi}\frac{\mathrm{d}}{\mathrm{d}x}\int_0^x \frac{\omega(s)-\omega(0)+\omega(0)\mathrm{d}s}{\sqrt{x-s}}, \\
&= \frac{1}{\pi}\frac{\mathrm{d}}{\mathrm{d}x}\left[\int_0^x \frac{\omega(x)-\omega(0)\mathrm{d}s}{\sqrt{x-s}} + \int_0^x \frac{\omega(0)\mathrm{d}s}{\sqrt{x-s}}\right], \\
&= \frac{1}{\pi}\frac{\mathrm{d}}{\mathrm{d}x}\left[2\int_0^x \sqrt{x-s}\omega_s(s)\mathrm{d}s + 2\sqrt{x}\omega(0)\right], \\
&= \frac{1}{\pi}\left[\frac{\omega(0)}{\sqrt{x}} + \int_0^x \frac{\omega_s(s)\mathrm{d}s}{\sqrt{x-s}}\right].
\end{aligned} \tag{A.1.35}$$

We will apply this result on (A.1.31). Let

$$\phi(s) = \int_s^1 \frac{\sqrt{\xi}\psi(\xi)\mathrm{d}\xi}{\sqrt{\xi-s}} \text{ and } \omega(x) = \int_0^x \sqrt{\lambda}f(\lambda)\mathrm{d}\lambda + 2c\sqrt{x}, \tag{A.1.36}$$

then (A.1.31) can be written as

$$\int_0^x \frac{\phi(s)\mathrm{d}s}{\sqrt{x-s}} = \omega(x). \tag{A.1.37}$$

Substituting $\omega(0) = 0$ and $\omega_x(x) = \frac{c}{\sqrt{x}} + \sqrt{x}f(x)$ into (A.1.34), we obtain

$$\begin{aligned}
\phi(x) &= \frac{1}{\pi}\left[\int_0^x \frac{\frac{c}{\sqrt{s}} + \sqrt{s}f(s)}{\sqrt{x-s}}\mathrm{d}s\right], \\
&= \frac{1}{\pi}\left[c\int_0^x \frac{\mathrm{d}s}{\sqrt{s}\sqrt{x-s}} + \int_0^x \frac{\sqrt{s}f(s)\mathrm{d}s}{\sqrt{x-s}}\right], \\
&= \frac{1}{\pi}\int_0^x \frac{\sqrt{s}f(s)\mathrm{d}s}{\sqrt{x-s}} + c.
\end{aligned} \tag{A.1.38}$$

Using (A.1.38), we find

$$\int_s^1 \frac{\sqrt{\xi}\psi(\xi)\mathrm{d}\xi}{\sqrt{\xi-s}} = \frac{1}{\pi}\int_0^s \frac{\sqrt{x}f(x)}{\sqrt{s-x}}\mathrm{d}x + c \tag{A.1.39}$$

The solution of the integral equation

$$\int_s^1 \frac{\varphi(\xi)\mathrm{d}\xi}{\sqrt{\xi-s}} = h(s) \tag{A.1.40}$$

can easily be deduced from Abel's equation. It is

$$\varphi(\xi) = -\frac{1}{\pi}\frac{\mathrm{d}}{\mathrm{d}\xi}\int_\xi^1 \frac{h(s)\mathrm{d}s}{\sqrt{s-\xi}}. \tag{A.1.41}$$

Let

$$\varphi(\xi) = \sqrt{\xi}\psi(\xi) \quad \text{and} \quad h(s) = \frac{1}{\pi}\int_0^s \frac{\sqrt{x}f(x)}{\sqrt{s-x}}\mathrm{d}x + c,$$

then the solution of (A.1.39), using (A.1.41), is

$$\begin{aligned}
\sqrt{\xi}\psi(\xi) &= -\frac{1}{\pi^2}\frac{\mathrm{d}}{\mathrm{d}\xi}\int_\xi^1 \frac{1}{\sqrt{s-\xi}}\left(\int_0^s \frac{\sqrt{x}f(x)}{\sqrt{s-x}}\mathrm{d}x + c\right)\mathrm{d}s \\
&= -\frac{1}{\pi^2}\frac{\mathrm{d}}{\mathrm{d}\xi}\int_\xi^1 \frac{1}{\sqrt{s-\xi}}\int_0^s \frac{\sqrt{x}f(x)\mathrm{d}x}{\sqrt{s-x}}\mathrm{d}s - \frac{1}{\pi}\frac{\mathrm{d}}{\mathrm{d}\xi}\int_\xi^1 \frac{c}{\sqrt{s-\xi}}\mathrm{d}s \\
&= \frac{c}{\pi\sqrt{1-\xi}} - \frac{1}{\pi^2}\frac{\mathrm{d}}{\mathrm{d}\xi}\int_\xi^1 \frac{1}{\sqrt{s-\xi}}\int_0^s \frac{\sqrt{x}f(x)\mathrm{d}x}{\sqrt{s-x}}\mathrm{d}s
\end{aligned} \tag{A.1.42}$$

Equation (A.1.42) is often taken to be the formula for the solution of (A.1.4) but it is not the standard one. In order to derive the standard formula we change the order of integration of the double integral on the right side of (A.1.42) to get

$$\begin{aligned}
\sqrt{\xi}\psi(\xi) = \frac{c}{\pi\sqrt{1-\xi}} &- \frac{1}{\pi^2}\frac{\mathrm{d}}{\mathrm{d}\xi}\left[\int_\xi^1 \sqrt{x}f(x)\int_x^1 \frac{\mathrm{d}s}{\sqrt{s-\xi}\sqrt{s-x}}\mathrm{d}x\right] \\
&- \frac{1}{\pi^2}\frac{\mathrm{d}}{\mathrm{d}\xi}\left[\int_0^\xi \sqrt{x}f(x)\int_\xi^1 \frac{\mathrm{d}s}{\sqrt{s-\xi}\sqrt{s-x}}\mathrm{d}x\right].
\end{aligned} \tag{A.1.43}$$

To proceed from here, we need the result

$$\int_{\max(\xi,x)}^1 \frac{\mathrm{d}s}{\sqrt{s-\xi}\sqrt{s-x}}\mathrm{d}x = \mathrm{In}\left|\frac{\sqrt{1-\xi}+\sqrt{1-x}}{\sqrt{1-\xi}-\sqrt{1-x}}\right|. \tag{A.1.44}$$

Consider the integral

$$\int \frac{\mathrm{d}s}{\sqrt{s-\xi}\sqrt{s-x}}. \tag{A.1.45}$$

To solve (A.1.45), let $u = s - x \Longrightarrow \mathrm{d}s = \mathrm{d}u$, then we have

$$\int \frac{\mathrm{d}s}{\sqrt{s-\xi}\sqrt{s-x}} = \int \frac{\mathrm{d}u}{\sqrt{u}\sqrt{u+x-\xi}}. \tag{A.1.46}$$

Again, let $v = \frac{\sqrt{u}}{\sqrt{x-\xi}} \Longrightarrow \mathrm{d}u = 2\sqrt{\xi-x}\sqrt{u}\mathrm{d}v$. Then,

$$\begin{aligned}
\int \frac{\mathrm{d}u}{\sqrt{u}\sqrt{u-x+\xi}} &= 2\int \frac{\mathrm{d}v}{\sqrt{v^2-1}}, \\
&= 2\mathrm{In}\left(\sqrt{v^2-1}+v\right), \\
&= 2\mathrm{In}\left(\frac{\sqrt{s-\xi}+\sqrt{s-x}}{\sqrt{\xi-x}}\right).
\end{aligned} \tag{A.1.47}$$

The integral (A.1.45) is given by

$$\int \frac{\mathrm{d}s}{\sqrt{s-\xi}\sqrt{s-x}} = 2\mathrm{In}\left(\frac{\sqrt{s-\xi}+\sqrt{s-x}}{\sqrt{\xi-x}}\right) + c_1. \tag{A.1.48}$$

For $\xi < x$, we have

$$\begin{aligned}\int_x^1 \frac{\mathrm{d}s}{\sqrt{s-\xi}\sqrt{s-x}} &= 2\mathrm{In}\left(\frac{\sqrt{s-\xi}+\sqrt{s-x}}{\sqrt{\xi-x}}\right) + c_1\Bigg|_x^1, \\ &= \mathrm{In}\left(\frac{\sqrt{1-\xi}+\sqrt{1-x}}{\sqrt{1-\xi}-\sqrt{1-x}}\right).\end{aligned} \tag{A.1.49}$$

Similarly, for the case $\xi > x$ we find

$$\int_\xi^1 \frac{\mathrm{d}s}{\sqrt{s-\xi}\sqrt{s-x}} = \mathrm{In}\left(\frac{\sqrt{1-\xi}+\sqrt{1-x}}{\sqrt{1-x}-\sqrt{1-\xi}}\right). \tag{A.1.50}$$

These results can be summarized as

$$\ln\left|\frac{\sqrt{1-\xi}+\sqrt{1-x}}{\sqrt{1-\xi}-\sqrt{1-x}}\right| = \begin{cases} \int_x^1 \frac{\mathrm{d}\sigma}{\sqrt{s-\xi}\sqrt{s-x}}, & x > \xi, \\ \int_\xi^1 \frac{\mathrm{d}s}{\sqrt{s-\xi}\sqrt{s-x}} & x < \xi. \end{cases} \tag{A.1.51}$$

Using (A.1.51), we find that

$$\sqrt{\xi}\psi(\xi) = \frac{c}{\pi\sqrt{1-\xi}} - \frac{1}{\pi^2}\frac{\mathrm{d}}{\mathrm{d}\xi}\left[\int_0^1 \ln\left|\frac{\sqrt{1-\xi}+\sqrt{1-x}}{\sqrt{1-\xi}-\sqrt{1-x}}\right|\sqrt{x}f(x)\mathrm{d}x\right]. \tag{A.1.52}$$

The second term on the right side of (A.1.52) is integrated as

$$\begin{aligned}\frac{\mathrm{d}}{\mathrm{d}\xi}\left[\int_0^1 \ln\left|\frac{\sqrt{1-\xi}+\sqrt{1-x}}{\sqrt{1-\xi}-\sqrt{1-x}}\right|\sqrt{x}f(x)\mathrm{d}x\right] &= \int_0^1 \frac{\mathrm{d}}{\mathrm{d}\xi}\ln\left|\frac{\sqrt{1-\xi}+\sqrt{1-x}}{\sqrt{1-\xi}-\sqrt{1-x}}\right|\sqrt{x}f(x)\mathrm{d}x, \\ &= \int_0^1 \frac{\sqrt{1-x}}{\sqrt{1-\xi}(x-\xi)}\sqrt{x}f(x)\mathrm{d}x.\end{aligned} \tag{A.1.53}$$

Equation (A.1.52) becomes

$$\psi(\xi) = \frac{c}{\sqrt{\xi(1-\xi)}} - \frac{1}{\pi^2\sqrt{\xi(1-\xi)}}\int_0^1 \frac{\sqrt{x(1-x)}f(x)\mathrm{d}x}{x-\xi}, \tag{A.1.54}$$

where c is an arbitrary constant arising from inversion of the singular integral.

B

APPENDIX B

B.1 SOLUTION OF THE DIMENSIONLESS FRACTURE HALF-WIDTH

We seek a solution of a Cauchy-type singular integral equation of the first kind in the interval $(-1,1)$ given by

$$P(\xi) = -\frac{1}{\pi}\fint_{-1}^{1}\frac{f'(\eta)\mathrm{d}\eta}{\eta-\xi}, \quad -1<\xi<1. \tag{B.1.1}$$

The inversion of the integral equation (B.1.1) has been obtained in [82]. We re-derive it here for completeness.

First, set $P^*(\xi) = -\pi P(\xi)$ for mathematical convenience to obtain

$$P^*(\xi) = \fint_{-1}^{1}\frac{f'(\eta)\mathrm{d}\eta}{\eta-\xi}, \quad -1<\xi<1. \tag{B.1.2}$$

From here, we move to introduce new variables so that we can represent equation (B.1.2) in the form of equation (A.1.4). Setting

$$\eta = 2t-1, \qquad \eta\in(-1,1)\Rightarrow t\in(0,1), \tag{B.1.3}$$

$$\xi = 2x-1, \qquad \xi\in(-1,1)\Rightarrow x\in(0,1), \tag{B.1.4}$$

we get $\eta-\xi = 2(t-x)$. Hence, equation (B.1.2) becomes

$$P^*(2x-1) = \fint_{0}^{1}\frac{f'(2t-1)2\mathrm{d}t}{2(t-x)}, \tag{B.1.5}$$

$$\text{or} \quad \fint_{0}^{1}\frac{\phi(t)\mathrm{d}t}{t-x} = q(x), \tag{B.1.6}$$

where $\phi(t) = f'(2t-1)$ and $q(x) = P^*(2x-1)$. The solution of (B.1.6) can easily be obtain as (see Appendix A)

$$\phi(x) = \frac{c}{\sqrt{x(1-x)}} - \frac{1}{\pi^2\sqrt{x(1-x)}}\fint_{0}^{1}\frac{\sqrt{t(1-t)}q(t)\mathrm{d}t}{t-x}, \tag{B.1.7}$$

where $0<x<1$ and c is an arbitrary constant. Now, substituting $t=\frac{1}{2}(\eta+1)$, $x=\frac{1}{2}(\xi+1)$, $\phi(x)=f'(\xi)$, $q(t)=P^*(\eta)$, $[t\in(0,1)\Rightarrow \eta\in(-1,1)$, $x\in(0,1)\Rightarrow\xi\in(-1,1)]$, we obtain

$$f'(\xi) = \frac{2c}{\sqrt{1-\xi^2}} - \frac{1}{\pi^2\sqrt{1-\xi^2}}\fint_{-1}^{1}\frac{\sqrt{1-\eta^2}P^*(\eta)\mathrm{d}\eta}{\eta-\xi}, \tag{B.1.8}$$

$$= \frac{2c}{\sqrt{1-\xi^2}} + \frac{1}{\pi\sqrt{1-\xi^2}}\fint_{-1}^{1}\frac{\sqrt{1-\eta^2}P(\eta)\mathrm{d}\eta}{\eta-\xi}. \tag{B.1.9}$$

We now change the limits of integration from (-1,1) to (0,1). To achieve this, we first prepare the integral by writing it in the form

$$\int_{-1}^{1} \frac{\sqrt{1-\eta^2}P(\eta)\mathrm{d}\eta}{\eta-\xi} = \int_{-1}^{0} \frac{\sqrt{1-r^2}P(r)\mathrm{d}r}{r-\xi} + \int_{0}^{1} \frac{\sqrt{1-\eta^2}P(\eta)\mathrm{d}\eta}{\eta-\xi}. \tag{B.1.10}$$

Set $r=-\eta \Longrightarrow \mathrm{d}r=-\mathrm{d}\eta$. Then, the first integral on right of (B.1.10) becomes

$$\int_{-1}^{0} \frac{\sqrt{1-r^2}P(r)\mathrm{d}r}{r-\xi} = -\int_{0}^{1} \frac{\sqrt{1-\eta^2}P(\eta)\mathrm{d}\eta}{\eta+\xi}. \tag{B.1.11}$$

Hence, equation (B.1.10) becomes

$$\int_{-1}^{1} \frac{\sqrt{1-\eta^2}P(\eta)\mathrm{d}\eta}{\eta-\xi} = \int_{0}^{1} \frac{\sqrt{1-\eta^2}P(\eta)\mathrm{d}\eta}{\eta-\xi} - \int_{0}^{1} \frac{\sqrt{1-\eta^2}P(\eta)\mathrm{d}\eta}{\eta+\xi}, \tag{B.1.12}$$

$$= 2\xi \int_{0}^{1} \frac{\sqrt{1-\eta^2}P(\eta)\mathrm{d}\eta}{\eta^2-\xi^2}. \tag{B.1.13}$$

Substituting (B.1.13) into (B.1.9), we obtain

$$f'(\xi) = \frac{2c}{\sqrt{1-\xi^2}} + \frac{2\xi}{\pi\sqrt{1-\xi^2}} \int_{0}^{1} \frac{\sqrt{1-\eta^2}P(\eta)\mathrm{d}\eta}{\eta^2-\xi^2}. \tag{B.1.14}$$

Using the fact that $f'(0)=0$, we find that $c=0$. Equation (B.1.14) becomes

$$f'(\xi) = \frac{2\xi}{\pi\sqrt{1-\xi^2}} \int_{0}^{1} \frac{\sqrt{1-\eta^2}P(\eta)\mathrm{d}\eta}{\eta^2-\xi^2}. \tag{B.1.15}$$

Integrating (B.1.15) with respect to ξ from x to 1 and using the boundary condition $f(1)=0$ gives

$$-f(x) = \frac{2}{\pi} \int_{x}^{1} \frac{\xi}{\sqrt{1-\xi^2}} \int_{0}^{1} \frac{\sqrt{1-\eta^2}P(\eta)}{\eta^2-\xi^2}\mathrm{d}\eta\mathrm{d}\xi. \tag{B.1.16}$$

Changing the order of integration, we obtain

$$\begin{aligned} -f(x) &= \frac{2}{\pi} \int_{0}^{1} \sqrt{1-\eta^2}P(\eta) \int_{x}^{1} \frac{\xi\mathrm{d}\xi\mathrm{d}\eta}{\sqrt{1-\xi^2}\,(\eta^2-\xi^2)}, \\ &= \frac{1}{\pi} \int_{0}^{1} \Phi(x,\eta)P(\eta)\mathrm{d}\eta, \end{aligned} \tag{B.1.17}$$

where

$$\Phi(x,\eta) = \ln\left|\frac{\sqrt{1-x^2}-\sqrt{1-\eta^2}}{\sqrt{1-x^2}+\sqrt{1-\eta^2}}\right|.$$

We now use the integration by parts method to determine the right side of (B.1.17). Let $u = P(\eta)$ and $\mathrm{d}v = \Phi(x,\eta)\mathrm{d}\eta$ then $\mathrm{d}u = P(\eta)\mathrm{d}\eta$ and $v = \int \Phi(x,\eta)\mathrm{d}\eta$. Thus,

$$\int_0^1 \Phi(x,\eta)P(\eta)\mathrm{d}\eta = P(\eta)\int \Phi(x,\eta)\mathrm{d}\eta\Big|_0^1 - \int_0^1 \left[\int \Phi(x,\eta)\mathrm{d}\eta\right] P(\eta)\mathrm{d}\eta. \tag{B.1.18}$$

Again, we use the integration by parts technique to determine the integral terms appearing on both terms on the right of (B.1.18). Let $u = \Phi(x,\eta)$ and $\mathrm{d}v = \mathrm{d}\eta$ then $\mathrm{d}u = \frac{2\eta\sqrt{1-x^2}}{\sqrt{1-\eta^2}(\eta^2-x^2)}\mathrm{d}\eta$ and $v = \eta$. Thus,

$$\begin{aligned}
\int \Phi(x,\eta)\mathrm{d}\eta &= \eta\Phi(x,\eta) - \int \frac{2\eta\sqrt{1-x^2}}{\sqrt{1-\eta^2}\,(\eta^2-x^2)}\mathrm{d}\eta, \\
&= \eta\Phi(x,\eta) - 2\sqrt{1-x^2}\sin^{-1}(\eta) + x\ln\left|\frac{x\sqrt{1-\eta^2}-\eta\sqrt{1-x^2}}{x\sqrt{1-\eta^2}+\eta\sqrt{1-x^2}}\right|, \\
&= k(x,\eta) - 2\sqrt{1-x^2}\sin^{-1}(\eta),
\end{aligned} \tag{B.1.19}$$

where

$$k(x,\eta) = \eta\Phi(x,\eta) + x\Psi(x,\eta),$$

with

$$\Psi(x,\eta) = \ln\left|\frac{x\sqrt{1-\eta^2}-\eta\sqrt{1-x^2}}{x\sqrt{1-\eta^2}+\eta\sqrt{1-x^2}}\right|.$$

Substituting (B.1.19) into (B.1.18), we find

$$\begin{aligned}
\int_0^1 \Phi(x,\eta)P(\eta)\mathrm{d}\eta &= P(\eta)\left[k(x,\eta) - 2\sqrt{1-x^2}\sin^{-1}(\eta)\right]\Big|_0^1 \\
&\quad - \int_0^1 \left[k(x,s) - 2\sqrt{1-x^2}\sin^{-1}(s)\right] P'(s)\mathrm{d}s, \\
&= -\pi\sqrt{1-x^2}P(1) + 2\sqrt{1-x^2}\int_0^1 \sin^{-1}(s)P'(s)\mathrm{d}s \\
&\quad - \int_0^1 k(x,s)P'(s)\mathrm{d}s, \\
&= -\pi\sqrt{1-x^2}P(1) + 2\sqrt{1-x^2}\left[\frac{\pi}{2}P(1) - \int_0^1 \frac{P(s)\mathrm{d}s}{\sqrt{1-s^2}}\right] \\
&\quad - \int_0^1 k(x,s)P'(s)\mathrm{d}s, \\
&= -2\sqrt{1-x^2}\int_0^1 \frac{P(s)\mathrm{d}s}{\sqrt{1-s^2}} - \int_0^1 k(x,s)P'(s)\mathrm{d}s
\end{aligned} \tag{B.1.20}$$

Using (B.1.20), (B.1.17) becomes

$$f(x) = \gamma\sqrt{1-x^2} + \frac{1}{\pi}\int_0^1 k(x,s)P'(s)\mathrm{d}s, \tag{B.1.21}$$

where γ represents the dimensionless stress intensity factor at the fracture tip and it is given by

$$\gamma = \frac{2}{\pi}\int_0^1 \frac{P(s)\mathrm{d}s}{\sqrt{1-s^2}}.$$

APPENDIX C

C.1 DIFFERENTIATION UNDER THE INTEGRAL SIGN

If $f(x,t)$ is a continuous and continuously differentiable function and the limits of integration $a(x)$ and $b(x)$ are continuous and continuously differentiable functions of x, then

$$\frac{\mathrm{d}}{\mathrm{d}x}\int_{a(x)}^{b(x)} f(x,t)\mathrm{d}t = f(x,b(x))\frac{\mathrm{d}}{\mathrm{d}x}b(x) - f(x,a(x))\frac{\mathrm{d}}{\mathrm{d}x}\cdot a(x) + \int_{a(x)}^{b(x)} \frac{\partial}{\partial x} f(x,t)\mathrm{d}t. \tag{C.1.1}$$

Using (C.1.1) and the fact that $v_x(t,\pm h(t,x),z) = 0$, we have that

$$\frac{\partial}{\partial x}\int_{-h(t,x)}^{h(t,x)} v_x(t,x,z)\mathrm{d}z = \int_{-h(t,x)}^{h(t,x)} \frac{\partial}{\partial x} v_x(t,x,z)\mathrm{d}z. \tag{C.1.2}$$

In this appendix, we will show using calculus that (C.1.2) holds only when the no slip boundary condition is applied. First, let

$$F(t,x,h(t,x)) = \int_{-h}^{h} v_x(t,x,z)\mathrm{d}z, \tag{C.1.3}$$

then

$$\frac{\mathrm{d}}{\mathrm{d}x}F(t,x,h(t,x)) = \frac{\partial F}{\partial x} + \frac{\partial F}{\partial h}\frac{\partial h}{\partial x}. \tag{C.1.4}$$

From the fundamental theorem of calculus and the no slip boundary condition

$$\frac{\partial}{\partial h}F(t,x,h) = v_x(t,x,h(t,x)) - v_x(t,x,-h(t,x)) = 0. \tag{C.1.5}$$

Thus,

$$\frac{\mathrm{d}}{\mathrm{d}x}F(t,x,h) = \frac{\partial}{\partial x}F(t,x,h). \tag{C.1.6}$$

Now,

$$\frac{\partial}{\partial x}F(t,x,h) = \lim_{\Delta x\to 0}\frac{F(t,x+\Delta x,h) - F(t,x,h)}{\Delta x}. \tag{C.1.7}$$

That is,

$$\begin{aligned}\frac{\partial F}{\partial x} &= \lim_{\Delta x\to 0}\frac{\int_{-h(t,x+\Delta x)}^{h(t,x+\Delta x)} v_x(t,x+\Delta x,z)\mathrm{d}z - \int_{-h(t,x)}^{h(t,x)} v_x(t,x,z)\mathrm{d}z}{\Delta x},\\ &= \lim_{\Delta x\to 0}\frac{1}{\Delta x}\left[\int_{-h(t,x+\Delta x)}^{h(t,x+\Delta x)} v_x(t,x+\Delta x,z)\mathrm{d}z - \int_{-h(t,x)}^{h(t,x)} v_x(t,x,z)\mathrm{d}z\right].\end{aligned}$$

(C.1.8)

Now,

$$\int_{-h(t,x+\Delta x)}^{h(t,x+\Delta x)} v_x(t,x+\Delta x,z)\mathrm{d}z = \int_{-h(t,x)}^{h(t,x+\Delta x)} v_x(t,x+\Delta x,z)\mathrm{d}z - \int_{-h(t,x)}^{-h(t,x+\Delta x)} v_x(t,x+\Delta x,z)\mathrm{d}z,$$

$$= \int_{-h(t,x)}^{h(t,x)} v_x(t,x+\Delta x,z)\mathrm{d}z + \int_{h(t,x)}^{h(t,x+\Delta x)} v_x(t,x+\Delta x,z)\mathrm{d}z - \int_{-h(t,x)}^{-h(t,x+\Delta x)} v_x(t,x+\Delta x,z)\mathrm{d}z. \tag{C.1.9}$$

Therefore, equation (C.1.8) becomes

$$\frac{\partial F}{\partial x} = \lim_{\Delta x\to 0}\frac{1}{\Delta x}\left[\int_{-h(t,x)}^{h(t,x)}(v_x(t,x+\Delta x,z)-v_x(t,x,z))\mathrm{d}z + \int_{h(t,x)}^{h(t,x+\Delta x)} v_x(t,x+\Delta x,z)\mathrm{d}z - \int_{-h(t,x)}^{-h(t,x+\Delta x)} v_x(t,x+\Delta x,z)\mathrm{d}z\right]. \tag{C.1.10}$$

By the mean value theorem,

$$\int_{h(t,x)}^{h(t,x+\Delta x)} v_x(t,x+\Delta x,z)\mathrm{d}z = (h(t,x+\Delta x)-h(t,x))v_x(t,x+\Delta x,\xi_1), \tag{C.1.11}$$

$$\int_{-h(t,x)}^{-h(t,x+\Delta x)} v_x(t,x+\Delta x,z)\mathrm{d}z = (h(t,x)-h(t,x+\Delta x))v_x(t,x+\Delta x,\xi_2), \tag{C.1.12}$$

where $h(t,x)\leqslant\xi_1\leqslant h(t,x+\Delta x)$ and $-h(t,x)\leqslant\xi_2\leqslant -h(t,x+\Delta x)$. Therefore,

$$\lim_{\Delta x\to 0}\frac{(h(t,x+\Delta x)-h(t,x))v_x(t,x+\Delta x,\xi_1)}{\Delta x} = 0, \text{ and} \tag{C.1.13}$$

$$\lim_{\Delta x\to 0}\frac{(h(t,x)-h(t,x+\Delta x))v_x(t,x+\Delta x,\xi_2)}{\Delta x} = 0. \tag{C.1.14}$$

Since $\xi_1 \to h(t,x)$ and $\xi_2 \to h(t,x)$ as $\Delta x \to 0$ and $v_x(t,x,h(t,x)) = 0$ for any x. Thus,

$$\frac{\partial F}{\partial x} = \int_{-h(t,x)}^{h(t,x)} \lim_{\Delta x \to 0} \left[\frac{v_x(t,x+\Delta x,z) - v_x(t,x,z)}{\Delta x} \right] \mathrm{d}z, \quad \text{(C.1.15)}$$

$$= \int_{-h(t,x)}^{h(t,x)} \frac{\partial}{\partial x} v_x(t,x,z) \mathrm{d}z. \quad \text{(C.1.16)}$$

That is,

$$\frac{\partial}{\partial x} \int_{-h(t,x)}^{h(t,x)} v_x(t,x,z) \mathrm{d}z = \int_{-h(t,x)}^{h(t,x)} \frac{\partial}{\partial x} v_x(t,x,z) \mathrm{d}z. \quad \text{(C.1.17)}$$

[1] M. Abdulkawi. "Solution of Cauchy type singular integral equations of the first kind by using differential transform method." In: *Applied Mathematical Modelling* 39 (2015), pp. 2107–2118.

[2] A.S. Abou-Sayed, C.E. Brechel, and R.J. Clifton. "In situ stress determination by hydrofracturing: a fracture mechanics approach." In: *Journal of Geophysical Research* 83 (B6) (1978), pp. 2851–62.

[3] D.J. Acheson. *Elementary fluid dynamics*. 1990.

[4] J. Adachi, E. Siebrits, A. Peirce, and J. Desroches. "Computer simulation of hydraulic fractures." In: *International Journal of Rock Mechanics and Mining Sciences* 44 (2007), pp. 739–757.

[5] J. Adams and C. Rowe. "Differentiating applications of hydraulic fracturing." In: *ISRM International Conference for Effective and Sustainable Hydraulic Fracturing*. International Society for Rock Mechanics and Rock Engineering. 2013.

[6] W. Ang. *Hypersingular integral equations in fracture analysis*. Elsevier, 2014.

[7] M. Anthonyrajah, D.P. Mason, and A.G. Fareo. "Propagation of a pre-existing turbulent fluid fracture." In: *International Journal of Non-Linear Mechanics* 54 (2013), pp. 105–114.

[8] S. Asadi, M.M. Javan, B. Bohloli, and S. Mutabashiani. "Experimental, numerical and Analytical investigation the initiation and propagation of hydraulic fracturing (Case Study: Sarvak Lime Stone)." In: *World Applied Science Journal* 22 (2013), pp. 637–646.

[9] R.D. Carter. "Derivation of the general equation for estimating the extent of the fractured area, Appendix I of optimum fluid characteristics for fracture extension." In: *Howard, G.C., Fast, C.R. (Eds.), Drilling and Production Practice. American Petroleum Institute, New York* (1957), pp. 261–269.

[10] A. Chakrabarti and G. V. Berghe. "Approximate solution of singular integral equations." In: *Applied mathematics letters* 17 (2004), pp. 553–559.

[11] B.C. Crittendon. "The mechanics of design and interpretation of hydraulic fracture treatments." In: *Journal of petroleum technology* 11 (1959), pp. 21–29.

[12] *D05 Chapter Introduction : NAG Library, Mark 26*. URL: https://www.nag.com/numeric/fl/nagdoc{_}fl26.2/html/d05/d05intro.html{\#}scope (visited on 11/01/2019).

[13] L.P. Dake. *Fundamentals of reservoir engineering*. Vol. 8. Elsevier, 1983.

[14] E. V. Dontsov. "An approximate solution for a plane strain hydraulic fracture that accounts for fracture toughness, fluid viscosity, and leak-off." In: *International Journal of Fracture* 205 (2017), pp. 221–237.

[15] M.J. Economides, A.D. Hill, C. Ehlig-Economides, and D. Zhu. *Petroleum production systems*. Pearson Education, 2013.

[16] M.J. Economides and K.G Nolte. *Reservoir stimulation*. Vol. 2. Prentice Hall Englewood Cliffs, NJ, 1989.

[17] S. Emerman, D.L Turcotte, and D.A. Spence. "Transport of magma and hydrothermal solutions by laminar and turbulent fluid fracture." In: *Phys. Earth Planet Int.* 36 (1986), pp. 276–284.

[18] Z. K. Eshkuvatov, N. M.A. Nik Long, and M. Abdulkawi. "Approximate solution of singular integral equations of the first kind with Cauchy kernel." In: *Applied Mathematics Letters* 22 (2009), pp. 651–657.

[19] R. Estrada and R. Kanwal. *Singular integral equations*. Springer Science & Business Media, 2012.

[20] A.G. Fareo. "Group invariant solutions for a pre-existing fracture driven by a non-Newtonian fluid in permeable and impermeable rock." PhD thesis. University of the Witwatersrand, 2013.

[21] A.G. Fareo and D.P. Mason. "A group invariant solution for a pre-existing fluid-driven fracture in permeable rock." In: *Nonlinear Analysis: Real world Applications* 12 (2011), pp. 767–779.

[22] A.G. Fareo and D.P. Mason. "A group invariant solution for a pre-existing fracture driven by power-law fluid in impermeable rock." In: *Comm Nonlinear Sci Numer Simulat* 18 (2013), pp. 3298–3316.

[23] A.G. Fareo and D.P. Mason. "Group invariant solution for a pre-existing fracture driven by power-law fluid in permeable rock." In: *International Journal of Modern Physics B* 30 (2016), 28n29. URL: http://www.worldscientific.com/doi/abs/10.1142/S0217979216400105.

[24] A.C. Fischer-Cripps. *Introduction to contact mechanics*. Vol. 101. Mechanical Engineering Series. Springer US, 2007.

[25] A.D. Fitt, A.D. Kelly, and C.P. Please. "Crack propagation models for rock fracture in a geothermal energy reservoir." In: *SIAM Journal on Applied Mathematics* 55 (1995), pp. 1592–1608.

[26] A.D. Fitt, A.D. Kelly, and C.P. Please. "Crack propagation models for rock fracture in a geothermal energy reservoir." In: *SIAM Journal on Applied Mathematics* 55 (1995), pp. 1592–1608.

[27] A.D. Fitt, D.P. Mason, and E.A. Moss. “Group invariant solution for a pre-existing fluid-driven fracture in impermeable rock.” In: *Z. Angew. Math. Phys.* 58 (2008), pp. 1049–1067.

[28] J. Geertsma and F. de Klerk. “A rapid method predicting width and extent of hydraulically induced fractures.” In: *J Pet Tech* 21 (1969), pp. 571–581.

[29] A.A. Griffith. “The phenomena of rupture and flows in solids.” In: *Philos. Trans. R. Soc.* 221 (1920), pp. 163–198.

[30] J. Hagoort, B.D. Weatherill, and A. Settari. “Modeling the propagation of waterflood-induced hydraulic fractures.” In: *Society of Petroleum Engineers Journal* 20 (1980), pp. 293–303.

[31] E. Harrison, W.F. Kieschnick, and W.J. McGuire. “The mechanics of fracture induction and extension.” In: *Petroleum Transactions, AIME* 201 (1954), pp. 252–263.

[32] D.R. Hartree. *Numerical Analysis*. Clarendon Press, Oxford, 1958.

[33] D.J. Hayes. “Origings of the stress intensity factor approach to fracture.” In: *Journal of strain analysis* 10 (1975), pp. 198–200.

[34] J.H. He. “Some asymptotic methods for strongly nonlinear equations.” In: *International journal of Modern physics B* 20 (2006), pp. 1141–1199.

[35] G.C. Howard and C.R. Fast. “Optimum fluid characteristics for fracture extension.” In: *Drilling and production practice*. Vol. 24. American Petroleum Institute. 1957, pp. 261–270.

[36] M.K. Hubbert. “The theory of ground-water motion.” In: *The Journal of Geology* 48 (1940), pp. 785–944. URL: http://www.jstor.org/stable/30057101.

[37] N.I. Ioakimidis. “The successive approximations method for the airfoil equation.” In: *Journal of computational and applied mathematics* 21 (1988), pp. 231–238.

[38] G.R. Irwin. *Fracture dynamics, Fracturing of Metals. American Society of Metals*. 1948.

[39] G.R. Irwin. “Analysis of stresses and strains near the end of a crack tranversing a plate.” In: *Journal of Applied mechanics* 24 (1957), pp. 361–364.

[40] L. Jing. “A review of techniques, advances and outstanding issues in numerical modelling for rock mechanics and rock engineering.” In: *International Journal of Rock Mechanics and Mining Sciences* 40 (2003), pp. 283–353.

[41] T. Kajishima and K. Taira. *Computational fluid dynamics: incompressible turbulent flows*. Springer International Publishing, 2016.

[42] S. Kanaun. "Hydraulic fracture crack propagation in an elastic medium with varying fracture toughness." In: *International Journal of Engineering Science* 120 (2017), pp. 15–30. URL: http://dx.doi.org/10.1016/j.ijengsci.2017.06.009.

[43] M.R.R. Kgatle and D.P. Mason. "Propagation of a linear hydraulic fracture with tortuosity." In: *International Journal of Non-Linear Mechanics* 61 (2014), pp. 39–53.

[44] S. Khristianovic and Y. Zheltov. "Formation of vertical fractures by means of highly viscous fluids." In: *In:4th World Petroleum Congress, Rome* (1995), pp. 579–586.

[45] S. Kim. "Solving singular integral equations using Gaussian quadrature and overdetermined system." In: *Computers & Mathematics with Applications* 35 (1998), pp. 63–71.

[46] P Kusmierczyk, M Wrobel, and G Mishuris. "Remarks on numerical simulation of the PKN model of hydrofracturing in proper variables. Various leak-off regimes." In: *International Journal of Fracture* 184 (2013), pp. 185–213.

[47] P. Kythe and P. Puri. *Computational methods for linear integral equations*. Birkhäuser Boston, 2011.

[48] I.M. Longman. "On the numerical evaluation of Cauchy principal values of integrals." In: *Mathematical Tables and Other Aids to Computation* 12 (1958), pp. 205–207.

[49] M. V. Madyarova. "Fluid-driven penny-shaped fracture in elastic medium." PhD thesis. University of Minnesota, 2003.

[50] K Maleknejad and M Hadizadeh. "A new computational method for Volterra-Fredholm integral equations." In: *Computers & Mathematics with Applications* 37 (1999), pp. 1–8.

[51] B.N. Mandal and A. Chakrabarti. *Applied singular integral equations*. CRC press, 2016.

[52] J.C. Mason and D.C. Handscomb. *Chebyshev polynomials*. CRC Press LLC, 2003.

[53] D.A. Mendelsohn. "A review of hydraulic fracture modelling - part I: general concepts, 2D models and motivation for 3D modelling." In: *ASME J. Energy Resour. Technol* 106 (1984), pp. 369–376.

[54] S. L. Mitchell, R. Kuske, and A. P. Peirce. "An asymptotic framework for finite hydraulic fractures including leak-off." In: *SIAM Journal on Applied Mathematics* 67 (2007), pp. 364–386.

[55] V.J. Monacella. *On ignoring the singularity in the numerical evaluation of Cauchy Principal Value integrals*. Vol. 2356. Department of the Navy, David Taylor Model Basin, 1967.

[56] S. Mondal and B. N. Mandal. “Solution of singular integral equations of the first kind with Cauchy kernel.” In: *Communications in Advanced Mathematical Sciences* 2 (2019), pp. 69–74.

[57] M.J.S. Mphaka. “Partial singular integro-differential equations models for dryout in boilers.” PhD thesis. University of Southampton, 2000.

[58] N.I. Muskhelishvili. *Singular Integral Equations*. Noordhoff, Groningen, 1953.

[59] A. Nasirisavadkouhi. *A comparison study of KGD, PKN and a modified P3D model*. 2015. DOI: 10.13140/RG.2.1.3860.7201. URL: http://rgdoi.net/10.13140/RG.2.1.3860.7201.

[60] M.W. Nchabeleng. “Hydraulic fracture with Darcy and non-Darcy flow in a porous medium.” MA thesis. University of the Witwatersrand, 2016.

[61] M.W. Nchabeleng and A.G. Fareo. “Group invariant solution for a fluid-driven permeable fracture with Darcy flow in porous rock medium.” In: *International Journal of Non-Linear Mechanics* 99 (2018), pp. 79–85.

[62] M.W. Nchabeleng and A.G. Fareo. “Group invariant solution for a fluid-driven fracture with a non-Darcy flow in porous medium.” In: *International Journal of Non-Linear Mechanics* 115 (2019), pp. 41–48.

[63] R.P. Nordgren. “Propagation of a vertical hydraulic fracture.” In: *Society of Petroleum Engineers Journal* 12 (1972), pp. 306–314.

[64] E. Orowan. “Fracture and strength of solids.” In: *Reports on progress in physics* 12 (1949), p. 185.

[65] T.W. Patzek and D.B. Silin. “Water injection into a low-permeability rock-1 hydrofracture growth.” In: *Transport in Porous Media* 43 (2001), pp. 537–555.

[66] T.K. Perkins and L.R. Kern. “Widths of hydraulic fractures.” In: *J Pet Tech* 13 (1961), pp. 937–949.

[67] M. Perkowska. “Mathematical and numerical modeling of hydraulic fractures for non-Newtonian fluids.” PhD thesis. Aberystwyth University, 2016.

[68] A. S. Peters. “A note on the integral equation of the first kind with a Cauchy Kernel.” In: *Communications on Pure and Applied Mathematics* 16 (1963), pp. 57–61.

[69] M. M. Rahman and M. K. Rahman. “A review of hydraulic fracture models and development of an improved pseudo-3D model for stimulating tight oil/gas sand.” In: *Energy Sources* 32 (2010), pp. 1416–1436.

[70] M. Rahman. *Integral equations and their applications*. WIT press, 2007.

[71] M.M. Rahman, M.M. Hossain, D.G. Crosby, M.K. Rahman, and S.S. Rahman. "Analyical numerical and experimental investigations of transverse fracture propagation from horizontal wells." In: *Journal of Petroleum Science and Engineering* 35 (2002), pp. 127–150.

[72] A.M. Rubin. "Propagation of magma-filled cracks." In: *Annu. Rev. Earth Planet. Sci.* 23 (1995), pp. 287–336.

[73] F. Rummel and R.B. Winter. "Application of laboratory fracture mechanics data to hydraulic fracturing field tests." In: *1st Japan-USA Symp. on Fracture Mechanics Approach, Hydraulic Fracture and Geothermal Energy, Sendai, Japan.* (1982), pp. 495–501.

[74] D. Saveljeva. "Quadratic and cubic spline collocation for Volterra integral equations." PhD thesis. University of Tartu, 2006.

[75] A. Seifi, T. Lotfi, T. Allahviranloo, and M. Paripour. "An effective collocation technique to solve the singular Fredholm integral equations with Cauchy kernel." In: *Advances in Difference Equations* 2017 (2017), p. 280. URL: http://dx.doi.org/10.1186/s13662-017-1339-3.

[76] F. Sheibani and J. Olson. "Stress intensity factor determination for three-dimensional crack using the displacement discontinuity method with applications to hydraulic fracture height growth and non-planar propagation paths." In: *ISRM International Conference for Effective and Sustainable Hydraulic Fracturing*. International Society for Rock Mechanics and Rock Engineering. 2013.

[77] N.N. Smirnov and V.P. Tagirova. "Self-similar solutions of the problem of formation of a hydraulic fracture in a porous medium." In: *Izvestiya Rossiiskoi Akademii Nauk* 42 (2007), pp. 70–82.

[78] G.D Smith. *Numerical solution of partial differential equations: finite difference methods*. Oxford University Press, 1994.

[79] I.N. Sneddon. "The distribution of stress in the neighbourhood of a crack in an elastic solid." In: *Proceedings of the Royal Society of London. Series A. Mathematical and Physical Sciences* 187 (1946), pp. 229–260.

[80] I.N. Sneddon and H.A. Elliot. "The opening of a Griffith crack under internal pressure." In: *Q Appl Math* 4 (1946), pp. 262–267.

[81] *Solving Integral Equations - (1) Definitions and Types – Gaurav Tiwari*. URL: https://gauravtiwari.org/solving-integral-equations-1-definitions-and-types/ (visited on 11/01/2019).

[82] D.A. Spence and P.W. Sharp. "Self-similar solution for elastohydrodynamic cavity flow." In: *Proc. R. Soc. London, Ser. A* 400 (1985), pp. 289–313.

[83] D.A. Spence and D.L. Turcotte. “Magma-driven propagation of cracks.” In: *J. Geophysical Research* 90 (1985), pp. 575–580.

[84] R. P. Srivastav and F. Zhang. “Solving Cauchy singular integral equations by using general quadrature-collocation nodes.” In: *Computers & Mathematics with Applications* 21 (1991), pp. 59–71.

[85] F. Stoeckhert, M. Molenda, S. Brenne, and M. Alber. “Fracture propagation in sandstone and slate - Laboratory experiments, acoustic emissions and fracture mechanics.” In: *Journal of Rock Mechanics and Geotechnical Engineering* 7 (2015), pp. 237–249.

[86] V.V. Tvardovsky. “Stress intensity factors for anisotropic layered composites: Part I-isolated collinear cracks.” In: *Theoretical and Applied Fracture Mechanics* 17 (1992), pp. 205–219.

[87] P. Valko and M.J. Economides. “Propagation of hydraulically induced fractures - a continuum damage mechanics approach.” In: *Int. J. Rock Mech. Min. Sci. Geomech. Abstr.* 31 (1994), pp. 221–229.

[88] P. Valko and M.J. Economides. *Hydraulic fracture mechanics*. Vol. 28. Wiley Chichester, 1995.

[89] P. Venkataraman and P. Rao. “Validation of Forchheimer‘s law for flow through porous media with converging boundaries.” In: *Journal of Hydraulic Engineering* 126 (2000), pp. 63–71.

[90] A.M. Wazwaz. “A reliable treatment for mixed Volterra–Fredholm integral equations.” In: *Applied Mathematics and Computation* 127 (2002), pp. 405–414.

[91] A.M. Wazwaz. *Linear and nonlinear integral equations methods and applications*. Springer Heidelberg Dordrecht London New York, 2011.

[92] A.M. Wazwaz. *A first course in integral equations*. World Scientific Publishing Company, 2015.

[93] C.H. Yew and X. Weng. *Mechanics of hydraulic fracturing*. Gulf Professional Publishing, 2014.

[94] K. Yildizdag, F. Weber, and H.H. Konietzky. *Hydraulic fracturing*. 2017. URL: https://docplayer.net/81323171-Hydraulic-fracturing-authors-kemal-yildizdag-fabian-weber-prof-dr-habil-heinz-konietzky-tu-bergakademie-freiberg-geotechnical-institute.html.

[95] C. Zeeb and H. Konietzky. “Simulating the hydraulic stimulation of multiple fractures in an anisotropic stress field applying the discrete element method.” In: *Energy Procedia* 76 (2015), pp. 264–272. URL: http://dx.doi.org/10.1016/j.egypro.2015.07.859.

[96] C. Zeeb, H. Konietzky, and D. Wolgast. “Simulation of hydro-mechanical fracture growth in single- and multi-fracture systems.” In: *Veröffentlichungen des Instituts für Geotechnik der TU Bergakademie Freiberg zum 43. Geomechanik-Kolloquium*. 2014, pp. 183–197. ISBN: 1611-1605.